ENGINEERING POLYMERIC NANOPARTICLES FOR NON-VIRAL DELIVERY OF NUCLEIC ACID DRUGS AND THE CRISPR/CAS9 GENE EDITING PLATFORM

by
Yuan Rui

A dissertation submitted to Johns Hopkins University in conformity with the requirements for the degree of Doctor of Philosophy

Baltimore, Maryland
June 2021

Abstract:

Gene therapy involves the introduction of exogenous nucleic acids into target cells to regulate gene expression. The recent discovery of the CRISPR/Cas9 gene editing system provides a powerful tool for site-specific editing of the host cell genome, further expanding the therapeutic potential of genetic medicine. Because of their high molecular weight and overall hydrophilicity, nucleic acids and proteins are inherently cell membrane impermeable. The efficacy of these biomacromolecules thus depends heavily on their ability to reach intracellular sites of action. Chemical gene delivery systems have been studied as promising vectors for gene therapy, and the recent development of lipid nanoparticle-based mRNA COVID-19 vaccines have demonstrated their efficacy and scalability. But more work still needs to be done to characterize and optimize non-viral nanoparticles for gene therapy applications. To this end, the work in this thesis sought to rationally engineer materials for delivery of different biomacromolecule cargos and validate their efficacy *in vitro* and *in vivo*.

Chapter one outlines the guiding aims of the thesis. Chapter two contains background information on intracellular delivery. Chapter three describes a collaborative work with Dr. John Laterra's lab using bio-reducible poly(beta-amino ester) (PBAE) nanoparticles to deliver cancer-inhibitory miRNAs to treat glioblastoma. Chapter four describes a study using plasmid DNA-containing nanoparticles to enable HSVtk suicide gene therapy to treat murine models of pediatric brain cancer. Chapter five details my work using PBAE nanoparticles to deliver DNA plasmids to enable CRISPR gene editing in mammalian cells. Chapter six further studies non-viral delivery of CRISPR gene editing tools using a series of bio-reducible, branched PBAE polymers to deliver Cas9 plasmid DNA and sgRNA in short RNA form. Chapter seven is an interesting study using carboxylated PBAE structures for intracellular delivery of proteins and also demonstrates the feasibility of non-viral CRISPR delivery in ribonucleoprotein form. Chapter eight explores the combined use of high-throughput imaging and a genetically-encoded galectin 8 endosomal disruption sensor to characterize intracellular gene delivery barriers *in vitro* as well as validate top structures for mRNA delivery *in vivo*. Chapter nine discusses my perspectives on exciting recent advances and future directions for the field of non-viral delivery.

Thesis Committee:

Jordan J. Green, Ph.D. *(primary advisor, reader)*

Professor, Department of Biomedical Engineering, Ophthalmology, Oncology, Neurosurgery, Materials Science & Engineering, and Chemical & Biomolecular Engineering

Johns Hopkins University School of Medicine

John J. Laterra, M.D/Ph.D. *(reader)*

Professor of Neurology, Oncology, and Neuroscience

Johns Hopkins University School of Medicine

Hai-Quan Mao, Ph.D.

Professor, Department of Materials Science & Engineering and Biomedical Engineering

Johns Hopkins University

Honggang Cui, Ph.D.

Associate Professor, Department of Chemical & Biomolecular Engineering

Johns Hopkins University

Acknowledgements

I would like to start by thanking all the mentors I have had the privilege to learn from and work with throughout my academic career. In my undergraduate studies, I am extremely grateful to my research advisor Dr. Brian Grady, who gave me my first research opportunity and encouraged me to pursue graduate studies. In graduate school, I would like to thank my primary research advisor Dr. Jordan Green for his mentorship and support throughout my PhD training. Dr. Green's encouragement, optimism, and patience helped me persevere through many failed studies, and the incredible amount of academic freedom he gave me allowed me to make mistakes and learn to be a more resilient and independent researcher. Special thanks go to Drs. John Laterra and Hernando Lopez-Bertoni, who were collaborators in our projects using miRNA to treat brain cancer as well as valuable advisors on career development. Thank you to my thesis committee members Dr. Hai-Quan Mao and Dr. Honggang Cui for your helpful discussion on data and your guidance in helping me navigate through my PhD. Likewise, this PhD benefited greatly from interactions with the faculty of the Translational Tissue Engineering Center (TTEC) including Dr. Jennifer Elisseeff, Dr. Josh Doloff, and Dr. Warren Grayson.

I would like to further thank the many undergraduate students and fellow graduate students who worked alongside me these past six years. Within the Green lab, I have had the privilege of mentoring undergraduate students Katie Sanders, Deepti Sudhakar, Shannelle Mendes, and Hannah Yamagata, as well as high school students Gabbie Quiñones and John Johnson. Their assistance with experiments was indispensable to my research projects and their enthusiasm for science was infectious, and I hope they found their time with me to be equally rewarding. I would like to thank past and present members of the Green lab – Dr. Kristen Kozielski, Dr. Randall Meyer, Dr. Jayoung Kim, Dr. Maziar Mohammadi, Dr. Ron Shmueli, Dr. Steph Tzeng, Dr. Johan Karlsson, Hannah Vaughan, Savannah Est-Witte, Elana Ben-Akiva, Kelly Rhodes, Katie Luly, Sarah Neshat, Sydney Shannon, Hongzhe Yu, and Erin Kavanagh; your eagerness to share your expertise and your camaraderie have made working in the lab so much easier and more enjoyable. Likewise, members from other labs on the floor have saved the day many times by giving advice or sharing

reagents; in particular, Sarah Somers, Ashley Farris, Lexi Rindone, Sami (Srujan) Singh, David Maestas, Dr. John Choi, Dr. Jordie Gilbert-Honick, Dr. Justin Morrissette-McAlmon, and Dr. Liam Chung.

These acknowledgments would not be complete without thanking my family. I would like to thank my partner in life and science, Dr. David Wilson. Meeting you and starting our little family together was one of the best things that's ever happened to me. I am so proud of all your achievements as a scientist, mentor, and father, and I'm eternally grateful for your unwavering support in all my endeavors. Thank you to our baby daughter Alice Marie, who accompanied me to lab and kept me company throughout my pregnancy and continues to be my little helper by snoring quietly on my lap as I type these words. Thank you to our wonderful cats Mavid Supernatant and Dorkin Winnifred for always being happy to see me when I come home, even on days when all my experiments failed. Thank you to my mom and dad for taking a leap of faith and coming to this country two decades ago, for pressuring me into getting a PhD (you were right, it was worth it), and for continuing to support me as a budding academic and a new mom. Likewise, thank you to my in-laws, Tim and Karen, for welcoming me into their family and always taking an interest in my work.

Table of contents

List of Tables

List of Figures

Chapter 1. Introduction to the Thesis

1.1 Objectives

The primary objective of this thesis was to develop biomaterials for non-viral delivery of genes and proteins and demonstrate their utility for cancer gene therapy in proof-of-concept animal studies. This work was accomplished broadly following the following aims:

1. Evaluate the efficacy of polymeric nanoparticles as nucleic acid delivery vehicles for cancer gene therapy.
    a. Identify nanoparticle formulations to deliver plasmid DNA to human brain cancer cells and validate their *in vivo* efficacy using HSVtk suicide gene therapy in mice.
    b. Engineer bio-reducible PBAEs for the delivery of small RNAs to treat glioblastoma.
2. Rational design and validation of polymers that enable CRISPR gene editing through delivery of different nucleic acid and protein cargos.
    a. Develop materials to enable CRISPR gene editing through combinatorial nucleic acid delivery.
    b. Design and validation of protein delivery materials to enable CRISPR editing *in vivo*.
3. Apply polymeric nanoparticle formulations to deliver mRNA *in vivo*.
    a. Develop high-throughput methods for polymer library synthesis and high content imaging-based *in vitro* screening.
    b. Investigate mRNA transfection after intravenous or intramuscular nanoparticle administration.

1.2 Summary of Contributions

Chapter 2: A background in non-viral delivery of biomacromolecules

- Review article – Kozielski K*, **Rui Y*,** Green JJ. Non-viral nucleic acid containing nanoparticles as cancer therapeutics. *Expert Opinion on Drug Delivery,* 13 (10) pp 1475-1487. (**2016**). *These authors contributed equally.

- Review article – **Rui Y***, Wilson DR*, Green JJ. Non-viral delivery to enable genome editing. *Trends in Biotechnology*, 37 (3), pp 281-293. (**2018**). *These authors contributed equally.

Chapter 3: Bioreducible Polymeric Nanoparticles Containing Multiplexed Cancer Stem Cell-regulating miRNAs inhibit Glioblastoma Growth and Prolong Survival

- Research article – Lopez-Bertoni H*, Kozielski KL*, **Rui Y***, Lal B, Vaughan H, Wilson DR, Mihelson N, Eberhart CG, Laterra J, Green JJ. Bioreducible polymeric nanoparticles containing multiplexed cancer stem cell-regulating miRNAs inhibit glioblastoma growth and prolong survival. *Nano Letters.* 18 (7), pp 4086–4094 (**2018**). *These authors contributed equally.
- Research talk – **Rui Y,** Lopez-Bertoni H, Kozielski KL, Lal B, Wilson DR, Laterra J, Green JJ. Environmentally-responsive polymeric nanoparticles for brain cancer gene therapy. Johns Hopkins Institute for Nanobiotechnology Student Research Forum. Baltimore, MD. 2019.

Chapter 4: Nonviral Polymeric Nanoparticles for Gene Therapy in Pediatric CNS Malignancies

- Research article – Choi J*, **Rui Y*,** Kim J*, Gorelick N, Wilson DR, Kozielski K, Mangraviti A, Sankey E, Brem H, Tyler B, Green JJ, Jackson EM. Nonviral polymeric nanoparticles for gene therapy in pediatric CNS malignancies. *Nanomedicine: Nanotechnology, Biology and Medicine*. 23 (**2020**). *These authors contributed equally.

Chapter 5: Poly(beta-amino ester) nanoparticles enable non-viral delivery of CRISPR/Cas9 plasmids for gene knockout and gene deletion

- Research article – **Rui Y**, Varanasi M, Mendes S, Yamagata HM, Wilson DR, Green JJ. Poly(beta-amino ester) nanoparticles enable non-viral delivery of CRISPR/Cas9 plasmids for gene knockout and gene deletion. *Molecular Therapy: Nucleic Acids.* 20, pp 661-672 (**2020**).
- Research talk – **Rui Y,** Wilson DR, Green JJ. Poly(beta-amino ester) nanoparticles for the delivery of CRISPR/Cas9 achieves efficient genome editing. Mid-Atlantic Biomaterials Day. Baltimore, MD. 2018.

- Research poster – **Rui Y,** Kozielski K, Wilson DR, Green JJ. Poly(β-amino ester) nanoparticles for delivery of CRISPR/Cas9 to primary human brain cancer cells. International Nanomedicine & Drug Delivery Symposium. Baltimore, MD. 2016

Chapter 6: Reducible Branched Ester-Amine Quadpolymers (rBEAQs) Co-delivering Plasmid DNA and RNA Oligonucleotides Enable CRISPR/Cas9 Genome Editing

- Research article – **Rui Y**, Wilson DR, Sanders K, Green JJ. Reducible branched ester amine quadpolymers (rBEAQs) co-delivering plasmid DNA and RNA oligonucleotides enable CRISPR/Cas9 genome editing. *ACS Applied Materials & Interfaces.* 11 (11), pp 10472-10480 (**2019**).
- Research talk – **Rui Y,** Wilson DR, Sanders K, Green JJ. Hyperbranched bioreducible poly(beta-amino ester)s for efficient delivery of siRNA. Biomedical Engineering Society National conference. Phoenix, AZ. 2017.
- Research poster – **Rui Y,** Wilson DR, Green JJ. Hyperbranched bioreducible poly(beta-amino ester)s for efficient delivery of siRNA. Johns Hopkins Women in STEM Symposium. Baltimore, MD. 2018.

Chapter 7: Carboxylated branched poly(beta-amino ester) nanoparticles enable robust cytosolic protein delivery and CRISPR/Cas9 gene editing

- Research article – **Rui Y**, Wilson DR, Choi J, Varanasi M, Sanders K, Karlsson J, Lim M, Green JJ. Carboxylated branched poly (B-amino ester) nanoparticles enable robust cytosolic protein delivery and CRISPR-Cas9 gene editing. *Science Advances*. 5 (12) (**2019**).
- Research talk – **Rui Y,** Wilson DR, Sanders K, Green JJ. Carboxylated branched poly(B-amino ester) nanoparticles enable robust intracellular protein delivery and CRISPR/Cas9 gene editing. Society for Biomaterials National Conference. Seattle, WA. 2019
- Research talk – **Rui Y,** Wilson DR, Sanders K, Green JJ. Carboxylated branched poly(B-amino ester) nanoparticles enable robust intracellular protein delivery and CRISPR/Cas9 gene editing. Wilmer Eye Institute Research Discussion (W.E.I.R.D.) Seminar Series. Baltimore, MD. 2019.

- Research poster – **Rui Y,** Wilson DR, Choi J, Varanasi M, Sanders K, Karlsson J, Lim M, Green JJ. Carboxylated branched poly(β-amino ester) nanoparticles enable robust intracellular protein delivery and CRISPR/Cas9 gene editing. US-Japan Symposium on Drug Delivery Systems. Maui, HI. 2019.
- Research poster – **Rui Y,** Wilson DR, Sanders K, Green JJ. Carboxylated branched poly(beta-amino ester) nanoparticles enable non-viral CRISPR/Cas9 gene editing via intracellular ribonucleoprotein delivery. American Society of Gene & Cell Therapy Annual Meeting. Washington D.C. 2019.

Chapter 8: Poly(beta-amino ester) Quadpolymer Structure Tunes Endosomal Escape, Cellular Uptake, and *In Vivo* Delivery of mRNA Nanoparticles

- Research article – **Rui Y,** Wilson DR, Tzeng SY, Yamagata HM, Sudhakar D, Conge M, Berlinicke CA, Zack DJ, Tuesca A, Green JJ. Poly(beta-amino ester) quadpolymer structure tunes endosomal escape, cellular uptake, and *in vivo* delivery of mRNA nanoparticles. (**2021**). Submitted.

Other contributions not included in written thesis:

- Research article – Karlsson J, Tzeng SY, Hemmati S, Luly KM, Choi O, **Rui Y**, Wilson DR, Kozielski KL, Quiñones -Hinojosa A, Green JJ. Photocrosslinked bioreducible polymeric nanoparticles for enhanced systemic siRNA delivery as cancer therapy. *Advanced Functional Materials*. pp 2009768 (**2021**).
- Research article – Lopez-Bertoni H, Kotchetkov IS, Mihelson N, Lal B, **Rui Y**, Ames H, Lugo-Fagundo M, Guerrero-Cazares H, Quiñones -Hinojosa A, Green JJ, Laterra J. A Sox2/miR-486-5p axis regulates survival of GBM cells by inhibiting tumor suppressor networks. *Cancer Research*. 80 (8), pp 1644-1655 (**2020**).
- Research article – Kim J, Mondal SK, Tzeng SY, **Rui Y**, Al-kharboosh R, Kozielski KL, Bhargav AG, Garcia CA, Quiñones-Hinojosa A, Green JJ. Poly(ethylene glycol)-poly(beta-amino ester)-based nanoparticles for suicide gene therapy enhance brain penetration and extend survival in a preclinical human glioblastoma orthotopic xenograft model. *ACS Biomaterials Science & Engineering*. 6 (5), pp 2943-2955 (**2020**).

- Research article – Mathios D, Hwang T, Xia Y, Phallen J, **Rui Y**, See AP, Maxwell R, Belcaid Z, Casaos J, Burger P, McDonald KL, Gallia G, Cope L, Kai M, Brem H, Pardoll D, Ha P, Green JJ, Velculescu V, Bettegowda C, Park CK, Lim M. Genome-wide investigation of intragenic DNA methylation identifies *ZMIZ1* gene as a prognostic marker in glioblastoma and multiple cancer types. *International Journal of Cancer*. 145, pp 3425-3435 (**2019**).
- Research article – Karlsson J, **Rui Y**, Kozielski K, Placone A, Choi O, Tzeng S, Kim J, Keyes J, Bogorad M, Gabrielson K, Guerrero-Cazares H, Quinones-Hinojosa A, Searson P, Green JJ. Engineered nanoparticles for systemic siRNA delivery to malignant brain tumors. *Nanoscale*. 11 (42), pp 20045-20057 (**2019**).
- Research article – Mishra B, Wilson DR, Sripathi SR, Suprenant MP, **Rui Y**, Wahlin KJ, Berlinicke CA, Green JJ, Zack DJ. A combinatorial library of biodegradable polyesters enables non-viral gene delivery to post-mitotic human stem cell-derived polarized RPE monolayers. *Regenerative Engineering and Translational Medicine*. pp 1-13 (**2019**).
- Research article – Kozielski K, Ruiz-Valls A, Tzeng S, Guerrero-Caszares H, **Rui Y**, Vaughan H, Gionet-Gonzales M, Vantucci C, Kim J, Schiapparelli P, Alkharboosh R, Quinones-Hinojosa A, Green JJ. Cancer-selective nanoparticles for combinatorial siRNA delivery to primary human GBM in vitro and in vivo. *Biomaterials*. 209 pp79-87. (**2019**).
- Research article – Wilson DR, **Rui Y**, Siddiq K, Routkevitch D, Green JJ. Differentially branched ester amine quadpolymers with amphiphilic pH-sensitive properties for efficient plasmid DNA delivery. *Molecular Pharmaceutics*. 16 (2), pp 655-668 (**2019**).
- Research article – Wilson DR, Routkevitch D, **Rui Y**, Quinones-Hinojosa A, Zack DJ, Green JJ. A triple-fluorophore labeled nucleic acid pH nanosensor to investigate non-viral gene delivery. *Molecular Therapy*. 25 (7), pp 1697-1709. (**2017**).
- Review article - Luly KM, Choi J, **Rui Y,** Green JJ, Jackson EM. Safety considerations for nanoparticle gene delivery in pediatric brain tumors. *Nanomedicine*. (**2020**).

- Review article - **Rui Y**, Quiñones G, Green JJ. Biodegradable and bioreducible poly(beta-amino ester) nanoparticles for intracellular delivery to treat brain cancer. *AIChE Journal*, 63 (5) pp 1470-1482. (**2017**).
- Review article - **Rui Y** and Green JJ. Overcoming Delivery Barriers in Immunotherapy for Glioblastoma. *Drug Delivery and Translational Research.* In press (**2021**).

Chapter 2.a Non-Viral Nucleic Acid Containing Nanoparticles as Cancer Therapeutics

Kozielski K[a]*, Rui Y [a]*, Green JJ[b]

[a]Department of Biomedical Engineering, the Institute for NanoBioTechnology, & the Translational Tissue Engineering Center, Johns Hopkins University School of Medicine, Baltimore, MD, USA; [b]Departments of Ophthalmology, Oncology, Neurosurgery, and Materials Science & Engineering, Johns Hopkins University School of Medicine, Baltimore, MD, USA

* These authors contributed equally to this work.

Abstract

Introduction: The delivery of nucleic acids such as DNA and short interfering RNA (siRNA) is promising for the treatment of many diseases, including cancer, by enabling novel biological mechanisms of action. Non-viral nanoparticles are a promising class of nucleic acid carriers that can be designed to be safer and more versatile than traditional viral vectors.

Areas covered: In this review, recent advances in the intracellular delivery of DNA and siRNA are described with a focus on non-viral nanoparticle-based delivery methods. Material properties that have enabled successful delivery are discussed as well as applications that have directly been applied to cancer therapy. Strategies to co-deliver different nucleic acids are highlighted, as are novel targets for nucleic acid co-delivery.

Expert opinion: The treatment of complex genetically-based diseases such as cancer can be enabled by safe and effective intracellular nucleic acid delivery of multiple nucleic acids. Non-viral nanoparticles can be fabricated to deliver multiple nucleic acids to the same cell simultaneously to prevent tumor cells from easily

compensating for the knockdown or overexpression of one genetic target. The continued innovation of new therapeutic modalities and non-viral nanotechnologies to provide target-specific and personalized forms of gene therapy hold promise for genetic medicine to treat diseases like cancer in the clinic.

Keywords: cancer, DNA, gene delivery, gene therapy, nanoparticle, polymer, siRNA

Article highlights:

- Obstacles to intracellular nucleic acid delivery include rapid clearance from circulation, tissue and tumor targeting, cellular internalization, endosomal escape, and intracellular release.
- Lipid-based and inorganic materials protect nucleic acids from degradation and condense them into nanoparticles for improved cellular uptake.
- Cationic polymers self-assemble into polyplexes with nucleic acids via electrostatic interactions and possess functional groups to aid in improved cellular uptake, endosomal escape through endosomal buffering, and intracellular cargo release via biodegradable linkages.
- Nanoparticle formulations optimized for the co-delivery of multiple DNA or siRNA cargos can be used to reach novel synergistic cancer therapy targets.
- Therapeutic modalities such as DNA, siRNA, and CRISPR/Cas technology may benefit from non-viral nanoparticle delivery platforms for the treatment of complex genetically-based diseases.

1. Introduction

The discovery that exogenous DNA introduced into isolated nuclei can be transcribed into mRNA [1] and lead to protein expression [2, 3] created the promise of gene therapy as a modality capable of treating myriad diseases. siRNA is a more recently discovered therapeutic modality and can be used to knock down gene expression through the RNA interference (RNAi) pathway. RNAi was initially discovered in *C. elegans* as a gene silencing pathway used as a natural mechanism for viral defense [4]. A strand of long, double-stranded RNA (dsRNA) is cleaved by the Dicer protein into 21-25 bp siRNAs [5]. siRNA is then incorporated into the RNA-induced silencing complex (RISC) where the sense strand is removed. The antisense strand is then used

as a template for complementary mRNA. mRNA that pairs with siRNA-RISC is cleaved, thus preventing translation and thereby gene expression. (For review, see Hannon [6].)

Early delivery methods of these nucleic acids often involved introducing nucleic acids by mechanical disruption of the cell membrane or direct injection [7, 8]. However, these methods are laborious and not clinically translatable. Viral methods of DNA and siRNA delivery are effective [9], yet often induce immunogenicity or tumorigenicity and are therefore limited for clinical translation [10]. Non-viral nucleic acid delivery has traditionally been considered less effective [11], but can be designed to avoid tumorigenesis and immune stimulation. Recent advances in nanoparticle vectors for nucleic acid delivery have continued to improve delivery efficacy while minimizing toxicity, but several obstacles remain that make successful delivery an ongoing challenge.

1.1 Obstacles to intracellular delivery

Due to their size and negative charge, nucleic acids cannot readily pass through the cell membrane to their intracellular sites of action (**Figure 2-1**). Nanocarriers can encapsulate nucleic acids to not only promote successful delivery into cells, but also to protect them from degradation by extracellular nucleases. Nanocarriers for nucleic acid delivery include liposomes that hold DNA and siRNA within their aqueous interiors [12-14], cationic polymers that bind anionic nucleic acids to form polyplexes [15, 16], and solid nanoparticles that can carry nucleic acids via covalent linkages [17]. For nanocarriers that electrostatically bind to nucleic acids, special considerations must be taken for short oligonucleotides like siRNA, which are much shorter and stiffer than plasmid DNA, and are therefore often harder to complex into nanoparticles [18, 19]. To prevent unwanted non-specific interactions between nanoparticles and biomolecules and cells, nanoparticles are frequently coated with hydrophilic polymers, such as polyethylene glycol (PEG) [20].

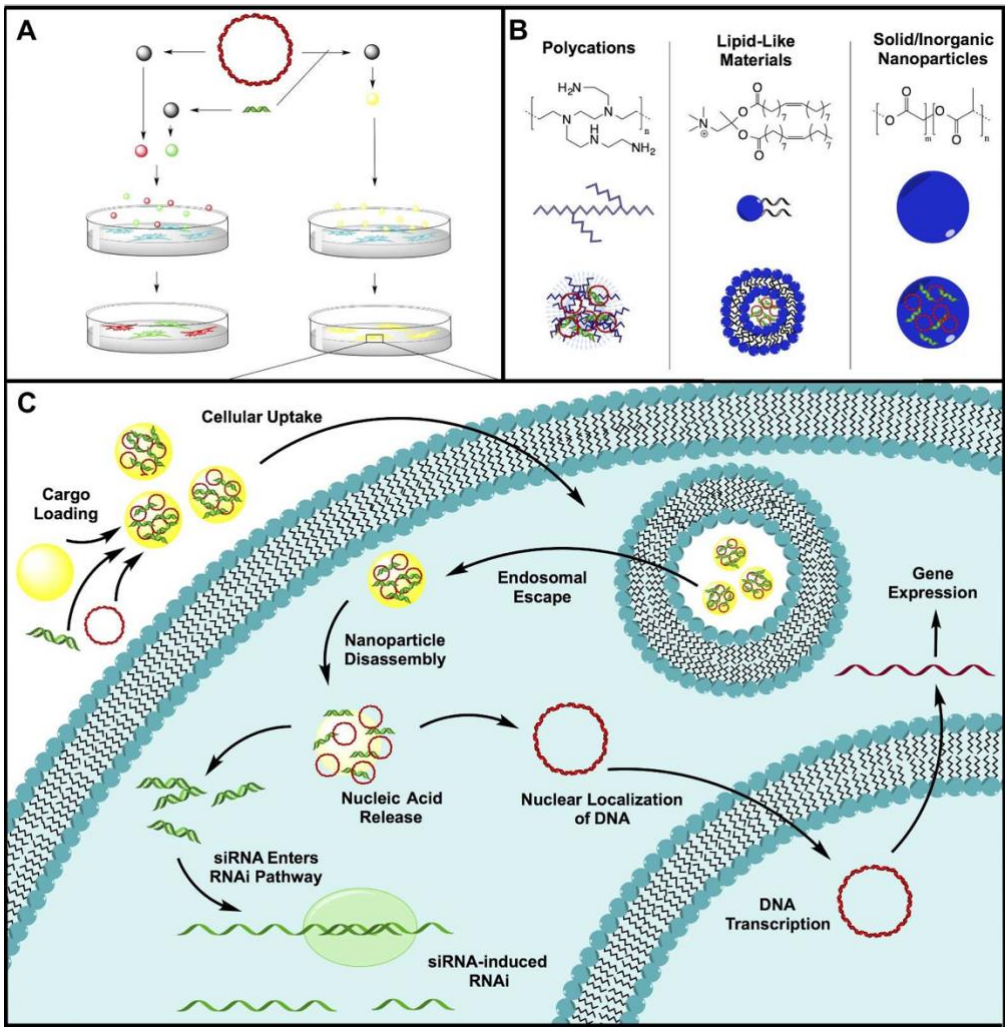

Figure 2-1. Overview of nanoparticle codelivery of DNA and siRNA. **(A)** Nanoparticles carrying DNA and siRNA cargoes separately yield little codelivery, while nanoparticles carrying both nucleic acids optimize coexpression. **(B)** There are multiple classes of non-viral nanoparticles for gene delivery. Each class with its own representative chemical structure (top), nanoparticle structure (center), and method of carrying nucleic acid (bottom). **(C)** There are multiple steps for successful intracellular delivery of DNA and siRNA.

For intracellular delivery, cells must take up the nucleic acid carrying nanoparticles. To enable cellular uptake, cell-penetrating peptides can be used to promote internalization directly through the cell membrane [21-23], or cationic nanoparticles can nonspecifically interact with the negatively charged cell surface to

promote endosomal uptake [24-27]. If internalized via endosomes, the nanoparticle must escape the endosome to prevent degradation in lysosomes, prevent recycling out of the cell, and to promote cytosolic delivery. This can be achieved with hydrophobic or amphiphilic biomaterials that can destabilize the endosomal membrane [28, 29]. Endosomal escape can also be achieved using the proton sponge mechanism, in which a nanomaterial may act as a buffer against endosomal acidification and eventually result in endosomal lysis. Although this mechanism has been challenged [30], it is the most widely accepted hypothesis to explain successful transfection when utilizing nanomaterials with titratable amines [31, 32].

For siRNA delivery, the nanocarrier must release its contents at the site of RNAi in the cytosol [33]. Several polymeric materials degrade hydrolytically and can thereby release siRNA as the polymer degrades [34, 35]. As the cytosol is approximately 1000 times more reducing than the extracellular space [36], nanomaterials may also employ bioreducible disulfide bonds to promote release targeted specifically to the cytosol. (For review, see Son *et al.*[37]) Nanocarriers delivering DNA may need to remain intact longer, as naked DNA is slow to diffuse in the cytosol and may be degraded by cytosolic nucleases on its way to the nucleus [38, 39]. Nuclear penetration is an additional major bottleneck to gene delivery. It has been shown that actively dividing cells are easier to transfect [40], and this can be an avenue to increase transfection in cancer cells compared to non-cancerous slower growing cells. In non-mitotic cells, attaching a nuclear localization signal peptide sequence to DNA is a strategy that improves nuclear penetration by using the cell's own nuclear import machinery [41]. Complexing DNA within a polymeric nanocarrier has been shown to increase nuclear association and permeability [42]. For all of these steps, nanomaterial properties are key in order to achieve intracellular nanoparticle-based DNA and siRNA delivery (**Table 2-1**). Table 1 also illustrates the evolution of nanomaterials used for non-viral gene delivery from readily available off-the-shelf chemicals to custom biomaterials designed specifically for intracellular nucleic acid delivery.

Non-viral Vector	Key Characteristics	Early Investigation	Representative Cancer Types
Calcium phosphate	Co-precipitate nucleic acids with calcium phosphate to form nanocrystals	1973[171]	Melanoma and breast cancer[172]; nasopharyngeal carcinoma[173]
Liposomes	Encapsulate nucleic acid cargo in aqueous interior	1980[174]	Colorectal cancer and breast cancer[175]; pancreatic islet cell tumors[176]; Lewis lung carcinoma[48]
PLL	Cationic polypeptide for nucleic acid binding	1987[16]	Lung cancer[177]; bladder cancer[178]
Gold	Chemically inert, easily functionalized; can be used for theranostic purposes	1990[179]	Breast cancer[180, 181]
Dendrimers	Highly branched polymers with greater shape control and end group density	1993 (PAA)[182]; 1999 (PPI)[183]	Breast cancer[184]; ovarian cancer[185]; epidermoid carcinoma and glioblastoma[186]
PEI	Titratable amines facilitate endosomal escape	1995[16, 99]	Neuroblatoma[149]; glioma and medulloblastoma[187]; glioma and hepatoma[150]
PLGA	Encapsulates nucleic acids through double emulsion process	1997[182, 183, 188]	Lung cancer[92]; prostate cancer[184-186, 189]
Cyclodextrin	Water-soluble polysaccharides that can complex with nucleic acids	1999[190]	Hepatoma[114]; leukemia[151]; breast and ovarian cancer[191]
Mesoporous silica	Solid material with porous structure allowing cargo adsorption on the outer surface and inside pores	2000[83]	Lung cancer[89]; ovarian cancer[87]; breast cancer[192]
PBAE	Contains hydrolizable ester bonds for greater biocompatability	2000[122]	Glioblastoma[125, 126, 170]; melanoma[129]; small cell lung cancer[135]; hepatoma[136]; prostate cancer[193]

Table 2-1. Key nanomaterials listed in chronological order of their initial investigation to illustrate the evolution of nanomaterials used for non-viral gene delivery. Representative cancer types that have been investigated using each material for therapeutic gene delivery are also listed.

2. Nanoparticles for DNA and siRNA delivery

2.1 Liposomes and lipid-based materials

Lipid-based nanoparticles are the most commonly used non-viral chemical method of intracellular nucleic acid delivery. Several commercially available transfection reagents including Lipofectamine® 2000 [43], 1,2-dioleoyl-3-trimethylammonium-propane (DOTAP) [44], RNAifect [44], TransIT-TKO and TransIT-siQuest [45] are all lipid-based. For DNA delivery, the molecular structure of the cationic lipid is an important factor in transfection efficacy as it determines how the liposome interacts with the cell membrane [46, 47]. These liposomes can be modified by conjugating targeting ligands on the surface [48] or adding cholesterol to improve cell binding and uptake [49]. In liposomes delivering siRNA, cholesterol is often added to formulations to increase membrane fluidity and thereby increase cell membrane fusion and cellular uptake [50, 51]. Other lipid-based approaches utilize modified structures of individual lipids to make it energetically easier for the liposome to leave the lamellar phase and disrupt the endosome, thus releasing nucleic acid cargo into the cytoplasm and preventing lysosomal degradation [24, 52, 53]. Liposomally delivered siRNA cargo simultaneously escapes the endosome and is released from its carrier into the cytosol, its site of action. Lipid hydrocarbon tail properties such as chain length and saturation have been shown to play a role in cell membrane fusogenicity and can be optimized to promote cellular uptake [54].

Factors other than efficacy must be considered when designing nanoparticle systems. For example, DOTAP forms stable nanoparticles that protect DNA from degradation [55] but has been shown to promote strong interferon responses in mice [44]. Chono *et al.* modified DOTAP with hyaluronic acid and were able to demonstrate reduced immunotoxicity as measured by inflammatory cytokine expression [56]. Functionalizing liposomes with a hydrophilic polymer poly(ethylene glycol) (PEG) has also been shown to reduce immune stimulation [57]. Semple *et al.* were able to show successful intravenous administration of siRNA using PEGylated lipids in non-human primates [58]. Interestingly, some groups have been able to take advantage of the immunogenic properties of DOTAP. Ott *et al.* showed that DOTAP nanoparticles in a DNA vaccine formulation induced greater antibody response compared to naked DNA [59]. Thus, DOTAP could potentially be used as an adjuvant as well as a carrier in DNA vaccines.

2.2 Inorganic nanoparticles

Calcium phosphate (CaP) nanoparticles enable DNA delivery via co-precipitation of CaP and DNA into nanoscale crystals [60-62]. Sokolova *et al.* synthesized nanoparticles with a CaP core and alternating DNA and CaP shells that protected DNA from degradation and improved transfection [63]. Methods to optimize CaP for siRNA delivery have often employed polymers. Polymethacrylate-PEG (PMA-PEG) block copolymers were coated onto the surface of CaP/siRNA nanoparticles and assisted in endosomal escape [64]. To improve loading of siRNA into CaP, Zhang *et al.* covalently functionalized siRNA with PEG and then co-precipitated siRNA and CaP [65].

Gold nanoparticles are advantageous for several types of gene delivery because they are safe, easy to chemically functionalize, and have the potential for diagnostic as well as therapeutic use [66, 67]. The particle surface can be modified by cationic groups such as quaternary ammonium salts to increase DNA binding [68]. Alternatively, anti-sense DNA oligonucleotides have been covalently linked to the surface of nanoparticles to induce gene knockdown [69]. Spherical nucleic acids, oligonucleotides arranged in a dense, oriented, and spherical configuration, have shown promise for intracellular delivery in multiple applications and are often designed by conjugation to an inorganic nanoparticle core, such as thiolated nucleic acids conjugated to gold nanoparticles [70, 71]. The covalent linker can also be modified to allow greater control of DNA release. Han *et al.* used a photoactive *o*-nitrobenzyl ester linker to control the spatial and temporal release of DNA by applying a near-UV light [72]. Alternative approaches to deliver siRNA using inorganic nanoparticles include combination with polymers. siRNA can be non-covalently layered onto gold nanoparticles by alternating layers of siRNA with the cationic polymer poly(ethylene imine) (PEI) [73]. A combinatorial approach was designed by Lee *et al.* in which siRNA was covalently linked to gold nanoparticles via disulfide bonds and then electrostatically coated with PBAEs in order to promote cell uptake and endosomal buffering [74].

Quantum dots such as CdSe/ZnS nanoparticles can be used as fluorophores as well as nucleic acid delivery vehicles [75-77]. DNA can be covalently conjugated onto the quantum dot using a peptide nucleic acid linker [78], or through non-covalent association with cationic polymers that are capped on the quantum

dot surface [79]. Methods for siRNA delivery commonly employ covalently linking siRNA to the quantum dot surface, often with a polymeric spacer [80, 81].

Mesoporous silicas are solid materials that have a honeycomb-like porous structure with empty channels (mesopores) that can encapsulate bioactive molecules.[82] This unique porous structure provides an inner and an outer surface onto which cargo can adsorb. Silica has been shown to have high affinity for the head groups of phospholipids that promotes its association with the cell membrane, enhancing cellular uptake through physical concentration of mesoporous silica nanoparticles (MSNs) on the cell surface [83, 84]. MSNs for DNA delivery require surface modification with cationic groups for DNA binding [85]. Similarly, MSNs have been coated with cationic polymers such as PEI [86] and PAA [87] to facilitate siRNA binding. In addition to nucleic acid binding on the outside, the internal surfaces of MSN mesopores have been used to encapsulate fluorescent dyes for intracellular tracking [88] or anticancer drugs for multimodal therapies [87]. Li *et al.* designed an MSN modified with PEI and the fusogenic peptide KALA encapsulating siRNA targeting vascular endothelial growth factor receptor [89]. When these particles were injected intratumorally into mice that had been subcutaneously inoculated with human lung cancer cells, they significantly inhibited tumor growth through the suppression of tumor neovascularization. These results demonstrate the potential of MSNs delivering nucleic acids as powerful anti-cancer therapies.

2.3 Polymeric nanoparticles

Poly(lactic-*co*-glycolic acid) (PLGA) nanoparticles are advantageous for several types of drug delivery due to their biodegradability and safety, and PLGA as a biomaterial has already been used in a number of FDA-approved devices. PLGA particles are typically synthesized via a simple emulsion-solvent evaporation process [90] and have a readily functionalizable surface chemistry that allows easy attachment of molecules to promote delivery functions like tissue homing and cellular uptake [91]. DNA can be encapsulated within PLGA particles through a double emulsion process or adsorbed onto the particle surface after surface treatment with bioadhesive agents such as Carbopol, a polyacrylic acid-based polymer [92]. Cationic polymers

such as chitosan or spermidine can be blended into PLGA particles, the latter of which was used by Woodrow *et al.* for intravaginal siRNA delivery [93].

More commonly employed polymers for polymeric gene delivery nanoparticles are often cationic and electrostatically interact with nucleic acids to form polyplexes. Early gene delivery strategies often employed poly(*L*-lysine) (PLL) due to its cationic nature [15, 16]. PLL particles delivering DNA have been modified by adding PEG groups to prevent particle aggregation in serum [94] and Kim *et al.* created a terplex system with stearyl-PLL, low density lipoprotein, and DNA that increased particle compactness and improved DNA binding [95]. PEG-PLL block copolymers have also been used for siRNA delivery [96], but were often so stable that the siRNA cargo could not be released. Miyata *et al.* enabled PEG-PLL nanoparticles to undergo cytoplasmic siRNA release by crosslinking PLL end chains with bioreducible disulfides [97]. A similar delivery system was later modified with the RGD integrin recognition peptide to promote *in vivo* tissue targeting [98].

PLL nanoparticles often are unable to escape the endosome. This realization led to the exploration of other cationic polymers such as PEI, a polymer that contains primary, secondary, and tertiary amines to enable both nucleic acid binding and more efficient endosomal escape [99]. Godbey *et al.* used extensive confocal microscopy experiments to elucidate the intracellular fate of PEI-DNA nanoparticles. They found that PEI particles aggregate in discrete patches on the cell surface before being internalized through endocytic vesicles; some particles then escape through lysed endosomes and localize to the nucleus [100]. The polymer structure can be tuned to modulate gene delivery as low molecular weight PEI cannot condense DNA as well as its high molecular weight counterpart but is less toxic than higher molecular weight PEI [101]. Modifications with targeting ligands and PEGylation have also been shown to improve particle stability and *in vivo* transfection [102]. PEI analogs optimized for siRNA delivery frequently employ lower molecular weight linear PEIs linked with disulfide bonds to enable degradation and siRNA release, as PEI itself contains no biodegradable moieties [103].

Similar polymeric materials such as poly(amido amine)s (PAAs) and poly(amido ethyleneimine)s (PAEIs) have been designed that have buffering capacities in the endosomal pH range superior to PEI [104]. Partial degradation of PAA dendrimers by heat treatment increases the dendrimer flexibility and has been

shown to lead to better transfection [105]. PEGylation further increases transfection efficacy and decreases toxicity [106]. PAA modifications for siRNA delivery employ disulfides linkages in the polymer backbone, and have shown superior siRNA delivery compared to PEI even in cells with comparable nanoparticle uptake [107-109]. This is likely due to the enhanced cytoplasmic siRNA release enabled by the inclusion of bioreducible disulfides. Modification of disulfide containing PAAs with PEG has shown a reduction in hemolysis and particle aggregation *in vivo*, but with reduced particle stability and decreases in gene knockdown [110].

Cyclodextrin-based nanoparticles are effective and have reached clinical trials. Cycldextrins are a class of water-soluble molecules of 6-9 glucose units that form a cone-shaped structure with a hydrophobic interior that can complex with various molecules, including nucleic acids [111]. Nanoparticles for DNA delivery can be made by conjugating cyclodextrin with polymers including PEI [112] and PAA [113], which condense DNA through electrostatic interactions. DNA can also be covalently linked to cyclodextrin via cationic adamantyl linkers [114]. For siRNA delivery, self-assembled nanoparticles can be made from cyclodextrin polymer, siRNA, and adamantane-PEG conjugates [115, 116]. These nanoparticles were used to deliver siRNA targeting the M2 subunit of ribonucleotide reductase in a Phase 1a/1b clinical trial which demonstrated siRNA activity in humans [116, 117].

Dendrimers are polymer structures that consist of a central core molecule from which highly branched arms extend out in an ordered and symmetric fashion. The stepwise method of dendrimer synthesis lends greater control of polymer size while the branching structure results in a higher density of terminal groups, offering unique surface characteristics and additional attachment sites for drugs or targeting moieties [118]. Two dendrimers that have been used for gene delivery are the PAAs mentioned above and polypropylenimine (PPI). PPI dendrimers with a butylenediamine (DAB) core have been shown to increase DNA binding with increasing dendrimer generations, with generation 2 providing the optimal balance between nucleic acid binding and toxicity [119]. Arginine has been conjugated to the terminal ends to increase membrane permeability and improve nuclear localization [120]. PPI nanoparticles for siRNA delivery have been modified with a disulfide crosslinking molecular cage on the surface to increase particle stability [121].

2.4 Poly(beta-amino ester) (PBAE) nanoparticles for DNA and siRNA delivery to cancer

PBAEs are a class of polymer that contains tertiary amines and ester bonds along the polymer backbone. These chemical moieties provide positive charge for nucleic acid binding, buffering to promote endosomal release, and hydrolytic degradability for cargo release [122]. PBAEs have been well studied for DNA delivery, and have been designed to deliver DNA more efficiently and with less cytotoxicity than commercially available reagents such as PEI and Lipofectamine® 2000 in several cell types [123, 124]. By changing the chemical properties of the PBAE, it is possible to design nanoparticles that selectively deliver DNA to certain cell types, while avoiding delivery to others [124]. PBAEs can also be designed to deliver DNA to cancer while avoiding healthy cells, thereby allowing for the delivery of cell-killing genes to tumor cells without off-target effects [125-127]. Additionally, PBAE-DNA nanoparticles can be fabricated, dried, and stored as a powder for at least two years at -20°C without losing function, highlighting their translational potential [125, 127].

Various modifications to the PBAE backbone have been made to allow controlled DNA release from PBAE nanoparticles. A light-responsive 2-nitrobenzene moiety was added to the PBAE backbone to allow quick and controlled DNA release upon UV radiation (**Figure 2-2**) [128]. Gu *et al.* electrostatically linked pH-sensitive carboxymethyl poly(L-histidine) groups to PBAE-DNA nanoparticles to neutralize the particle's positive surface charge and increase buffering capacity; this modification decreased erythrocyte agglutination and enhanced the particle's tumor targeting capabilities after intravenous injection [129].

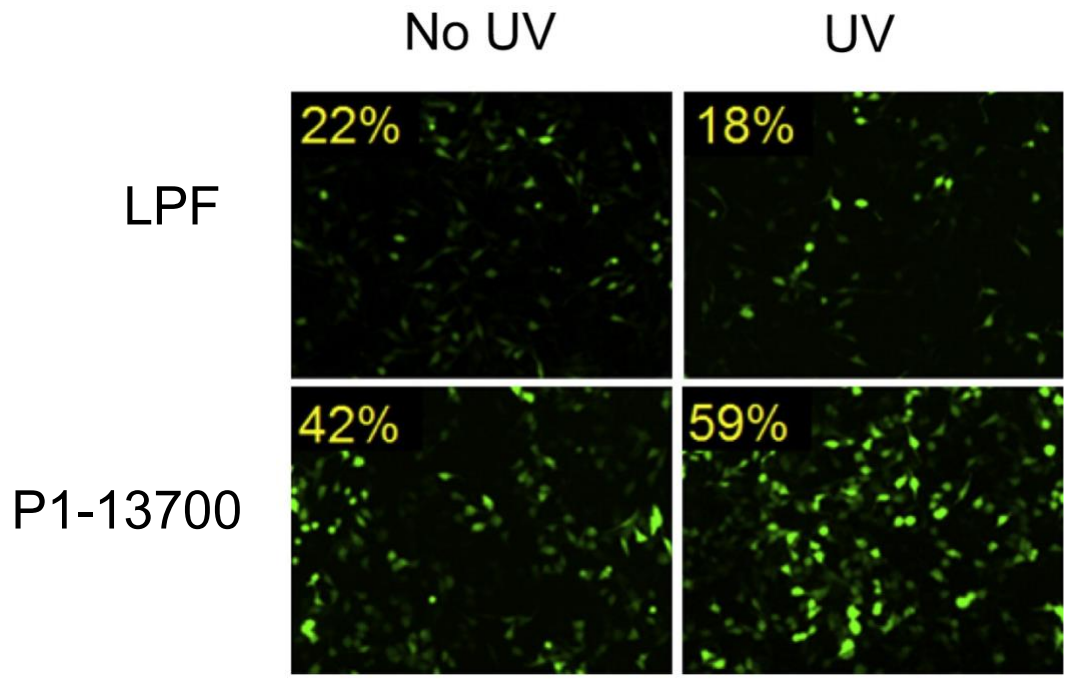

Figure 2-2. Light-responsive PBAE nanoparticles (P1-13700) delivering an EGFP plasmid to Hela cells with or without 2 minutes of UV irradiation; Lipofectamine™ 2000 (LPF) was used as a control. PBAE transfection efficacy increased with UV treatment, which broke 2-nitrobenzene linkers in the polymer backbone and allowed controlled DNA release. Reproduced with permission [128].

Due to the physical differences between DNA and siRNA described above, PBAE-based siRNA delivery had initially been difficult without the addition of other delivery vectors such as gold nanoparticles [74]. Hong *et al.* took the approach of modifying the siRNA itself. They designed complementary DNA/siRNA strands that self-assembled to form a dendrimeric siRNA structure; these siRNA dendrimers had higher charge density and structural flexibility, which allowed them to form stable particles with PBAE formulations that had been optimized for DNA delivery [130]. Tzeng *et al.* modified the polymer structure by end-capping traditional PBAEs with a disulfide-containing small molecule and showed successful siRNA delivery to both cancer cells and mesenchymal stem cells [131, 132]. The addition of the degradable disulfide moiety enabled this polymer structure to form polyplexes at a higher polymer:siRNA mass ratio (wt/wt) without causing significant toxicity, even though the disulfide bonds were only at the polymer end-caps.

Building on this work, Kozielski *et al.* designed a novel disulfide containing monomer to form disulfide bonds within every repeat unit [133]. This monomer, 2,2'-disulfanediylbis(ethane-2,1-diyl) diacrylate, was referred to as "BR6" as it was the reducible form of a well-established PBAE monomer known as "B6," hexane-1,6-diyl diacrylate [134]. PBAE nanoparticles made from BR6 were shown to bind siRNA with the same strength as particles made from its non-reducible analog but quickly released its siRNA cargo in a reducing environment, unlike the conventional non-bioreducible PBAEs. Furthermore, these particles achieved gene knockdown *in vitro* that was significantly higher than that achieved by Lipofectamine® 2000 (**Figure 2-3**) and was shown to preferentially deliver siRNA to brain cancer cells while avoiding delivery to healthy brain cells.

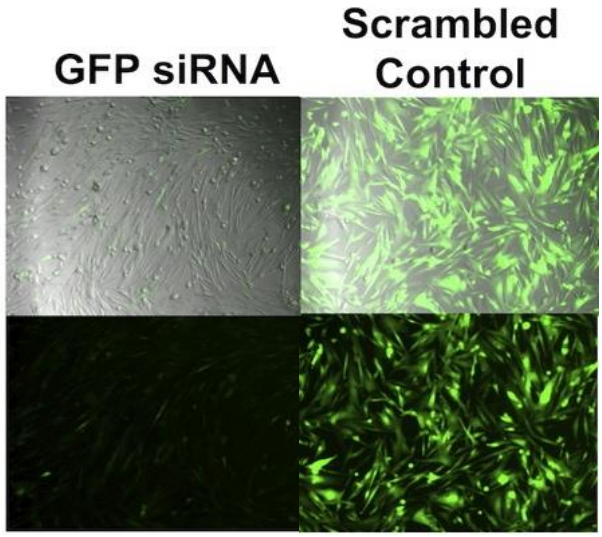

Figure 2-3. Phase contrast (**top**) and fluorescence (**bottom**) images of GFP+ GBM cells with bioreducible PBAE (R647) nanoparticles delivering either an siRNA targeting GFP (**left**) or a scrambled control RNA (**right**) [170].

The ability to effectively bind and deliver both DNA and siRNA make PBAEs an attractive option for gene delivery in cancer therapies. PBAE nanoparticles delivering the p53 tumor suppressor gene inhibited tumor growth in a small cell lung cancer mouse model after intratumoral injection [135]. A nanoparticle with a PBAE-DNA core and a pullulan-methotrexate shell showed enhanced circulation time and targeted delivery to hepatoma cells *in vivo*, with high levels of particle accumulation and transfection in the tumor [136]. For

more controlled long-term release, Segovia *et al.* encapsulated PBAE-siRNA particles in a PAA-dextran aldehyde hydrogel; when implanted in a breast cancer model, they saw a high level of knockdown even after 7 days [137]. Our group is particularly interested in the use of PBAE nanoparticles for the treatment of glioblastoma. Glioblastoma (GBM), a grade IV glioma, is one of the most deadly human cancers with a median survival of only 15 months following treatments such as tumor resection, chemotherapy and radiotherapy [138-140]. Polymeric nanoparticles for the intracellular delivery of nucleic acids enable new modalities of treatment for many cancer cell types, including GBM. By tuning the PBAE polymer structure, we were able to form PBAE nanoparticles that preferentially delivered nucleic acids to brain tumor initiating cells, a cell population that is believed to be responsible for tumor recurrence [127]. High levels of transfection were seen when PBAE particles delivering a GFP reporter gene were injected into an orthotopic GBM murine model [125]. In addition, these particles were able to achieve a therapeutic effect. PBAE nanoparticles delivering DNA encoding the herpes simplex virus-derived thymidine kinase (HSVtk) were injected intracranially in a rat GBM model while the ganciclovir pro-drug was administered systemically [126]. The PBAE nanoparticles penetrated through the whole brain tumor volume (a length of approximately 2 mm) and HSVtk catalyzed the phosphorylation of ganciclovir into its active form to enable killing of brain cancer cells, resulting in significant survival benefits [126].

Further modifications of PBAEs such as synthesis of dendrimeric versions of the polymers are interesting future directions for enhanced nucleic acid delivery. Cutlar *et al.* synthesized a highly branched PBAE that showed higher transfection efficacy when compared to linear counterparts as they could better condense their DNA cargo [141]. Zhou *et al.* synthesized a dendrimeric ester nanoparticle that successfully delivered microRNAs to a liver cancer model and achieved significant survival benefits [142]. The authors hypothesized that the increased nucleic acid binding capacity and degradability of these polyester dendrimers contributed to successful RNA delivery while maintaining low hepatotoxicity. Indeed, dendrimeric PBAEs may produce smaller, more compact nanoparticles that contain more polymer end groups, which could increase biomaterial-mediated cell specificity. This may be especially relevant for cancer therapy, including brain cancer therapy, where smaller particle sizes can increase particle penetration and transport.

2.5 Methods for DNA and RNA co-delivery

Despite the physical differences between DNA and RNA that present different challenges for their intracellular delivery, several strategies have been developed for co-delivery in order to achieve novel therapeutic goals. In designing nanoparticle formulations, it is particularly important to also ensure that each of the different nucleic acids to be delivered reaches the target cells at the desired ratios. To enable co-delivery to the same cell, loading different nucleic acids into the same particles (rather than delivering a combination of particles, each with its own cargo) has been show to increase the co-expression of delivered nucleic (**Figure 2-4**) [143]. As polyplexes are formed through self-assembly between cationic polyelectrolytes and anionic polyelectrolytes, with larger more multivalent polyelectrolytes leading to enhanced stability, carrier DNA can be complexed into the same polyplexes as siRNA as a strategy to stabilize the particle for enhanced siRNA delivery [144]. This can be an effective way to achieve gene knockdown and expression in the same cell to achieve synergistic therapeutic effects [145, 146]. Another way to complex multiple nucleic acids in the same particle is through layer-by-layer (LbL) assembly. Elbakry *et al.* used LbL to synthesize a particle with a gold core, 11-mercaptoundecanoic acid coating, and PEI-siRNA layers to condense siRNA into a particle and achieve effective knockdown [73]. Bishop *et al.* adopted a similar strategy but added DNA, siRNA, and PBAE layers [147]. This strategy can be used to deliver multiple nucleic acid cargos as well as control their relative release times.

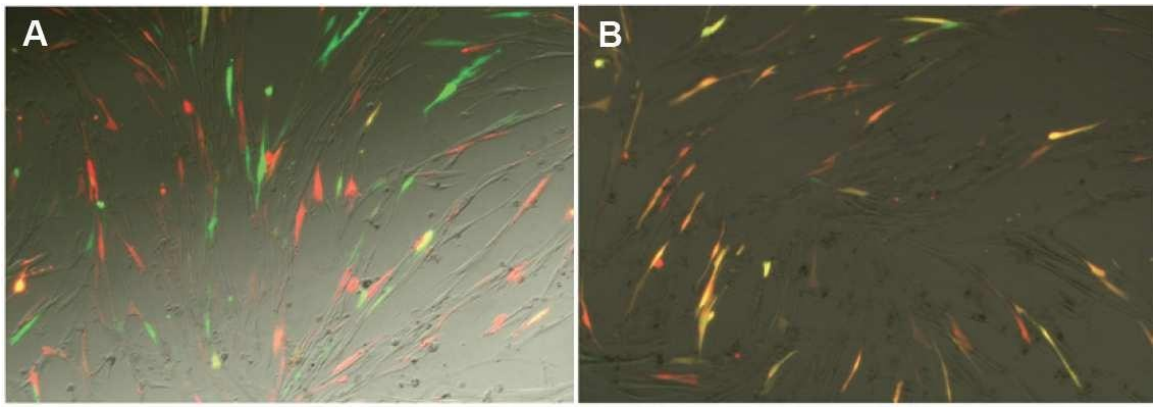

Figure 2-4. (**A**) Nanoparticles carrying either GFP or DsRed plasmid DNA are blended following nanoparticle fabrication, resulting in particles containing only one type of plasmid. Transfection of IMR90

human fibroblasts with this nanoparticle combination yields little codelivery, as indicated by few cells coexpressing GFP and DsRed (yellow cells). (**B**) Nanoparticles formed using a blend of GFP and DsRed plasmids yield particles containing both plasmids, and coexpression is high. Reproduced with permission [143].

3. Conclusion

Non-viral nanoparticle technologies for DNA and siRNA delivery have advanced rapidly, with many complementary biomaterial and particle designs. Several promising delivery platforms involving lipid-based, inorganic, and polymeric nanocarriers have been developed with strong *in vivo* efficacies, some of which have entered clinical trials. The interest in these technologies is due to the large potential for gene delivery and siRNA-induced gene knockdown to treat diseases caused by aberrant gene expression, such as cancer, and the need to obtain safe and effective delivery methods. Non-viral nanoparticles have the potential to fulfill this promise. Continuing to investigate the barriers to intracellular delivery as well as to innovate the nanotechnologies capable of overcoming these barriers may one day allow genetic medicine to clinically treat genetically based diseases such as cancer.

4. Expert Opinion

As polymeric nanoparticle-based gene therapy shows increasing promise against cancer *in vitro* and for local administration *in vivo*, increasing attention is being turned towards strategies to allow the systemic delivery of these particles to treat metastatic cancer. A common method employs PEGylation, which shields the particles from interacting with serum proteins or off-target cells. For example, PEGylation of PLL, PEI, and PAA-based nanoparticles has been shown to enhance their circulation time and reduce hemolysis and serum-induced aggregation [110, 148]. Such a strategy could greatly enhance the ability of newer types of non-viral nanoparticles, such as PBAE-based nanoparticles, to enable them to circulate effectively and diffuse through tissue, improving their translational potential for use in cancer applications.

PEG can also be used as a linking molecule onto which targeting ligands may be conjugated to enable nanoparticle targeting to cellular receptors. Ligands that have successfully been conjugated to

PEGylated nanocarriers for cancer targeting include the RGD peptide sequence targeting integrins in tumor vasculature [149] as well as folate [150] and transferrin [151], molecules whose receptors are overexpressed in many cancer cell types. This strategy takes advantage of PEG's ability to increase nanocarrier serum stability, reduce non-specific uptake, and better enable the display of targeting moieties on the nanoparticle surface, resulting in higher particle accumulation in the tumor. However, one potential concern with PEGylated electrostatic polyplex nanocarrier systems is that while the charge masking properties of PEG have been shown to increase nanoparticle colloidal stability in serum, they may also decrease particle complexation stability. Kichler *et al.* showed that in a PEI polymer covalently endcapped with high molecular weight PEG, the resulting nanoparticles could not protect their DNA cargo from nuclease degradation and resulted in poor transfection when compared to un-PEGylated PEI [152]. Similarly, Mao *et al.* showed that in PEI-PEG block copolymers, formulations with lower molecular weight PEG at higher substitution levels resulted in large, loosely structured particles that could not effectively condense siRNA and resulted in poor knockdown [153]. The charge shielding capability of PEG molecules protect cationic polymers from serum aggregation but also reduce their ability to electrostatically bind to nucleic acid cargos. To create a PEGylated polymer for successful nanoparticle formation, it is crucial to balance these opposing forces, such as through the addition of crosslinks or by adding non-PEGylated polymers to the co-complex to increase its stability.

Another strategy for systemic delivery is coating the particle with peptides to decrease toxicity, enhance circulation time, and enable particle targeting to specific organs or tumors [154]. Simberg *et al.* coated a peptide sequence to iron oxide particles that targeted clotted plasma proteins in leaky tumor vasculature [155]. These particles in turn induced more clots and amplified the effect. PBAE nanoparticles electrostatically coated with poly(glutamic acid) based peptide sequences reduced *in vivo* toxicity and could enable targeting to specific organs based on peptide sequence differences and nanoparticle properties [156]. Peptide coating can allow nanoparticles to remain in circulation for longer periods of time and can enhance particle targeting and uptake through ligand-mediated endocytosis. An important area for future research in the field is the investigation of new types of nanoparticle coatings that enable greater specific intracellular delivery to on-target cancer cells (perhaps in a manner specific to the receptors on a patient's particular

tumor), while preventing intracellular delivery to off-target cells. In addition, such next generation coating must enable prolonged circulation times, including resistance to clearance by neutralizing antibodies, even after multiple previous treatments of the next-generation nanoparticles.

The clustered regularly interspaced short palindromic repeats (CRISPR)/CRISPR-associated (Cas) system is a recently discovered genome editing tool with many potential therapeutic applications. The CRISPR/Cas9 system derives from a bacterial defense mechanism, where foreign DNA segments are transcribed into a dual-RNA complex and used to recognize and silence invading targets through double-stranded breaks (DSB) induced by the Cas9 endonuclease [157]. A single chimeric sgRNA was recently developed that can activate site-specific cleavage by Cas9 [158]. The resulting DSB can be repaired through error-prone non-homologous end joining, leading to indels that knock out gene function, or homology-directed repair upon introduction of a donor repair template [159]. The CRISPR/Cas9 system has been successfully used in human cells to introduce permanent changes in the genome [159, 160], making it a powerful tool for gene editing to treat diseases like cancer.

Only a handful of studies have been done using non-viral methods to deliver the CRISPR/Cas9 system. Jinek *et al.* constructed a plasmid encoding Cas9 and the sgRNA and delivered it using commercial transfection agents. However, they were only able to achieve editing efficiencies in the range of 6-8% [161]. Sun *et al.* constructed DNA nanoclews by packing sgRNA and the Cas9 protein into DNA strands that are partially complementary to the sgRNA and coating the outside with PEI (**Figure 2-5**); the DNA nanoclew system achieved a 36% editing efficiency [162]. The low editing efficiency seen by many groups may be due to poor delivery efficacy of the Cas9 plasmid or sgRNA. Co-delivery of the two using non-viral nanoparticles, such as biodegradable polymeric nanoparticles, is a potential way to increase expression and gene editing efficacy. Strategies such as a layer-by-layer approach can be used to package the Cas9 plasmid and sgRNA using polymers that are suitable for each and to control their intracellular temporal release.

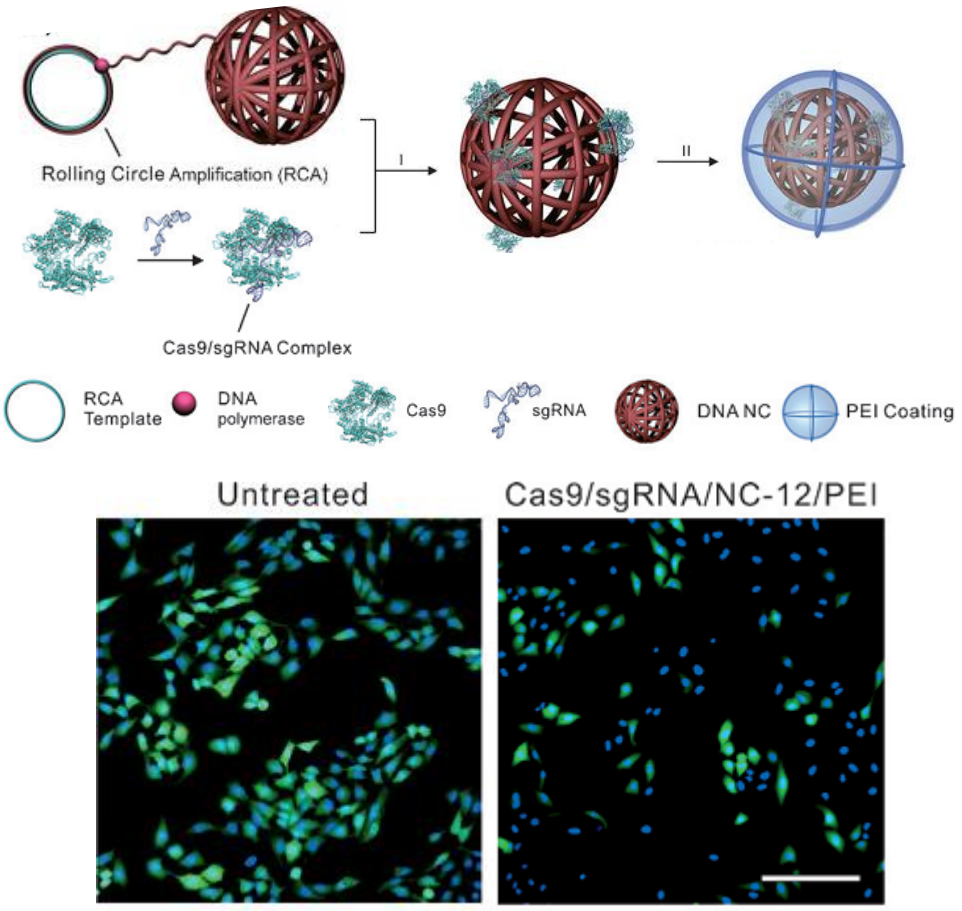

Figure 2-5. (**Top**) Assembly schematic of DNA nanoclew (DNA-NC) carrying Cas9 and sgRNA. Cas9 and sgRNA were incubated together and complexed with the DNA-NC; a PEI coating was then applied to the outside to facilitate endosomal escape . (**Bottom**) Fluorescence microscopy images of EGFP+ U2OS cells with or without treatment with DNA-NC delivering Cas9 and EGFP-specific sgRNA. Cas9-induced DNA cleavage resulted in significant EGFP gene knockout. Reproduced with permission [162].

Another interesting target for the co-delivery of DNA and siRNA is the TNF-related apoptosis-inducing ligand (TRAIL) system. TRAIL induces apoptosis in many transformed cell lines by binding to the death receptors DR4 and DR5 on the cell surface [163, 164]. Its apoptotic function is selective for transformed and tumor cells [165], and exhibits a bystander effect [166]. These properties make TRAIL an attractive delivery target for cancer treatment as it can produce a cancer-specific, self-amplifying apoptotic effect. However, it has been shown that many cancer cell types resist TRAIL action. One explanation for this

phenomenon is the presence of decoy receptors DcR1 and DcR2, which lack functional intracellular death domains [167]. Studies have shown that DcR2 is upregulated in some TRAIL-resistant breast and prostate cancers [168, 169]. siRNA knockdown of DcR2 in these cells sensitized them to TRAIL-induced apoptosis. When TRAIL plasmids were delivered to the same cells, their tumorigenic potential was significantly reduced. This suggests that co-delivery of siRNA to knock down decoy receptors and DNA to upregulate TRAIL expression can work synergistically to cause cancer cell apoptosis and may be a promising target for polymeric nanoparticle delivery. Similarly, other siRNA and DNA co-delivery strategies may enable breakthroughs against cancer resistance and are enabled by non-viral nanoparticles.

Treatment of genetically-based diseases such as cancer often requires a combinatorial approach, as cells can often compensate for the knockdown or overexpression of one genetic target. For the proposed treatment strategies suggested herein, co-delivery of DNA and RNA is required to occur within the same cells, not simply within the bulk of a tissue or tumor. While the materials optimal for DNA and siRNA often vary, a treatment strategy requiring co-delivery would ideally require a material optimized to deliver both. As previously demonstrated [143], a blend of nanoparticles containing different cargos is less likely to co-deliver both cargos to the same cells. Conversely, particles containing the cargo blended within each nanoparticle results in high co-delivery rates. Temporal control of DNA and RNA release [147] is also imperative for systems which would require DNA transcription and siRNA-induced knockdown to occur in a non-simultaneous fashion. Future nanoparticle designs that would have the sophistication and control to combinatorially deliver multiple types of nucleic acids against multiple targets have the potential to address the heterogeneity and mutational capabilities of genetic diseases such as cancer.

References

1. J. L. Manley, P. A. Sharp and M. L. Gefter. RNA synthesis in isolated nuclei: in vitro initiation of adenovirus 2 major late mRNA precursor. Proceedings of the National Academy of Sciences 1979; 76: 160-4

2. M. Manthorpe, F. Cornefert-Jensen, J. Hartikka, et al. Gene therapy by intramuscular injection of plasmid DNA: studies on firefly luciferase gene expression in mice. Human gene therapy 1993; 4: 419-31

3. F. Liu, Y. Song and D. Liu. Hydrodynamics-based transfection in animals by systemic administration of plasmid DNA. Gene therapy 1999; 6: 1258-66

4. A. Fire, S. Q. Xu, M. K. Montgomery, et al. Potent and specific genetic interference by double-stranded RNA in Caenorhabditis elegans. Nature 1998; 391: 806-11•**This seminal paper describes the RNAi pathway in *C. elegans* and led to the development of siRNA as a gene silencing modality.**

5. E. Bernstein, A. A. Caudy, S. M. Hammond, et al. Role for a bidentate ribonuclease in the initiation step of RNA interference. Nature 2001; 409: 363-6

6. G. J. Hannon. RNA interference. nature 2002; 418: 244-51

7. M. A. Hickman, R. W. Malone, K. Lehmann-Bruinsma, et al. Gene expression following direct injection of DNA into liver. Human gene therapy 1994; 5: 1477-83

8. J. C. Clemens, C. A. Worby, N. Simonson-Leff, et al. Use of double-stranded RNA interference in Drosophila cell lines to dissect signal transduction pathways. Proceedings of the National Academy of Sciences of the United States of America 2000; 97: 6499-503

9. M. A. Rosenfeld, W. Siegfried, K. Yoshimura, et al. Adenovirus-Mediated Transfer of a Recombinant alpha 1-Antitrypsin Gene to the Lung Epithelium in Vivo. Science 1991; 252: 431-4

10. C. E. Thomas, A. Ehrhardt and M. A. Kay. Progress and problems with the use of viral vectors for gene therapy. Nature Reviews Genetics 2003; 4: 346-58••**This article reviewed the limitations and safety concerns associated with viral vectors for gene delivery.**

11. D. W. Pack, A. S. Hoffman, S. Pun, et al. Design and development of polymers for gene delivery. Nature Reviews Drug Discovery 2005; 4: 581-93

12. C. R. Alving, E. A. Steck, W. L. Chapman, Jr., et al. Therapy of leishmaniasis: superior efficacies of liposome-encapsulated drugs. Proceedings of the National Academy of Sciences 1978; 75: 2959-63.

13. K. Vadiei, G. Lopez-Berestein, R. Perez-Soler, et al. In vitro evaluation of liposomal cyclosporine. International Journal of Pharmaceutics 1989; 57: 133-8

14. G. L. Scherphof, J. Dijkstra, H. H. Spanjer, et al. Uptake and intracellular processing of targeted and nontargeted liposomes by rat Kupffer cells in vivo and in vitro. Ann N Y Acad Sci. 1985; 446: 368-84.

15. E. Wagner, C. Plank, K. Zatloukal, et al. Influenza-Virus Hemagglutinin-Ha-2 N-Terminal Fusogenic Peptides Augment Gene-Transfer by Transferrin Polylysine DNA Complexes - toward a Synthetic Virus-Like Gene-Transfer Vehicle. Proceedings of the National Academy of Sciences 1992; 89: 7934-8

16. G. Y. Wu and C. H. Wu. Receptor-mediated in vitro gene transformation by a soluble DNA carrier system. Journal of Biological Chemistry 1987; 262: 4429-32**••This paper first introduced PLL as a potential nucleic acid delivery material.**

17. D. A. Giljohann, D. S. Seferos, A. E. Prigodich, et al. Gene regulation with polyvalent siRNA-nanoparticle conjugates. Journal of the American Chemical Society 2009; 131: 2072-3

18. P. J. Hagerman. Flexibility of RNA. Annu Rev Bioph Biom 1997; 26: 139-56

19. P. Kebbekus, D. E. Draper and P. Hagerman. Persistence length of RNA. Biochemistry-Us 1995; 34: 4354-7

20. M. Ogris, S. Brunner, S. Schuller, et al. PEGylated DNA/transferrin-PEI complexes: reduced interaction with blood components, extended circulation in blood and potential for systemic gene delivery. Gene Therapy 1999; 6: 595-605

21. A. D. Frankel and C. O. Pabo. Cellular uptake of the tat protein from human immunodeficiency virus. Cell 1988; 55: 1189-93

22. M. Green and P. M. Loewenstein. Autonomous functional domains of chemically synthesized human immunodeficiency virus tat *trans*-activator protein. Cell 1988; 55: 1179-88

23. T. B. Wyman, F. Nicol, O. Zelphati, et al. Design, synthesis, and characterization of a cationic peptide that binds to nucleic acids and permeabilizes bilayers. Biochemistry-Us 1997; 36: 3008-17

24. I. Hafez, N. Maurer and P. Cullis. On the mechanism whereby cationic lipids promote intracellular delivery of polynucleic acids. Gene Therapy 2001; 8: 1188-96

25. Y. Xu and F. C. Szoka Jr. Mechanism of DNA release from cationic liposome/DNA complexes used in cell transfection. Biochemistry-Us 1996; 35: 5616-23

26. O. Zelphati and F. C. Szoka Jr. Mechanism of oligonucleotide release from cationic liposomes. Proceedings of the National Academy of Sciences 1996; 93: 11493-8

27. A. Verma and F. Stellacci. Effect of Surface Properties on Nanoparticle-Cell Interactions. Small 2010; 6: 12-21

28. J. H. Felgner, R. Kumar, C. N. Sridhar, et al. Enhanced Gene Delivery and Mechanism Studies with a Novel Series of Cationic Lipid Formulations. Journal of Biological Chemistry 1994; 269: 2550-61

29. A. El Ouahabi, M. Thiry, V. Pector, et al. The role of endosome destabilizing activity in the gene transfer process mediated by cationic lipids. Febs Lett 1997; 414: 187-92

30. R. V. Benjaminsen, M. A. Mattebjerg, J. R. Henriksen, et al. The Possible "Proton Sponge" Effect of Polyethylenimine (PEI) Does Not Include Change in Lysosomal pH. Molecular therapy : the journal of the American Society of Gene Therapy 2013; 21: 149-57

31. N. D. Sonawane, F. C. Szoka and A. S. Verkman. Chloride accumulation and swelling in endosomes enhances DNA transfer by polyamine-DNA polyplexes. Journal of Biological Chemistry 2003; 278: 44826-31

32. A. E. Nel, L. Madler, D. Velegol, et al. Understanding biophysicochemical interactions at the nano-bio interface. Nat Mater 2009; 8: 543-57

33. H. Kawasaki and K. Taira. Short hairpin type of dsRNAs that are controlled by tRNAVal promoter significantly induce RNAi-mediated gene silencing in the cytoplasm of human cells. Nucleic acids research 2003; 31: 700-7

34. D. M. Lynn and R. Langer. Degradable poly (beta-amino esters): synthesis, characterization, and self-assembly with plasmid DNA. Journal of the American Chemical Society 2000; 122: 10761-8

35. K. A. Woodrow, Y. Cu, C. J. Booth, et al. Intravaginal gene silencing using biodegradable polymer nanoparticles densely loaded with small-interfering RNA. Nat Mater 2009; 8: 526-33

36. O. W. Griffith. Biologic and pharmacologic regulation of mammalian glutathione synthesis. Free Radical Biology and Medicine 1999; 27: 922-35

37. S. Son, R. Namgung, J. Kim, et al. Bioreducible Polymers for Gene Silencing and Delivery. Accounts of Chemical Research 2012; 45:

38. G. L. Lukacs, P. Haggie, O. Seksek, et al. Size-dependent DNA mobility in cytoplasm and nucleus. Journal of Biological Chemistry 2000; 275: 1625-9

39. D. Lechardeur, K. J. Sohn, M. Haardt, et al. Metabolic instability of plasmid DNA in the cytosol: a potential barrier to gene transfer. Gene therapy 1999; 6: 482-97

40. S. Brunner, T. Sauer, S. Carotta, et al. Cell cycle dependence of gene transfer by lipoplex, polyplex and recombinant adenovirus. Gene therapy 2000; 7: 401-7

41. M. A. Zanta, P. Belguise-Valladier and J.-P. Behr. Gene delivery: a single nuclear localization signal peptide is sufficient to carry DNA to the cell nucleus. Proceedings of the National Academy of Sciences 1999; 96: 91-6

42. G. Grandinetti and T. M. Reineke. Exploring the Mechanism of Plasmid DNA Nuclear Internalization with Polymer-Based Vehicles. Molecular Pharmaceutics 2012; 9: 2256-67

43. B. Dalby, S. Cates, A. Harris, et al. Advanced transfection with Lipofectamine 2000 reagent: primary neurons, siRNA, and high-throughput applications. Methods 2004; 33: 95-103

44. Z. Ma, J. Li, F. T. He, et al. Cationic lipids enhance siRNA-mediated interferon response in mice. Biochemical and Biophysical Research Communications 2005; 330: 755-9

45. D. Palliser, D. Chowdhury, Q. Y. Wang, et al. An siRNA-based microbicide protects mice from lethal herpes simplex virus 2 infection. Nature 2006; 439: 89-94

46. J. Smisterová, A. Wagenaar, M. C. A. Stuart, et al. Molecular shape of the cationic lipid controls the structure of cationic lipid/dioleylphosphatidylethanolamine-DNA complexes and the efficiency of gene delivery. Journal of Biological Chemistry 2001; 276: 47615-22

47. R. Koynova, L. Wang, Y. Tarahovsky, et al. Lipid phase control of DNA delivery. Bioconjugate chemistry 2005; 16: 1335-9

48. V. P. Torchilin, T. S. Levchenko, R. Rammohan, et al. Cell transfection in vitro and in vivo with nontoxic TAT peptide-liposome–DNA complexes. Proceedings of the National Academy of Sciences 2003; 100: 1972-7

49. K. Crook, B. J. Stevenson, M. Dubouchet, et al. Inclusion of cholesterol in DOTAP transfection complexes increases the delivery of DNA to cells in vitro in the presence of serum. Gene therapy 1998; 5: 137-43

50. J. J. Lu, R. Langer and J. Z. Chen. A novel mechanism is involved in cationic lipid-mediated functional siRNA delivery. Molecular Pharmaceutics 2009; 6: 763-71

51. M. Umeda, S. Nojima and K. Inoue. Effect of lipid composition on HVJ-mediated fusion of glycophorin liposomes to erythrocytes. J Biochem-Tokyo 1985; 97: 1301-10

52. I. M. Hafez and P. R. Cullis. Roles of lipid polymorphism in intracellular delivery. Adv Drug Deliver Rev 2001; 47: 139-48

53. D. C. Litzinger and L. Huang. Phosphatidylethanolamine Liposomes - Drug Delivery, Gene-Transfer and Immunodiagnostic Applications. Biochim. Biophys. Acta 1992; 1113: 201-27

54. J. Heyes, L. Palmer, K. Bremner, et al. Cationic lipid saturation influences intracellular delivery of encapsulated nucleic acids. Journal of Controlled Release 2005; 107: 276-87

55. I. Moret, J. Esteban Peris, V. M. Guillem, et al. Stability of PEI–DNA and DOTAP–DNA complexes: effect of alkaline pH, heparin and serum. Journal of Controlled Release 2001; 76: 169-81

56. S. Chono, S. D. Li, C. C. Conwell, et al. An efficient and low immunostimulatory nanoparticle formulation for systemic siRNA delivery to the tumor. Journal of Controlled Release 2008; 131: 64-9

57. A. D. Judge, G. Bola, A. C. H. Lee, et al. Design of Noninflammatory Synthetic siRNA Mediating Potent Gene Silencing in Vivo. Mol Ther 2006; 13: 494-505

58. S. C. Semple, A. Akinc, J. Chen, et al. Rational design of cationic lipids for siRNA delivery. Nature Biotechnology 2010; 28: 172-6

59. G. Ott, M. Singh, J. Kazzaz, et al. A cationic sub-micron emulsion (MF59/DOTAP) is an effective delivery system for DNA vaccines. Journal of Controlled Release 2002; 79: 1-5

60. C. Chen and H. Okayama. High-efficiency transformation of mammalian cells by plasmid DNA. Molecular and cellular biology 1987; 7: 2745-52

61. M. Jordan, A. Schallhorn and F. M. Wurm. Transfecting mammalian cells: optimization of critical parameters affecting calcium-phosphate precipitate formation. Nucleic acids research 1996; 24: 596-601

62. H. Tolou. Administration of oligonucleotides to cultured cells by calcium phosphate precipitation method. Analytical biochemistry 1993; 215: 156-8•**This paper introduced the use of co-precipitation of nucleic acids with calcium phosphote crystals as a method for DNA delivery.**

63. V. V. Sokolova, I. Radtke, R. Heumann, et al. Effective transfection of cells with multi-shell calcium phosphate-DNA nanoparticles. Biomaterials 2006; 27: 3147-53

64. Y. Kakizawa, S. Furukawa, A. Ishii, et al. Organic-inorganic hybrid-nanocarrier of siRNA constructing through the self-assembly of calcium phosphate and PEG-based block aniomer. Journal of Controlled Release 2006; 111: 368-70

65. M. Zhang, A. Ishii, N. Nishiyama, et al. PEGylated Calcium Phosphate Nanocomposites as Smart Environment-Sensitive Carriers for siRNA Delivery. Advanced Materials 2009; 21: 3520-5

66. P. S. Ghosh, C. K. Kim, G. Han, et al. Efficient gene delivery vectors by tuning the surface charge density of amino acid-functionalized gold nanoparticles. 2008;

67. E. E. Connor, J. Mwamuka, A. Gole, et al. Gold nanoparticles are taken up by human cells but do not cause acute cytotoxicity. Small 2005; 1: 325-7

68. K. K. Sandhu, C. M. McIntosh, J. M. Simard, et al. Gold Nanoparticle-Mediated Transfection of Mammalian Cells. Bioconjugate Chemistry 2002; 13: 3-6

69. N. L. Rosi, D. A. Giljohann, C. S. Thaxton, et al. Oligonucleotide-Modified Gold Nanoparticles for Intracellular Gene Regulation. Science 2006; 312: 1027-30

70. J. I. Cutler, E. Auyeung and C. A. Mirkin. Spherical nucleic acids. Journal of the American Chemical Society 2012; 134: 1376-91

71. G. Han, C. C. You, B. j. Kim, et al. Light-Regulated Release of DNA and Its Delivery to Nuclei by Means of Photolabile Gold Nanoparticles. Angewandte Chemie 2006; 118: 3237-41

72. A. Elbakry, A. Zaky, R. Liebl, et al. Layer-by-Layer Assembled Gold Nanoparticles for siRNA Delivery. Nano Letters 2009; 9: 2059-64

73. J. S. Lee, J. J. Green, K. T. Love, et al. Gold, poly (beta-amino ester) nanoparticles for small interfering RNA delivery. Nano letters 2009; 9: 2402-6•**This paper described an early system using PBAE coating of gold nanoparticles to delivery siRNA.**

74. A. M. Derfus, W. C. W. Chan and S. N. Bhatia. Intracellular delivery of quantum dots for live cell labeling and organelle tracking. Advanced Materials 2004; 16: 961-6

75. X. Gao, Y. Cui, R. M. Levenson, et al. In vivo cancer targeting and imaging with semiconductor quantum dots. Nature Biotechnology 2004; 22: 969-76

76. X. Wu, H. Liu, J. Liu, et al. Immunofluorescent labeling of cancer marker Her2 and other cellular targets with semiconductor quantum dots. Nature Biotechnology 2002; 21: 41-6

77. C. Srinivasan, J. Lee, F. Papadimitrakopoulos, et al. Labeling and Intracellular Tracking of Functionally Active Plasmid DNA with Semiconductor Quantum Dots. Mol Ther 2006; 14: 192-201

78. P. Zhang and W. Liu. ZnO QD@PMAA-co-PDMAEMA nonviral vector for plasmid DNA delivery and bioimaging. Biomaterials 2010; 31: 3087-94

79. A. M. Derfus, A. A. Chen, D. H. Min, et al. Targeted quantum dot conjugates for siRNA delivery. Bioconjugate Chemistry 2007; 18: 1391-6

80. A. A. Chen, A. M. Derfus, S. R. Khetani, et al. Quantum dots to monitor RNAi delivery and improve gene silencing. Nucleic acids research 2005; 33: e190-e

81. I. I. Slowing, J. L. Vivero-Escoto, C.-W. Wu, et al. Mesoporous silica nanoparticles as controlled release drug delivery and gene transfection carriers. Adv Drug Deliver Rev 2008; 60: 1278-88

82. D. Luo and W. M. Saltzman. Enhancement of transfection by physical concentration of DNA at the cell surface. Nat Biotech 2000; 18: 893-5

83. S. Mornet, O. Lambert, E. Duguet, et al. The Formation of Supported Lipid Bilayers on Silica Nanoparticles Revealed by Cryoelectron Microscopy. Nano Letters 2005; 5: 281-5

84. D. J. Bharali, I. Klejbor, E. K. Stachowiak, et al. Organically modified silica nanoparticles: A nonviral vector for in vivo gene delivery and expression in the brain. Proceedings of the National Academy of Sciences of the United States of America 2005; 102: 11539-44

85. T. Xia, M. Kovochich, M. Liong, et al. Polyethyleneimine Coating Enhances the Cellular Uptake of Mesoporous Silica Nanoparticles and Allows Safe Delivery of siRNA and DNA Constructs. ACS Nano 2009; 3: 3273-86

86. A. M. Chen, M. Zhang, D. Wei, et al. Co-delivery of Doxorubicin and Bcl-2 siRNA by Mesoporous Silica Nanoparticles Enhances the Efficacy of Chemotherapy in Multidrug-Resistant Cancer Cells. Small 2009; 5: 2673-7

87. I. Roy, T. Y. Ohulchanskyy, D. J. Bharali, et al. Optical tracking of organically modified silica nanoparticles as DNA carriers: A nonviral, nanomedicine approach for gene delivery. Proceedings of the National Academy of Sciences of the United States of America 2005; 102: 279-84

88. X. Li, Y. Chen, M. Wang, et al. A mesoporous silica nanoparticle – PEI – Fusogenic peptide system for siRNA delivery in cancer therapy. Biomaterials 2013; 34: 1391-401

89. A. M. Tinsley-Bown, R. Fretwell, A. B. Dowsett, et al. Formulation of poly(d,l-lactic-co-glycolic acid) microparticles for rapid plasmid DNA delivery. Journal of Controlled Release 2000; 66: 229-41•**This paper described the double emulsion process commonly used to encapsulate nucleic acid cargo in PLGA particles.**

90. J. Zhou, T. R. Patel, M. Fu, et al. Octa-functional PLGA nanoparticles for targeted and efficient siRNA delivery to tumors. Biomaterials 2012; 33: 583-91

91. W. Zou, C. Liu, Z. Chen, et al. Studies on bioadhesive PLGA nanoparticles: A promising gene delivery system for efficient gene therapy to lung cancer. International Journal of Pharmaceutics 2009; 370: 187-95

92. K. A. Woodrow, Y. Cu, C. J. Booth, et al. Intravaginal gene silencing using biodegradable polymer nanoparticles densely loaded with small-interfering RNA. Nat Mater 2009; 8: 526-33

93. A.-G. Ziady, C. R. Gedeon, T. Miller, et al. Transfection of Airway Epithelium by Stable PEGylated Poly-L-lysine DNA Nanoparticles in Vivo. Mol Ther 2003; 8: 936-47

94. J.-S. Kim, B.-I. Kim, A. Maruyama, et al. A new non-viral DNA delivery vector: the terplex system. Journal of Controlled Release 1998; 53: 175-82

95. M. L. Patil, M. Zhang and T. Minko. Multifunctional Triblock Nanocarrier (PAMAM-PEG-PLL) for the Efficient Intracellular siRNA Delivery and Gene Silencing. ACS Nano 2011; 5: 1877-87

96. K. Miyata, Y. Kakizawa, N. Nishiyama, et al. Block catiomer polyplexes with regulated densities of charge and disulfide cross-linking directed to enhance gene expression. Journal of the American Chemical Society 2004; 126: 2355-61

97. R. J. Christie, Y. Matsumoto, K. Miyata, et al. Targeted Polymeric Micelles for siRNA Treatment of Experimental Cancer by Intravenous Injection. ACS Nano 2012; 6: 5174-89

98. O. Boussif, F. Lezoualc'h, M. A. Zanta, et al. A Versatile Vector for Gene and Oligonucleotide Transfer into Cells in Culture and in vivo: Polyethylenimine. Proceedings of the National Academy of Sciences of the United States of America 1995; 92: 7297-301•• **This was the first paper to demonstrate the versatility and efficacy of PEI as a gene delivery vector.**

99. W. T. Godbey, K. K. Wu and A. G. Mikos. Tracking the intracellular path of poly(ethylenimine)/DNA complexes for gene delivery. Proceedings of the National Academy of Sciences 1999; 96: 5177-81•**This paper provides a detailed illustration of intracellular PEI nanoparticle fate after cellular uptake.**

100. K. Kunath, A. von Harpe, D. Fischer, et al. Low-molecular-weight polyethylenimine as a non-viral vector for DNA delivery: comparison of physicochemical properties, transfection efficiency and in vivo distribution with high-molecular-weight polyethylenimine. Journal of Controlled Release 2003; 89: 113-25

101. E. Kleemann, M. Neu, N. Jekel, et al. Nano-carriers for DNA delivery to the lung based upon a TAT-derived peptide covalently coupled to PEG–PEI. Journal of Controlled Release 2005; 109: 299-316

102. M. Breunig, C. Hozsa, U. Lungwitz, et al. Mechanistic investigation of poly (ethylene imine)-based siRNA delivery: disulfide bonds boost intracellular release of the cargo. Journal of Controlled Release 2008; 130: 57-63

103. L. V. Christensen, C. W. Chang, W. J. Kim, et al. Reducible poly(amido ethylenimine)s designed for triggered intracellular gene delivery. Bioconjugate Chemistry 2006; 17: 1233-40

104. M. X. Tang, C. T. Redemann and F. C. Szoka. In Vitro Gene Delivery by Degraded Polyamidoamine Dendrimers. Bioconjugate Chemistry 1996; 7: 703-14

105. D. Luo, K. Haverstick, N. Belcheva, et al. Poly(ethylene glycol)-Conjugated PAMAM Dendrimer for Biocompatible, High-Efficiency DNA Delivery. Macromolecules 2002; 35: 3456-62

106. J. H. Jeong, L. V. Christensen, J. W. Yockman, et al. Reducible poly(amido ethylenimine) directed to enhance RNA interference. Biomaterials 2007; 28: 1912-7

107. P. Vader, L. J. van der Aa, J. F. J. Engbersen, et al. Disulfide-Based Poly(amido amine)s for siRNA Delivery: Effects of Structure on siRNA Complexation, Cellular Uptake, Gene Silencing and Toxicity. Pharmaceutical Research 2011; 28: 1013-22

108. L. J. van der Aa, P. Vader, G. Storm, et al. Optimization of poly(amido amine)s as vectors for siRNA delivery. Journal of Controlled Release 2011; 150: 177-86

109. P. Vader, L. J. van der Aa, J. F. J. Engbersen, et al. Physicochemical and Biological Evaluation of siRNA Polyplexes Based on PEGylated Poly (amido amine) s. Pharmaceutical Research 2012; 29: 352-61

110. S. Li and W. C. Purdy. Cyclodextrins and their applications in analytical chemistry. Chemical Reviews 1992; 92: 1457-70••**This paper describes the structure and functionality of cyclodextrins as a nanocarrier for cargo such as nucleic acids.**

111. C. Yang, H. Li, S. H. Goh, et al. Cationic star polymers consisting of α-cyclodextrin core and oligoethylenimine arms as nonviral gene delivery vectors. Biomaterials 2007; 28: 3245-54

112. H. Arima, F. Kihara, F. Hirayama, et al. Enhancement of Gene Expression by Polyamidoamine Dendrimer Conjugates with α-, β-, and γ-Cyclodextrins. Bioconjugate Chemistry 2001; 12: 476-84

113. V. Burckbuchler, V. Wintgens, C. Leborgne, et al. Development and Characterization of New Cyclodextrin Polymer-Based DNA Delivery Systems. Bioconjugate Chemistry 2008; 19: 2311-20

114. M. E. Davis. The First Targeted Delivery of siRNA in Humans via a Nanoparticle : From Concept to Clinic. 2009; 6: 659-68

115. M. E. Davis, J. E. Zuckerman, C. H. J. Choi, et al. Evidence of RNAi in humans from systemically administered siRNA via targeted nanoparticles. Nature 2010; 464: 1067-70••**This article demonstrated**

evidence of siRNA efficacy in humans for the first time in a clinical trial with cyclodextrin nanocarriers.

116. J. E. Zuckerman, I. Gritli, a. Tolcher, et al. Correlating animal and human phase Ia/Ib clinical data with CALAA-01, a targeted, polymer-based nanoparticle containing siRNA. Proceedings of the National Academy of Sciences 2014; 111: **••This article described the results of the first clinical trial using a synthetic vector (cyclodextrin) to systemically delivery siRNA.**

117. C. Dufès, I. F. Uchegbu and A. G. Schätzlein. Dendrimers in gene delivery. Adv Drug Deliver Rev 2005; 57: 2177-202

118. B. H. Zinselmeyer, S. P. Mackay, A. G. Schatzlein, et al. The Lower-Generation Polypropylenimine Dendrimers Are Effective Gene-Transfer Agents. Pharmaceutical Research 19: 960-7

119. T.-i. Kim, J.-u. Baek, C. Zhe Bai, et al. Arginine-conjugated polypropylenimine dendrimer as a non-toxic and efficient gene delivery carrier. Biomaterials 2007; 28: 2061-7

120. O. Taratula, O. B. Garbuzenko, P. Kirkpatrick, et al. Surface-engineered targeted PPI dendrimer for efficient intracellular and intratumoral siRNA delivery. Journal of Controlled Release 2009; 140: 284-93

121. D. M. Lynn and R. Langer. Degradable Poly(β-amino esters): Synthesis, Characterization, and Self-Assembly with Plasmid DNA. Journal of the American Chemical Society 2000; 122: 10761-8**••This paper introduced PBAEs as a cationic polymer capable of forming nanoparticles with nucleic acids.**

122. S. Y. Tzeng, L. J. Higgins, M. G. Pomper, et al. Student award winner in the Ph.D. category for the 2013 society for biomaterials annual meeting and exposition, april 10-13, 2013, Boston, Massachusetts : biomaterial-mediated cancer-specific DNA delivery to liver cell cultures using synthetic poly(beta-amino ester)s. Journal of biomedical materials research. Part A 2013; 101: 1837-45

123. R. B. Shmueli, J. C. Sunshine, Z. Xu, et al. Gene delivery nanoparticles specific for human microvasculature and macrovasculature. Nanomedicine 2012; 8: 1200-7

124. H. Guerrero-Cázares, S. Y. Tzeng, N. P. Young, et al. Biodegradable Polymeric Nanoparticles Show High Efficacy and Specificity at DNA Delivery to Human Glioblastoma in Vitro and in Vivo. ACS Nano 2014; 8: 5141-53

125. A. Mangraviti, S. Y. Tzeng, K. L. Kozielski, et al. Polymeric Nanoparticles for Nonviral Gene Therapy Extend Brain Tumor Survival in Vivo. ACS Nano 2015; 9: 1236-49••**This paper demonstrated that intrtumoral injection of PBAE-DNA nanoparticles diffused through tumor tissue and achieved significant survival benefits.**

126. S. Y. Tzeng, H. Guerrero-Cázares, E. E. Martinez, et al. Non-viral gene delivery nanoparticles based on poly(β-amino esters) for treatment of glioblastoma. Biomaterials 2011; 32: 5402-10

127. X. Deng, N. Zheng, Z. Song, et al. Trigger-responsive, fast-degradable poly(β-amino ester)s for enhanced DNA unpackaging and reduced toxicity. Biomaterials 2014; 35: 5006-15

128. J. Gu, X. Wang, X. Jiang, et al. Self-assembled carboxymethyl poly (l-histidine) coated poly (β-amino ester)/DNA complexes for gene transfection. Biomaterials 2012; 33: 644-58

129. C. A. Hong, A. A. Eltoukhy, H. Lee, et al. Dendrimeric siRNA for efficient gene silencing. Angewandte Chemie 2015; 127: 6844-8

130. S. Y. Tzeng and J. J. Green. Subtle changes to polymer structure and degradation mechanism enable highly effective nanoparticles for siRNA and DNA delivery to human brain cancer. Advanced Healthcare Materials 2013; 2: 468-80

131. S. Y. Tzeng, B. P. Hung, W. L. Grayson, et al. Cystamine-terminated poly(beta-amino ester)s for siRNA delivery to human mesenchymal stem cells and enhancement of osteogenic differentiation. Biomaterials 2012; 33: 8142-51••**This paper demonstrated that the addition of disulfide-containing molecules to PBAE polymer can improve siRNA delivery.**

132. K. L. Kozielski, S. Y. Tzeng and J. J. Green. A bioreducible linear poly(beta-amino ester) for siRNA delivery. Chemical Communications 2013; 49: 5319 - 21••**This paper first reported the development of the BR6 PBAE monomer, which includes bioreducible disulfide bonds in every polymer repeat unit and facilitated PBAE delivery of siRNA.**

133. J. Chen, X. Qiu, J. Ouyang, et al. pH and reduction dual-sensitive copolymeric micelles for intracellular doxorubicin delivery. Biomacromolecules 2011; 12: 3601-11

134. C. D. Kamat, R. B. Shmueli, N. Connis, et al. Poly(β-amino ester) Nanoparticle Delivery of TP53 Has Activity against Small Cell Lung Cancer In Vitro and In Vivo. Molecular Cancer Therapeutics 2013; 12: 405-15

135. Y. Liu, Y. Wang, C. Zhang, et al. Core–Shell Nanoparticles Based on Pullulan and Poly(β-amino) Ester for Hepatoma-Targeted Codelivery of Gene and Chemotherapy Agent. ACS Applied Materials & Interfaces 2014; 6: 18712-20

136. N. Segovia, M. Pont, N. Oliva, et al. Hydrogel doped with nanoparticles for local sustained release of siRNA in breast cancer. Advanced healthcare materials 2015; 4: 271-80

137. K. L. Chaichana, P. Zadnik, J. D. Weingart, et al. Multiple resections for patients with glioblastoma: prolonging survival. J Neurosurg 2013; 118: 812-20

138. M. J. McGirt, K. L. Chaichana, M. Gathinji, et al. Independent association of extent of resection with survival in patients with malignant brain astrocytoma. Journal of Neurosurgery 2009; 110: 156-62

139. R. Stupp, W. P. Mason, M. J. van den Bent, et al. Radiotherapy plus Concomitant and Adjuvant Temozolomide for Glioblastoma. New England Journal of Medicine 2005; 352: 987-96

140. L. Cutlar, D. Zhou, Y. Gao, et al. Highly Branched Poly (β-Amino Esters): Synthesis and Application in Gene Delivery. Biomacromolecules 2015; 16: 2609-17

141. K. Zhou, L. H. Nguyen, J. B. Miller, et al. Modular degradable dendrimers enable small RNAs to extend survival in an aggressive liver cancer model. Proceedings of the National Academy of Sciences 2016; 113: 520-5

142. N. S. Bhise, R. B. Shmueli, J. Gonzalez, et al. A novel assay for quantifying the number of plasmids encapsulated by polymer nanoparticles. Small 2012; 8: 367-73

143. S.-D. Li and L. Huang. Targeted Delivery of Antisense Oligodeoxynucleotide and Small Interference RNA into Lung Cancer Cells. Molecular Pharmaceutics 2006; 3: 579-88

144. H. Chang Kang and Y. H. Bae. Co-delivery of small interfering RNA and plasmid DNA using a polymeric vector incorporating endosomolytic oligomeric sulfonamide. Biomaterials 2011; 32: 4914-24

145. Y. Chen, X. Zhu, X. Zhang, et al. Nanoparticles Modified With Tumor-targeting scFv Deliver siRNA and miRNA for Cancer Therapy. Mol Ther 2010; 18: 1650-6

146. C. J. Bishop, S. Y. Tzeng and J. J. Green. Degradable polymer-coated gold nanoparticles for co-delivery of DNA and siRNA. Acta Biomaterialia 2015; 11: 393-403

147. A. Akinc, M. Thomas, A. M. Klibanov, et al. Exploring polyethylenimine-mediated DNA transfection and the proton sponge hypothesis. The journal of gene medicine 2005; 7: 657-63

148. R. M. Schiffelers, A. Ansari, J. Xu, et al. Cancer siRNA therapy by tumor selective delivery with ligand-targeted sterically stabilized nanoparticle. Nucleic acids research 2004; 32: e149-e

149. B. Liang, M.-L. He, Z.-P. Xiao, et al. Synthesis and characterization of folate-PEG-grafted-hyperbranched-PEI for tumor-targeted gene delivery. Biochemical and Biophysical Research Communications 2008; 367: 874-80

150. N. C. Bellocq, S. H. Pun, G. S. Jensen, et al. Transferrin-Containing, Cyclodextrin Polymer-Based Particles for Tumor-Targeted Gene Delivery. Bioconjugate Chemistry 2003; 14: 1122-32

151. A. Kichler, M. Chillon, C. Leborgne, et al. Intranasal gene delivery with a polyethylenimine–PEG conjugate. Journal of Controlled Release 2002; 81: 379-88

152. S. Mao, M. Neu, O. Germershaus, et al. Influence of Polyethylene Glycol Chain Length on the Physicochemical and Biological Properties of Poly(ethylene imine)-graft-Poly(ethylene glycol) Block Copolymer/SiRNA Polyplexes. Bioconjugate Chemistry 2006; 17: 1209-18

153. J. Xie, K. Chen, H.-Y. Lee, et al. Ultrasmall c(RGDyK)-Coated Fe3O4 Nanoparticles and Their Specific Targeting to Integrin αvβ3-Rich Tumor Cells. Journal of the American Chemical Society 2008; 130: 7542-3

154. D. Simberg, T. Duza, J. H. Park, et al. Biomimetic amplification of nanoparticle homing to tumors. Proceedings of the National Academy of Sciences 2007; 104: 932-6

155. T. J. Harris, J. J. Green, P. W. Fung, et al. Tissue-specific gene delivery via nanoparticle coating. Biomaterials 2010; 31: 998-1006

156. E. Deltcheva, K. Chylinski, C. M. Sharma, et al. CRISPR RNA maturation by trans-encoded small RNA and host factor RNase III. Nature 2011; 471: 602-7

157. M. Jinek, K. Chylinski, I. Fonfara, et al. A Programmable Dual-RNA–Guided DNA Endonuclease in Adaptive Bacterial Immunity. Science 2012; 337: 816-21**••This paper reported the invention of the single guide RNA for the CRISPR/Cas system that can induce Cas9 cleavage, simplifying the system and allowing for easier application of CRISPR/Cas as a gene editing tool.**

158. P. Mali, L. Yang, K. M. Esvelt, et al. RNA-Guided Human Genome Engineering via Cas9. Science 2013; 339: 823-6**•This paper demonstrated the versatility of the CRISPR/Cas9 system in gene editing in various cell lines using the newly-devloped single guide RNA.**

159. L. Cong, F. A. Ran, D. Cox, et al. Multiplex Genome Engineering Using CRISPR/Cas Systems. Science 2013; 339: 819-23**•This paper demonstrated the application of CRISPR/Cas9 technology to human cells.**

160. M. Jinek, A. East, A. Cheng, et al. RNA-programmed genome editing in human cells. eLife 2013; 2:

161. W. Sun, W. Ji, J. M. Hall, et al. Self-Assembled DNA Nanoclews for the Efficient Delivery of CRISPR–Cas9 for Genome Editing. Angewandte Chemie 2015; 127: 12197-201

162. S. R. Wiley, K. Schooley, P. J. Smolak, et al. Identification and characterization of a new member of the TNF family that induces apoptosis. Immunity 1995; 3: 673-82

163. G. Pan, K. O'Rourke, A. M. Chinnaiyan, et al. The Receptor for the Cytotoxic Ligand TRAIL. Science 1997; 276: 111-3

164. A. Ashkenazi, R. C. Pai, S. Fong, et al. Safety and antitumor activity of recombinant soluble Apo2 ligand. The Journal of Clinical Investigation 104: 155-62

165. S. Kagawa, C. He, J. Gu, et al. Antitumor activity and bystander effects of the tumor necrosis factor-related apoptosis-inducing ligand (TRAIL) gene. Cancer research 2001; 61: 3330-8

166. A. Ashkenazi and V. M. Dixit. Apoptosis control by death and decoy receptors. Current Opinion in Cell Biology 1999; 11: 255-60

167. A. D. Sanlioglu, E. Dirice, C. Aydin, et al. Surface TRAIL decoy receptor-4 expression is correlated with TRAIL resistance in MCF7 breast cancer cells. BMC Cancer 2005; 5: 1-17

168. A. D. Sanlioglu, B. Karacay, I. T. Koksal, et al. DcR2 (TRAIL-R4) siRNA and adenovirus delivery of TRAIL (Ad5hTRAIL) break down in vitro tumorigenic potential of prostate carcinoma cells. Cancer Gene Ther 2007; 14: 976-84

169. K. L. Kozielski, S. Y. Tzeng, B. A. H. d. Mendoza, et al. Bioreducible Cationic Polymer-Based Nanoparticles For Efficient and Environmentally Triggered Cytoplasmic siRNA Delivery to Primary Human Brain Cancer Cells. ACS Nano 2014; 8: 3232-41

170. F. L. Graham and A. J. van der Eb. A new technique for the assay of infectivity of human adenovirus 5 DNA. Virology 1973; 52: 456-67

171. M. Kester, Y. Heakal, T. Fox, et al. Calcium Phosphate Nanocomposite Particles for In Vitro Imaging and Encapsulated Chemotherapeutic Drug Delivery to Cancer Cells. Nano Letters 2008; 8: 4116-21

172. T. Liu, A. Tang, G. Zhang, et al. Calcium phosphate nanoparticles as a novel nonviral vector for efficient transfection of DNA in cancer gene therapy. Cancer biotherapy & radiopharmaceuticals 2005; 20: 141-9

173. R. Fraley, S. Subramani, P. Berg, et al. Introduction of liposome-encapsulated SV40 DNA into cells. Journal of Biological Chemistry 1980; 255: 10431-5

174. R. B. Campbell, D. Fukumura, E. B. Brown, et al. Cationic charge determines the distribution of liposomes between the vascular and extravascular compartments of tumors. Cancer research 2002; 62: 6831-6

175. G. Thurston, J. W. McLean, M. Rizen, et al. Cationic liposomes target angiogenic endothelial cells in tumors and chronic inflammation in mice. Journal of clinical investigation 1998; 101: 1401

176. R. J. Cristiano and J. A. Roth. Epidermal growth factor mediated DNA delivery into lung cancer cells via the epidermal growth factor receptor. Cancer gene therapy 1995; 3: 4-10

177. M. Tanaka, G. C. Fraizer, J. De La Cerda, et al. Connexin 26 enhances the bystander effect in HSVtk/GCV gene therapy for human bladder cancer by adenovirus/PLL/DNA gene delivery. Gene therapy 2001; 8: 139-48

178. N. S. Yang, J. Burkholder, B. Roberts, et al. In vivo and in vitro gene transfer to mammalian somatic cells by particle bombardment. Proceedings of the National Academy of Sciences 1990; 87: 9568-72

179. R. K. Visaria, R. J. Griffin, B. W. Williams, et al. Enhancement of tumor thermal therapy using gold nanoparticle–assisted tumor necrosis factor-α delivery. Molecular Cancer Therapeutics 2006; 5: 1014-20

180. F. Wang, Y.-C. Wang, S. Dou, et al. Doxorubicin-Tethered Responsive Gold Nanoparticles Facilitate Intracellular Drug Delivery for Overcoming Multidrug Resistance in Cancer Cells. ACS Nano 2011; 5: 3679-92

181. J. Haensler and F. C. Szoka. Polyamidoamine cascade polymers mediate efficient transfection of cells in culture. Bioconjugate Chemistry 1993; 4: 372-9

182. C. Loup, M. A. Zanta, A. M. Caminade, et al. Preparation of Water-Soluble Cationic Phosphorus-Containing Dendrimers as DNA Transfecting Agents. Chemistry–A European Journal 1999; 5: 3644-50

183. P. Wang, X.-H. Zhao, Z.-Y. Wang, et al. Generation 4 polyamidoamine dendrimers is a novel candidate of nano-carrier for gene delivery agents in breast cancer treatment. Cancer Letters 2010; 298: 34-49

184. M. L. Patil, M. Zhang, O. Taratula, et al. Internally Cationic Polyamidoamine PAMAM-OH Dendrimers for siRNA Delivery: Effect of the Degree of Quaternization and Cancer Targeting. Biomacromolecules 2009; 10: 258-66

185. S. Koppu, Y. J. Oh, R. Edrada-Ebel, et al. Tumor regression after systemic administration of a novel tumor-targeted gene delivery system carrying a therapeutic plasmid DNA. Journal of Controlled Release 2010; 143: 215-21

186. O. Veiseh, F. M. Kievit, J. W. Gunn, et al. A ligand-mediated nanovector for targeted gene delivery and transfection in cancer cells. Biomaterials 2009; 30: 649-57

187. D. H. Jones, S. Corris, S. McDonald, et al. Poly(dl-lactide-co-glycolide)-encapsulated plasmid DNA elicits systemic and mucosal antibody responses to encoded protein after oral administration. Vaccine 1997; 15: 814-7

188. O. V. Chumakova, A. V. Liopo, V. G. Andreev, et al. Composition of PLGA and PEI/DNA nanoparticles improves ultrasound-mediated gene delivery in solid tumors in vivo. Cancer Letters 2008; 261: 215-25

189. H. Gonzalez, S. J. Hwang and M. E. Davis. New Class of Polymers for the Delivery of Macromolecular Therapeutics. Bioconjugate Chemistry 1999; 10: 1068-74

190. H. Huang, H. Yu, G. Tang, et al. Low molecular weight polyethylenimine cross-linked by 2-hydroxypropyl-γ-cyclodextrin coupled to peptide targeting HER2 as a gene delivery vector. Biomaterials 2010; 31: 1830-8

191. H. Meng, W. X. Mai, H. Zhang, et al. Codelivery of an optimal drug/siRNA combination using mesoporous silica nanoparticles to overcome drug resistance in breast cancer in vitro and in vivo. ACS nano 2013; 7: 994-1005

192. D. G. Anderson, W. Peng, A. Akinc, et al. A polymer library approach to suicide gene therapy for cancer. Proceedings of the National Academy of Sciences of the United States of America 2004; 101: 16028-33

Chapter 2.b Non-viral Delivery to Enable Genome Editing

Yuan Rui[1,2,‡], David R. Wilson[1-3,‡], Jordan J. Green[1-9]

[1]Biomedical Engineering, [2]Translational Tissue Engineering Center, [3]Institute for Nanobiotechnology, [4]Materials Science and Engineering, [5]Ophthalmology, [6]Neurosurgery, [7]Oncology, [8]Chemical & Biomolecular Engineering, [9]Bloomberg~Kimmel Institute for Cancer Immunotherapy, Johns Hopkins University School of Medicine, Baltimore, MD 21231, USA.

[‡]These authors contributed equally.

Abstract

Genome editing technologies such as zinc finger nucleases, transcription activator-like effector nucleases, and the clustered regularly interspaced short palindromic repeat/CRISPR-associated protein system have revolutionized biological research. Each biotechnology consists of a DNA binding protein that can be programmed to recognize and initiate double stranded breaks for site-specific gene modification. These technologies have the potential to be harnessed to cure diseases caused by aberrant gene expression. In order to be successful therapeutically, their functionality depends on their safe and efficient delivery into the cell nucleus. This review discusses the challenges in the delivery of genome editing tools and highlights recent innovations in non-viral delivery that have potential to overcome these limitations and advance the translation of genome editing towards patient care.

Keywords: ZFN, TALEN, CRISPR/Cas, Non-viral, Gene Editing

Glossary

ZFN: Zinc Finger Nucleases are *FokI* based, targeted DNA cleaving proteins that can introduce double stranded breaks targeted by triplet DNA bp recognizing zinc finger motifs

TALEN: Transcription Activator-Like Effector Nucleases are *FokI* based nucleases that are targeted to specific DNA sequences by central repeat domains in which 33-35 amino acids specify a single target DNA base

CRISPR: Clustered Regularly Interspaced Short Palindromic Repeats refers to the RNA targeted, DNA cleaving system originating in bacteria that has been re-appropriated for RNA guided DNA cleavage in mammalian cells

Cas: CRISPR associated protein, frequently Cas9 from *S. aureus* or *S. pyogenes*

PAM: Protospacer Adjacent Motifs are a short (2-6 bp) region of DNA recognized by the CRISPR associated proteins as non-bacterial in origin and are required to mediate CRISPR cleavage at RNA targeted. The canonical PAM sequence is 5'-NGG-3' but other Cas variants with different PAM sequences have been discovered or engineered.

DSB: Double stranded breaks occur when both strands of DNA are cleaved, triggering DNA repair pathways

NHEJ: Non-Homologous End-Joining is the primary, non-specific repair pathway of double-stranded break ligation in mammalian cells

HDR: Homology Directed Repair occurs when a donor template containing a gene insert flanked by homology arms that are complementary to DNA sequences flanking the cut site is present after double-stranded breaks

HITI: Homology-Independent Target Integration introduces gene inserts via donor templates that do not contain homology arms

RNP: Ribonucleoproteins in the context of CRISPR refers to the assembled complex of gRNA and Cas protein that can actively induce DNA cleavage

ZFNs, TALENs, and CRISPR/Cas

Zinc **F**inger **N**ucleases (**ZFNs**) (see **Glossary**) and **T**ranscription **A**ctivator-**l**ike **E**ffector **N**ucleases (**TALENs**) are hybrid restriction enzymes comprised of a DNA binding domain and a DNA cleavage domain based on the *FokI* endonuclease [1]. In contrast to ZFNs and TALENs, both of which use protein structures to recognize DNA sequences, the **C**lustered **R**egularly **I**nterspaced **S**hort **P**alindromic **R**epeat/**C**RISPR-**a**ssociated **s**ystem (**CRISPR/Cas)** enables DNA recognition through RNA-defined specificity. This simplifies the design of a target-specific gene editing complex to a short guide RNA (sgRNA) with a 20 bp complementarity with the target DNA sequence, as opposed to a new protein array, though the target sequence must be upstream of a protospacer adjacent motif (PAM) sequence [2, 3]. **Table 2-2** summarizes the characteristics of each gene editing system. Gene editing technologies continue to advance rapidly and recent reviews have provided coverage of many physical and chemical strategies for intracellular delivery of macromolecules that can potentially be adopted for gene editing applications as well as strategies for specific modification of genome editing proteins [4, 5]. In this review, we provide in-depth discussion of the most recent studies on non-viral gene editing, most of which were published in the last year, with an emphasis on the utilization of nanoparticle-based delivery vehicles.

	DNA binding domain	DNA cleavage domain	Mechanism for target specificity	Challenges and restrictions
ZFN	Zinc finger protein repeats	*Fok*I endonuclease	Each zinc finger protein recognizes 3 bp DNA	Target sequence length must be multiple of 3; longer target sequence requires larger protein
TALEN	Central repeat domains of transcription activator-like effector proteins	*Fok*I endonuclease	Each TALE protein unit recognizes 1 bp DNA	Cloning of TALE repeat arrays can be technically challenging; longer target sequence requires larger protein
CRISPR/Cas9	Cas9 endonuclease in complex with sgRNA	Cas9 endonuclease	20 bp targeting region of sgRNA confers specificity through DNA-RNA complementarity	Target sequence must be upstream of PAM site

Table 2-2. Comparison of ZFN, TALEN, and CRISPR/Cas gene editing systems.

All three gene editing systems result in sequence-specific DNA cleavage, at which point the cell's own DNA repair machinery can be harnessed to achieve gene modification. In the absence of a donor DNA template, double stranded breaks (**DSBs**) are repaired through error-prone non-homologous end joining (**NHEJ**), which introduces small indels that can shift the reading frame and result in gene knockout. When a donor DNA template is present, entire genes can be knocked in at the cut site. This is commonly achieved through homology directed repair (**HDR**) [6, 7], although some studies have shown higher integration rates through a process termed homology-independent targeted integration (**HITI**) [8]. The DNA binding capabilities of these genome editing enzymes have been further harnessed to enable site-specific single base pair editing [9, 10] and epigenetic [11, 12] or transcriptional [13, 14] modulation of gene expression.

In order for gene editing complexes to be functionally active, they must first be delivered into the cell nucleus, necessitating delivery across both the plasma and nuclear membranes. Historically, the most common way to achieve this is through the use of viral vectors, in which nucleic acids coding for the enzyme complexes are packaged into viruses and delivered to a target cell. While viral vectors are often highly effective, the complexity and challenge associated with scale-up of virus production, potential for insertional mutagenesis, and possible immune responses against the viral vector limit their use in a therapeutic capacity [15]. Viral vector cargo size limitations additionally limit efficacy particularly in AAV systems, which can necessitate editing enzymes and donor templates to be packaged into separate viral particles [16, 17]. Non-viral delivery methods have emerged as a viable alternative as they can be engineered to largely avoid these problems, but they require substantial improvements in order to reach the efficacy of their viral counterparts. Challenges to non-viral delivery include protection of nucleic acid or protein cargo from degradation, opsonization, and immune avoidance, as well as delivery to specific cell targets and cellular compartments. Recent research has further highlighted risks of host humoral and cell mediated immunity to the Cas9 protein [18] as well as double-stranded break P53 responses associated with genome editing that risk selection of P53 deficient edited cells [19, 20] that have yet to be overcome with any delivery strategy.

Cargo selection: DNA, mRNA, or Protein

Plasmid DNA

Genome editing complexes can be delivered by non-viral vectors in the form of plasmid DNA, a format that offers flexibility in design as DNA sequences can be easily incorporated into plasmids using simple molecular cloning techniques. However, gene editing efficiency is often limited by the efficiency of nuclear delivery and gene expression that is required to generate the final gene editing protein complexes. Upon systemic injection, DNA nanoparticles face multiple barriers before successful delivery to target tissues **(Figure 2-6)**. Nanoparticles with highly positive surface charges are prone to serum protein adsorption, aggregation, premature cargo release [21], and nanoparticle clearance by immune cells [22]. Coating nanoparticles with hydrophilic molecules such as poly(ethylene glycol) (PEG) is a common anti-fouling strategy that has been shown to reduce immune stimulation and increase circulation time [23], however anti-PEG responses resulting in accelerated clearance upon repeated administration may limit the applicability of PEGylation in the clinic for some applications [24]. Nanoparticle size is another important feature as molecules smaller than 5.5 nm in diameter have been shown to experience rapid clearance from the kidneys [25]. Complexation into nanoparticles decreases renal clearance of DNA by increasing its size beyond the renal filtration limit, and nanoparticles effective for gene delivery have been found to fall in the range of 100-250 nm in diameter [26].

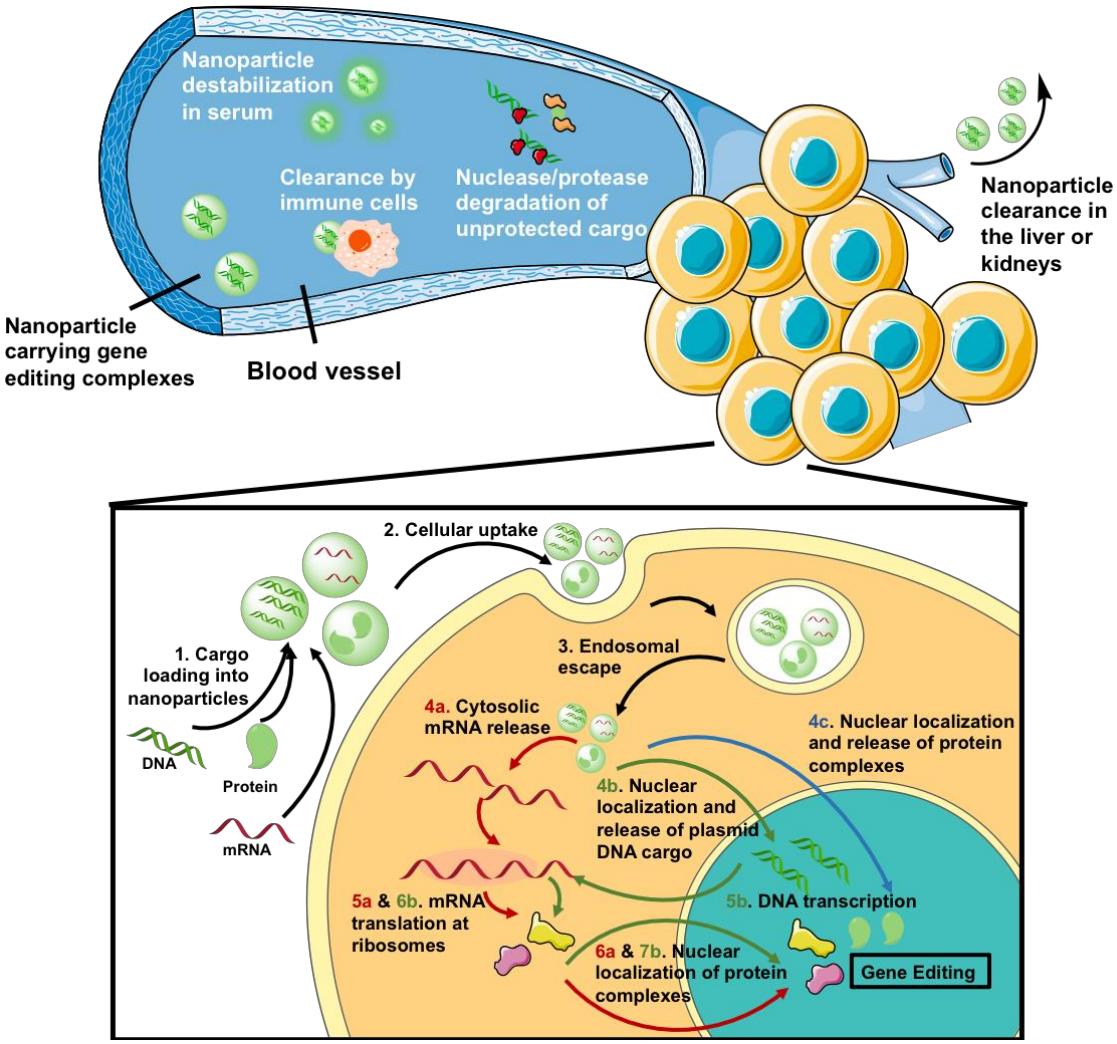

Figure 2-6. Extracellular and intracellular obstacles for non-viral delivery of gene editing tools.

Systemically injected nanoparticles carrying gene editing complexes must protect their cargo from destabilizing serum components, enzyme degradation, and clearance by immune cells or in the liver and kidneys. Upon reaching the target tissue, they face further intracellular delivery barriers. Protein or nucleic acid cargo must be (1) encapsulated in nano-carriers for (2) efficient intracellular uptake to occur. Upon endocytosis into the cell, nanoparticles need to (3) escape from degradative endo-lysosomal compartments. For mRNA delivery, cargo release should occur in the cytosol (4a) to enable mRNA translation at the ribosomes (5a). For DNA delivery, plasmid DNA needs to traffic to the nucleus (4b) where DNA can be transcribed into mRNA (5b); the mRNA transcript must then enter the cytosol to be translated into protein (6b). Protein complexes, whether synthesized in the cell (6a and 7b) or delivered directly by the nanocarrier

(4c), must localize to the nucleus for gene editing to occur. Intracellular delivery steps common to all cargo formats are shown in black arrows and those specific to mRNA, plasmid DNA, and protein complexes are shown in red, green, and blue arrows, respectively.

Upon arrival at target cells, nanoparticles must first cross the cell membrane. Cellular uptake can be enabled by attaching cell-penetrating peptides on nanoparticle surfaces to promote direct internalization [27] or through non-specific interactions between cationic nanoparticles and the anionic cell surface [28, 29]. If internalized via endocytosis, nanoparticles must also escape from degradative endo-lysosomal compartments. Many materials have been proposed to escape the endosome via the debated proton sponge mechanism, where nanomaterials containing uncharged amines at neutral pH acquire charge during endosome acidification, leading to polymer swelling and membrane destabilization for transient endosomal escape [30]. Several recent studies suggest that upon protonation in the acidifying endosome, polycations such as polyethylenimine (PEI) cause endosomal deformation and increase the permeability of the endosomal membrane, allowing nanoparticles to leak out through small pores [31, 32]. Finally, plasmid DNA must localize to the nucleus, which can be facilitated by nanomaterials that expedite cytosolic and nuclear trafficking [33]. In rapidly dividing cells, nuclear entry of plasmids generally occurs following nuclear membrane breakdown during cell division but in post-mitotic cells, import to the nucleus generally occurs through nuclear pores, which can be facilitated by transcription factor binding sequences in the plasmid that bind to importins [33]. Gene editing complexes face an additional trafficking step as proteins synthesized at cytosolic ribosomal sites must again localize to the nucleus to bind to and cleave genomic DNA. This could be especially challenging for the CRISPR/Cas system as Cas9 endonucleases must also bind sgRNA in the nucleus before they can form functional gene editing units. Utilization of minicircle DNA, which is more efficient on a per-mass basis and less immunogenic than plasmid DNA due to elimination of bacterial expression sequences, offers an alternative to some of these challenges and has been utilized for delivery of CRISPR [34], ZFN and TALEN [35] systems. The reduced size of minicircles compared to plasmids facilitates their cytosolic trafficking and nuclear import while the removal of sequences of bacterial origin reduces transcriptional silencing associated with plasmid DNA sequences [36].

Delivery of genome editing factors as DNA sequences also carries a substantial risk of unintentional genomic integration, which can induce insertional mutagenesis due to incorporation of highly active promoter elements in chromosomal DNA or disruption of tumor suppressor genes [37]; while the risk of insertional mutagenesis with non-viral delivery of plasmid DNA is generally much lower than with DNA viral vectors, this risk must be taken into account for translationally relevant therapies. Finally, plasmid DNA delivery is generally not feasible for cell types that are refractory to plasmid DNA transfection. This is especially problematic in immune cells, where it has been demonstrated that the same delivery system that enabled up to 50% editing in human embryonic kidney cells achieved less than 4% editing in $CD4^+$ T cells [38]. This could potentially be due to the fact that T cells can sense the intracellular presence of foreign nucleic acids [39], leading to an innate immune response and prompting the need for other delivery methods.

mRNA

Another nucleic acid delivery cargo to enable genome editing is mRNA, which can be synthesized from a DNA template using *in vitro* transcription. mRNA delivery circumvents the need for nuclear localization of the nucleic acid cargo as protein expression can occur following cytosolic delivery, and protein expression is detectable as short as 4-6 hours post-transfection [40, 41]. This virtually eliminates the risk of insertional mutagenesis and also reduces the probability of off-target effects as the duration of protein expression is much shorter for mRNA compared to DNA. Studies have shown that Cas9 protein expression can be effectively undetectable 72 hours post-transfection with mRNA *in vitro* [41] and 24 hours post-injection *in vivo* [40]. One major challenge for mRNA delivery is that in CRISPR applications, the delivery of Cas9 mRNA and sgRNA may require specialized materials as the two have very different lengths and different kinetics of expression. One study showed that the optimal condition for an RNA-mediated CRISPR/Cas9 editing system required the Cas9 mRNA to be delivered 24 hours before sgRNA delivery [42]. For gene insertion applications, the need for a donor template DNA may also necessitate an alternative delivery mechanism as Wang and colleagues demonstrated when the authors used electroporation to deliver mRNA coding for ZFNs and a viral vector to deliver donor DNA [43].

Proteins

Delivery of gene editing protein complexes synthesized outside the cell eliminates the need for intracellular transcription and translation, and gene editing can occur immediately following intranuclear delivery. This could potentially boost gene editing efficacy in post-mitotic or hard-to-transfect cells, in which limits to the cell's transcriptional or translational capacity could result in lower gene editing efficacy when using plasmid DNA or mRNA. On the other hand, this method also reduces the cargo's ability to enable cell type specificity as transcriptional targeting cannot be used. In the case of CRISPR/Cas9, there is the additional concern that the Cas9 protein variant from the bacterial species *S. pyogenes* and *S. Aureas* have both been shown to be recognized by antibodies in greater than 60% of human patients [18], which could result in rapid clearance of these proteins upon systemic delivery. Furthermore, Cas9 and TALENs generally cannot cross the cell membrane on their own, though ZFNs have been shown to have some inherent cell membrane permeability [44]. Due to the nucleic acid binding nature of the Cas9 protein, unmodified SpCas9 possesses a net charge of +20, which becomes further positively charged with addition of a nuclear localization signal (NLS) peptide [45]. This net positive charge of the Cas9 protein can be neutralized with protein engineering, by inclusion of a glutamate tag up to 20 amino acids long, which enabled direct cytosolic delivery when Cas9/sgRNA complexes were assembled with arginine-gold nanoparticles [45]. An alternative strategy to increase the plasma membrane permeability of genome editing enzymes is to fuse multiple viral SV40 nuclear localization signal (NLS) domains onto these proteins, which was reported to enable editing without an additional vector material both *in vitro* and *in vivo* [46, 47]. Similarly, cell-penetrating peptides have been conjugated to Cas9 and gRNAs directly to facilitate uptake and endosomal escape as self-condensed cationic nanoparticles, although these particles mediated <10% knockout efficiency *in vitro* in HEK293T cells [48].

Physical Delivery Methods

Delivery methods that physically disrupt the cell and nuclear membranes have been used extensively for delivery of ZFNs, TALENs and CRISPR but are generally limited to *ex vivo* delivery. Gene editing proteins or their DNA or RNA precursors have been directly injected into cells or embryos through the

process of microinjection and have been successfully used to generate disease models in rodents, but this technique is highly limited in the number of cells that can be edited in a timely manner [49, 50]. Other physical methods include electroporation, in which an electric field causes small pores to temporarily form in the cell membrane to allow nucleic acids and proteins to pass through, and nucleofection, which combines electroporation with chemically-enhanced delivery. Many groups have utilized electroporation to deliver nucleic acids or proteins for ZFNs, TALENs or CRISPR RNPs directly in manners that have been extensively reviewed, with many on-going clinical trials utilizing electroporation for delivery to T-cells [4]. Overall, physical delivery methods have a high potential to be used for *ex vivo* editing of isolated circulating lymphocytes *ex vivo*, which could potentially then be adoptively transferred into a patient for cellular therapy.

Additionally, hydrodynamic injection has been used *in vivo* to induce expression of Cas9 and gRNA from plasmid DNA in the liver of rodents, although this method is not regarded as translatable to humans [51]. Other physical delivery methods include direct mechanical disruption of cellular membranes via micro-constriction [52] or induction of cell uptake and endosomal escape of Cas9 RNP complexes via manipulation of osmotic potential [53]. D'Astolfo and colleagues utilized hypertonic solutions to trigger macropinocytosis *in vitro* followed by endosomal disruption mediated by zwitterionic propanebetaines to deliver Cas9 RNP complexes, providing an alternative to electroporation or physical membrane disruption [53].

Chemical material-based delivery approaches for genome editing

Nanoparticle material	Cargo format	Main findings	Refs
PEG-PEI-cholesterol lipopolymer	Plasmid DNA	50% knockout of VEGF gene in osteosarcoma cells *in vitro* and *in vivo*	[57]
Lipid-assisted PEG-PLGA	Plasmid DNA	Macrophage-specific knockout of netrin-1; 30% *in vitro* and 20% *in vivo*	[58]
Zwitterionic amino lipid	Cas9 mRNA and in vitro transcribed sgRNA	Achieved gene deletion-mediated turning on of mCherry expression in Ai9 mice *in vivo*	[42]
Lipofectamine 2000®	Ribonucleoprotein complex	24% knockout of eGFP *in vitro* in neuron-derived mouse embryonic stem cells and 13% knockout *in vivo* in mouse cochlea hair cells	[59]

PEG-lipid	Cas9 mRNA and in vitro transcribed sgRNA	97% knockout of mouse transthyretin protein in liver cells for; sustained for at least 12 months following single systemic injection	[61]
Polymer and gold nanoparticle	Ribonucleoprotein complex	5.4% homology-directed repair in mouse *mdx* Duchenne muscular dystrophy model after intramuscular injection	[67]
PEI coated on DNA nanoparticle	Ribonucleoprotein complex	~40% GFP knockout *in vitro* and 25% knockout *in vivo* in U2OS cells following intratumoral injection	[69]
Cationic cell-penetrating polypeptide	Plasmid DNA	35% gene deletion, 67% protein knockdown, and reduced tumor growth by >71% in HeLa cells after intratumoral injections *in vivo*	[70]

Table 2-3. Examples of non-viral nanoparticle-mediated CRISPR delivery.

Lipids and lipid-like materials

Chemical approaches to non-viral delivery utilize biomaterials to form nanostructures that encapsulate genome-editing cargos and then shuttle them into cells (see **Figure 2-7** for chemical structures of these materials). Many lipids and lipid-like materials have been developed for the intracellular delivery of nucleic acids such as oligonucleotides [54], mRNA [55], and plasmid DNA [56]. For genome editing applications, these materials have largely been used to deliver genome editing tools in the form of nucleic acids (see **Table 2-3** for summary). Plasmid DNA encoding a Cas9-sgRNA complex targeting VEGF was delivered using a PEG-PEI-cholesterol lipopolymer and achieved ~50% gene knockout in osteosarcoma cells *in vitro* and *in vivo* [57] while a CRISPR DNA construct with a CD68 promoter was delivered using lipid-containing PEG-PLGA nanoparticles to enable macrophage-specific gene editing, resulting in 30% gene knockout *in vitro* and 20% *in vivo* [58]. Cas9 mRNA and *in vitro* transcribed sgRNAs were delivered by Miller and colleagues using a zwitterionic amino lipid library [42] and by Jiang and colleagues using N^1,N^3,N^5-tris(2-aminoethyl)benzene-1,3,5- tricarboxamide (TT) based lipid-like nanoparticles [40] for gene editing *in vitro* and *in vivo* **(Figure 2-8)**. Noting the ability to deliver the RNAs despite their vastly different sized (100 nt for sgRNA and >4500 nt for mRNA), the lipidoid nanoparticles engineered by Miller and colleagues achieved 95% knockout *in vitro* and detectable editing in the liver, lungs and kidney.

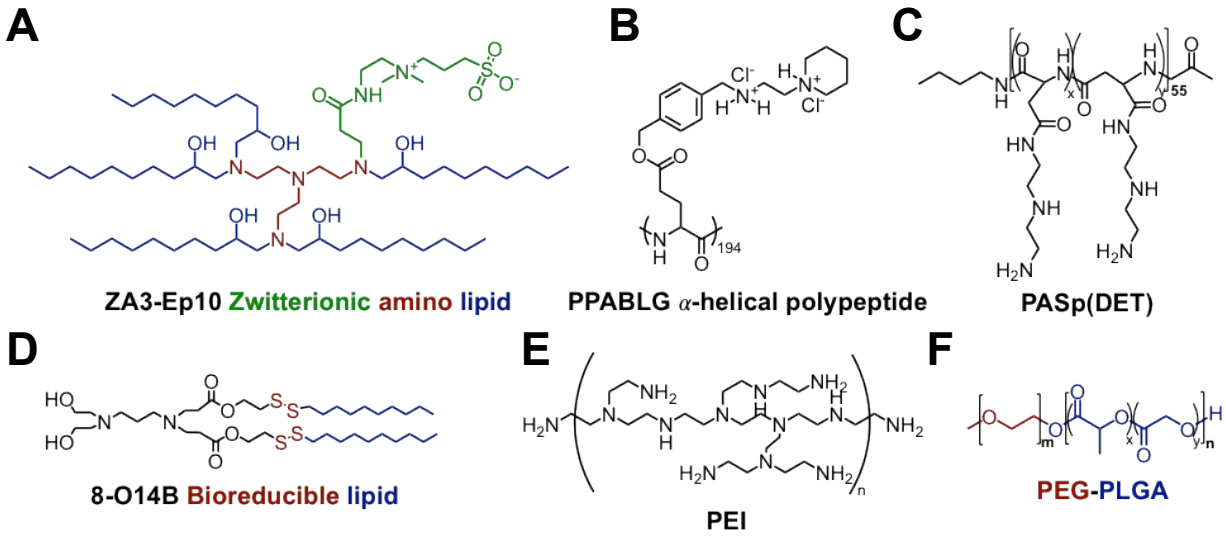

Figure 2-7. Chemical structures of materials that have been used to deliver non-viral gene editing complexes. (A) Zwitterionic amino lipid were used to deliver Cas9 mRNA and sgRNA [42]; **(B)** PPABLG polypeptides condensed plasmid DNA into nanoparticles for CRISPR editing [70]; **(C)** PASp(DET) coating enabled endosomal escape of CRISPR-gold constructs [67]; **(D)** bioreducible lipids enabled intracellular delivery of RNP complexes [60]; **(E)** PEI was used in hybrid nanoparticle systems to deliver the CRISPR system as RNPs [69] and plasmid DNA [57]; **(F)** PEG-PLGA nanoparticles enabled CRISPR editing in macrophages *in vivo* [58].

Lipid materials have also been explored as vehicles for genome editing proteins. Zuris and colleagues engineered Cas9 and TALENs fused to anionic GFP proteins to increase the negative surface charge of these proteins and complexed them with the commercially-available cationic lipid transfection reagent Lipofectamine 2000™ and demonstrated 24% gene knockout in neuron-derived mouse embryonic stem cells *in vitro* and 13% gene knockout in mouse cochlea hair cells *in vivo* [59]. Likewise, Wang and colleagues utilized more effective bioreducible lipid nanoparticles to deliver charge neutralized Cas9 RNP complexes for up to 70% knockout *in vitro* [60]. Lipid materials have also shown impressive levels of gene editing after systemic delivery, primarily in the liver. Finn and colleagues reported that lipid nanoparticles formulated with PEG-lipids showed excellent serum stability, and when used to deliver Cas9 mRNA and sgRNAs targeting the mouse transthyretin gene in liver cells resulted in >97% reduction in serum protein levels that persisted for at

least 12 months after a single systemic injection [61]. Yin and colleagues utilized the highly effective lipid cKK-E12 lipid nanoparticle formulation for co-delivery to the liver of Cas9 mRNA and sgRNA highly modified for enhanced efficacy, demonstrating 80% gene knockout primarily in hepatocytes [62]. Importantly, lipid nanoparticles also have the ability to complement viral delivery strategies for genome editing to improve tissue specificity; Yin and colleagues reported using lipid nanoparticles to deliver Cas9 mRNA non-virally to the liver, while using AAV encoding a sgRNA and HDR DNA template to achieve 6% editing correction of hepatocytes [63]. Using biologically derived materials, Kim and colleagues used cancer-derived exosomes as the delivery vehicle for plasmid DNA encoding a CRISPR/Cas system and showed efficient and targeted editing in an ovarian cancer model [64]. An exosome-liposome hybrid vector developed by Lin and colleagues enabled CRISPR-interference in mesenchymal stem cells, which could not be transfected using liposomes alone [65]. These results showcase the great potential of lipid formulations for *in vivo* delivery of genome editing tools to treat genetic diseases, rivaling that of viral mediated delivery for some tissues such as the liver.

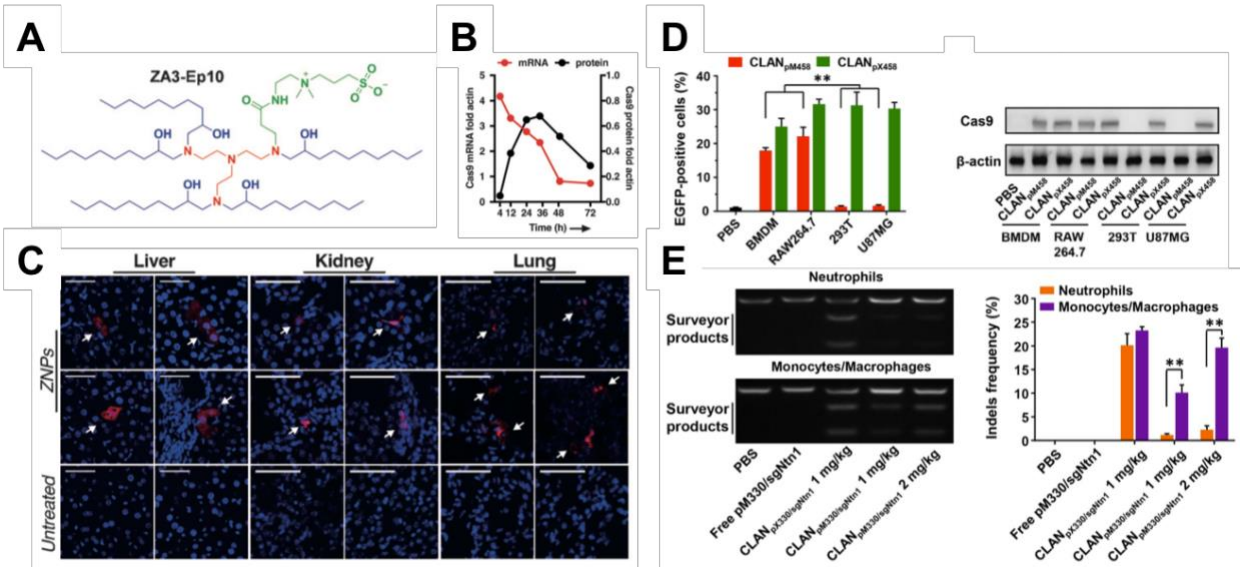

Figure 2-8. Lipid-containing delivery systems enable gene editing after systemic injections *in vivo*. **(A)** Structure of the zwitterionic amino lipid used by Miller *et al.* [42] to formulate nanoparticles delivering the CRISPR/Cas9 system in the form of Cas9 mRNA and sgRNA. **(B)** Expression profile of Cas9 after mRNA delivery. **(C)** Systemic injection of these zwitterionic lipid nanoparticles achieved gene editing in the liver,

kidney, and lung (as indicated by red fluorescence). Reproduced with permission from [42]. **(D)** Cationic lipid-assisted PEG-*b*-PLGA nanoparticles (CLAN) developed by Luo *et al.* [58] delivering the CRISPR/Cas9 system in the form of plasmid DNA showed preferential expression in macrophages (BMDM and RAW264.7) when using a macrophage-specific promoter (pM458). **(E)** Systemic injection of these nanoparticles enabled macrophage-specific gene editing in mice. Reproduced with permission from [58].

Polymeric materials

Polymeric materials have been used for the delivery of DNA, mRNA, and oligonucleotides [66]. For the delivery of genome editing tools, polymers have often been used in multi-component delivery systems to promote endosomal escape **(Figure 2-9)**. Lee and colleagues used the endosomal disruptive polymer poly(*N*-(*N*-(2-aminoethyl)-2-aminoethyl) aspartamide) to coat Cas9-sgRNA RNPs adsorbed onto gold nanoparticles and used this vehicle, which they termed CRISPR-Gold, to correct the dystrophin gene in a mouse model of Duchenne muscular dystrophy *in vivo*; despite an *in vivo* HDR frequency of only 5% following intramuscular injection, these nanoparticles mediated a statistically measurable increase in muscle strength compared to scramble nanoparticles [67]. CRISPR-Gold has been utilized in follow-up work to mediate genome editing in rodent brains following local injection using both Cas9 and Cfp1, managing to reduce mRNA and protein levels of the target gene by up to 50% [68]. In an alternative approach, Sun and colleagues used rolling circle amplification to create DNA nanoclews that enabled encapsulation of RNP complexes in a DNA based particle core that were then coated with the cationic polymer polyethylenimine (PEI) and achieved CRISPR-mediated gene editing *in vitro* of up to 28% knockout compared to <2% knockout with PEI only as well as an estimated 25% knockout of eGFP *in vivo* following intratumoral injection of the nanoparticles [69]. Recent work by the labs of Cheng and Leong have demonstrated the promise of a cationic α-helical polypeptide to deliver Cas9 and sgRNA plasmids for enhanced efficiency at gene editing *in vitro* and *in vivo* [70], leading to 67% targeted protein knockdown in HeLa cells *in vivo* following repeated intratumoral injections and reducing tumor growth by >71%, consequently significantly extending survival in the HeLa xenograft mouse model [70]. These strategies, using cationic polymers to deliver either nucleic acids, nucleic acid neutralized RNP

complexes, or anionic modified RNP complexes, have all relied upon local delivery due to the cationic nature of the particles being utilized presenting potential systemic delivery challenges. While this relatively high efficacy of cationic polymer-based materials for local delivery is promising in mice, for certain applications, it may face challenges in scale-up to patients due to the larger length scales required for sufficient transport and therapeutic coverage.

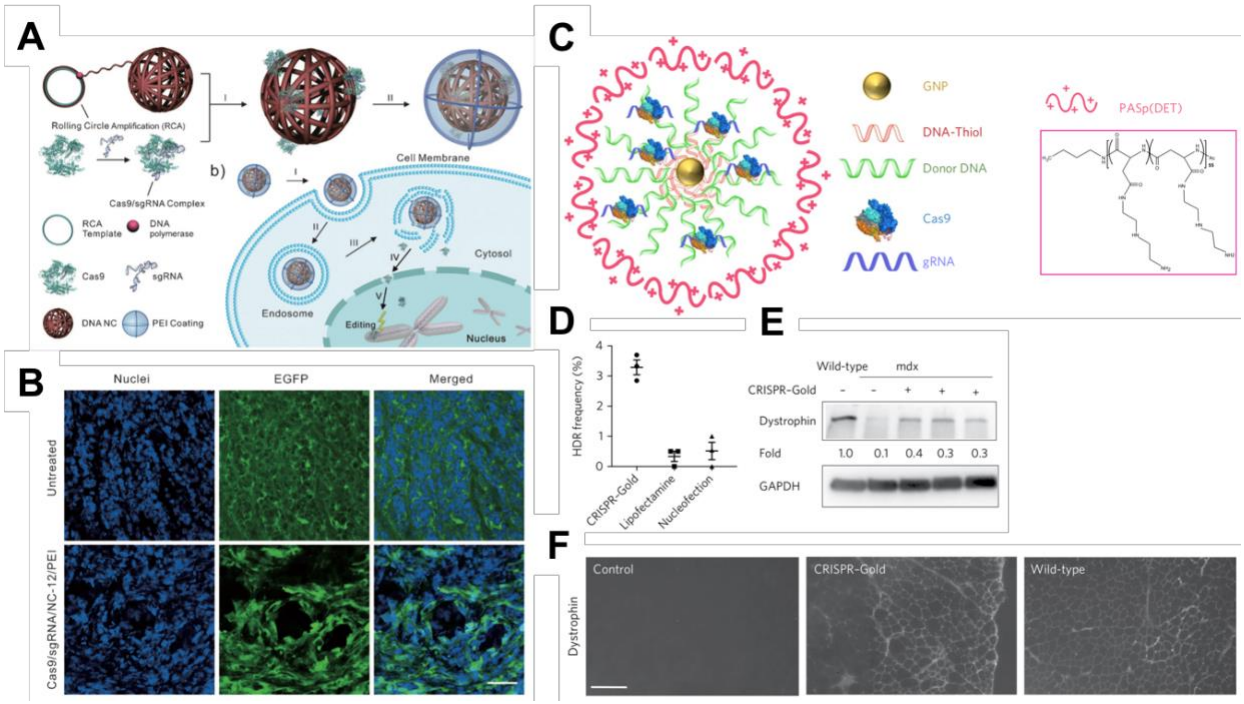

Figure 2-9. Hybrid delivery systems for CRISPR/Cas9 using polymers to facilitate cellular uptake and endosomal escape. (A) Assembly schematic for the DNA nanoclew system in which Cas9-sgRNA RNPs are assembled into nanocomplexes with DNA nanoparticles coated with the cationic polymer PEI. **(B)** DNA nanoclews enabled knockout of an eGFP gene *in vivo.* Reproduced with permission from [69]. **(C)** Assembly schematic for CRISPR-gold, which complexed RNPs with gold nanoparticles and a PASp(DET) polymer. CRISPR-gold corrected the dystrophin gene in primary myoblasts from the *mdx* mouse model for Duchenne muscular dystrophy *in vitro* (D&E), and enabled restoration of the dystrophin gene *in vivo* after intramuscular injection (F). Reproduced with permission from [67].

Advances in systemic delivery strategies could be utilized to give polymeric gene editing delivery vehicles greater reach. The most commonly used strategy is PEGylation, in which the hydrophilic molecule

polyethylene glycol (PEG) is used to reduce fouling of the nanoparticle surface and increase circulation time [23]. More recently, the use of zwitterionic materials have gained interest as another strategy for systemic delivery. Recent advances in the field of systemic siRNA delivery are applicable to genome editing machinery nucleic acids or proteins; particularly, use of zwitterionic materials including cationic quaternary ammonium sulfonamide amino lipids [71] and zwitterionic phosphorylcholine-based polymer corona in a diblock polymer have been shown to improve systemic delivery and offer more effective alternatives to PEGylation [72].

Another avenue to explore is the use of polymeric materials to deliver gene editing proteins. In contrast to nucleic acid delivery, where cationic polymers are typically used to condense anionic nucleic acids into nanoparticles via electrostatic interactions, protein delivery platforms must be more flexible to accommodate protein molecules of various surface charges. Chang and colleagues reported a protein delivery system composed of a dendrimer end-capped with guanidyl groups to facilitate protein binding through hydrogen bonding and salt bridges as well as phenyl groups to promote endocytosis and endosomal escape [73]. This polymer successfully encapsulated proteins of different sizes and surface charges and promoted the efficient intracellular delivery of functionally-intact proteins *in vitro*. Yan and colleagues employed a different strategy in which thin polymer shells were synthesized around individual protein molecules *in situ*, resulting in a core-shell architecture in which polymer shells were covalently linked to the protein cores [74]. The authors showed that this system protected proteins against protease degradation and enabled efficient cellular uptake *in vitro* and *in vivo* of proteins that retained their efficacy following intracellular delivery without relying on electrostatic charge based interactions, which is beneficial for gene editing protein complexes and Cas9 RNP complexes which possess regions of varying charge. Recently, several groups have reported the use of zinc/imidazole-based metal-organic frameworks (MOF) for intracellular protein delivery [75, 76]. These MOF nanoparticles have been demonstrated to effectively protect protein cargo from protease digestion and were used by Alsaiari and colleagues to enable intracellular delivery of CRISPR RNPs, though the editing efficiency was quite low (30% gene knockout in CHO cells *in vitro*) and further optimization of this system is required [77]. Overall, these strategies could be adapted to delivering gene editing protein complexes, which

are mostly impermeable to cell membranes on their own and unsuitable for encapsulation using cationic polymers as they have slightly cationic surface charges.

Concluding Remarks and Future Perspectives

In August 2017, the FDA approved the first therapeutic that involved a gene therapy step as a medicine in the United States [78]. Tisagenlecleucel, a cell-based cancer immunotherapy for children and young adults with B-cell lymphoblastic leukemia, uses viruses to insert a gene encoding chimeric antigen receptors (CARs) into patient-derived T cells and infuses these CAR T cells back into the patient. This drug has achieved remission in >80% of patients who had been refractory to traditional radiation therapy [79]. Subsequently, the first gene therapy in the United States for use *in vivo* to directly treat a genetic disease was approved by the FDA in December 2017 [80]. The therapy, voretigene neparvovec-rzyl, uses an adeno-associated virus (AAV2) to deliver RPE65 cDNA to patients with biallelic RPE65 mutation-associated retinal dystrophy and demonstrated improved vision without product-related serious adverse events [81]. The approval of these first gene therapy-based medicines in the United States marks the beginning of an exciting new era of precision medicine in which gene-based therapeutics, such as gene editing technologies, are being brought to market.

While these impressive steps forward bode well for the future clinical translation of gene editing technologies, their efficacy largely depends on the efficiency of intracellular delivery and the suitability of the delivery system for the genetic cargo being delivered. Viral delivery systems can be effective but can also have significant limitations to cargo size as well as potential adverse effects such as insertional mutagenesis and immunogenicity, which may limit many applications to modifying cells *ex vivo* for re-infusion into patients as in the case with CAR T cells [82]. The field is moving quickly as clinical trials have begun in China using CRISPR to engineer CAR T cells targeting lung cancer [83] and in the UK using TALENs to engineer CAR T cells targeting pediatric leukemia [84], and the first CRISPR-engineered CAR T cell clinical trials in the US were recently approved [85]. Non-viral platforms could expand the scope of gene editing therapies by facilitating safe and effective direct delivery to native cells *in vivo*. Recent studies using a non-viral polymer and

gold nanoparticle hybrid system resulted in effective correction of disease phenotypes in muscle cells after intramuscular injection [67]. Clinically-relevant levels of gene editing in the liver were achieved from systemic injections of lipid nanoparticles that could be promising in treating a host of inherited liver diseases such as primary hyperoxaluria type 1, transthyretin amyloidosis, and hepatitis B [61]. Other advances in achieving more targeted delivery of gene editing tools could be used to decrease the chances of off-target editing. Even with these advances, much work still needs to be done in order to adapt gene editing technologies to treat various disease types in a safe and effective way (see Outstanding Questions). Innovating genome editing complexes as well as nanostructured delivery vehicles with higher specificity, enhanced efficiency, and lower toxicity brings these promising technologies closer to the clinic, where they have the potential to precisely cure genetic diseases instead of merely treating disease symptoms.

Outstanding Questions

What cargo type should gene editing molecules be delivered as to maximize editing efficiency while minimizing off-target effects and immunogenicity in the most cell types?

What type of non-viral delivery vehicle would best enable clinically relevant levels of gene editing in humans?

Are gene editing technologies safe to use as a systemically delivered drug in light of P53 damage responses to double stranded DNA breaks?

What is the best way to develop and implement gene editing technologies to treat diseases in which the same disease phenotype can be caused by multiple different genotypes in different patients?

Acknowledgements

Y.R. and D.W. thank the NSF for graduate fellowships. The authors would like to thank the Bloomberg~Kimmel Institute for Cancer Immunotherapy, Research to Prevent Blindness / Dr. H. James and Carole Free Catalyst Award, and the NIH (R01EB022148) for support.

References

1. Mani, M. et al. (2005) Binding of two zinc finger nuclease monomers to two specific sites is required for effective double-strand DNA cleavage. Biochemical and Biophysical Research Communications 334 (4), 1191-1197.

2. Mojica, F.J.M. et al. (2009) Short motif sequences determine the targets of the prokaryotic CRISPR defence system. Microbiology 155 (3), 733-740.

3. Deltcheva, E. et al. (2011) CRISPR RNA maturation by trans-encoded small RNA and host factor RNase III. Nature 471 (7340), 602.

4. Yin, H. et al. (2017) Delivery technologies for genome editing. Nature reviews Drug discovery 16 (6), 387.

5. Wang, H.-X. et al. (2017) CRISPR/Cas9-based genome editing for disease modeling and therapy: challenges and opportunities for nonviral delivery. Chem Rev 117 (15), 9874-9906.

6. Moehle, E.A. et al. (2007) Targeted gene addition into a specified location in the human genome using designed zinc finger nucleases. Proceedings of the National Academy of Sciences 104 (9), 3055.

7. Yoshimi, K. et al. (2016) ssODN-mediated knock-in with CRISPR-Cas for large genomic regions in zygotes. Nature communications 7, 10431.

8. Suzuki, K. et al. (2016) In vivo genome editing via CRISPR/Cas9 mediated homology-independent targeted integration. Nature 540, 144.

9. Kim, Y.B. et al. (2017) Increasing the genome-targeting scope and precision of base editing with engineered Cas9-cytidine deaminase fusions. Nat Biotechnol 35 (4), 371-376.

10. Rees, H.A. et al. (2017) Improving the DNA specificity and applicability of base editing through protein engineering and protein delivery. Nature Communications 8, ncomms15790.

11. Hilton, I.B. et al. (2015) Epigenome editing by a CRISPR-Cas9-based acetyltransferase activates genes from promoters and enhancers. Nature biotechnology 33 (5), 510.

12. Amabile, A. et al. (2016) Inheritable silencing of endogenous genes by hit-and-run targeted epigenetic editing. Cell 167 (1), 219-232.

13. Polstein, L.R. and Gersbach, C.A. (2012) Light-Inducible Spatiotemporal Control of Gene Activation by Customizable Zinc Finger Transcription Factors. Journal of the American Chemical Society 134 (40), 16480-16483.

14. Konermann, S. et al. (2014) Genome-scale transcriptional activation by an engineered CRISPR-Cas9 complex. Nature 517, 583.

15. Kotterman, M.A. et al. (2015) Viral vectors for gene therapy: translational and clinical outlook. Annual review of biomedical engineering 17, 63-89.

16. Yang, Y. et al. (2016) A dual AAV system enables the Cas9-mediated correction of a metabolic liver disease in newborn mice. Nat Biotechnol 34 (3), 334.

17. Yu, W. et al. (2017) Nrl knockdown by AAV-delivered CRISPR/Cas9 prevents retinal degeneration in mice. Nature Communications 8, 14716.

18. Charlesworth, C.T. et al. (2018) Identification of Pre-Existing Adaptive Immunity to Cas9 Proteins in Humans. bioRxiv, 243345.

19. Ihry, R.J. et al. (2018) p53 inhibits CRISPR–Cas9 engineering in human pluripotent stem cells. Nat Med, 1.

20. Haapaniemi, E. et al. (2018) CRISPR–Cas9 genome editing induces a p53-mediated DNA damage response. Nat Med, 1.

21. Liu, J. et al. (2005) Influence of serum protein on polycarbonate-based copolymer micelles as a delivery system for a hydrophobic anti-cancer agent. Journal of Controlled Release 103 (2), 481-497.

22. Jones, S.W. et al. (2013) Nanoparticle clearance is governed by Th1/Th2 immunity and strain background. The Journal of Clinical Investigation 123 (7), 3061-3073.

23. Suk, J.S. et al. (2016) PEGylation as a strategy for improving nanoparticle-based drug and gene delivery. Advanced drug delivery reviews 99, 28-51.

24. Ando, H. et al. (2018) Reactivity of IgM antibodies elicited by PEGylated liposomes or PEGylated lipoplexes against auto and foreign antigens. J Control Release 270, 114-119.

25. Choi, H.S. et al. (2007) Renal Clearance of Nanoparticles. Nature biotechnology 25 (10), 1165-1170.

26. Sunshine, J.C. et al. (2012) Uptake and transfection with polymeric nanoparticles are dependent on polymer end-group structure, but largely independent of nanoparticle physical and chemical properties. Mol Pharm 9 (11), 3375-83.

27. Freimann, K. et al. (2018) Formulation of Stable and Homogeneous Cell-Penetrating Peptide NF55 Nanoparticles for Efficient Gene Delivery In Vivo. Molecular Therapy - Nucleic Acids 10, 28-35.

28. Verma, A. and Stellacci, F. (2010) Effect of surface properties on nanoparticle–cell interactions. Small 6 (1), 12-21.

29. Lin, J. and Alexander-Katz, A. (2013) Cell Membranes Open "Doors" for Cationic Nanoparticles/Biomolecules: Insights into Uptake Kinetics. ACS Nano 7 (12), 10799-10808.

30. Stewart, M.P. et al. (2016) Challenges in carrier-mediated intracellular delivery: moving beyond endosomal barriers. Wiley Interdisciplinary Reviews: Nanomedicine and Nanobiotechnology 8 (3), 465-478.

31. Vermeulen, L.M.P. et al. (2018) Endosomal Size and Membrane Leakiness Influence Proton Sponge-Based Rupture of Endosomal Vesicles. ACS Nano 12 (3), 2332-2345.

32. Clark, S.R. et al. (2018) Determining the effects of PEI adsorption on the permeability of 1,2-dipalmitoylphosphatidylcholine/bis(monoacylglycero)phosphate membranes under osmotic stress. Acta Biomaterialia 65, 317-326.

33. Vaughan, E.E. et al. (2006) Intracellular trafficking of plasmids for gene therapy: mechanisms of cytoplasmic movement and nuclear import. Curr Gene Ther 6 (6), 671-681.

34. Chen, Z. et al. (2017) Targeted Delivery of CRISPR/Cas9-Mediated Cancer Gene Therapy via Liposome-Templated Hydrogel Nanoparticles. Advanced Functional Materials 27 (46).

35. Dad, A.B. et al. (2014) Enhanced gene disruption by programmable nucleases delivered by a minicircle vector. Gene Ther 21 (11), 921.

36. Chen, Z.-Y. et al. (2003) Minicircle DNA vectors devoid of bacterial DNA result in persistent and high-level transgene expression in vivo. Mol Ther 8 (3), 495-500.

37. Yin, H. et al. (2014) Non-viral vectors for gene-based therapy. Nat Rev Genet 15 (8), 541-555.

38. Mandal, Pankaj K. et al. (2014) Efficient Ablation of Genes in Human Hematopoietic Stem and Effector Cells using CRISPR/Cas9. Cell Stem Cell 15 (5), 643-652.

39. Monroe, K.M. et al. (2014) IFI16 DNA Sensor Is Required for Death of Lymphoid CD4 T Cells Abortively Infected with HIV. Science 343 (6169), 428.

40. Jiang, C. et al. (2017) A non-viral CRISPR/Cas9 delivery system for therapeutically targeting HBV DNA and pcsk9 in vivo. Cell Research 27, 440.

41. Liang, X. et al. (2015) Rapid and highly efficient mammalian cell engineering via Cas9 protein transfection. J Biotechnol 208, 44-53.

42. Miller, J.B. et al. (2017) Non-Viral CRISPR/Cas Gene Editing In Vitro and In Vivo Enabled by Synthetic Nanoparticle Co-Delivery of Cas9 mRNA and sgRNA. Angewandte Chemie International Edition 56 (4), 1059-1063.

43. Wang, J. et al. (2016) Highly efficient homology-driven genome editing in human T cells by combining zinc-finger nuclease mRNA and AAV6 donor delivery. Nucleic Acids Research 44 (3), e30-e30.

44. Gaj, T. et al. (2012) Targeted gene knockout by direct delivery of zinc-finger nuclease proteins. Nature Methods 9, 805.

45. Mout, R. et al. (2017) Direct cytosolic delivery of CRISPR/Cas9-ribonucleoprotein for efficient gene editing. ACS nano 11 (3), 2452-2458.

46. Liu, J. et al. (2015) Improved Cell-Penetrating Zinc-Finger Nuclease Proteins for Precision Genome Engineering. Molecular Therapy. Nucleic Acids 4 (3), e232.

47. Staahl, B.T. et al. (2017) Efficient genome editing in the mouse brain by local delivery of engineered Cas9 ribonucleoprotein complexes. Nat Biotechnol 35 (5), 431-434.

48. Ramakrishna, S. et al. (2014) Gene disruption by cell-penetrating peptide-mediated delivery of Cas9 protein and guide RNA. Genome Res.

49. Wefers, B. et al. (2013) Direct production of mouse disease models by embryo microinjection of TALENs and oligodeoxynucleotides. Proceedings of the National Academy of Sciences 110 (10), 3782.

50. Geurts, A.M. et al. (2009) Knockout Rats via Embryo Microinjection of Zinc-Finger Nucleases. Science 325 (5939), 433.

51. Yin, H. et al. (2014) Genome editing with Cas9 in adult mice corrects a disease mutation and phenotype. Nat Biotechnol 32 (6), 551.

52. Han, X. et al. (2015) CRISPR-Cas9 delivery to hard-to-transfect cells via membrane deformation. Science advances 1 (7), e1500454.

53. D'Astolfo, D.S. et al. (2015) Efficient intracellular delivery of native proteins. Cell 161 (3), 674-690.

54. Wang, Y. et al. (2015) Delivery of oligonucleotides with lipid nanoparticles. Advanced drug delivery reviews 87, 68-80.

55. Hajj, K.A. and Whitehead, K.A. (2017) Tools for translation: non-viral materials for therapeutic mRNA delivery. Nature Reviews Materials 2, 17056.

56. de Lima, M.C.P. et al. (2001) Cationic lipid–DNA complexes in gene delivery: from biophysics to biological applications. Advanced drug delivery reviews 47 (2-3), 277-294.

57. Liang, C. et al. (2017) Tumor cell-targeted delivery of CRISPR/Cas9 by aptamer-functionalized lipopolymer for therapeutic genome editing of VEGFA in osteosarcoma. Biomaterials 147, 68-85.

58. Luo, Y.-L. et al. (2018) Macrophage-Specific in Vivo Gene Editing Using Cationic Lipid-Assisted Polymeric Nanoparticles. ACS Nano.

59. Zuris, J.A. et al. (2015) Cationic lipid-mediated delivery of proteins enables efficient protein-based genome editing in vitro and in vivo. Nat Biotechnol 33 (1), 73.

60. Wang, M. et al. (2016) Efficient delivery of genome-editing proteins using bioreducible lipid nanoparticles. Proceedings of the National Academy of Sciences 113 (11), 2868.

61. Finn, J.D. et al. (2018) A Single Administration of CRISPR/Cas9 Lipid Nanoparticles Achieves Robust and Persistent In Vivo Genome Editing. Cell Reports 22 (9), 2227-2235.

62. Yin, H. et al. (2017) Structure-guided chemical modification of guide RNA enables potent non-viral in vivo genome editing. Nature Biotechnology 35, 1179.

63. Yin, H. et al. (2016) Therapeutic genome editing by combined viral and non-viral delivery of CRISPR system components in vivo. Nat Biotechnol 34 (3), 328.

64. Kim, S.M. et al. (2017) Cancer-derived exosomes as a delivery platform of CRISPR/Cas9 confer cancer cell tropism-dependent targeting. J Control Release 266, 8-16.

65. Lin, Y. et al. (2018) Exosome–Liposome Hybrid Nanoparticles Deliver CRISPR/Cas9 System in MSCs. Advanced Science 5 (4), 1700611.

66. Yin, H. et al. (2014) Non-viral vectors for gene-based therapy. Nature Reviews Genetics 15, 541.

67. Lee, K. et al. (2017) Nanoparticle delivery of Cas9 ribonucleoprotein and donor DNA in vivo induces homology-directed DNA repair. Nature Biomedical Engineering 1 (11), 889-901.

68. Lee, B. et al. (2018) Nanoparticle delivery of CRISPR into the brain rescues a mouse model of fragile X syndrome from exaggerated repetitive behaviours. Nature Biomedical Engineering 2 (7), 497.

69. Sun, W. et al. (2015) Self-assembled DNA nanoclews for the efficient delivery of CRISPR–Cas9 for genome editing. Angewandte Chemie International Edition 54 (41), 12029-12033.

70. Wang, H.-X. et al. (2018) Nonviral gene editing via CRISPR/Cas9 delivery by membrane-disruptive and endosomolytic helical polypeptide. Proceedings of the National Academy of Sciences.

71. Miller, J.B. et al. (2018) Development of Cationic Quaternary Ammonium Sulfonamide Amino Lipids for Nucleic Acid Delivery. ACS Applied Materials & Interfaces 10 (3), 2302-2311.

72. Jackson, M.A. et al. (2017) Zwitterionic Nanocarrier Surface Chemistry Improves siRNA Tumor Delivery and Silencing Activity Relative to Polyethylene Glycol. ACS Nano 11 (6), 5680-5696.

73. Chang, H. et al. (2017) Rational Design of a Polymer with Robust Efficacy for Intracellular Protein and Peptide Delivery. Nano letters 17 (3), 1678-1684.

74. Yan, M. et al. (2009) A novel intracellular protein delivery platform based on single-protein nanocapsules. Nature Nanotechnology 5, 48.

75. Chen, T.-T. et al. (2018) Biomineralized Metal-Organic Framework Nanoparticles Enable Intracellular Delivery and Endo-Lysosomal Release of Native Active Proteins. Journal of the American Chemical Society.

76. Cheng, G. et al. (2018) Self-Assembly of Extracellular Vesicle-like Metal–Organic Framework Nanoparticles for Protection and Intracellular Delivery of Biofunctional Proteins. Journal of the American Chemical Society.

77. Alsaiari, S.K. et al. (2017) Endosomal Escape and Delivery of CRISPR/Cas9 Genome Editing Machinery Enabled by Nanoscale Zeolitic Imidazolate Framework. Journal of the American Chemical Society 140 (1), 143-146.

78. Ledford, H. (2017) Engineered cell therapy for cancer gets thumbs up from FDA advisers. Nature 547 (7663), 270.

79. Bach, P.B. et al. (2017) FDA Approval of Tisagenlecleucel: Promise and Complexities of a $475 000 Cancer Drug. Jama 318 (19), 1861-1862.

80. Fischer, A., FDA approves novel gene therapy to treat patients with a rare form of inherited vision loss, FDA, FDA.gov, 2017.

81. Russell, S. et al. (2017) Efficacy and safety of voretigene neparvovec (AAV2-hRPE65v2) in patients with RPE65-mediated inherited retinal dystrophy: a randomised, controlled, open-label, phase 3 trial. The Lancet 390 (10097), 849-860.

82. Eyquem, J. et al. (2017) Targeting a CAR to the TRAC locus with CRISPR/Cas9 enhances tumour rejection. Nature 543 (7643), 113.

83. Cyranoski, D. (2016) Chinese scientists to pioneer first human CRISPR trial. Nature News 535 (7613), 476.

84. Qasim, W. et al. (2017) Molecular remission of infant B-ALL after infusion of universal TALEN gene-edited CAR T cells. Science Translational Medicine 9 (374).

85. Reardon, S. (2016) First CRISPR clinical trial gets green light from US panel. Nature News.

Chapter 3: Bioreducible Polymeric Nanoparticles Containing Multiplexed Cancer Stem Cell-regulating miRNAs inhibit Glioblastoma Growth and Prolong Survival

Hernando Lopez-Bertoni[1,2,‡], Kristen L. Kozielski[3,‡], Yuan Rui[3,‡], Bachchu Lal,[1,2] Hannah Vaughan[3], David R. Wilson[3], Nicole Mihelson[1,2], Charles G. Eberhart[4,5,6], John Laterra[1,2,6,7,*] and Jordan J. Green[3,5,6,8,9,10,*]

[1]Hugo W. Moser Research Institute at Kennedy Krieger, [2]Department of Neurology, [3]Department of Biomedical Engineering, Institute for NanoBioTechnology, and the Translational Tissue Engineering Center, [4]Department of Pathology, [5]Department of Ophthalmology, [6]Department of Oncology, [7]Department of Neuroscience, [8]Departments of Materials Science & Engineering and Chemical & Biomolecular Engineering, [9]Department of Neurosurgery, [10]Bloomberg~Kimmel Institute for Cancer Immunotherapy, Johns Hopkins University School of Medicine, Baltimore, Maryland 21231, United States

[‡] These authors contributed equally.

Abstract

Despite our growing molecular understanding of glioblastoma (GBM), treatment modalities remain limited. Recent developments in mechanisms of cell fate regulation and nanomedicine provide new avenues to treat and manage brain tumors via delivery of molecular therapeutics. Here we have developed bioreducible poly(beta-amino ester) nanoparticles that demonstrate high intracellular delivery efficacy, low cytotoxicity, escape from endosomes, and promotion of cytosol-targeted environmentally-triggered cargo release for

miRNA delivery to tumor-propagating human cancer stem cells. In this report, we combined this nanobiotechnology with newly discovered cancer stem cell inhibiting miRNAs to develop self-assembled miRNA-containing polymeric nanoparticles (nano-miRs) to treat gliomas. We show that these nano-miRs effectively intracellularly deliver single and combination miRNA mimics that inhibit the stem cell phenotype of human GBM cells *in vitro*. Following direct intratumoral infusion, these nano-miRs were found to distribute through the tumors, inhibit the growth of established orthotopic human GBM xenografts, and cooperatively enhance response to standard-of-care γ–radiation. Co-delivery of two miRNAs, miR-148a and miR-296-5p, within the bioreducible nano-miR particles enabled long-term survival from GBM in mice.

KEYWORDS: miRNA, polymer, bioreducible, brain cancer, cancer stem cell, nanomedicine

Introduction

More than 50,000 new cases of malignant brain cancer are diagnosed in the U.S. each year with glioblastoma (GBM) being the most common and deadly form.[1] Despite aggressive treatment consisting of surgical resection and radiotherapy/chemotherapy, the median life expectancy for GBM patients is only 14-20 months, highlighting the need for new therapeutic approaches.[2] Treatment options for GBM remain limited in part due to tumor cell resistance to chemotherapy/radiation and the difficulty in delivering newer targeting therapeutics to the brain.[3-4] GBMs are highly heterogeneous at the cellular level and contain cells that vary in their capacity to propagate tumor growth as revealed through single cell sequencing, RNA-profiling[5] and studies of intra-tumoral evolution.[6] Among these different cell subpopulations are multi-potent stem-like cells (also referred to as cancer stem cells or CSCs) that are critical determinants of tumor propagation, therapeutic resistance, and recurrence following treatment.[7] Epigenetic mechanisms that support this stem-like tumor-propagating phenotype represent a vulnerability amenable to therapeutic targeting.[8] Non-coding RNAs, in particular miRNAs, are emerging as critical epigenetic regulators of cell fate and oncogenesis.[9] miRNAs selectively inhibit gene expression primarily by targeting mRNA for degradation usually via complementary 3'-UTR seed sequences. Numerous miRNAs have been found to regulate tumorigenesis and cancer cell stemness by targeting tumor-suppressing or tumor promoting transcripts.[10] We recently showed that the

coordinated actions of Oct4 and Sox2 induce a CSC state in GBM cells through a mechanism that involves the down-regulation of a network of miRNAs through promoter DNA methylation.[11-12] We further showed that the repression of two of these miRNAs, miR-148a and miR-296-5p, is required for the induction of GBM tumor propagating capacity by Oct4/Sox2 and that their reconstitution using viral expression vectors efficiently inhibits the GBM stem-like phenotype.[11-12]

Therapeutically translating these advances in the molecular drivers of GBM stem cells remains a challenge.[13] Viral gene delivery is promising but there remain potential limitations to clinical translation due to factors such as scalability, limited cargo size, and potential tumorigenic and immunogenic effects.[14-15] Non-viral vectors such as polymeric nanoparticles can be designed to circumvent many of these problems, but traditional cationic polymers such as poly(L-lysine) (PLL) and polyethylenimine (PEI) that encapsulate nucleic acid cargoes into nanoparticles by electrostatically-driven self-assembly are generally ineffective for utilization *in vivo* and have been shown to be minimally effective for delivery of relatively small RNA molecules.[16] Poly(beta-amino ester)s (PBAEs) are newer synthetic cationic polymers that promote superior gene delivery versus PEI, in part, as they contain hydrolytically-cleavable ester bonds, which reduces cytotoxicity as well as enhances cargo release.[17] Like many gene delivery vehicles, PBAEs were first optimized for DNA delivery. Because RNA oligos (e.g. miRNA) are shorter and stiffer than plasmid DNA, they are often harder to complex into nanoparticles,[18] and the materials that are effective for DNA delivery are often ineffective for RNA delivery.[19]

In this report we create new nanoparticles consisting of state-of-the-art polymeric nanobiotechnology with newly discovered cancer stem cell inhibiting miRNAs to develop miRNA delivering nanoparticles (nano-miRs) to treat gliomas. We develop and characterize nanoparticles utilizing bioreducible and cationic PBAE polymers capable of safely and efficiently shuttling miRNA into GBM cells, enabling escape out of the endosomes into the cytosol, and exhibiting an environmentally-triggered release of miRNA upon entering the cytosolic compartment. For the first time, we demonstrate the use of modified PBAE-based polymers for the effective delivery of miRNA mimics and observed that they inhibit the stem cell phenotype of human GBM cells. Further, we show that this new bioreducible PBAE-based nanomedicine spreads through

established tumors *in vivo* and can be effective for therapeutic *in vivo* delivery of miRNA, and consequently, oligonucleotides in general. Critically, the delivery of these tumor-suppressing miRNAs using these biomaterials inhibited the growth of established GBM xenografts and led to significant long-term survival in mouse models. Our findings demonstrate that identifying and validating stem cell-regulating miRNAs in combination with advances in nanomedicine can impact the development of therapies for targeting the human CSC population and treating GBM.

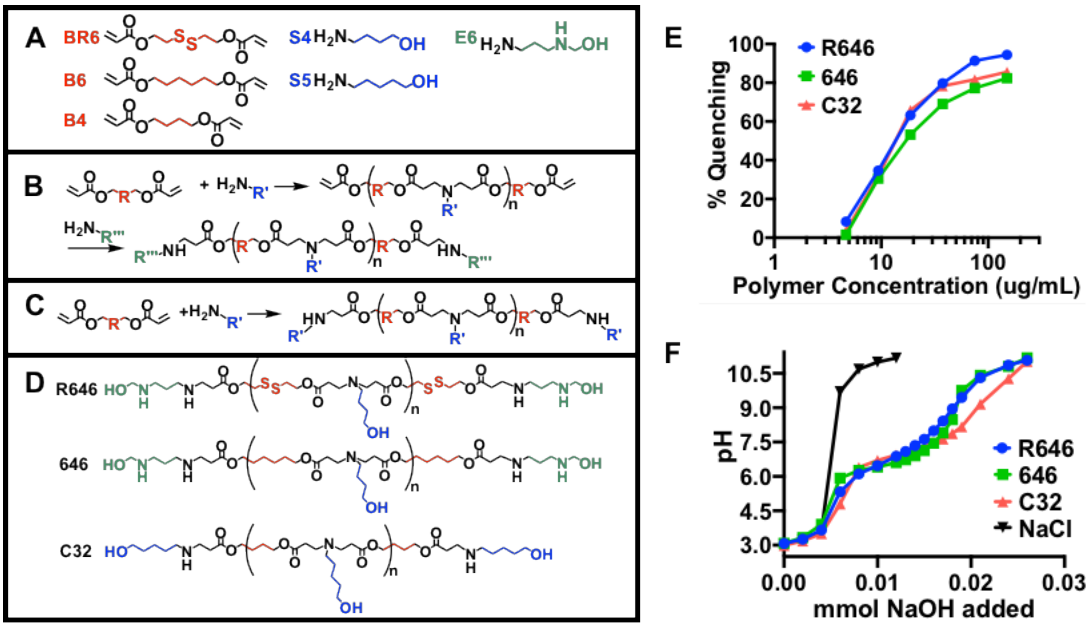

Figure 3-1: PBAE synthesis, miRNA complexation and buffering capacity. (A) PBAE monomer structures are shown. (B) Polymer R646 was synthesized using a Michael addition reaction between monomers BR6 and S4 at a 1.01:1 BR6:S4 ratio. The resulting acrylate-terminated polymer was endcapped with monomer E6 to yield BR6-S4-E6 (R646). Polymer 646 was synthesized via a similar method using monomer B6 instead of BR6. (C) Polymer C32 was synthesized by reacting B4 with S5 at a 1:1.2 B4:S5 ratio, resulting in an amino alcohol terminated polymer. (D) Chemical structures of R646, 646, and C32. (E) Polymer-miRNA competitive binding assay; polymer to miRNA binding strength is assessed by quenching of YO-PRO®-1 Iodide fluorescence over increasing polymer concentrations. (F) Acid-base titration curves for PBAE polymers with 150 mM aqueous NaCl for comparison. pH was adjusted to pH 3 with HCl and titrated with NaOH.

Results and Discussion

Bioreducible PBAE nano-miRs encapsulate miRNAs into nanoparticles, effectively release them in a reducing cytosolic environment and deliver miRNAs to human GBM *in vitro.* To investigate the miRNA delivery capabilities of bioreducibe PBAE nano-miRs and compare their performance with previous iterations of non-reducible PBAEs, we synthesized bioreducible polymer R646, its non-reducible analog 646, and C32 – a non-reducible PBAE that has been shown to be very effective at delivering DNA[20] (Figure 3-1). The bioreducible monomer 2,2'-disulfanediylbis(ethane-2,1-diyl)diacrylate (BR6) was copolymerized with 4-amino-1-butanol (S4) via a Michael Addition reaction at a 1.01:1 BR6:S4 ratio, and the resulting acrylate-terminated polymer was endcapped with 2-(3-aminopropylamino)ethanol (E6) to synthesize the polymer BR6-S4-E6 (R646). Polymer 646 was synthesized using the same procedure, but using the non-reducible hexane-1,6-diyl diacrylate (B6) instead of BR6. Finally, polymer C32, which has been shown to successfully deliver plasmid DNA to human prostate cancer xenografts in mouse models, was synthesized by copolymerizing 1,4-butanediol diacrylate (B4) and 5-amino-1-pentanol (S5) at a 1:1.2 B4:S5 ratio following the method reported by Anderson et al.[20] Polymers were characterized with gel permeation chromatography for molecular weight and polydispersity (Table 3-S1 and Figure 3-S14) and NMR for polymer structure (Figures 3-S15, 3-S16, and 3-S17). YO-PRO®-1 Iodide competition binding assay, in which YO-PRO®-1 Iodide fluoresces upon binding miRNA and is quenched as it is displaced by polymer, shows that these PBAEs bound miRNA with equivalent binding affinity. pH titration curves were determined for the polymers using acid-base titration and showed they have equivalent buffering capacity in the physiologically-relevant range of pH 6-7.4, as indicated by a gradual slope at this pH range (Figure 3-1). As all three polymers have a similar structure (linear PBAE polymers that contain a similar tertiary amine repeat unit in the backbone, Figure 3-1D), their buffering capacity is similar. To determine the optimal nano-miR formulations required to deliver miRNA to GBM cells, we prepared nano-miRs at increasing polymer: miRNA weight-weight ratios (w/w). We optimized nano-miR w/w ratios *in vitro* in human GBM1A CSCs at a miRNA dose of 90 nM with a minimum acceptable cell viability of 75%. At this dosage, R646 nano-miRs maintained cell viability of greater than 75% at 150 w/w while 646 and C32 achieved the same at 37 w/w (Figure 3-2A). Additionally,

incubating GBM1A or GBM1B neurospheres with R646 nano-miRs using the conditions described above for 3 hrs or 24 hrs did not have adverse effects on cell viability (Figure 3-S1). At these optimal w/w ratios, cellular uptake of fluorescently labeled miRNAs was assessed via flow cytometry. We found that R646 nano-miRs achieved nearly 60-fold higher cellular uptake of miRNA compared to 646 and C32 nano-miRs encapsulating the same amount of miRNA (Figure 3-2B). This is most likely due to the fact that R646 attenuated cytotoxicity, allowing us to formulate R646 nano-miRs at a much higher w/w ratio and resulting in smaller and more stable nanoparticles compared to C32 and 646. Lastly, we assessed functional delivery of bio-active miRNAs using the different nano-miR formulations. Polymers were complexed with either a non-targeting control miRNA (Ctrl) or a combination of miRNA mimics miR-148a and miR-296-5p (Comb). Three days after transfection, functional delivery was assessed through qRT-PCR analysis of the expression of Dnmt1 and Hmga1, which are known targets of these two miRNAs.[11-12] We found that R646 nano-miRs significantly reduced the expression of both targets while 646 and C32 nano-miRs did not (Figure 3-2C-D). Unlike R646 nano-miRs, canonical PBAEs did not show meaningful, statistically significant target gene knockdown, demonstrating the need for improved materials for polymeric nanoparticle-mediated miRNA delivery (Figure 3-S2). In order to rule out the possibility that differences in polymer molecular weight contributed to the observed difference in transfection efficacy, we synthesized R646 and 646 of similar molecular weight and used these polymers to deliver control or combination miRNA mimics. Our results showed that R646 nano-miRs again achieved significantly higher target gene knockdown and lower cytotoxicity compared to 646 nano-miRs formulated with matching molecular weight polymers , indicating that polymer characteristics beyond molecular weight are responsible for the superior performance of bioreducible R646 nano-miRs (Figure 3-S3). Furthermore, target gene knock-down by R646 nano-miRs was found to be somewhat more efficient than that achieved by commercially available RNAiMax and substantially more efficient than that achieved by commercially available PEI and Lipofectamine 3000 (Figure 3-S4).

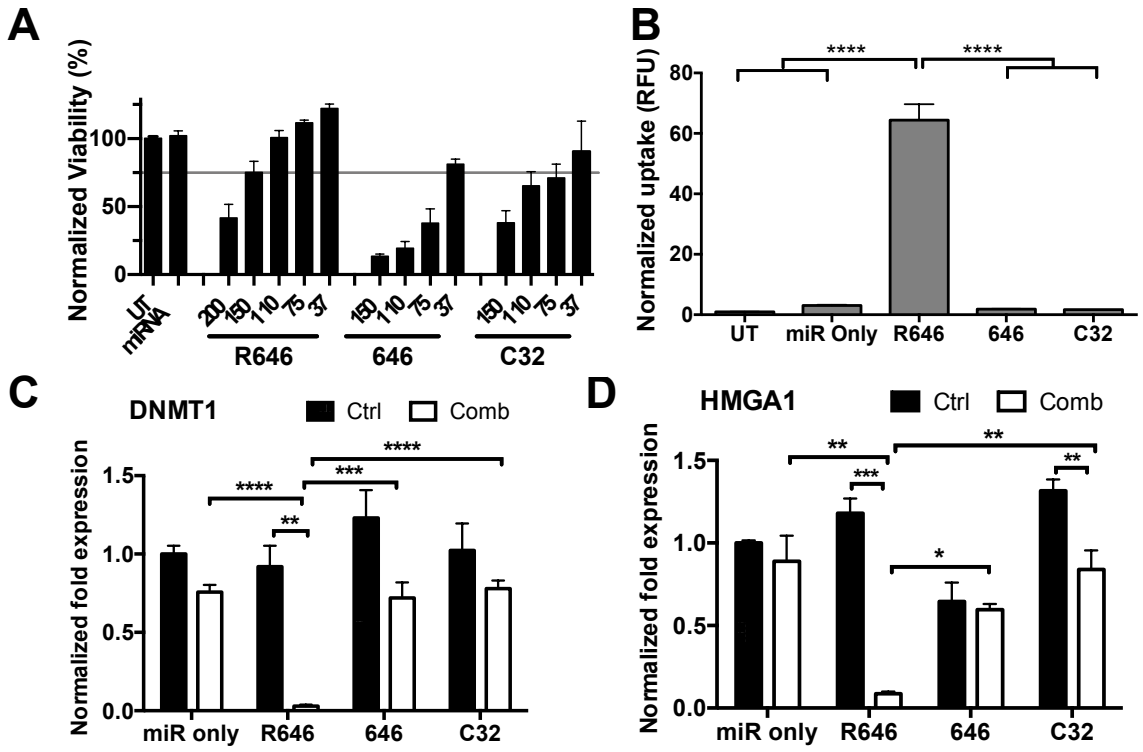

Figure 3-2: Polymer R646 attenuates cytotoxicity compared to non-reducible PBAE and effectively delivers miRNAs to GBM cells. (A) Nano-miR formulations were screened in GBM1A cells to identify optimal nano-miR formulation with >75% relative viability. Numbers on the x-axis indicate polymer-miRNA w/w ratios. (B) Nano-miR uptake was measured using flow cytometry after treating cells with nano-miRs loaded with Cy5-labeled miRNA. R646 nano-miRs had significantly higher cell uptake (****P<0.0001) than all other conditions assessed by One-way ANOVA with Tukey post hoc tests. (C) qRT-PCR analysis of expression of Dnmt1 and Hmga1 in GBM1A 3 days after treatment with nano-miRs delivering a non-targeting control miRNA (Ctrl) or a combination of miRNA mimics miR-148a and miR-296-5p (Comb). Fold expression was normalized to cells treated with Ctrl miRNA only. R646 showed statistically significant knockdown in expression of (C) Dnmt1 and (D) Hmga1 assessed by Holm-Sidak corrected multiple t-tests between matched Ctrl and Comb (**P< 0.01; ***P<0.001). Bars show mean + SEM of three (qRT-PCR) or four wells (viability and uptake). For each target, R646 nano-miRs delivering the combination of miRNA mimics also showed significantly higher knockdown than all other conditions as assessed by One-way ANOVA with Tukey post hoc tests (*P<0.05).

We characterized the physical properties of the three nano-miR formulations by measuring nanoparticle hydrodynamic diameter via dynamic light scattering (DLS) and nanoparticle tracking analysis (NTA), zeta-potential by electrophoretic light scattering, and nanoparticle morphology by transmission electron microscopy (TEM). Diluted with PBS to a buffer condition of 150 mM and pH 7.4 to mimic physiological conditions, nano-miR size measured via NTA showed number-averaged hydrodynamic diameters of approximately 100 nm for all three formulations while DLS showed that R646 nano-miRs have an intensity-weighted z-average hydrodynamic diameter of approximately 200 nm, while 646 and C32 nano-miRs had z-average hydrodynamic diameters of greater than one micron, indicating the presence of aggregates in their particle distributions (Figure 3-3A). Interestingly, we also performed DLS size measurements before PBS dilution (measurement in 25 mM sodium acetate buffer, pH 5) and found that all nano-miRs were below 200 nm in diameter (Figure 3-S5). Thus, the canonical PBAE nano-miRs were prone to aggregation after the initial self-assembly and following dilution into neutral physiological buffer. This suggests that the high w/w ratio that we were able to use with bioreducible polymer R646 (as this polymer was engineered to be less cytotoxic) resulted in nano-miRs that had complexed miRNA more strongly, which reduced nano-miR aggregation in higher salt and pH environments. Zeta-potential was slightly positive for R646 nano-miRs and essentially neutral for 646 and C32 nano-miRs (Figure 3-3B). TEM images show that all formulations formed spherical nanoparticles with R646 nano-miRs appearing slightly smaller than the 646 nano-miRs and C32 nano-miRs (Figure 3-3C and Figure 3-S6). As R646 nano-miRs degrade in water due to the hydrolytic ester linkages within the R646 polymer, we wanted to evaluate whether the R646 nano-miRs could be formulated dry in a manner suitable for storage that would also facilitate *in vivo* use. We utilized a lyophilization procedure with sugar as a cryoprotectant and found that R646 nano-miRs maintained their physical properties following lyophilization with no significant change in nanoparticle diameter assessed by DLS or TEM (Figure 3-S7).[21]

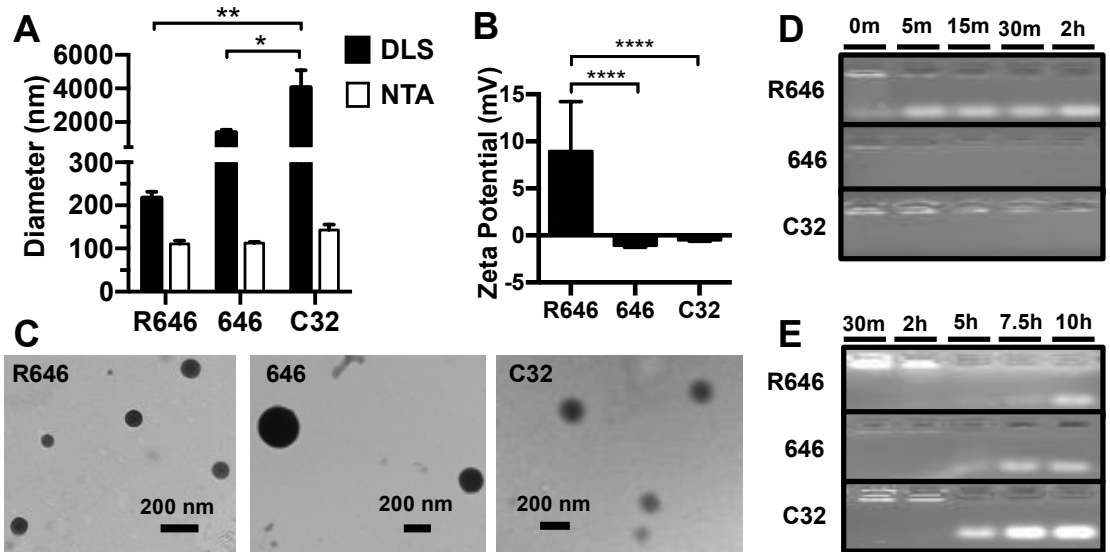

Figure 3-3: Polymer R646 forms nanoparticles with miRNA and effectively releases miRNA in a reducing environment. (A) Nanoparticle hydrodynamic diameter as measured using intensity-weighted (DLS) or number-average (NTA) measurement showed that R646 nano-miRs had a statistically smaller hydrodynamic diameter via DLS as assessed by One-way ANOVA with Tukey post hoc tests (**P<0.001) **(B)** Nanoparticle zeta-potential as measured via electrophoretic light scattering showed R646 nano-miRs had a statistically significantly higher zeta potential assessed by One-way ANOVA with Tukey post hoc tests (****P<0.0001). **(C)** TEM images of nano-miRs showed dried particle size and spherical morphology. **(D)** Gel retention assay performed in 5 mM glutathione mimicking the intracellular environment showed short-term miRNA release in reducing conditions. miRNA that was tightly bound within non-bioreducible PBAE nanoparticles was unable to run down the gel. **(E)** Gel retention assay performed in artificial CSF mimicking the extracellular environment in the brain showed long-term miRNA release in non-reducing conditions. Bars show mean + SEM of three independently prepared samples.

To determine miRNA release kinetics, we performed a gel retention assay, in which nano-miRs were loaded into an agarose gel, and tightly bound RNA would be unable to electrophorese under an applied voltage. We incubated the nano-miRs in 5 mM glutathione (GSH) to mimic the reducing cytosolic space in the intracellular environment.[22] In the presence of GSH, miRNA from bioreducible R646 nano-miRs began to release almost instantaneously, and was completely released within 5 minutes; non-reducible 646 and C32

nano-miRs, in contrast, did not release miRNA even after 2 hr incubation (Figure 3-3D). We incubated the nanoparticles in artificial cerebrospinal fluid (aCSF) to mimic the redox and ionic environment in the brain extracellular space[23] for longer times and found that for all nano-miR formulations, miRNA began to release after 5 hr and was completely released by 10 hr. (Figure 3-3E) These results indicate that R646 nano-miRs are able to release miRNA cargo rapidly in a stimuli-responsive manner upon entry into the reducing intracellular space due to the reduction of disulfide bonds in the polymer backbone, while non-reducible 646 and C32 nano-miRs hold on to their cargo for much longer and eventually release miRNA after the slower hydrolysis of ester bonds.

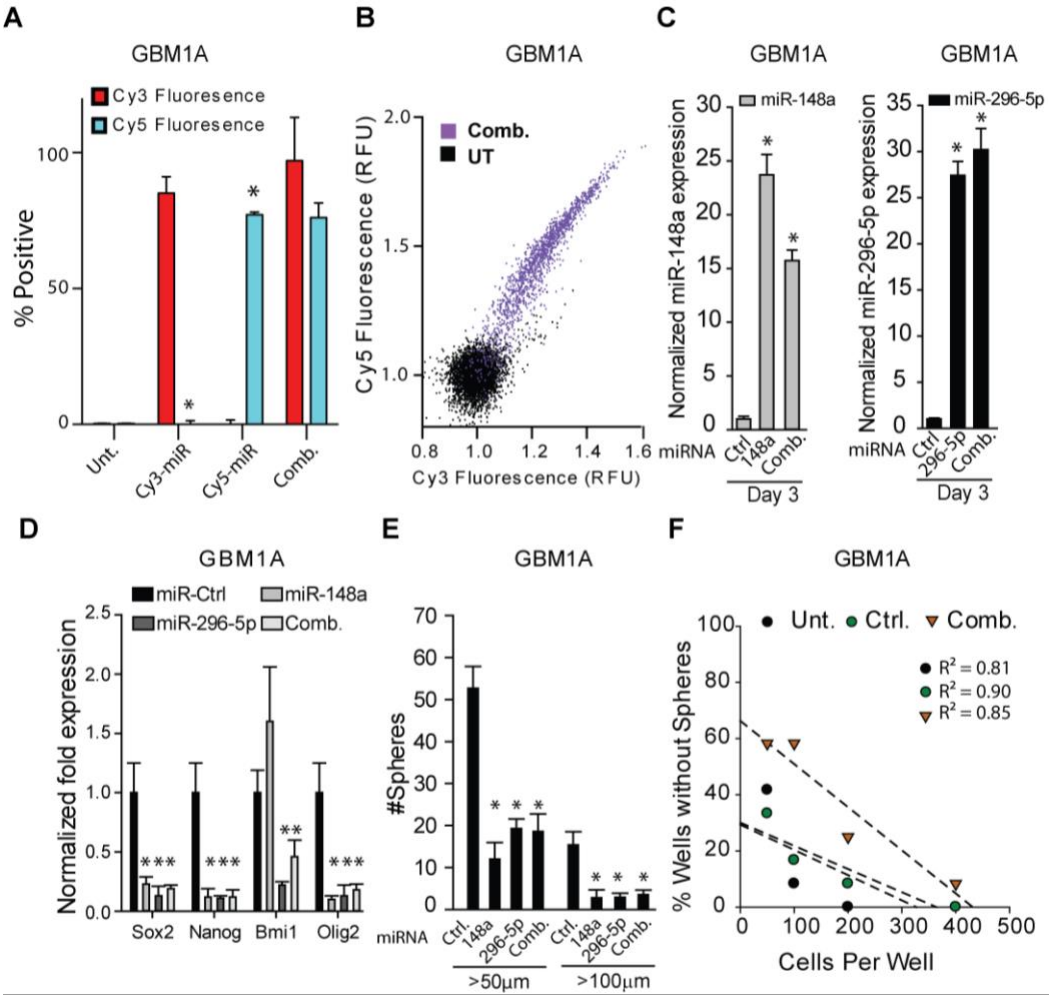

Figure 3-4: R646 nano-miRs can deliver multiple different miRNAs and inhibit the GBM stem cell phenotype. (A) Flow cytometry data of GBM1A neurospheres treated with R646 nano-miRs carrying either Cy3-labeled miRNA (Cy3-miR), Cy5-labeled miRNA (Cy5-miR), both RNAs (comb.) and completely

untreated (Unt.). Fluorescence signal of cells treated with nano-miRs carrying both miRNAs were normalized against the single miRNA groups. Bars show mean + SEM of four wells. **(B)** Flow cytometry plot of cells treated with nano-miRs carrying both labeled miRNAs compared to the untreated population shows proportional uptake of both miRNAs. **(C)** Expression of mature miR-148a and miR-296-5p was measured by qRT-PCR 3 days after transfection. **(D)** qRT-PCR analysis to measure expression of stem cell markers in GBM1A neurospheres transfected with nano-miRs. **(E)** Equal numbers of GBM1A transfected with nano-miRs were cultured in neurosphere medium containing EGF/FGF for 12 days and neurosphere numbers (>100μm diameter) were quantified by computer-assisted image analysis. **(F)** Limiting dilution analyses of GBM1A transfected with control (Ctrl.) or miR-148a+miR-296-5p combination (Comb.) nano-miRs. Untransfected cells (Unt.) were used as negative control. Cells were plated in a limiting dilution manner, and the number of wells containing spheres was counted after 14 days to compare stem cell frequencies. One-way ANOVA with Tukey post hoc tests was used when performing multiple comparisons and $p<0.05$ considered statistically significant. *$p<0.05$

With the goal of simultaneously delivering multiple miRNA constructs, we investigated whether R646 nano-miRs were able to co-deliver two different miRNA mimics (miR-148a and miR-296-5p) to the same cell. To this end, we made nano-miRs containing either Cy3-labeled miRNA, Cy5-labeled miRNA, or both miRNAs (comb.). For nano-miRs containing both miRNAs, we mixed the two anionic RNAs together before adding the cationic polymer for nanoparticle self-assembly to enable miRNA multiplexing. Flow cytometry experiments investigating cellular uptake showed that cells treated with nano-miRs carrying both miRNAs increased proportionally in fluorescence (Figure 3-4A, B). Confocal imaging showed that endosomes in these cells contained both Cy3 and Cy5 fluorescence, confirming that the nano-miRs not only delivered both miRNAs into the same cell but also into the same endosomes, which indicates that two different miRNAs can be complexed into the same nano-miR delivery system (Figure 3-S8A). We also saw detectable levels of diffuse Cy5 fluorescence distributed throughout the cytosol and nucleus at 2h, suggesting that the R646 nano-miRs effectively escaped the endosome (Figure 3-S8B). In contrast, cytosolic RNA molecules have previously been difficult to image with scanning laser confocal microscopy following leading

non-viral gene delivery methods such as lipid nanoparticle mediated delivery.[24-25] We also stained cells treated with Cy5-labeled miRNA nano-miRs with a lysosomal dye (pKa 4.5) and found that endosomes with Cy5 signal did not colocalize with lysosomes at 2h , consistent with efficient endosomal escape prior to detectable lysosomal targeting. Our results show that a significant number of R464 nano-miRs effectively avoided lysosomal degradation and released their miRNA cargo in the cytosol. This is a significant improvement over traditional cationic polymers and nanomedicine delivery systems, for which lysosomal degradation has been a limitation.[26-27] Overall, these results indicate that bioreducible R646 nano-miRs outperformed nano-miRs constructed from non-reducible polymers 646 and C32 by attenuating cytotoxicity, increasing cellular uptake of miRNA cargo, and effectively delivering bio-active miRNAs to the cytoplasm of GBM cells. We therefore chose to use R646 nano-miRs to assess *in vitro* and *in vivo* delivery of our GBM-regulating miRNA mimics.

Mature miRNA mimics labeled with Dy547 were complexed with bioreducible R646 to formulate PBAE nano-miRs and used to transfect multicellular GBM neurospheres. Fluorescence from the Dy547-labeled miRNA was readily detectable in the multicellular spheres starting 3 hrs after the transfection and persisted for at least 9 days (Figure 3-S9A and Figure 3-S19). We recently showed that miR-148a and miR-296-5p are repressed as part of an epigenetic program by which GBM cells become stem-like and tumor propagating.[11-12] We also found that reconstituting these miRNAs individually using viral vectors inhibits the stem cell phenotype and tumor-propagating potential of GBM cells.[11-12] To assess the bioactivity of R646-delivered miRNAs, nano-miRs carrying control miRNA (miR-Ctrl), miR-148a mimic, miR-296-5p mimic, or miR-148a+miR-296-5p (comb.) were used to transfect GBM neurospheres. Total RNA concentrations were held fixed at 120 nM, and miR-148a or miR-296-5p were either blended with miR-Ctrl or one another, so that the total amount of each functional miRNA remained at 60 nM in all conditions.

Expression of mature miRNAs was measured using qRT-PCR 3 days after transfection. Transfecting GBM neurospheres with miR-148a or with miR-296-5p nano-miRs increased intracellular miRNA levels by 24-fold and 27-fold, respectively (Figure 3-4C), and these miRNAs remained substantially elevated (15-20 fold) for up to 12 days (the last time point examined) (Figure 3-S19C). The combination nano-miRs simultaneously increased miR-148a and miR-296-5p levels by 16-fold and 30-fold respectively (Figure 3-4C).

To directly evaluate the effects of these nano-miRs on the GBM stem cell phenotype, two patient-derived neurosphere lines were transfected using nano-miRs and sphere forming capacity, a quantitative marker of cell stemness and self-renewal, was measured. miRNA delivery by this approach significantly inhibited sphere-forming capacity (Figure 3-4E and 3-4F and Figure 3-S9C and 3-S9D) concurrent with the decreased expression of stem cell markers Sox2, Nanog, Bmi1, and Olig2 (Figure 3-4D and Figure 3-S9B) and also inhibited previously described miR-148a and miR-296-5p targets, Dnmt1 and Hmga1, respectively (Figure 3-2C and 3-2D). These results supported the use of our novel bioreducible PBAE polymeric nano-miRs to deliver bio-active miRNAs to GBM xenografts *in vivo*.

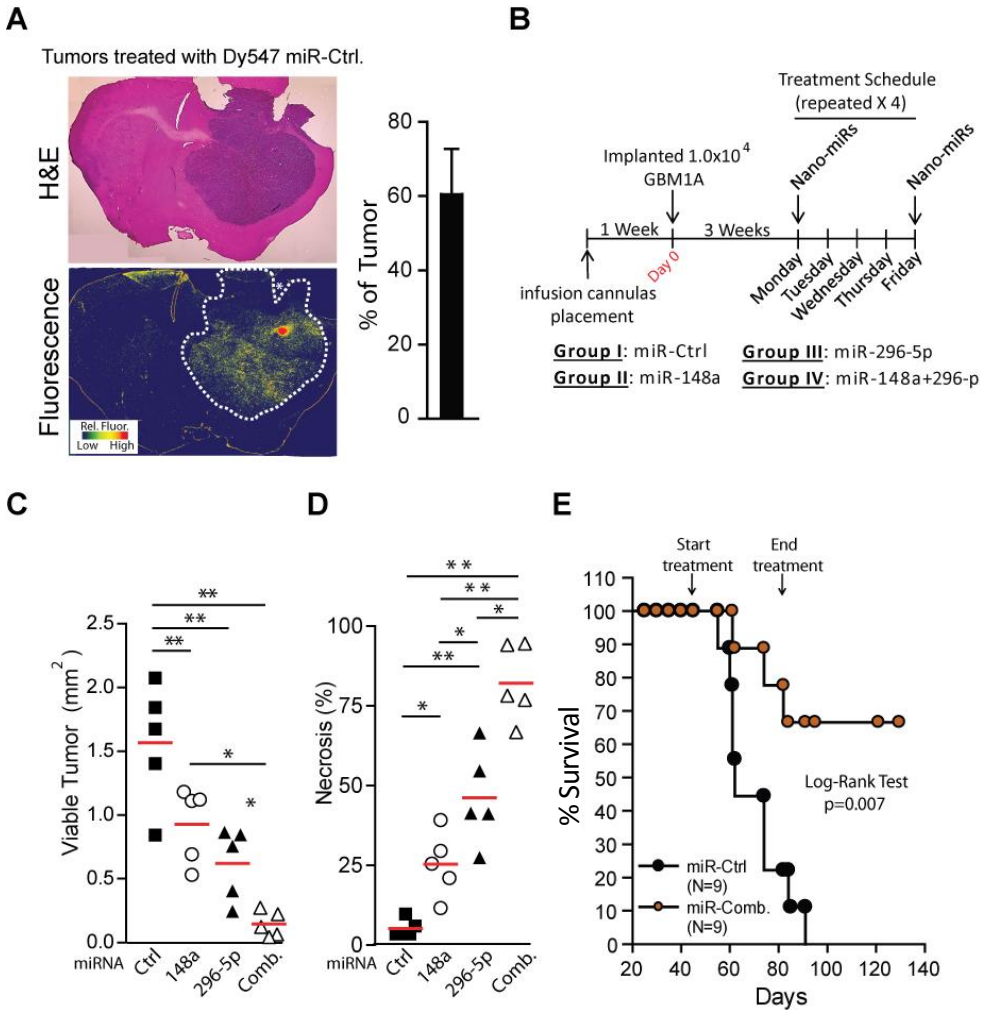

Figure 3-5: miR-148a and miR-296-5p co-delivery using R646 nano-miRs inhibits GBM tumor growth and extends survival *in vivo*. (A) miR-Ctrl labeled with Dy547 was visualized 3 days after the last

infusion using fluorescence microscopy and compared to adjacent H&E stained sections. The intra-tumoral distribution of the nano-miRs was calculated as the ratio of fluorescence area divided by tumor area X 100 in brain sections with the highest cross-sectional area of tumor (N=3 mice per group; right panel). **(B)** Schematic summarizing treatment schedule for *in vivo* delivery of nano-miRs. Animals were sacrificed 42 days after cell implantation and maximum tumor cross-sectional areas following treatment with nano-miRs representing viable tumor tissue **(C)** and necrotic tumor tissue **(D)** were quantified from H&E stained sections using ImageJ software. For each cohort, R646 nano-miRs delivering the bioactive miRNA mimics showed significantly lower viable tumor area and higher necrotic area than the animals receiving control (Ctrl.) nano-miR as assessed by One-way ANOVA with Tukey post hoc tests (**$p<0.01$ and *$p<0.05$). **(E)** Kaplan-Meier survival curves comparing mice treated with control nano-miRs (miR-Ctrl) or miR-148a+miR296-5p nano-miRs (miR-Comb.). Therapy in the survival study was initiated 45 days after tumor cell implantation. Survival was compared across arms using the log-rank test (N=9). (**$p<0.01$, *$p< 0.05$).

Bioreducible PBAE nano-miRs spread through brain tumor xenografts to deliver miRNAs. To circumvent the delivery obstacle posed by the blood brain barrier, we used direct intra-tumoral delivery to test the biological effects of our nano-miRs *in vivo*.[28] Trans-cranial cannulas were placed with their tips within the right caudate/putamen of mice. One week after cannula placement, animals were implanted with Oct4/Sox2 induced cancer stem cells (iCSCs)[11] via the cannula. iCSCs generate aggressive rapidly growing xenografts and represent a demanding model to assess miRNA biodistribution and *in vivo* bioactivities. R646 nano-miR delivery was started 3 weeks after cell implantation. Twice per week for 3 weeks animals received slow infusions of nano-miRs containing either Dy547-labeled control miRNA or miR-148a via the cannula. Brains were collected and histopathologic sections were visualized using fluorescence microscopy and compared to the adjacent H&E stained counterparts. Dy547-labled miRNA was found to be distributed through approximately 60% of these large rapidly growing tumors when evaluated 25 days after the first nano-miR infusion and 3 days after the last infusion (Figure 3-5A). To determine if the miRNAs delivered by this protocol retained their biological function, we measured the expression of Dnmt1 and Dnmt3b, two well

described miR-148a targets.[11] Tumors treated with miR-148a nano-miRs had significantly lower expression levels of both Dnmt1 and Dnmt3b compared to control treated animals (Figure 3-S10). To investigate the therapeutic potential of miRNA delivery using R646 biodegradable PBAE nanoparticles in comparison to ionizing radiation (I.R.), a standard of care treatment modality for GBM, tumors were established as described above and treated with 148a nano-miR +/- I.R. (Figure 3-S11). Intra-tumoral delivery of miR-148a nano-miRs to a pre-established tumor more effectively decreased tumor size and tumor vascularity and increased tumor cell apoptosis as measured by caspase 3 activation than I.R. treatment alone. Combining 148a nano-miRs with I.R. generated cooperative and potentially synergistic anti-tumor responses.

miRNA co-delivery via bioreducible PBAE nano-miRs inhibits tumor growth and prolongs animal survival in an orthotopic model of human GBM. We have recently reported that viral-based transgenic expression of either miR-148a or miR-296-5p differentiated GBM stem cells and inhibited their self-renewal as spheres. We also found that these miRNAs independently inhibit the capacity of GBM stem cells to propagate glioma xenografts *in vivo*.[11-12] We asked if reconstituting both of these stem cell inhibiting miRNAs using non-viral R646 nano-miRs would have cooperative effects on pre-established GBM xenografts. Human GBM derived neurospheres (GBM1A), which generate tumors that closely recapitulate the growth pattern and pathology of clinical GBM,[29] were implanted in animals using an experimental paradigm similar to the one described above (Figure 3-5B). Tumors were then treated with R646 nano-miRs containing control miRNA, miR-148a, miR-296-5p, or a combination of miR-148a+miR-296-5p. Tumor burden in brains collected after 28 days of treatment quantified by computer-assisted morphometry was significantly decreased in all three groups treated with active miRNA, with the most profound effect seen in animals treated with the miRNA combination (Figure 3-5C and Figure 3-S12A). We also saw an increase in tumor tissue necrosis (Figure 3-5D) and apoptosis (Figure 3-S12B), as measured by histopathology and cleaved caspase 3 immunohistochemistry, respectively. We find that while miR cooperativity was limited during *in vitro* evaluation, miR cooperativity is potent *in vivo* and consistent with our understanding of these two miRs targeting complementary tumor-promoting mechanisms. The substantial decrease in tumor burden observed

in mice treated with the multiplex nano-miRs and the more modest effects observed when delivering miR-148a alone in both this patient-derived GBM model and the more aggressive engineered iCSC model predicted the therapeutic survival advantage of miR-148a + miR-296-5p multiplex nano-miRs.

To rigorously test the efficacy of our nano-miR therapy in a survival study, animals bearing pre-established intracranial GBM1A glioma xenografts received either control or miR-148a + miR-296-5p multiplex nano-miRs beginning on post-implantation day 45 and continued twice per week for 6 weeks. Surviving animals began to show signs of weight loss so treatment was stopped after 6 weeks (12 injections) on post-implantation day 87. All treated animals regained weight one week after ending treatment. All 9 animals treated with control nanomiRs were either dead or premorbid requiring euthanasia by post-implantation day 90. In contrast, 6 of 9 nano-miR-treated animals remained alive and healthy by post-implantation day 133, at which time the experiment was terminated (Figure 3-5E). Histological analysis of the surviving animals euthanized at post-implantation day 133 revealed that 4 out of the 6 had no detectable tumor (Figure 3-S13).

Conclusions

There is a need to develop and translate new treatment strategies for glioblastoma that are designed to target the subpopulation of CSCs that drive tumor propagation, therapeutic resistance, and tumor recurrence following conventional treatments.[30] These CSCs are highly plastic and exist in a state of dynamic flux between CSC and non-CSC states.[31] The epigenetic mechanisms driving these phenotypic transitions represent unexploited vulnerabilities amenable to therapeutic biological targeting.[4, 8] Approaches based on the premise that reconstituting CSC-inhibiting miRNA toward the goal of normalizing dysregulated networks in cancer hold great promise.[32] As is becoming evident, miRNAs regulate cell phenotypes by modulating multiple gene targets simultaneously. The broad targetome of naturally occurring miRNAs has numerous advantages over siRNAs that are engineered to target individual genes within multi-genic processes such as CSC regulation.[32] We recently identified two candidate therapeutic miRNAs, miR-148a and miR-296-5p, based on their repression during the induction of GBM stemness and tumor-propagating capacity by Oct4/Sox2.[11-12] We now show that reconstituting these miRNAs using non-viral bioreducible PBAE nano-

miRs offers a therapeutic approach distinct from conventional cytotoxic therapy (e.g ionizing radiation or temozolomide) that has been shown to be insufficiently effective against CSC pools and clinical GBM.[30, 33]

A central challenge to developing nucleic acid-based modalities for targeting tumor-propagating CSCs is identifying and developing a suitable delivery vehicle. An optimal miRNA carrier for intra-tumoral delivery should be able to stably encapsulate miRNA, including combinations of miRNA, and protect it while in the extracellular environment and then quickly release it in the cytosolic environment. Our bioreducible R646 nano-miRs were found to fulfill these requirements. Using a gel retention assay, we were able to show that the R646 nano-miRs fully encapsulated the miRNA in non-bioreducible conditions and then released the miRNA in a triggered manner within 5 minutes when in a cytosol-like reducing environment. The quick intracellular release of miRNA is dually important, as it significantly reduces cytotoxicity compared to non-reducible PBAEs and cationic polymer such as PEI (Figure 3-2A and S4A), allowing higher polymer-to-miRNA weight/weight ratios to be used and smaller, more stable nanoparticles to be formed (Figure 3-3A and S5). Furthermore, it allows the miRNA to enter into cellular pathways necessary for miRNA function.[34-35]

Particle sizing analysis revealed that the R646 nano-miRs are approximately 100 nm in diameter (Figure 3-3A). *In vivo* tumor distribution studies revealed that these nanoparticles can spread through brain tumor tissue following direct intra-tumor infusion, distributing particles through established tumors with at least 60% coverage (Figure 3-5A). This represents a length scale of ~2 mm from the cannula infusion site following a 5 μL infusion to reach the tumor margins. The finding that the nano-miRs could spread through the GBM tumors is consistent with the finding that this treatment led to long-term survivors in the majority of the combination miRNA treated animals (Figure 3-5E). In comparison, non-bioreducible PBAE/DNA nanoparticles delivered via an intratumoral infusion were recently observed to spread through a similar length-scale of approximately 2 mm in 9L rat glioma tumors following a larger volume 25 μL infusion[36] and PEGylated non-bioreducible PBAE/DNA nanoparticles spread through a length-scale of ~2 mm in the brains of Fischer 344 rats following a 20 μL infusion.[37] Thus, for non-viral nucleic acid delivery to brain tumors, the R646 polymeric nanoparticles, small and with relatively neutral surface charge, appear to be potent vehicles that are able to spread through brain tumors sufficiently to have therapeutic effect. In our

current study, the functional efficacy of bioreducible nano-miRs *in vivo* was validated and is especially significant as oligonucleotides are known to be more difficult to deliver by electrostatic polyplex nanoparticles than plasmid DNA molecules are, as oligonucleotides are typically 100-fold smaller and consequently orders of magnitude less multivalent than plasmids.

Once at the surface of individual cancer cells, the nano-miRs are able to be internalized effectively as demonstrated in our *in vitro* cellular uptake studies (Figure 3-2 and Figure 3-S9). Once internalized into a cell, the tertiary amines of the PBAE polymers can facilitate avoidance of lysosomes and endosomal escape by a sufficiently large fraction of nano-miRs that the released miRNA can be detected in the cytosol (Figure 3-1E and Figure 3-S8B). Through these mechanisms, the nano-miRs are able to effectively increase the intracellular levels of multiplexed cargo miRNA 15-30 fold (Figure 3-4C) with retention of anti-CSC bioactivity (Figure 3-4D-F).

Combinations of miRNAs that inhibit multiple pathways required for tumorigenesis should more efficiently impede tumor growth and propagation while at the same time reducing the emergence of resistance.[30, 32] To reduce the possibility of cytostatic effects or tumors developing resistance, we explored two treatment modalities by either combining I.R. treatment with nano-miR-148a delivery or targeting two parallel pathways that contribute to GBM cell stemness and tumor propagation using R646 biodegradable PBAE nanoparticles to co-deliver miR-148a and miR-296-5p. miR-148a nano-miRs and ionizing radiation cooperatively inhibited tumor xenograft growth. This result is consistent with the relative resistance of GSCs to cytotoxic therapeutics and our current and previous findings that miR-148a inhibits GBM cell stemness.[11, 33] Co-delivering both miR-148a and miR-296-5p as multiplexed nano-miRs *in vivo* increased tumor cell death and reduced tumor burden more significantly than either miRNA delivered alone (Figure 3-5 and Figure 3-S13). This cooperative therapeutic effect *in vivo* is consistent with the concept that cancers will be more responsive to strategies designed to target multiple complementary tumor-promoting pathways by normalizing miRNA networks and their multiple targetomes than to single miRNA or highly specific siRNA therapeutics.

To our knowledge, our current report is the first time that a bioreducible PBAE-based system has been evaluated for oligonucleotide delivery *in vivo*. Moreover, it is the first time that PBAE-based nanomaterials have been formulated for miRNA delivery *in vitro* or *in vivo*. The results presented in this study demonstrate the promise of using R646 nano-miR systems in combination with cancer stem cell-inhibitory miRNAs as nanomedicine to impact the development of biological therapies for treating GBM.

Author Contributions

The manuscript was written through contributions of all authors. All authors have given approval to the final version of the manuscript. ‡ Hernando Lopez-Bertoni, Kristen L. Kozielski, Yuan Rui contributed equally.

Funding Sources

The authors would like to thank the following organizations for financial support: American Brain Tumor Association (HLB), the ARCS Foundation (KK), NSF Graduate Research Fellowship DGE-0707427 (DRW) and DGE-1232825 (YR), the Bloomberg~Kimmel Institute for Cancer Immunotherapy (JG), Research to Prevent Blindness / Dr. H. James and Carole Free Catalyst Award (JG), Microscopy Core Grant (S10 OD016374) and the United States NIH grants R01NS073611 (JL), R01EB016721 (JG), F31CA196163 (KK), and R01CA195503 (JG).

References

1. Ostrom, Q. T.; Gittleman, H.; de Blank, P. M.; Finlay, J. L.; Gurney, J. G.; McKean-Cowdin, R.; Stearns, D. S.; Wolff, J. E.; Liu, M.; Wolinsky, Y., et al., *Neuro-oncology* **2016,** *18 Suppl 1*, i1-i50.

2. Seystahl, K.; Wick, W.; Weller, M., *Crit Rev Oncol Hematol* **2016,** *99*, 389-408.

3. Tamai, I.; Tsuji, A., *J Pharm Sci* **2000,** *89* (11), 1371-88.

4. Lopez-Bertoni, H.; Li, Y.; Laterra, J., *Biol Med (Aligarh)* **2015,** *7* (Suppl 2).

5. Patel, A. P.; Tirosh, I.; Trombetta, J. J.; Shalek, A. K.; Gillespie, S. M.; Wakimoto, H.; Cahill, D. P.; Nahed, B. V.; Curry, W. T.; Martuza, R. L., *Science* **2014,** *344* (6190), 1396-1401.

6. Sottoriva, A.; Spiteri, I.; Piccirillo, S. G. M.; Touloumis, A.; Collins, V. P.; Marioni, J. C.; Curtis, C.; Watts, C.; Tavaré, S., *Proc Natl Acad Sci U S A.* **2013,** *110* (10), 4009-4014.

7. Lathia, J. D.; Mack, S. C.; Mulkearns-Hubert, E. E.; Valentim, C. L.; Rich, J. N., *Genes & Dev.* **2015,** *29* (12), 1203-17.

8. Mack, S. C.; Hubert, C. G.; Miller, T. E.; Taylor, M. D.; Rich, J. N., *Nat Neurosci.* **2016,** *19* (1), 10-9.

9. Esquela-Kerscher, A.; Slack, F. J., *Nat Rev Cancer* **2006,** *6* (4), 259-69.

10. Sato, F.; Tsuchiya, S.; Meltzer, S. J.; Shimizu, K., *FEBS J* **2011,** *278* (10), 1598-609.

11. Lopez-Bertoni, H.; Lal, B.; Li, A.; Caplan, M.; Guerrero-Cazares, H.; Eberhart, C. G.; Quinones-Hinojosa, A.; Glas, M.; Scheffler, B.; Laterra, J., et al., *Oncogene* **2014**.

12. Lopez-Bertoni, H.; Lal, B.; Michelson, N.; Guerrero-Cazares, H.; Quinones-Hinojosa, A.; Li, Y.; Laterra, J., *Oncogene* **2016**.

13. Tzeng, S. Y.; Green, J. J., *Ther Deliv* **2013,** *4* (6), 687-704.

14. Thomas, C. E.; Ehrhardt, A.; Kay, M. A., *Nat Rev Genet* **2003,** *4* (5), 346-358.

15. Verma, I. M.; Somia, N., *Nature* **1997,** *389* (6648), 239-242.

16. Wu, G. Y.; Wu, C. H., *J Biol Chem* **1987,** *262* (10), 4429-32.

17. Lynn, D. M.; Langer, R., *J Am Chem Soc* **2000,** *122* (44), 10761-10768.

18. Hagerman, P. J., *Annu Rev Bioph Biom* **1997,** *26*, 139-156.

19. Tzeng, S. Y.; Green, J. J., *Adv Healthc Mater* **2013,** *2* (3), 468-480.

20. Anderson, D. G.; Peng, W.; Akinc, A.; Hossain, N.; Kohn, A.; Padera, R.; Langer, R.; Sawicki, J. A., *Proc Natl Acad Sci U S A* **2004,** *101* (45), 16028-16033.

21. Tzeng, S. Y.; Guerrero-Cázares, H.; Martinez, E. E.; Sunshine, J. C.; Quiñones-Hinojosa, A.; Green, J. J., *Biomaterials* **2011,** *32* (23), 5402-10.

22. Griffith, O. W., *Free Radic Biol Med* **1999,** *27* (9-10), 922-935.

23. Davson, H., **1970**.

24. Wittrup, A.; Ai, A.; Liu, X.; Hamar, P.; Trifonova, R.; Charisse, K.; Manoharan, M.; Kirchhausen, T.; Lieberman, J., *Nature biotechnology* **2015,** *33* (8), 870-876.

25. Gilleron, J.; Querbes, W.; Zeigerer, A.; Borodovsky, A.; Marsico, G.; Schubert, U.; Manygoats, K.; Seifert, S.; Andree, C.; Stöter, M., et al., *Nat Biotechnol* **2013,** *31* (7), 638-46.

26. Wilson, D. R.; Routkevitch, D.; Rui, Y.; Mosenia, A.; Wahlin, K. J.; Quinones-Hinojosa, A.; Zack, D. J.; Green, J. J., *Mol Ther* **2017**.

27. Benjaminsen, R. V.; Mattebjerg, M. A.; Henriksen, J. R.; Moghimi, S. M.; Andresen, T. L., *Mol Ther* **2013,** *21* (1), 149-157.

28. Lal, B.; Xia, S.; Abounader, R.; Laterra, J., *Clin Cancer Res* **2005,** *11* (12), 4479-86.

29. Galli, R.; Binda, E.; Orfanelli, U.; Cipelletti, B.; Gritti, A.; De Vitis, S.; Fiocco, R.; Foroni, C.; Dimeco, F.; Vescovi, A., *Cancer Res* **2004,** *64* (19), 7011-21.

30. Kalkan, R., *Clin Med Insights Oncol* **2015,** *9*, 95-103.

31. Li, Y.; Laterra, J., *Cancer Res* **2012,** *72* (3), 576-80.

32. Rupaimoole, R.; Slack, F. J., *Nat Rev Drug Discov* **2017,** *16* (3), 203-222.

33. Bao, S.; Wu, Q.; McLendon, R. E.; Hao, Y.; Shi, Q.; Hjelmeland, A. B.; Dewhirst, M. W.; Bigner, D. D.; Rich, J. N., *Nature* **2006,** *444* (7120), 756-60.

34. Elbakry, A.; Zaky, A.; Liebl, R.; Rachel, R.; Goepferich, A.; Breunig, M., *Nano Lett* **2009,** *9* (5), 2059-2064.

35. Gary, D. J.; Puri, N.; Won, Y. Y., *J Control Release* **2007,** *121* (1), 64-73.

36. Mangraviti, A.; Tzeng, S. Y.; Kozielski, K. L.; Wang, Y.; Jin, Y.; Gullotti, D.; Pedone, M.; Buaron, N.; Liu, A.; Wilson, D. R., et al., *ACS Nano* **2015,** *9* (2), 1236-49.

37. Mastorakos, P.; Song, E.; Zhang, C.; Berry, S.; Park, H. W.; Kim, Y. E.; Park, J. S.; Lee, S.; Suk, J. S.; Hanes, J., *Small* **2016,** *12* (5), 678-85.

Supplementary:

Materials and Methods

Materials

All chemicals used to synthesize bioreducible monomer disulfanediylbis(ethane-2,1-diyl) diacrylate (BR6) were purchased from Sigma-Aldrich (St. Louis, MO) and used without further purification. All other monomers used for polymer synthesis were purchased from Alfa Aesar (Ward Hill, MA). The following mature miRNA mimics used in the study were purchased from Dharmacon (GE Healthcare): hsa-miR-148a-3p (C-300540-05-0005), hsa-miR-296-5p (C-300659-03-0005), and microRNA Hairpin Inhibitor Transfection Control with Dy547 (IP-004500-01-05). Fluorophore-labeled miRNA mimics were custom synthesized by Sigma-Aldrich (St. Louis, MO): HMC0002_Cy3s and HMC0002_Cy5s. Yo-Pro-1 iodide was purchased from Thermofisher.

GBM neurosphere culture

GBM-derived neurosphere lines (GBM1A and GBM1B) were originally derived and characterized by Vescovi and colleagues [1] and the iCSC line (previously designated A172-iGSC) was developed by us [2]. Neurospheres were cultured in serum-free medium containing DMEM/F-12 (Invitrogen, Carlsbad, CA, USA), supplemented with 1% BSA, 20 ng/ml epidermal growth factor (EGF) and 10 ng/ml fibroblast growth factor (FGF). All cell lines used in the study were tested for mycoplasma and were STR profiled.

Polymer synthesis

Bioreducible monomer BR6 was synthesized as previously described.[3] Briefly, the acrylation of bis(2-hydroxyethyl) disulfide was carried out in tetrahydrofuran (THF) anhydrous conditions with acryloyl chloride as the acrylation reagent and in the presence of triethylamine (TEA). Following overnight reaction at room temperature, the TEA HCl precipitate was removed via filtration, THF was removed via rotary evaporation, and the impure product was dissolved in dichloromethane (DCM). The product was purified using aqueous washes of Na_2CO_3, followed by water, after which DCM was removed via rotary evaporation.

Polymers R646 and 646 were synthesized using a method similar to Kozielski *et al.*[4] in which monomer BR6 or hexane-1,6-diyl diacrylate (B6) was polymerized at a 1.01:1 molar ratio with monomer 4-amino-1-butanol (S4) at 500 mg/mL in THF at 60°C for 24 h. Polymers were endcapped in THF at 100 mg/mL with 0.2 M 2-(3-aminopropylamino)ethanol (E6) at room temperature for 1 h while stirring. Unreacted monomers

were removed by precipitating out polymer using diethyl ether, centrifuging at 3220 RCF, and decanting off ether. This was repeated, and the polymer was stored under vacuum to allow ether to evaporate. Polymer C32 was synthesized using a method similar to Anderson *et al.*[5] in which monomer 1,4-butanediol diacrylate (B4) was polymerized at a 1:1.2 molar ratio with monomer 5-amino-1-pentanol (S5) without solvent at 90°C for 24 h. Unreacted monomers were removed by the ether purification process described above. The final polymer product was dissolved in dimethyl sulfoxide (DMSO) at 100 mg/mL and stored at -20°C under desiccant.

Gel permeation chromatography

All polymers used in this study were dissolved in BHT-stabilized tetrahydrofuran with 5% DMSO and 1% piperidine, filtered through a 0.2 μm PTFE filter, and measured with gel permeation chromatography (Waters, Milford, MA) equipped with styragel column and refractive index detector to determine molecular weight distribution relative to linear polystyrene standards. The calculated M_W, M_N and PDI of all polymers are shown in **Supplemental Table 1**.

^{1}H-NMR

Polymers were dissolved in deuterated chloroform with tetramethylsilane as an internal standard. NMR spectra were acquired using a 500 mHz Bruker NMR and analyzed using TopSpin 3.5 software. NMR spectra for polymers R646, 646 and C32 are shown in Figures 3-S13, 3-S14, and 3-S15, respectively.

YO-PRO®-1 Iodide polymer-miRNA competitive binding assay

miRNA mimic was dissolved at 2 μM in 25 mM NaAc and added to YO-PRO®-1 Iodide dye (1 μM in NaAc) at a 1:2 miRNA: YO-PRO v/v ratio; 75 μL of this solution was distributed to each well of a black opaque 96-well plate. Polymers were also dissolved in NaAc at various concentrations; 25 μL of polymer solution was added to the miRNA/YO-PRO mix at a final concentration 0.5 μM for miRNA and YO-PRO, respectively, and 96 to 6 μg/mL polymer. The solution was mixed by pipetting, incubated at room temperature for 15 minutes while protected from direct light, and YO-PRO fluorescence was read using a BioTek® Synergy 2 multi-mode plate reader. Fluorescence quenching correlates with polymer binding to miRNA and displacing the YO-PRO dye.

pH titrations

All titrations were performed using a SevenEasy pH Meter (Mettler Toledo) with 10 mg of polymer dissolved in 10 mL of 100 mM NaCl acidified with HCL as previously described[6]. Polymer was then titrated from pH 3.0 to pH 11.0 using 100 mM NaOH added stepwise with pH of the solution recorded after each addition.

Cytotoxicity

GBM1A neurospheres were dissociated into single cells and plated on laminin-coated 96-well tissue culture plates (15,000 cells/well, 100 μL medium/well) and allowed to adhere for 48 hours. Polymers were dissolved in NaAc at the desired concentration and added to Dy547-labeled control miRNA (miCtrl) in a 1:1 volume ratio. The solution was mixed by pipetting and nano-miRs were allowed to form for 10 minutes. The resulting nano-miRs were added directly to the cell culture medium at a final RNA concentration of 90 nM and final polymer-miRNA weight ratios (w/w) of 150, 110, 75, and 37. Nano-miRs were incubated with the cells at 37°C for 2 hours, after which the particles and cell culture media were removed and fresh media was added. 24 hours after transfection, an MTS assay (CellTiter Aqueous One, Promega, Madison, WI) was performed according to manufacturer's instructions.

Nanoparticle uptake

Cy5-labeled miRNA mimic was diluted with unlabeled miRNA to a final concentration of 20% labeled miRNA by weight. Transfections were then carried out using a final miRNA dose of 90 nM with viability optimized w/w ratios for each nano-miR ratio of 150 w/w for R646 and 37 w/w for 646 and C32 (15,000 cells/well, 100 μL medium/well). Following a 2-hour incubation period, cell culture medium containing nanoparticles were removed and cells were gently washed with PBS. Cells were then detached from the plate using Accutase® Cell Detachment Solution (Sigma-Aldrich), diluted in FACS buffer (2% FBS in PBS), and pelleted by centrifugation. In a duplicate set of plates, cells were washed again with heparin in 150 mM PBS (50 μg/mL) to remove surface associated but non-endocytosed nanoparticles [7]. Heparin washing was shown to remove a fraction of polyplexes (Figure 3-S16). All cells were then analyzed using high-throughput flow cytometry. Cellular uptake was quantified using the geometric mean of fluorescence from each well using the

Cy5 signal from the FL4 detector (emission: 675/25 nm). The persistence of the cellular uptake of fluorescently labeled miRNA was evaluated over time (Figure 3-S17).

Confocal microscopy

GBM1A cells were plated on laminin coated Nunc Lab-Tek chambered borosilicate coverglass well plates (155411; Thermo Fisher) at 37,500 cells/well 48 hours prior to imaging. R646 nano-miRs were formed with Cy3-miRNA, Cy5-miRNA, or both at a miRNA dose of 90 nM per well and 150 w/w. After one hour of incubation, cells were gently washed to remove polyplex nanoparticles and stained for imaging. Nuclei were stained with Hoechst 33342 (1:2000 dilution) and lysosomes were labeled with Cell Navigator Lysosome Staining dye (AAT Bioquest, Sunnyvale, CA) that has a pKa of 4.5 to accumulate in acidic vesicles. Excess stain was washed away and cells were imaged in live cell imaging solution at 37°C in 5% CO_2. Images were acquired with equal exposure times using a Zeiss LSM 780 microscope with Zen software and 63x oil immersion lens. Specific laser channels used were 405 nm diode, 488 nm argon, 561 nm solid-state, and 639 nm diode lasers.

Functional delivery of bio-active miRNAs in vitro

GBM1A cells were transfected as described above with nano-miRs carrying Dy547-labeled control miRNA (miCtrl), or a combination of miR-148a+miR-296-5p (Comb.). A final miRNA dose of 90 nM was used (for Comb. nano-miRs, miR-148a and miR-296-5p were each at a final concentration of 45 nM) and polymer-miRNA w/w ratios of 150 and 37 were tested. Cells were incubated with nano-miRs for 2 hours and harvested 3 days after transfection; qRT-PCR analysis of Dnmt1 and Hmga1 – targets of miR-148a and miR-296-5p – was performed to assess miRNA delivery efficacy. R646 combination miR-148a and miR-296-5p nano-miRs were also found to reduce cell numbers without drastically inducing cell death (Figure 3-S18).

Optimization and* in vitro *screening of standard transfection reagents

BPEI 25 kDa (Sigma Aldrich) was dissolved in 150 mM sodium chloride and mixed with miRNA to yield polyplexes at weight ratios between 0.5 to 32 of BPEI to miRNA. Polyplexes were added to GBM1A cells to give a miRNA concentration of 90 nM and incubated for two hours, after which media was fully changed. Cellular viability was assessed by MTT assay 24 hours later to select a permissible BPEI concentration (Figure

3-S3). At the BPEI concentration that had ≥ 75% viability (1 w/w) and miRNA dose of 90 nM was selected for *in vitro* delivery of bio-active miRNA experiments (as described above).

Commercial reagents Lipofectamine™ 3000 and Lipofectamine™ RNAiMAX (ThermoFisher) were used according to manufacturer's instructions.

Transmission Electron Microscopy

Nano-miRs were synthesized as described above. The solution was placed onto a carbon-coated copper 400 mesh TEM grid and allowed to settle for 30 minutes. Grids were then counter-stained with uranyl acetate (0.5% in distilled water) for 3 minutes, and allowed to dry. Particles were imaged using a Philips/FEI BioTwin CM120 transmission electron microscope.

Nanoparticle Tracking Analysis

Nano-miRs were prepared as described above and diluted in PBS at a 1:500 v/v ratio prior to loading particles into a NanoSight NS300. Particles were tracked and their size and concentration determined using NanoSight NTA 3.2 software. All measurements were repeated with three samples of nano-miRs to determine batch-to-batch variability. All particle concentrations represented are scaled so that they report the number of particles per volume that would be present in the *in vitro* transfection wells. The loading of miRNA molecules per particle was calculated by dividing the dose of miRNA in each transfection by the number of particles per well **(**Table 3-S3).

Dynamic Light Scattering

Nano-miRs were prepared as described above. Nano-miR size was measured using Dynamic Light Scattering (DLS) via a Malvern Zetasizer NanoZS immediately after particle formation in 25 mM NaAc and after dilution in PBS at a 1:6 v/v ratio. Zeta potential was measured by electrophoretic light scattering using a Malvern Zetasizer NanoZS and analyzed with the Smoluchowski model. Nano-miRs were measured from three separate formulations to account for synthesis variability. Nano-miR hydrodynamic diameter is reported as the mean ± SEM of the Z-average diameter.

Gel retention analysis of nano-miRs in non-reducing vs. reducing conditions

Nano-miRs were formed as previously described, and diluted at a 1:100 v/v ratio in either artificial cerebrospinal fluid (aCSF) or PBS containing 5 mM glutathione (GSH). aCSF is a solution of ions that mimics the ionic composition of human CSF [8]. Glutathione is present in human cells' cytosol in concentrations ranging from 1 – 8 mM, while extracellular concentrations range from 5 – 50 μM.[9] Nano-miRs were incubated in either solution at 37°C while shaking, and samples were removed at 0 min, 5 min, 15 min, 30 min, and 2 h for particles incubated in 5 mM GSH, and 30 min, 2 h, 5 h, 7.5 h, and 10 h for particles incubated in aCSF. Upon removal of the nano-miRs, 30 mg/mL sucrose was added as a cryoprotectant, and samples were frozen at -80°C to stop the polymer degradation reaction. Particles were thawed and loaded into a 1% w/v agarose gel containing 1 μg/mL ethidium bromide and electrophoresed at 100 mV for 15 min, after which gels were visualized using UV light exposure.

Nano-miR lyophilization

Nano-miRs were formed as previously described in 25 mM NaAc buffer, pH 5.0 by mixing solutions of R646 polymer and miRNA in a 1:1 ratio. Because injection volume is limited for *in* vivo delivery, nano-miRs for all lyophilized samples were synthesized using the same polymer to miRNA w/w ratio as in all earlier studies (150 w/w), but the total polymer concentration was 5 mg/mL to enable a higher dose to be delivered in the limited cannula injection volume. Endotoxin free sucrose initially dissolved at 500 mg/mL was then added to the nano-miRs for a final concentration of 30 mg/mL sucrose as a cryoprotectant. Nano-miRs were then aliquoted to tubes and frozen at -80°C and lyophilized overnight at ~20 Pa and -45°C. For *in vitro* characterization and *in vivo* utilization, lyophilized nano-miRs were resuspended using deionized water to a final polymer concentration of 16.7 mg/mL and a final isotonic sucrose concentration of 100 mg/mL.

qRT-PCR and miRNA expression

Total RNA was extracted from cells using RNeasy Mini Kit (Qiagen). cDNA was made by reverse-transcribing 1 μg of total RNA using MuLV Reverse Transcriptase and Oligo (dT) primers (Applied Biosystems). qRT-PCR was performed with a Bio-Rad CFX detection System (Bio-Rad) and expression of target genes was measured using Power SYBR green PCR kit (Applied Biosystems). Samples were amplified in

triplicate and relative gene expression was analyzed using Bio-Rad CFX manager software and normalized to 18S RNA. Primer sequences used were previously described [2, 10].

For miRNA analysis, total RNA including small RNA was extracted using miRNeasy kit and 1 μg of total RNA was used as template to generate cDNA using miScript II RT kit according to manufacturer's protocol. Mature miRNA expression was detected using miScript SYBR green PCR kit using probes for RNU6 (Cat.# MS00033740), miR-148a (MS00003556), and miR-296-5p (Cat. # MS00016401). All kits and probes used to detect mature miRNAs were purchased from Qiagen.

Fluorescence imaging of intra-tumoral nanoparticle distribution

To determine intra-tumor distribution of Dy547-labeled control nano-miRs, we took overlapping images of the tumor sections using 10X magnification. The fluorescent threshold was set automatically by the Q-Capture Pro software (Q-Imaging Corp.) using the tumor margin most distal to the injection site as reference. All the images were taken using the same parameters (35-40 pictures per section) and subsequently merged and subject to background reduction and smoothening using the Photomerge function in Adobe Photoshop. Background fluorescence was minimized by subtracting the fluorescence signal of images of control brains (not infused with nanoparticles) from that of images of brains infused with nanoparticles. Total tumor areas as defined by H&E staining were compared to the fluorescing areas and expressed as % of tumor.

Intra-cranial nano-miR delivery

The procedure for intra-cranial cannula implantation was adapted from Moreno-Estelles et. al. [11] Stainless steel guide and dummy cannulas were custom ordered from PlasticsOne (Roanoke, VA). The guide cannula (26 gauge) was designed to have a Decon® mesh under the pedestal and cut 3 mm from the mesh. The guide cannula is capped with a screw-on dummy cannula 6.5 mm long so that a 0.5 mm projection extends past the guide to prevent blockage. Prior to surgical placement of cannulas, mice were anesthetized using a Ketamine (100mg/Kg)/Xylazine (10mg/kg) cocktail and mounted on a stereotactic frame. A rostro-caudal incision was made with a scalpel, the skin is spread apart, the surface of the skull was exposed, and

cannulas were placed at coordinates: AP (antero-posterior) 0.0 (0 mm from bregma), L (lateral) 0.8 (0.8 mm right from mid-sagital line).

Lyophilized and resuspended nano-miRs were slowly infused (5□ L) into the brains (0.5□ L/min with a 2 min wait at the end) twice a week as described for each experiment. At the end of the experiment animals were anesthetized and then sacrificed by perfusion using 4% paraformaldehyde (PFA) according to methods approved by the Animal Use and Care Committee at Johns Hopkins University. All the sectioning and histological analysis was performed in-house. Whole brains were collected and soaked in 4% PFA for 2 days then washed 1X with PBS and soaked in 30% sucrose over-night at 4°C then flash frozen using dry ice. Brains were embedded in Tissue-Tek® O.C.T. Compound (VWR, Radnor, PA) and 20 □ m sections were cut using the CryoStat system from Microm (Walldorf, Germany). All tumor sections were analyzed by a neuropahologist in a blinded fashion. For ionizing radiation experiments, a subset of animals received radiation either alone or in combination with the nano-miR therapy. Radiation was administered starting 3 weeks after tumor cell implantation. Tumor-bearing mice were gently restrained in a 50ml ventilated plastic centrifuge tube encapsulated in lead cylinders to protect normal body parts from radiation. This ensures only the tumor-bearing brain will be irradiated. Animals received 300 cGy (or sham irradiation) once a week for 3 weeks using a collimator ^{137}Cs source. These radiation doses were without adverse side effects.

Necrosis and apoptosis quantification

Tumor sections were analyzed by a neuropathologist for histologic features of GBM and areas of necrosis and apoptosis. To measure apoptosis, tissue sections were subject to Immunohistochemical staining using cleaved Caspase 3 antibody (Cell Signaling, #9664) and positive cells per field were counted from pictures taken using 10X magnification and an automated ImageJ script. To measure necrosis, the total area of tumor and the necrotic area within each tumor were identified by an expert neuropathologist (Dr. Charles G. Eberhart) and quantified using ImageJ software from images taken at 10X magnification and represented as (area of necrotic tissue/area of total tumor tissue)*100.

Tumor formation in vivo and animal survival

A transcranial cannula was placed so that the tip is in the right caudate/putamen of female athymic nude NCR Nu/Nu mice (8-week old). One week after cannula placement, animals received either GBM1A or iCSC tumor propagating stem cells ($1.0x10^4$ neurospheres) via the cannula and assigned into different treatment groups in a non-blinded, randomized manner [11]. Using the same cannula, the control cohort received nano-miRs loaded with control miRNA labeled with Dy547 and the experimental group received nano-miRs loaded with the indicated miRNAs.

The number of animals used for each experiment is indicated in the corresponding figure legend. Tumor growth inhibition was determined by computer-assisted morphometric quantification of tumor area in H&E-stained histologic sections using ImageJ software and volumes calculated using volume = (square root of maximum cross-sectional area)^3 as previously described [12]. Data for all *in vivo* experiments are shown as the mean tumor area distribution of all animals used in the study. All animal procedures were approved by the Johns Hopkins Institutional Animal Care and Use Committee (Protocol# MO14M307), and were in accordance with the NIH Guide for the Care and Use of Laboratory Animals.

Statistical Analysis

All experiments were performed in triplicates and repeated at least twice in each cell model ($N \geq 6$). Two group comparisons were analyzed for variation and significance using a two-tailed, type 1 *t*-test and *p* values lower than 0.05 were considered significant and symbolized by an asterisk in the graphs. One-way ANOVA with Tukey post hoc tests were used to analyze experiments with multiple simultaneous comparisons. Survival data was compiled using the Kaplan-Meier methodology and compared across arms using the log-rank test (Mantel-Cox), with *p* values lower than 0.05 was considered statistically significant.

Supplemental Figures:

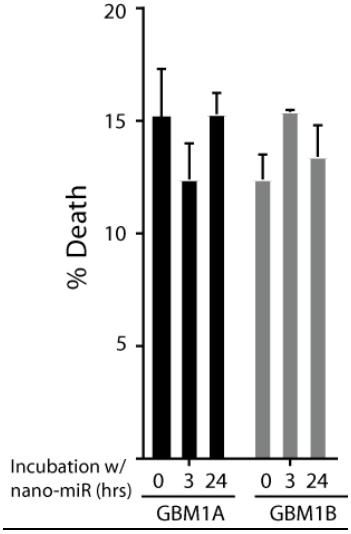

Figure 3-S1: GBM1A and GBM1B neurospheres were dissociated into single cells and transfected with nano-miRs carrying miR-Ctrl (120 nM) using R646 polymer (150 w/w). Cell death was measured using trypan blue exclusion 3hrs and 24hrs after incubation with nano-miRs.

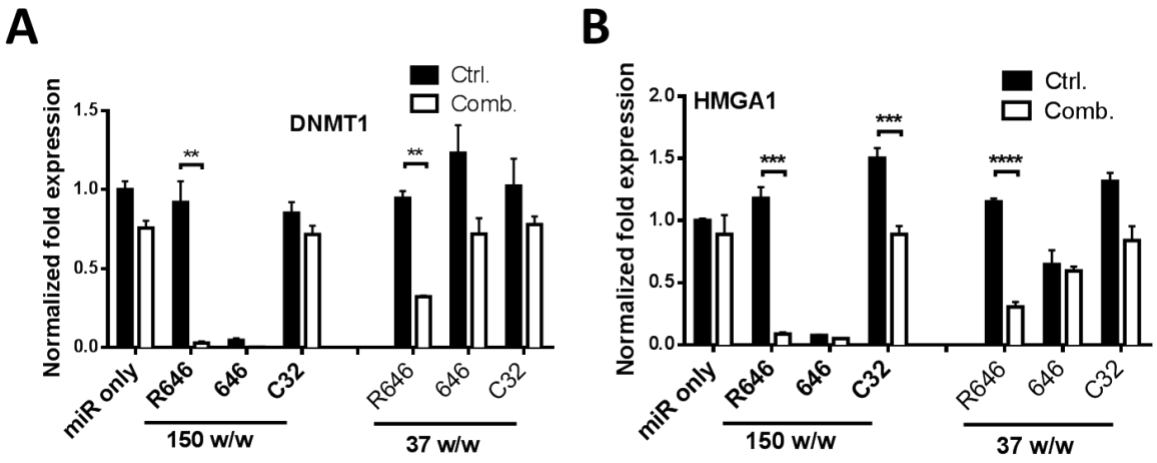

Figure 3-S2. Functional screen results of different nano-miR formulations delivering a non-targeting control (Ctrl) or a combination of miRNA mimics miR-148a and miR-296-5p. Effects on expression of miRNA-target genes, DNMT1 and HMGA1, are shown. **p<0.01, ***p<0.001, and ****p<0.0001

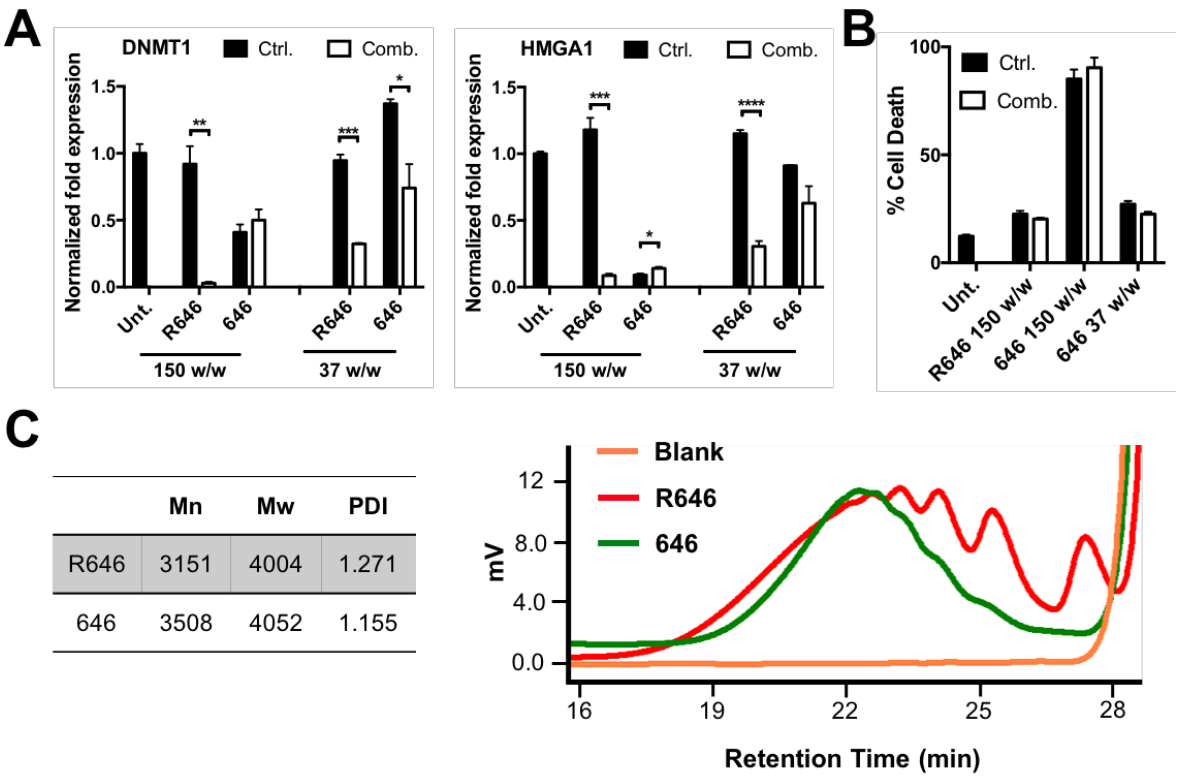

Figure 3-S3. Functional screen using R646 and 646 polymers of similar molecular weight. Nano-miRs were used to deliver a non-targeting control (Ctrl) or a combination of miRNA mimics miR-148a and miR-296-5p (Comb). **(A)** Effects on expression of miRNA-target genes, DNMT1 and HMGA1, are shown. *p<0.05, **p<0.01, ***p<0.001, and ****p<0.0001. **(B)** Cell viability measured 3 days post-transfection. **(C)** GPC data for the two polymers used in this experiment.

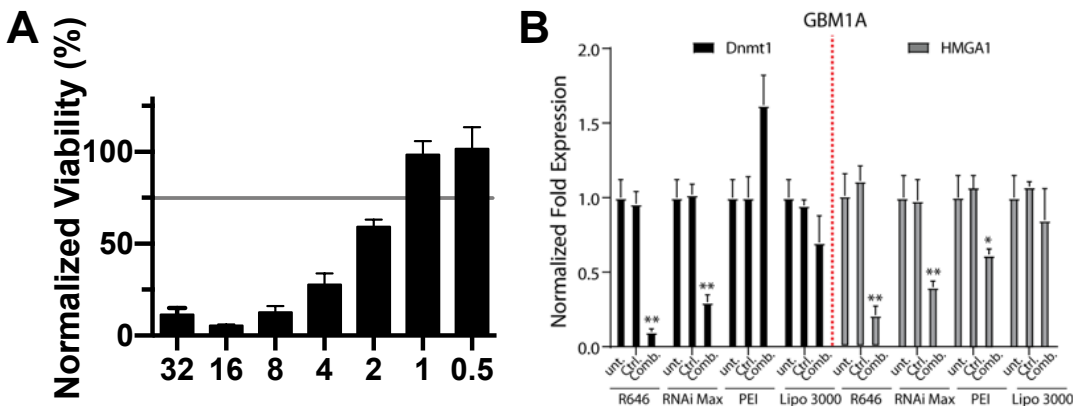

Figure 3-S4. *in vitro* screening of standard transfection reagents PEI, Lipofectamine 3000, and RNAiMAX. **(A)** PEI-miRNA formulations were screened in GBM1A cells to identify optimal formulations with >75% relative viability. Numbers on the x-axis indicate polymer-miRNA w/w ratios. **(B)** Functional delivery of a non-targeting control (Ctrl) or a combination of miRNA mimics miR-148a and miR-296-5p by standard transfection reagents as assessed by qRT-PCR quantification of the expression of miRNA target genes DNMT1 and HMGA1. All results are normalized to the untreated control (unt.).

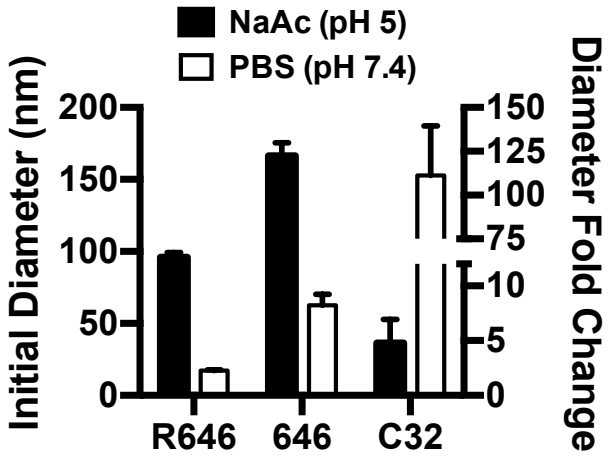

Figure 3-S5: Nano-miR size in different pH and molarity buffers. DLS measurement of nano-miR size in 25 mM sodium acetate (pH 5) and fold change in diameter after 1:6 dilution in 150 mM PBS (pH 7.4) show different nano-miR response to changes in buffer pH and salt content.

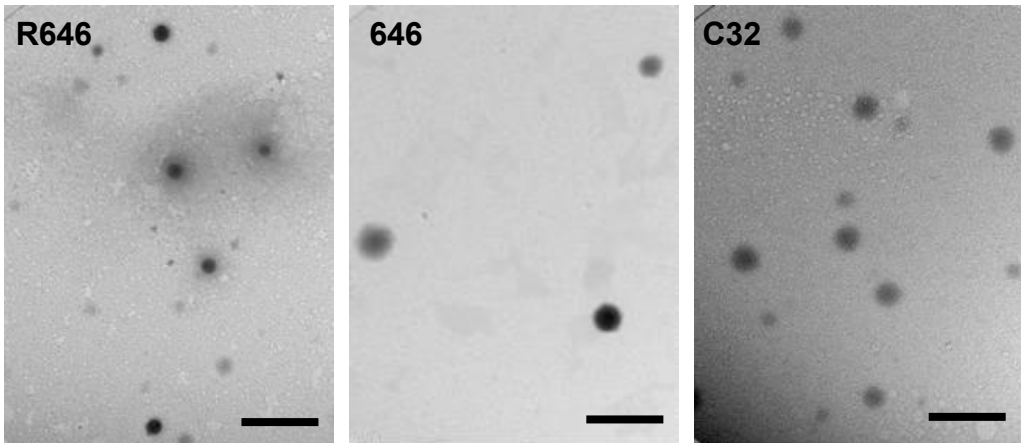

Figure 3-S6: Additional TEM images showing nano-miR dried size and spherical morphology. Scale bar 400 nm.

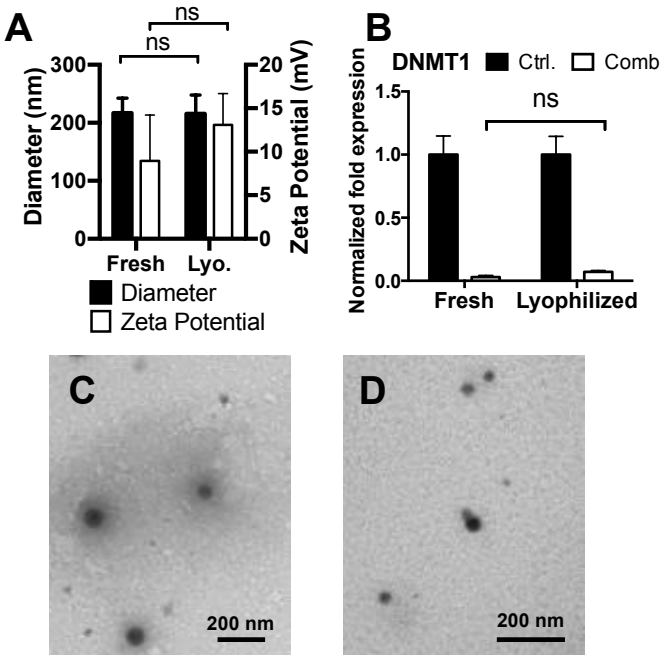

Figure 3-S7: The increased polymer concentration and lyophilization process involved in making nano-miRs does not change their physical properties and miRNA delivery capabilities. **(A)** Fresh and lyophilized R646 nano-miR showed no statistical difference ($p > 0.05$) in size or zeta potential. **(B)** Functional delivery of miRNA mimics using fresh or lyophilized nano-miRs resulted the same level of knockdown of the target DNMT1. TEM images of fresh **(C)** and lyophilized **(D)** nano-miRs show similar size and morphology.

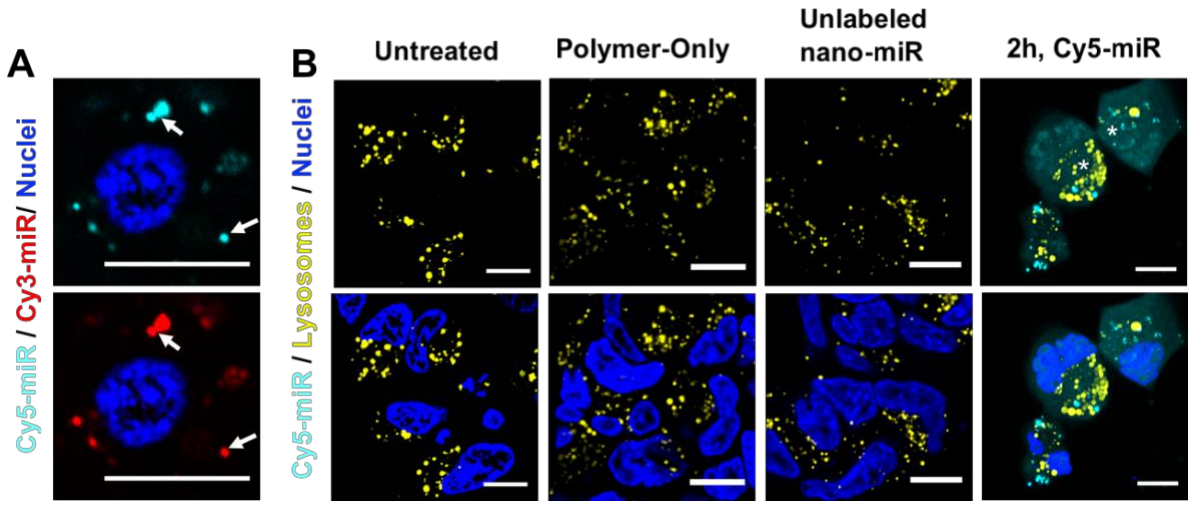

Figure 3-S8. R646 nanoparticles can deliver multiple different miRNAs to the same cell and escape from endosomes. Confocal microscopy images of cells treated with (A) R646 nano-miRs carrying Cy3 (red) and Cy5 (cyan) labeled miRNAs show endosomal colocalization (indicated by white arrows) two hours following uptake. (B) Nano-miRs carrying Cy5 labeled miRNA (cyan) avoid lysosomes (yellow) at two hours after uptake. Cytosolic miRNA was detectable at two hours after uptake compared to controls (white asterisk). Scale bars are 10 μm.

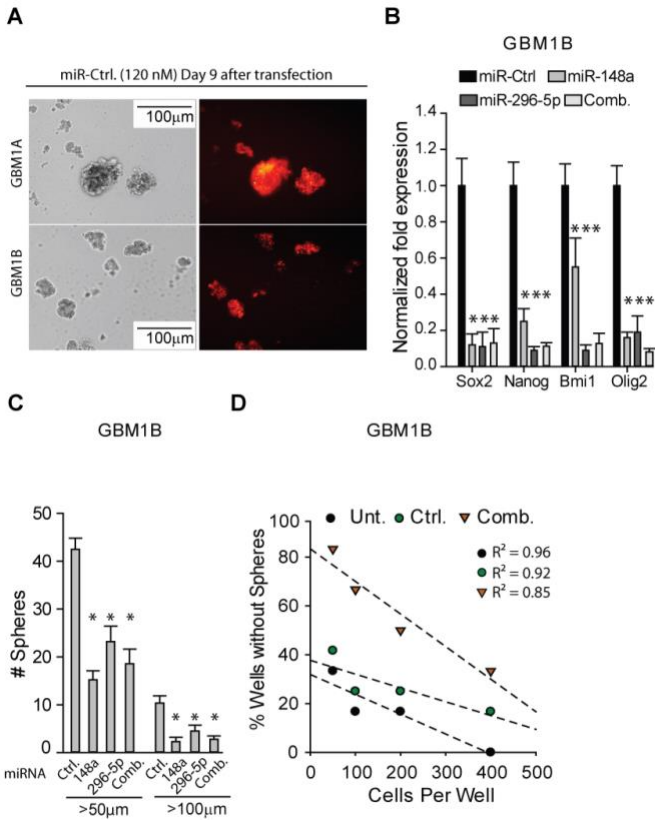

Figure 3-S9: R646 nano-miRs inhibit the GBM stem cell phenotype. GBM1A and GBM1B neurospheres were dissociated into single cells, seeded onto plates pre-treated with Poly-L-Lysine and transfected as described in the ***Methods*** section with nano-miRs carrying miR-Ctrl, miR-148a, miR-296-5p, or the combination (120 nM) using R646 polymer (150 w/w). **(A)** Nano-miR-Ctrl labeled with Dy547 was visualized in the enlarging multicellular spheres 9 days after transfection using fluorescence microscopy. **(B)** qRT-PCR analysis to measure expression of stem cell markers in GBM1B neurospheres transfected with nano-miRs. **(C)** Equal numbers of GBM1B cells transfected with nano-miRs were cultured in neurosphere medium containing EGF/FGF for 12 days and neurosphere numbers (>100μm diameter) were quantified by computer-assisted image analysis. **(D)** Limiting dilution analyses of GBM1B cells transfected with control (Ctrl.) or miR-148a+miR-296-5p combination (Comb.) nano-miRs. Untransfected cells (Unt.) were used as negative control. Cells were plated in a limiting dilution manner, and the number of wells containing spheres was counted after 14 days to compare stem cell frequencies. One-way ANOVA with Tukey post hoc tests was used when performing multiple comparisons and $p<0.05$ considered statistically significant.* $p<0.05$

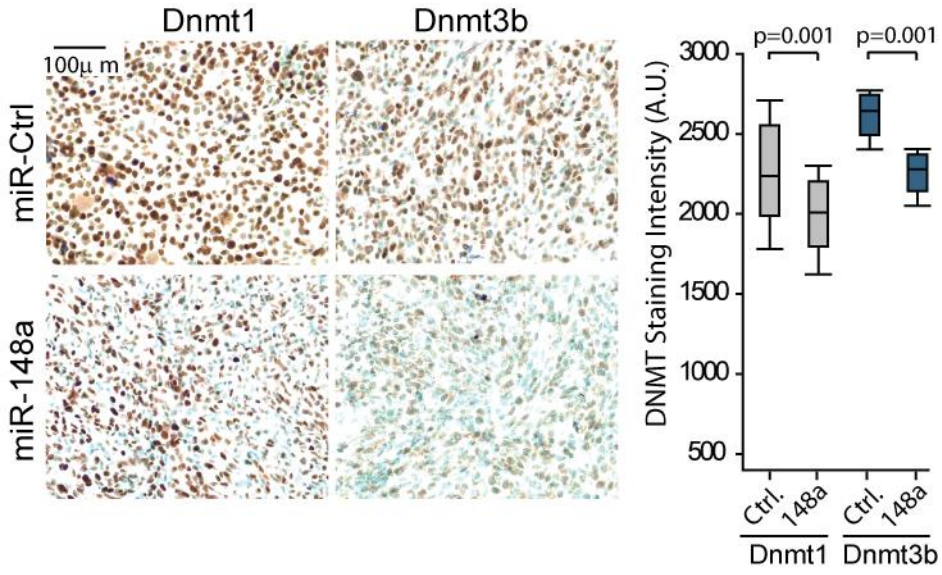

Figure 3-S10: miR-148a delivery using R646 nano-miRs reduces DNMT1 and DNMT3B expression *in vivo*. Immunohistochemical analysis of Dnmt1 and Dnmt3b in tumor sections treated with miR-Ctrl or miR-148a (left panel). Quantification of Dnmt1 and Dnmt3b expression in tumor sections treated with miR-Ctrl. or miR-148a using computer-assisted densitometry analysis (right panel; N=4 mice per group).

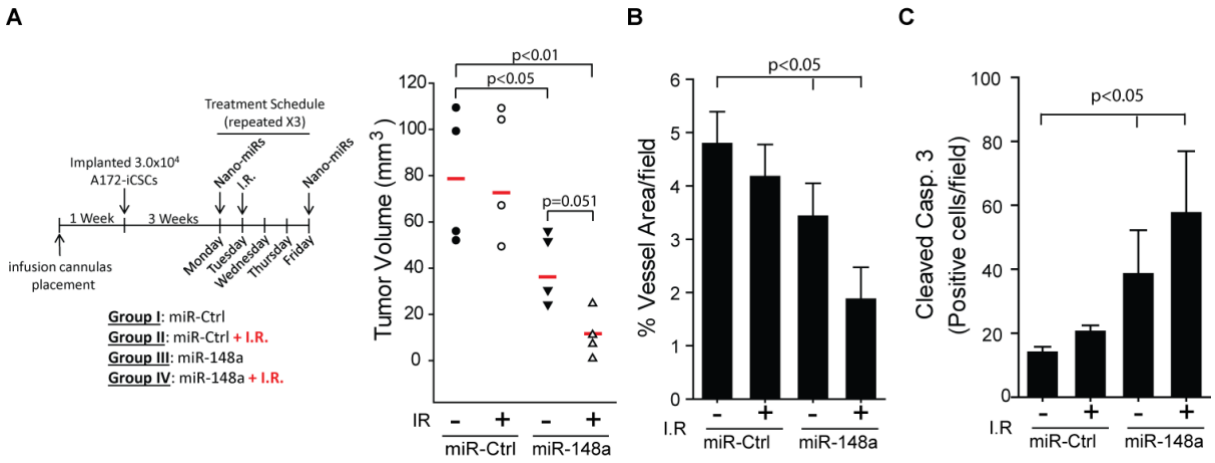

Figure 3-S11: miR-148a delivery using R646 nano-miRs reduces GBM tumor growth *in vivo* and enhances response to ionizing radiation (I.R.) as a standard of care. **(A) Left panel:** Schematic outlining *in vivo* experimental procedure. **Right panel:** Tumor-bearing animals received control nano-miR, 148a nano-miR, control nano-miR+I.R. (300 cGy/dose X 3), or 148a nano-miR+I.R as shown. Maximum tumor cross-sectional areas were determined in H&E stained sections using ImageJ software and tumor volumes calculated as described in *Materials and Methods*. Vessel density **(B)** and Apoptotic index **(C)** were measured in tumor sections by analysis of anti-laminin and anti-cleaved caspase 3 immunohistochemistry, respectively. One-way ANOVA with Tukey post hoc tests was used when performing multiple comparisons and $p<0.05$ considered statistically significant.

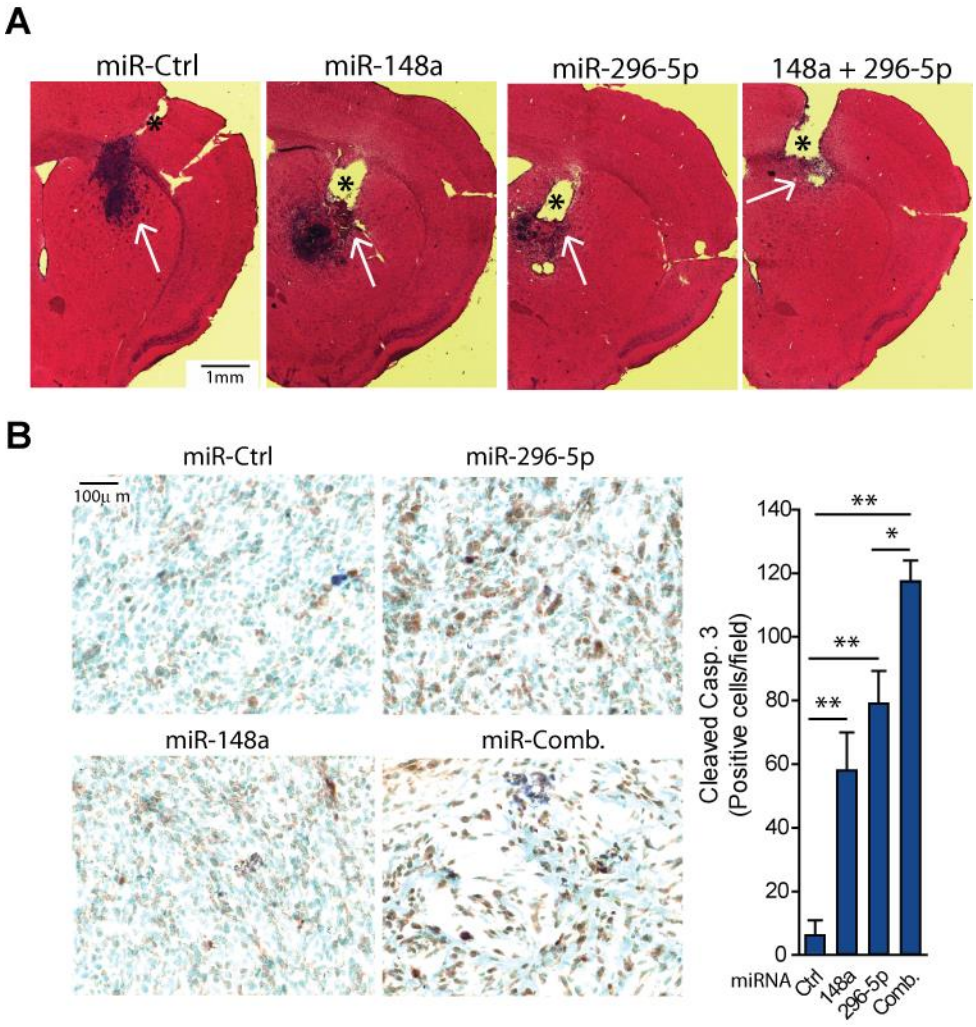

Figure 3-S12: miR-148a and miR-296-5p co-delivery using R646 nano-miRs inhibits GBM tumor growth. **(A)** Representative H&E stained brain sections from mice implanted with GBM1A neurosphere cells (N=5 for each group) treated with the indicated nano-miRs (* marks infusion cannula tracks). **(B)** Apoptotic index was measured in tumor sections by analysis of anti-cleaved caspase 3 immunohistochemistry. One-way ANOVA with Tukey post hoc tests was used when performing multiple comparisons and $p<0.05$ considered statistically significant. (**$p<0.01$, *$p< 0.05$).

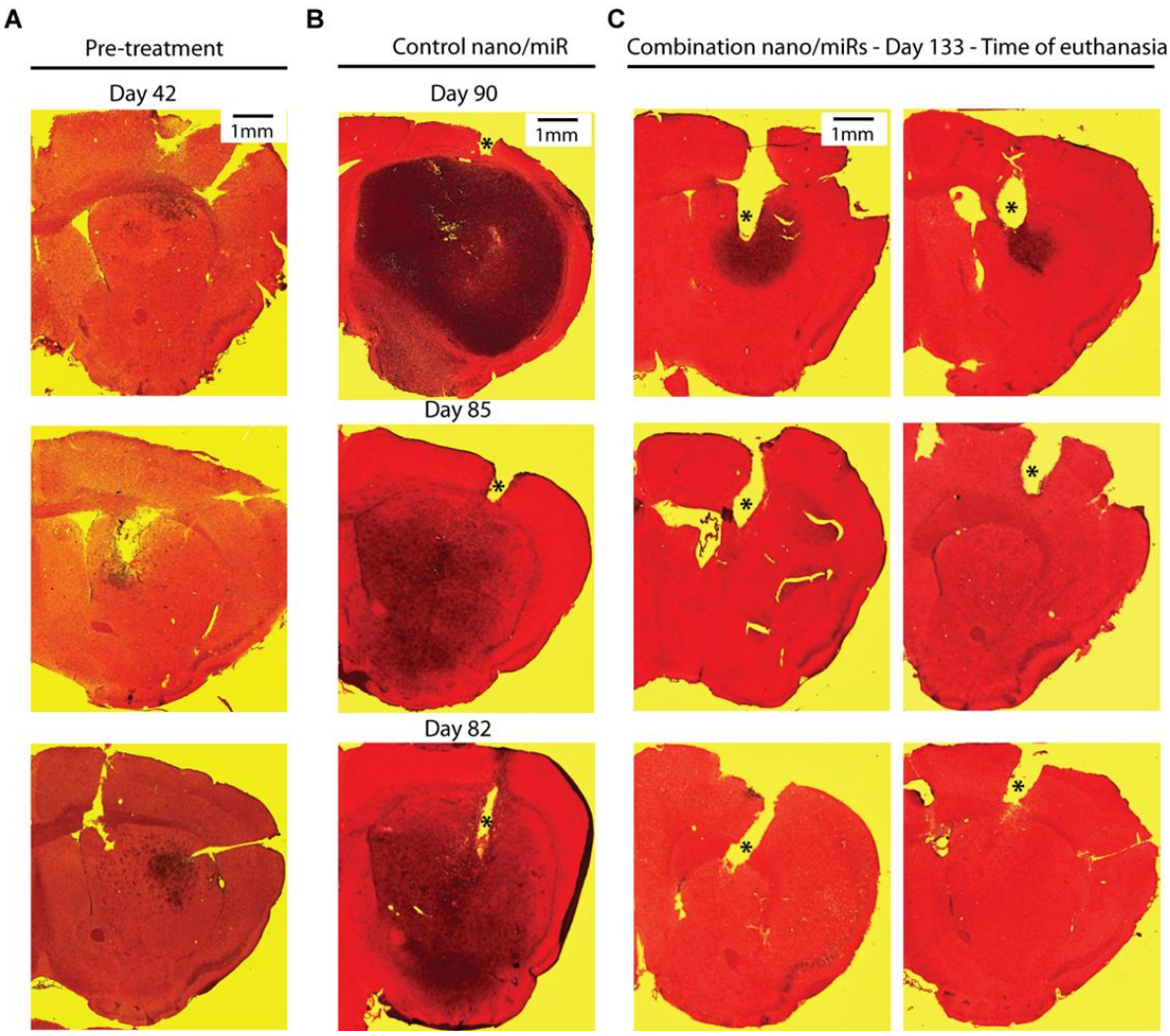

Figure 3-S13: Histological analysis of brains collected from survival study. Representative H&E stained sections showing the histology of the tumors **(A)** 42 days post-implantation before starting treatment, **(B)** the last 3 animals that died in the control group, **(C)** and the 6 long-term survivors. The * marks infusion cannula tracks.

Polymer	M_N	M_W	PDI
R646	2949	3978	1.349
646	5317	7313	1.375
C32	5630	10491	1.863

Table 3-S1: Gel permeation chromatography (GPC) results indicating the number average (M_N) and weight average (M_W) molecular weight and polydispersity (PDI) of each polymer.

A

	Reducible R646			Non-reducible 646		
	Mn	Mw	PDI	Mn	Mw	PDI
Pre-endcap	2052	2430	1.184	2517	3212	1.276
Post-endcap, no ether wash	1955	2276	1.162	2457	3061	1.231
Post-endcap, ether wash	2162	2731	1.263	3047	3617	1.273

B

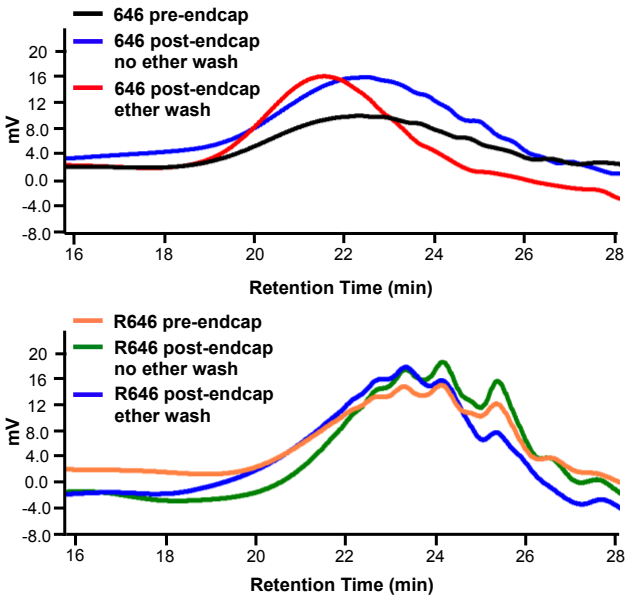

Figure 3-S14: Gel permeation chromatography (GPC) experiments determining the effect of polymer endcapping on molecular weight. The molecular weight of bioreducible R646 and non-reducible 646 were characterized at each step of the polymer synthesis process. **(A)** Molecular weight data and **(B)** GPC traces are shown.

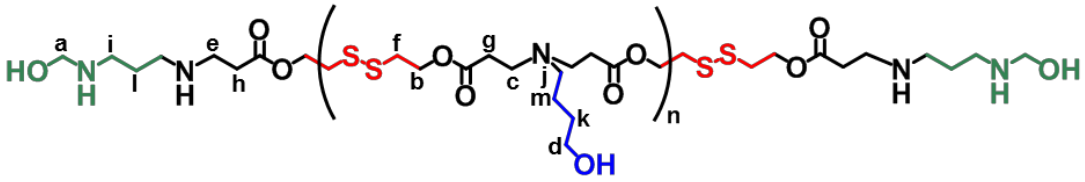

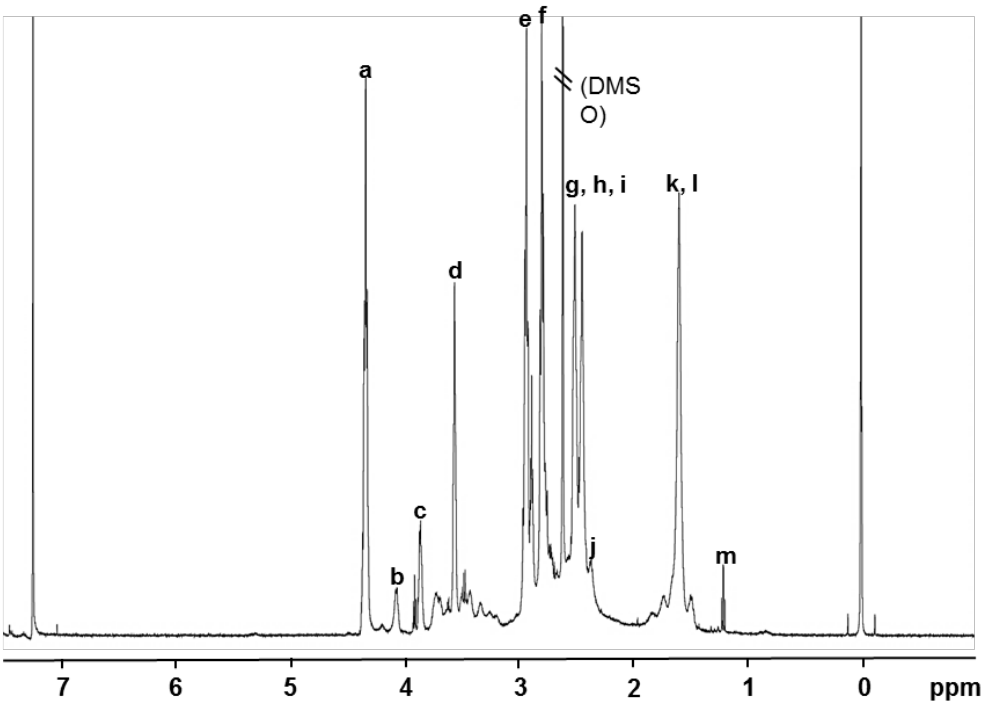

Figure 3-S15: H^1-NMR spectrum of polymer R646 ($CDCl_3$, 500 MHz). Proton peaks are labeled with letters corresponding to protons on the structure of R646.

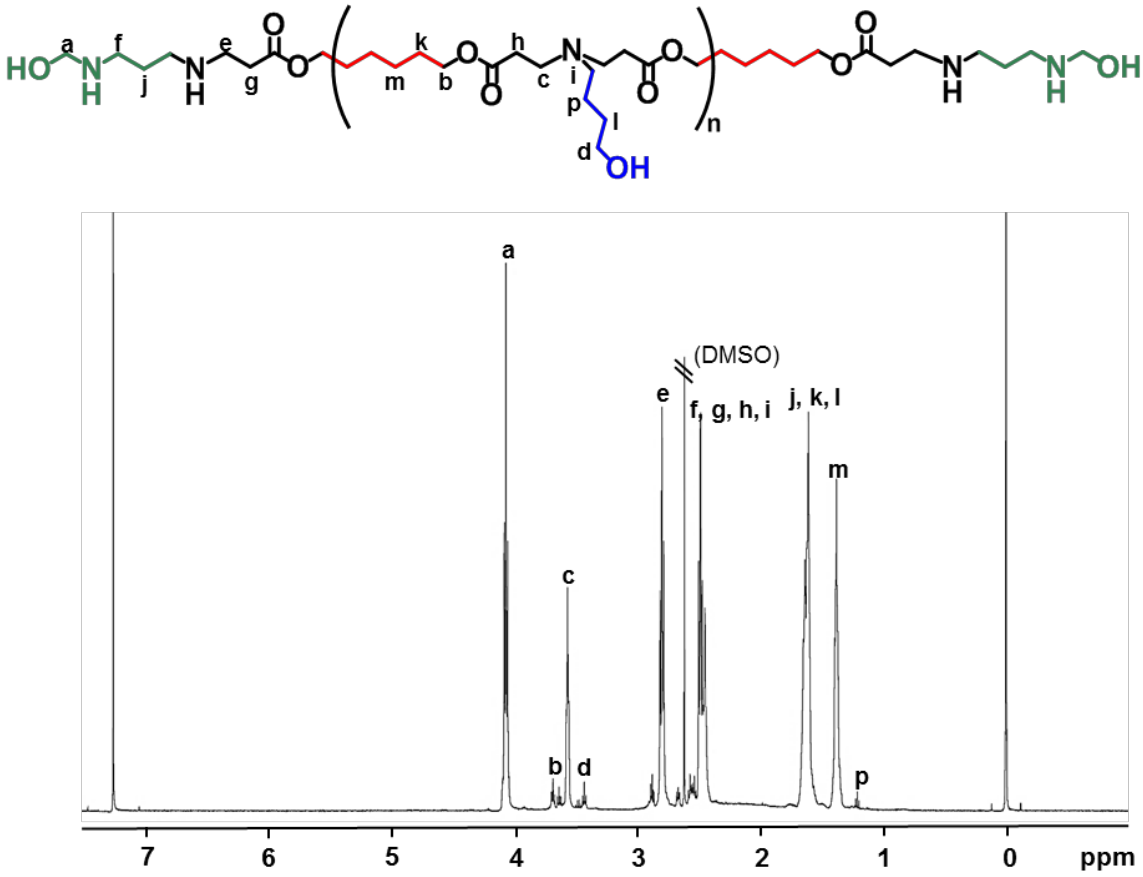

Figure 3-S16: H^1-NMR spectrum of polymer 646 ($CDCl_3$, 500 MHz). Proton peaks are labeled with letters corresponding to protons on the structure of 646.

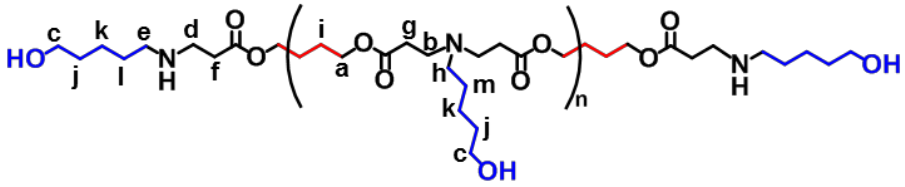

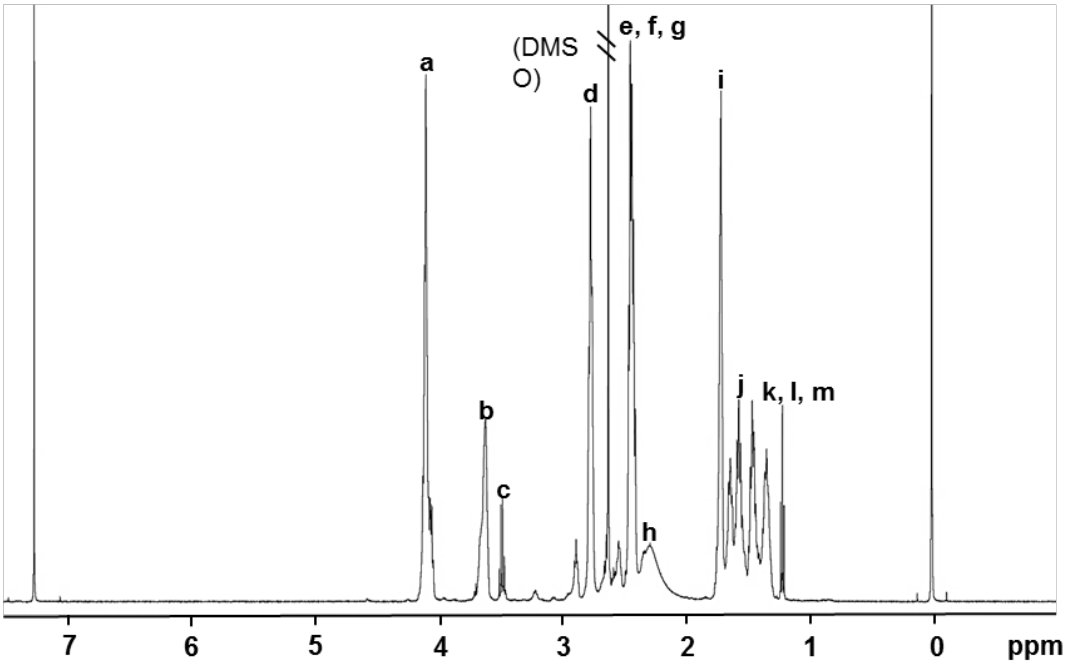

Figure 3-S17: H^1-NMR spectrum of polymer C32 ($CDCl_3$, 500 MHz). Proton peaks are labeled with letters corresponding to protons on the structure of C32.

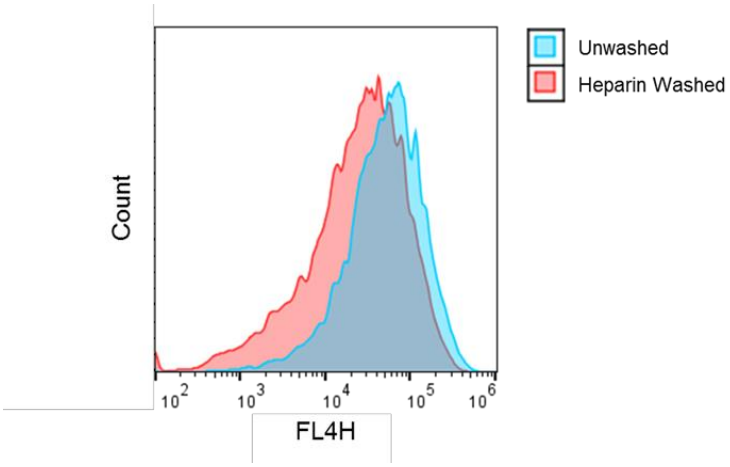

Figure 3-S18: Effects of heparin washing on uptake experiments. Flow cytometry plot of cells treated with R646 nano-miRs encapsulating Cy5-tagged miRNA show changes in average cellular fluorescence with and without a heparin wash to remove nano-miRs adhering to the cell surface.

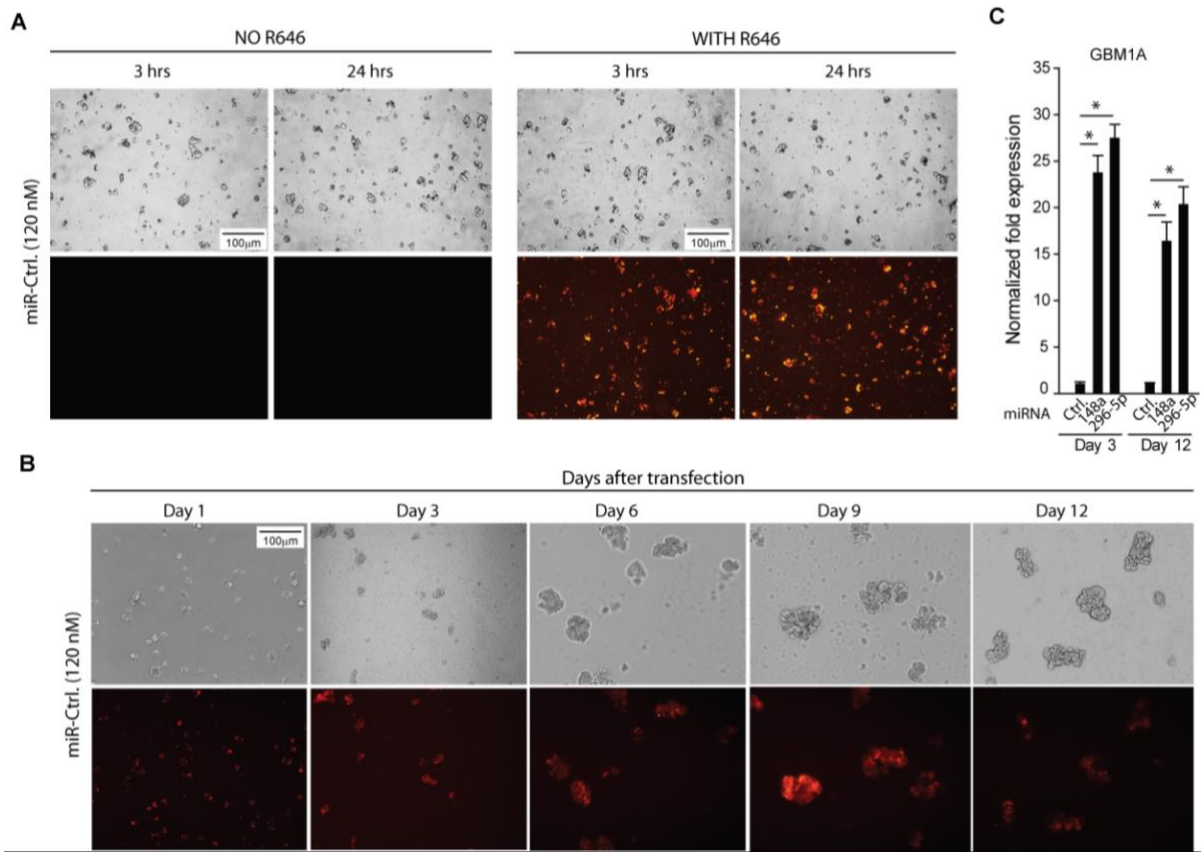

Figure 3-S19: Persistence of R646 nanoparticle-mediated intracellular delivery of labeled control miRNA to GBM neurospheres. GBM1A neurospheres were dissociated into single cells, and transfected with miR-Ctrl (120 nM) with and without R646 polymer (150 w/w). **(A)** miR-Ctrl labeled with Dy547 was visualized 3 hr and 24hrs after transfection using fluorescence microscopy. **(B)** Dy547-labeled control miRNA (miR-Ctrl) delivered to GBM neurospheres was detectable via fluorescence microscopy through at least 12 days following transfection. *$p< 0.05$ **(C)** qRT-PCR to measure expression of mature miR-148a and mature miR-296-5p 3 and 12 days after nano-miR transfection in GBM1A neurospheres. *$p<0.05$*

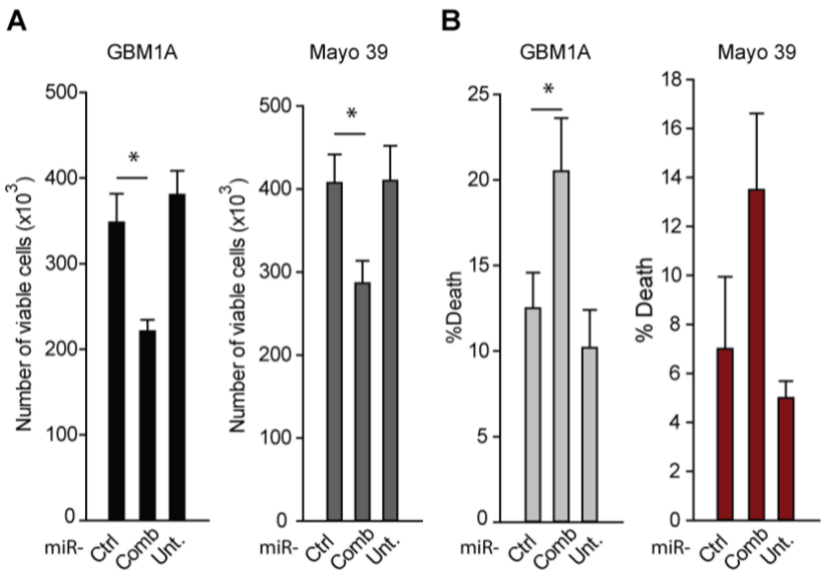

Figure 3-S20: R646 nano-miRs reduce cell numbers without drastically inducing cell death. GBM1A and Mayo39 GBM cells were transfected with miR-Ctrl or miR-148a/miR-296-5p combination (120 nM) using R646 polymer. Untreated (unt.) cells were used as control for nanoparticle toxicity. Nano-miRs were incubated with cells for 2 hours. Cell number **(A)** and viability **(B)** was measured 4 days after transfection using Trypan blue. *$p< 0.05$

Polymer	Nanoparticle Concentration (particles/mL)	miRNA Molecules per Particle
R646	$4.9 \pm 0.8 \times 10^{11}$	120 ± 20
646	$5.3 \pm 0.4 \times 10^{11}$	100 ± 9
C32	$3.7 \pm 0.3 \times 10^{11}$	150 ± 20

Table 3-S2: Nano-miR concentration as measured by NTA and the calculated miRNA molecules per particle for each nano-miR formulation. As all miRNA loaded was bound in nano-miRs **(Figure 7- 3E)** and a dose of 90 nM miRNA was used in the nano-miR formulation, miRNA molecules per particle was calculated using the equation:

$$\text{RNA loading} = \frac{\text{RNA Concentration}}{\text{NP Concentration}}.$$

Chapter 4: Nonviral Polymeric Nanoparticles for Gene Therapy in Pediatric CNS Malignancies

John Choi[1,*], Yuan Rui[2,3,*], Jayoung Kim[2,3,*], Noah Gorelick[1], David R. Wilson[2,3], Kristen Kozielski[2,3], Antonella Mangraviti[1], Eric Sankey[1], Henry Brem[1,2,4], Betty Tyler[1], Jordan J. Green[1,2,3,4,5,6,#], and Eric M. Jackson[1,#]

[1]Department of Neurosurgery, Johns Hopkins University School of Medicine, [2]Department of Biomedical Engineering, Johns Hopkins University School of Medicine, [3]The Institute for Nanobiotechnology and the Translational Tissue Engineering Center, Johns Hopkins University School of Medicine, [4]Departments of Ophthalmology and Oncology, Johns Hopkins University School of Medicine, [5]Departments of Materials Science & Engineering and Chemical & Biomolecular Engineering, Johns Hopkins University, [6]Bloomberg~Kimmel Institute for Cancer Immunotherapy, Johns Hopkins University School of Medicine.

[*]These authors contributed equally

Abstract

Together, medulloblastoma (MB) and atypical teratoid/rhabdoid tumors (AT/RT) represent two of the most prevalent pediatric brain malignancies. Current treatment involves radiation, which has high risks of developmental sequelae for patients under the age of three. New safer and more effective treatment modalities are needed. Cancer gene therapy is a promising alternative, but there are challenges with using viruses in pediatric patients. We developed a library of poly(beta-amino ester) (PBAE) nanoparticles and evaluated their efficacy for plasmid delivery of a suicide gene therapy to pediatric brain cancer models—specifically herpes simplex virus type I thymidine kinase (HSVtk), which results in controlled apoptosis of transfected cells. *In vivo,* PBAE-HSVtk treated groups had a greater median overall survival in mice implanted

with AT/RT (*p=0.0083 vs. control*) and MB (*p<0.0001 vs. control*). Our data provides proof of principle for using biodegradable PBAE nanoparticles as a safe and effective nanomedicine for treating pediatric CNS malignancies.

Keywords: Pediatrics, Cancer, Medulloblastoma, Atypical teratoid/rhabdoid tumor, Poly(Beta-Amino Ester) nanoparticle

Background

Malignant CNS tumors are the most common solid tumor in children.[1] Of those, medulloblastoma (MB) accounts for about 20 percent of all pediatric CNS tumors.[2] However, in children younger than 6 months of age, atypical teratoid/rhabdoid tumors (AT/RT) are the most common malignant central CNS tumor.[3] Historically, it has been difficult to distinguish these two cancers based on radiology alone, particularly since both occur almost exclusively in the cerebellum. Current diagnostic criteria of AT/RT require immunohistochemistry (IHC) characterization of SMARCB1/INI1 or evidence of SMARCA4/BRG1 deletion and/or mutation of 22q11.2 to distinguish it from MB.[4-5]

Of note, the prevalence of these two tumors in pediatric populations younger than three years of age complicates treatment; chemotherapy is often used to delay or avoid radiotherapy in infantile medulloblastoma,[6] while lack of effective therapies for AT/RT often requires use of initial radiotherapy for treatment despite the risk of neurologic sequelae that arises from early childhood radiation.[7] Even with radiation and surgery, patients with AT/RT report a dismal prognosis with median overall survival of 1 year.[8-9] Therefore, expansion of new treatment modalities for these malignancies is imperative for improving mortality outcomes in these pediatric populations.

We recently explored the potential of a new nanomedicine, poly(beta-amino ester) (PBAE) nanoparticles containing plasmid DNA encoding the suicide gene herpes simplex virus I thymidine kinase (HSVtk), as a gene therapy for treating adult glioma.[10] We found that in a preclinical glioma rat study, the nanoparticles could spread through the tumor and there was a significant increase in median overall survival

in vivo.[10] The well-characterized safety profile and effectiveness of PBAE nanoparticles for gene delivery—along with the ability to engineer these particles to avoid unwanted immunogenic risks—make them a promising candidate for pediatric malignancies,[11-15] although this direction has not been previously investigated. Of note, there has been a recent emergence of interest in using nanoparticles for gene delivery in pediatric malignancies, with cationic lipid-polymer hybrid nanoparticles (CLPNs) showing *in vivo* transfection efficacy in childhood rhabdomyosarcoma.[16]

Specifically, PBAEs are a class of polymeric nanoparticles that can be engineered to contain primary, secondary, and tertiary amines with hydrolytically cleavable ester bonds that allow for effective DNA binding and encapsulation, endocytosis within the host cell, subsequent endosomal escape, and intracellular DNA release for transcription and translation of the exogenous gene of interest.[17] Previous studies have shown that PBAEs can be safe and effective DNA delivery vectors both *in vitro* across multiple tissue types as well as *in vivo* in retinal and brain tissue.[11-13] Furthermore, PBAE polymers degrade quickly under physiological conditions, thereby minimizing nanoparticle cytotoxicity as well as maximizing successful delivery of nucleic acids.[18] Notably, PBAEs also demonstrate biomaterial-mediated cell type specificity, and are able to selectively transfect tumor tissue over healthy tissue in the brain[13, 19] and liver.[20-21]

Additionally, convection-enhanced delivery (CED) has been shown to be an effective method for locally delivering PBAEs to tumor sites *in vivo* by maintaining a pressure gradient that enhances diffusion of the particles throughout the tumor mass.[22] In a previous study, we demonstrated increased distribution of particles using CED *in vivo*.[10] Therefore, this study aims to investigate the efficacy of PBAE nanoparticles for intracellular delivery of nucleic acids such as plasmid DNA encoding HSVtk to show proof of principle that these polymeric nanoparticles can be used as a safe and effective method for treatment delivery in MB and AT/RT.

Methods

Materials

Small molecule monomers: 1,4-butanediol diacrylate (B4; CAS 1070-70-8), 3-amino-1-propanol (S3, CAS 156-87-6), 4-amino-1-butanol (S4, CAS 13325-10-05), 5-amino-1-pentanol (S5, CAS 2508-29-4), and 1-(3-aminopropyl)-4-methylpiperazine (E7, CAS 4572-031) were purchased from Alfa Aesar (Ward Hill, MA, USA); 1,5-pentanediol diacrylate (B5, CAS 36840-85-4) was purchased from Dajac Laboratories (Feasterville-Trevose, PA, USA); 2-(3-aminopropylamino)ethanol (E6; CAS 4461-39-6) was purchased from Sigma Aldrich (St. Louis, MO, USA). Lipofectamine™ 2000 and Lipofectamine 3000™ were purchased from ThermoFisher (Waltham, MA, USA). 25 kD branched poly(ethylenimine) was purchased from Sigma Aldrich (St. Louis, MO, USA). The pEGFP-N1 plasmid (GFP) was purchased from Elim Biopharmaceuticals (Hayward, CA, USA) and the herpes simplex virus type 1-derived thymidine kinase (HSVtk) gene was cloned into the pcDNA3.1 vector; both plasmids were amplified by Aldeveron (Fargo, ND, USA). For cell staining in *in vitro* cell killing assays, Hoechst 33342 and propidium iodide were purchased from Invitrogen (Carlsbad, CA, USA). CellTiter 96 AQ_{ueous} One MTS assay was purchased from Promega (Madison, Wisconsin, USA). Ganciclovir was purchased from Invivogen (Carlsbad, CA, USA).

Polymer Synthesis and Characterization

B and S monomers were reacted at a molar ratio of 1.1:1 at 90°C with stirring overnight to form acrylate-terminated base polymers. Base polymers were then dissolved in anhydrous THF at 167 mg/mL and added to end-capping E monomers (0.5 M in THF) at a 3:2 volume ratio and allowed to react at room temperature with stirring for 1 hour, at which time polymers were washed twice in diethyl ether to remove unreacted monomers and oligomers. Solvents were removed in a vacuum desiccant chamber for 2 days, at which point polymers were dissolved in DMSO at 100 mg/mL, and single-use aliquots were stored at -20°C with desiccant.

Nuclear magnetic resonance spectroscopy (NMR) was used to characterize polymer structure via ^1H NMR in $CDCl_3$ (Bruker 500 MHz) and analyzed using TopSpin 3.5 software (Billerica, MA, USA). Gel

permeation chromatography (Waters, Milford, MA) measurements were performed to measure polymer molecular weight and polydispersity. Polymers were dissolved in BHT-stabilized tetrahydrofuran and 5% DMSO and 1% piperidine, filtered through a 0.2 μm PTFE filter and measured against linear polystyrene standards.

Nanoparticle Characterization

Nanoparticles were prepared in the same manner as for transfections and diluted in 150 mM PBS to determine nanoparticle characteristics in neutral isotonic buffer. Hydrodynamic diameter was measured via dynamic light scattering at 1:6 dilution in PBS using a Malvern Zetasizer NanoZS (Malvern Panalytical, Malvern, UK). Zeta potential was measured via electrophoretic light scattering on the same Malvern Zetasizer. For characterization of lyophilized nanoparticles, nanoparticles were first resuspended in water following the same procedure as *in vivo* experiments and then diluted in PBS to the same polymer concentration as freshly prepared nanoparticles before measurement using dynamic light scattering. Transmission electron microscopy (TEM) images were acquired using a Philips CM120 (Philips Research, Cambridge, MA, USA). Nanoparticles were prepared at a polymer concentration of 1.8 mg/mL in 25 mM sodium acetate buffer (NaAc), and 30 μL were added to 400-square mesh carbon-coated TEM grids and allowed to dry for 20 min, at which point grids were rinsed with ultrapure water and allowed to fully dry before imaging.

Cell Culture

Human BT-12 atypical teratoid/rhabdoid tumor (AT/RT) cells (obtained from C. Eberhart's laboratory, Johns Hopkins University, Baltimore, MD, USA) were cultured in Dulbecco's Modified Eagle Media (DMEM; ThermoFisher, Waltham, MA, USA) supplemented with 10% FBS and 1% penicillin/streptomycin. D425 group 3 medulloblastoma cells (obtained from C. Eberhart's laboratory, Johns Hopkins University, Baltimore, MD, USA) were cultured in Minimum Essential Medium (MEM;

ThermoFisher, Waltham, MA, USA) supplemented with non-essential amino acids, 10% FBS, and 1% penicillin/streptomycin.

Transfection

BT-12 cells were seeded onto 96 well tissue culture plates at a density of 15,000 cells per well in 100 μL complete medium and allowed to adhere for 48 hours before transfection. D425 cells were seeded at a density of 15,000 cells per well 24 hours prior to transfection (transfection was done with cells in suspension as D425s did not adhere to tissue culture plates). To form nanoparticles, plasmid DNA and polymer were first dissolved separately in 25 mM NaAc buffer (pH 5) at the desired concentration and then mixed together at a 1:1 volume ratio. Nanoparticles were allowed to self-assemble for 10 minutes at room temperature before being added to cells. Nanoparticles were incubated with cells for 2 hours, at which time cells were replenished with fresh complete medium. To test the transfection efficacy of lyophilized nanoparticles, nanoparticles were first resuspended in water and then added to cells in complete cell culture medium to achieve a final DNA dose matching that delivered by freshly prepared nanoparticles (600 ng DNA per well). Nanoparticle-mediated cytotoxicity was assessed 24 hours post-transfection using CellTiter 96 AQ_{ueous} One MTS cell proliferation assay (Promega, Madison, Wisconsin, USA) following manufacturer's instructions. Transfection efficacy was assessed 48 hours post-transfection via flow cytometry using a BD Accuri C6 flow cytometer (BD Biosciences, Franklin Lakes, NJ, USA). N = 4 +/- SEM.

Transfections using commercially-available non-viral transfection reagents Lipofectamine 2000™ and Lipofectamine 3000™ (ThermoFisher, Waltham, MA, USA) were performed according to manufacturer instructions.

Nanoparticle Uptake and Endocytosis Pathway Inhibition

Cellular uptake of nanoparticles was measured using nanoparticles encapsulating 20% Cy5-labeled DNA (prepared using previously published protocols[23]) and 80% unlabeled plasmid DNA. Nanoparticles were prepared and added to cells in the same manner as for *in vitro* transfections described above. After 2 h

incubation with cells, nanoparticles were removed and cells were washed once with PBS before being prepared for flow cytometry experiments. Nanoparticle uptake was quantified both as percentage of cells with Cy5 fluorescence after gating against untreated cells as well as by using the geometric mean Cy5 fluorescence intensity normalized to that of untreated cells.

To investigate the relationship between polymer structure and endocytosis pathways leading to nanoparticle uptake and transfection, BT-12 cells were pre-treated with small molecule drugs inhibiting specific endocytosis pathways for 1 h prior to the addition of nanoparticles. Endocytosis inhibitors were used at the highest concentrations that did not lead to significant levels of inhibitor-mediated cytotoxicity and are as follows: 16 μg/mL chlorpromazine, 1.5 mg/mL methyl-β-cyclodextrin, 36 μg/mL genistein, and 3.5 μg/mL cytochalasin-D. After 1 h pre-incubation with inhibitors, nanoparticles were added to cells and incubated for an additional 2 h, after which cells were prepared for flow cytometry for uptake experiments or replenished with fresh complete media for transfection experiments.

In Vitro HSVtk Cell Killing Assay

For HSVtk cell killing assays, transfection was performed as described above using HSVtk and GFP plasmids, respectively. Ganciclovir (Invivogen, San Diego, CA, USA) was resuspended in PBS at 5 mg/mL following manufacturer's instructions and diluted to desired concentrations using complete cell culture media. On days 1, 3, and 5 after transfection, cells were treated with fresh ganciclovir-containing media. On day 7 post-transfection, cells were stained with Hoechst 33342 nuclear stain (1:1000 dilution) and propidium iodide (1:500 dilution) for 20 minutes and imaged and analyzed using Cellomics Arrayscan VTI with live cell imaging module. Cell killing was calculated by normalizing live cell numbers in treated wells to those in untreated wells.

Tumor Implantation

All animal work was done in strict adherence of the policies and guidelines of the Johns Hopkins University Animal Care and Use Committee (ACUC Mouse Protocol Mo17M185). For intracranial tumor

implantation, 6-8 week old male athymic nude mice (Charles River, Wilmington, MA, USA) were anesthetized using a Ketamine (100 mg/kg)/Xylazine (10 mg/kg) cocktail and mounted on a stereotactic frame. A rostro-caudal incision was made with a scalpel, the skin was spread apart, the surface of the skull was exposed and cleaned with 100% ethanol, and a small hole was made using an electric drill in the skull 2 mm posterior to the coronal suture and 2 mm lateral to the sagittal suture. Stainless steel cannulas (C212SG PlasticsOne®, Roanoke, VA, USA) were implanted into the hole in the skull. 5e5 BT-12 cells and 1.25e5 D425 cells were respectively implanted into mouse brains into the left striatum through cannulas.

In Vivo Nanoparticle Administration

Xenograft tumors were allowed to form for 10 days for BT-12 and 7 days for D425, at which time nanoparticle administration began. For *in vivo* injections, nanoparticles were lyophilized after initial formation as described previously.[24] Briefly, nanoparticles were formulated at *in vitro* optimized polymer-to-DNA w/w ratio but with the total polymer concentration at 5 mg/mL; sucrose was added at a final concentration of 30 mg/mL as a cryoprotectant. Lyophilized nanoparticles were resuspended in sterile water at a final isotonic sucrose concentration of 100 mg/mL immediately before intracranial administration. Mice were anesthetized, and the original incision was opened. Convection-enhanced delivery (CED) was performed using a 26-gauge needle stereotactically placed at a depth of 3 mm and an UltraMicroPump (UMP3) with SYS-Micro4 Controller (World Precision Instruments, Sarasota, FL, USA) was used to infuse nanoparticles at a rate of 0.5 μL/min.[25] 10 μL nanoparticles were injected per animal, after which the needle was maintained in the cortex for another 5 min to avoid backflow. Following needle removal, the incision was closed and the animal was allowed to awaken and recover.

HSVtk Survival Studies

After tumor inoculation, mice were randomized and divided into 3 groups (n=10), each group receiving GFP nanoparticles, HSVtk nanoparticles, or sham PBS treatment, respectively. Mice implanted with BT-12 were treated with 447 nanoparticles (90 w/w) while mice implanted with D425 were treated with 537

nanoparticles (90 w/w). Mice received nanoparticle infusions on days indicated in **Figure 4-6** for a total of 3 infusions. All mice received intraperitoneal administration of 50 mg/kg ganciclovir daily on days 10-40 for BT-12 implanted mice and days 7-28 for D425 implanted mice after the first nanoparticle infusion. Animals were monitored daily and assessed for neurological impairment.

Data Analysis and Statistics

All *in vitro* experiments were performed with n=4 unless otherwise noted. Survival data was compiled using the Kaplan-Meier methodology and compared across arms using the Mantel-Cox log-rank test. All statistical tests were performed using the GraphPad Prism6 software.

Results

PBAE nanoparticles enable efficient DNA delivery to AT/RT and MB cells in vitro

We synthesized a small library of PBAEs by co-polymerizing small molecule monomers via Michael addition reactions between amines and diacrylates following previously reported protocols (**Figure 4-1A**).[26] Briefly, diacrylate "B" monomers were reacted with primary amine-containing "S" monomers (90°C, overnight) to produce acrylate-terminated polymers, which were then end-capped with amine-containing "E" monomers (25°C, 1 hour). The presence of acrylate-terminated polymers following the first step of synthesis was confirmed via ^{1}H NMR with three characteristic acrylate peaks in the 5.5-6.5 ppm range, which disappeared after end-capping reaction (**Figure 4-S1**). The cationic polymers were mixed with anionic plasmid DNA in acidic buffer to self-assemble into nanoparticles, which were found to be 100-200 nm in diameter with slightly positive surface charges (**Figure 4-1B**).

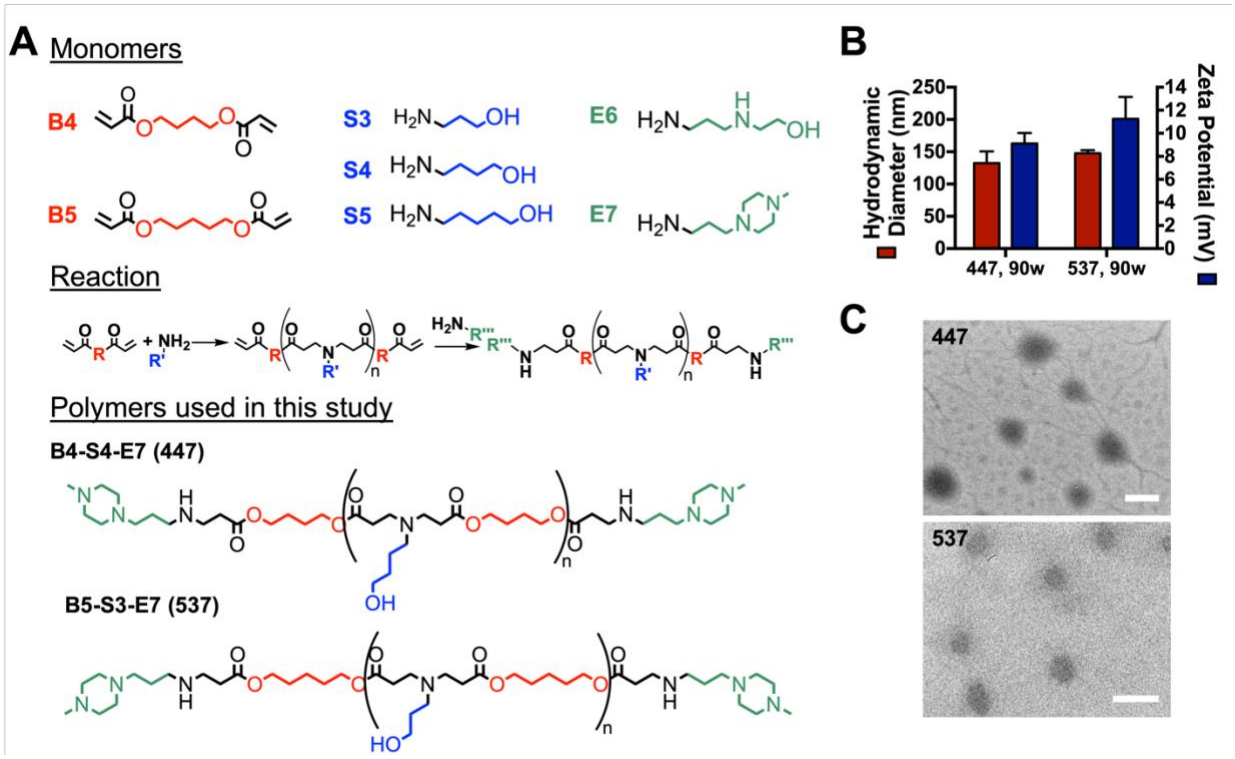

Figure 4-1. PBAE chemical structures and nanoparticle characteristics. (A) PBAEs are synthesized from B, S, and E monomers via Michael addition reactions. Structures of top polymers used in this study are shown. **(B)** Hydrodynamic diameter and zeta potential measurements of top nanoparticle formulations as measured by dynamic light scattering, n = 3. **(C)** Representative TEM images of 447 and 537 nanoparticles, respectively; scale bar = 200 nm.

We performed nanoparticle transfection screens on two cell lines established from pediatric patient samples; D425 is a well-characterized Group 3 medulloblastoma cell line,[27] and BT-12 is a highly-cited AT/RT cell line that has been used in pre-clinical studies using HDAC inhibitors,[28] IGF-IR antisense oligonucleotides,[29] and neutralizing antibodies[30-31] for exploring treatment.[32-33] Using a GFP reporter plasmid for the initial nanoparticle screen, we found that several PBAE nanoparticle formulations enabled >50% transfection in both cell lines with minor levels of cytotoxicity (**Figure 4-2**). PBAE nanoparticles also enabled significantly higher transfection compared to commercially-available transfection reagents such as 25 kD branched PEI and Lipofectamine 3000™ (**Figure 4-3**). Based on our screening results, we chose polymer 1-(3-aminopropyl)-4-methylpiperazine end-capped poly(1,4-butanediol diacrylate-co-4-amino-1-butanol) (447)

at a polymer-to-DNA weight-to-weight (w/w) ratio of 90 as the optimal formulation for BT-12 and polymer 1-(3-aminopropyl)-4-methylpiperazine end-capped poly(1,5-pentanediol diacrylate-co-3-amino-1-propanol) (537) at 90 w/w for D425.

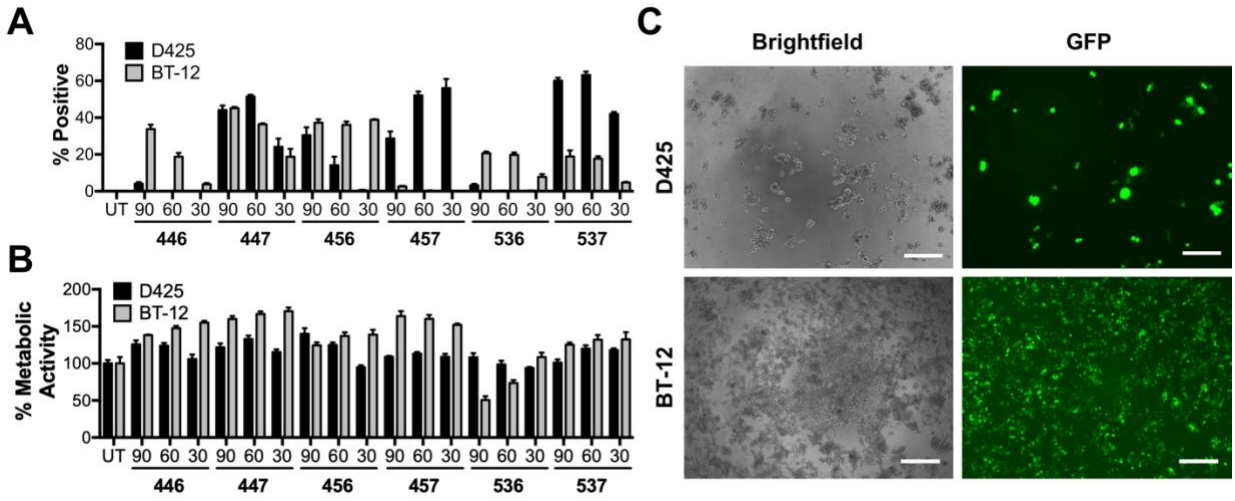

Figure 4-2. *In vitro* nanoparticle screening in D425 and BT-12 cells. Transfection efficacy shown as percent GFP positive cells **(A)** and **(B)** metabolic activity after treatment with different nanoparticle formulations; n = 4. **(C)** Fluorescence microscopy images of both cell lines transfected with their respective optimal nanoparticle formulations (537, 90 w/w for D425; 447, 90 w/w for BT-12); scale bar = 200 μm.

We performed nanoparticle uptake experiments in which nanoparticle were formulated to deliver 20% Cy5 labeled DNA, and we characterized nanoparticle uptake in BT-12 cells by assessing intracellular Cy5 fluorescence. Our results showed that 447 90 w/w and 537 90 w/w nanoparticle formulations resulted in the highest levels of cellular uptake as measured by the geometric mean Cy5 fluorescence intensity (**Figure 4-4**). These optimized nanoparticle formulations were used for their respective cell lines for the remaining experiments. Uptake pathways leading to transfection were further investigated using an endocytosis pathway inhibition assay in which BT-12 cells were pre-treated with small molecule drugs inhibiting clathrin-mediated endocytosis, lipid raft-mediated endocytosis, caveolin-mediated endocytosis, and macropinocytosis, respectively, before incubation with nanoparticles. Our results demonstrated that polymer end-group structure played an important role in determining the pathway through which nanoparticles were internalized.

For example, 446 nanoparticle uptake was significantly inhibited by methyl-β-cyclodextrin, which was not the case for 447 or 537.

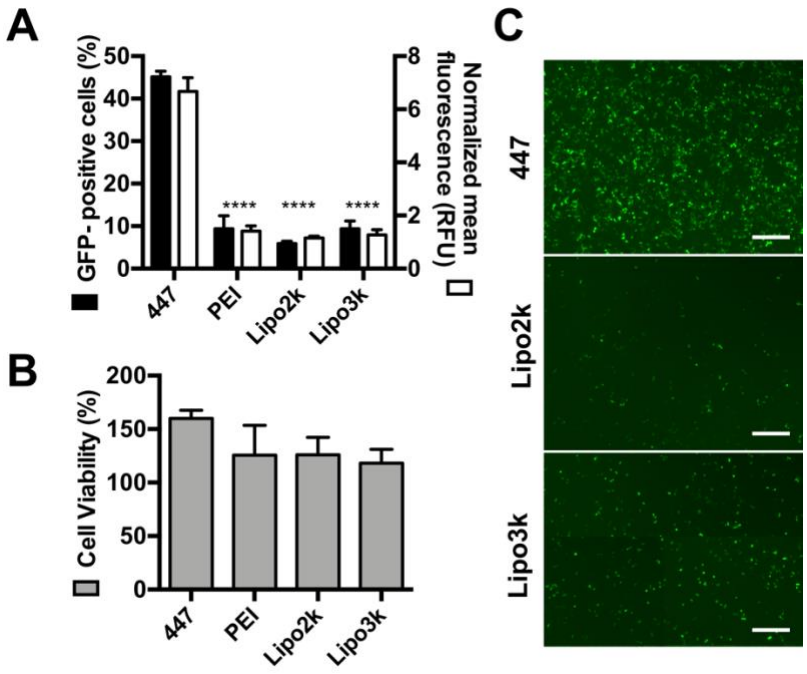

Figure 4-3. PBAE nanoparticles enable higher transfection than commercially-available transfection reagents. (A) Formulation 447 nanoparticles enabled significantly higher transfection in BT-12 cells compared to 3 commercially-available transfection reagents; statistical significance assessed by ordinary one-way ANOVA Dunnett's multiple comparisons test (n = 4; ****$p<0.001$). **(B)** Nanoparticles caused negligible levels of cytotoxicity; metabolic activity/cell viability measured by MTS assay and normalized to non-transfected control (n = 4). **(C)** Fluorescence microscopy images of cells transfected with different reagents; scale bar = 200 μm.

PBAE-HSVtk nanoparticles activate ganciclovir prodrug to induce cell killing in vitro

We next investigated the *in vitro* cell killing capabilities of PBAE nanoparticles encapsulating the HSVtk suicide gene. 447 nanoparticles delivering a plasmid encoding HSVtk or GFP were used to transfect BT-12 cells. Transfected and untransfected controls were replenished with cell culture media containing varying doses of ganciclovir (GCV) on days 1, 3, and 5 post-transfection. Live/dead cell imaging on day 7 post-transfection revealed that GCV treatment in HSVtk transfected cells resulted in >65% cell death at all 3

GCV doses (**Figure 4-5**). Similar treatment in GFP-transfected cells did not incur any cytotoxicity, suggesting that cell killing required GCV activation by cells expressing HSVtk. Untransfected cells treated with GCV also did not incur appreciable cytotoxicity, indicating that the GCV doses used did not cause non-specific cell death.

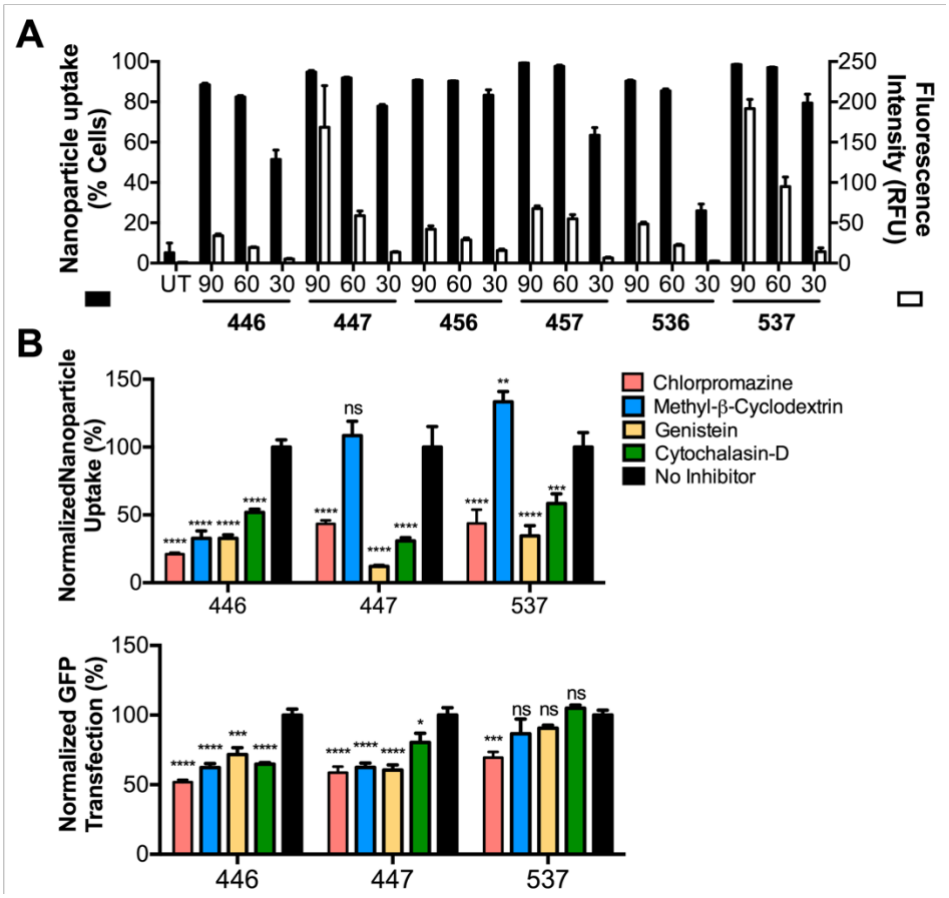

Figure 4-4: Effect of endocytosis pathway on nanoparticle uptake and transfection. (A) Cellular uptake of nanoparticles encapsulating Cy5-labled DNA. Nanoparticle uptake is expressed as the percentage of cells containing Cy5 signal as well as the geometric mean Cy5 fluorescence intensity (n = 4). **(B)** Uptake (top) and transfection (bottom) of select polymers (all nanoparticles were formulated at 90 w/w) after endocytosis pathway inhibition (n = 4). Chlorpromazine was used to inhibit clathrin-mediated endocytosis; methyl-β-cyclodextrin – lipid raft-mediated endocytosis; genistein – caveolin-mediated endocytosis, and cytochalasin-D – macropinocytosis. Uptake and transfection are expressed as the fluorescence intensity of each inhibitor-treated condition normalized to the no inhibitor group. Statistical significance was determined using 2-way

ANOVA with Dunnett's multiple comparisons test as compared to the no inhibitor group for each polymer (*p ≤ 0.05, **p ≤ 0.01, ***p ≤ 0.001, **** p ≤ 0.0001.)

Nanoparticles administered via CED significantly prolong survival in mouse xenograft models in vivo

The robustness of PBAE nanoparticles delivering HSVtk suicide gene therapy was further evaluated in two orthotopic mouse xenograft models, using BT-12 and D425 cells, respectively. Nanoparticles encapsulating either HSVtk or GFP were formulated at the same optimal w/w as *in vitro* experiments and lyophilized with sucrose as a cryoprotectant following previously published protocols,[10, 24] for ease of storage and to facilitate future manufacturing scalability. To validate our nanoparticle lyophilization procedure, lyophilized nanoparticles were resuspended in water following the same procedure was for *in vivo* injections and characterized using dynamic light scattering. We found that lyophilized nanoparticles were not statistically different in hydrodynamic diameter or zeta potential compared to freshly prepared nanoparticles (**Figure 4-S2**). Furthermore, lyophilized nanoparticles achieved similar levels of *in vitro* transfection as fresh nanoparticles delivering the same DNA dose, further confirming that lyophilization did not significantly alter nanoparticle properties.

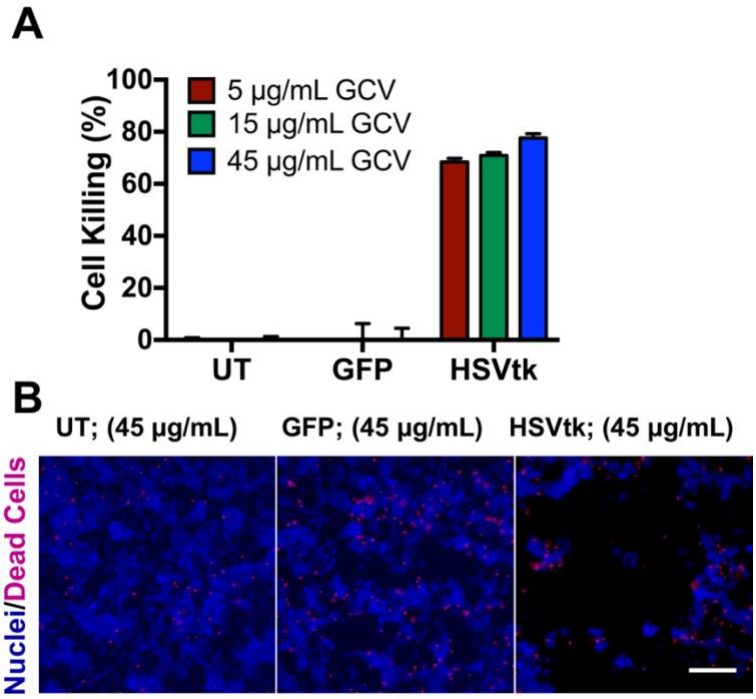

Figure 4-5. PBAE nanoparticles delivering HSVtk enables cell killing *in vitro*. (A) BT-12 cells were transfected with nanoparticles encapsulating either GFP or HSVtk plasmid DNA (447, 90 w/w, 600 ng/well), and only cells transfected with HSVtk showed high levels of cell death upon GCV treatment. Un-transfected cells (UT) were treated with GCV only as negative control. (n = 4). **(B)** Fluorescence microscopy images of BT-12 cells treated with indicated nanoparticle formulations at 45 μg/mL GCV 7 days post-transfection. Cells were stained with Hoechst 33342 nuclear dye (blue) or propidium iodide for dead cells (magenta). Scale bar = 100 μm.

To evaluate *in vivo* nanoparticle efficacy in intracranial tumor models, athymic nude mice were inoculated with 5e5 BT-12 cells or 1.25e5 D425 cells, respectively. Tumors were allowed to form for 7-10 days, after which time nanoparticle treatment began at day 7 for mice implanted with BT-12 cells and day 10 for mice implanted with D425 cells. Each treatment group received 3 nanoparticle infusions through convection-enhanced delivery (CED); mice received 2 μg total DNA dose for each infusion. The first day of treatment was designated as day 0, at which point survival tracking began. Mice also received daily intraperitoneal (i.p.) injections of GCV for the entirety of the treatment period (**Figure 4-6**).

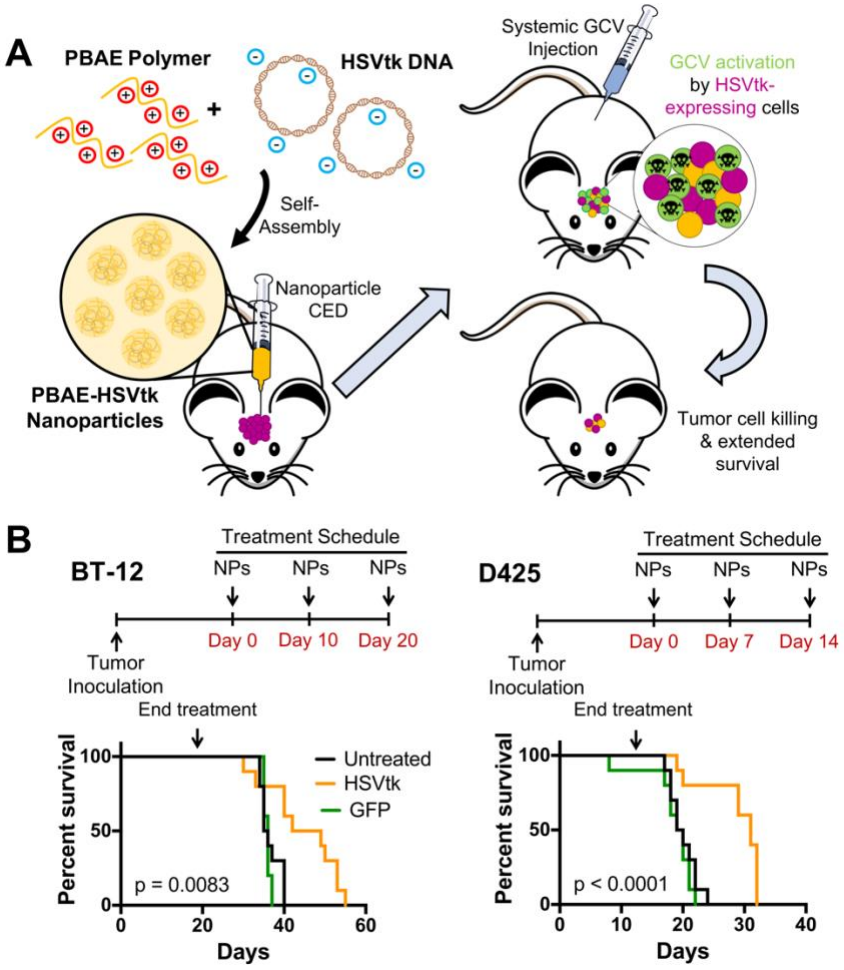

Figure 4-6. Convection-enhanced delivery of PBAE nanoparticles significantly extended survival in mouse orthotopic xenograft models *in vivo*. (A) Schematic of *in vivo* study: PBAEs self-assembled into nanoparticles with plasmid DNA, which were infused intratumorally via CED; mice also received intraperitoneal injections of GCV prodrug, which were activated in transfected cells, leading to tumor cell killing and extended survival. **(B)** Treatment schedule and Kaplan-Meier survival curves for each tumor model; n = 10 animals per group.

In both tumor models, survival of the GFP nanoparticle group closely followed that of the untreated control group, mirroring the results of our *in vitro* cell killing assay. Nanoparticles delivering HSVtk significantly extended survival in both tumor models ($p = 0.0083$ for BT-12 and $p < 0.0001$ for D425, as determined by Mantel-Cox log-rank tests). Mice bearing BT-12 tumors had median survival of 35 days when untreated, and survival was extended to 42 days (20% longer) with HSVtk nanoparticles. D425 tumors were

more aggressive, with untreated median survival at 19 days and with HSVtk nanoparticle treatment, median overall survival at 31 days (63% longer) (**Figure 4-6)**.

Discussion

In this work, we synthesized a small library of poly(beta-amino ester)s (PBAEs) and examined their ability to functionally deliver plasmid DNA encoding a suicide gene to pediatric CNS malignancies. The small size of the nanoparticles (**Figure 4-1**) contributed to successful delivery to BT-12 (an AT/RT cell line) and D425 (a MB cell line) *in vitro*. Within the same polymer type, transfection efficacy generally increased with increasing polymer-DNA w/w ratio while cell viability decreased (**Figure 4-2**); both phenomenon could be partly explained by the fact that higher polymer doses increase the positive charge of the nanoparticles as well as the number of positively-charged molecules interacting with cells overall, which could simultaneously increase nanoparticle uptake and cytotoxicity by perturbing and disrupting the cellular membrane.[34]

While polymer 447 was equally effective at transfecting both cell lines (45% GFP positive in BT-12 and D425), some polymers were only effective at transfecting one cell line and not the other. For example, 446 enabled transfection exclusively in BT-12 while 457 exclusively transfected D425. To investigate the mechanism by which polymer structure affects transfection efficacy, we studied nanoparticles formulated with polymers 446, 447, and 537 at 90 w/w and their interactions with BT-12 cells. From **Figure 4-2A**, we see that 446 and 447 nanoparticles enabled similar levels of transfection in this cell line while 537 nanoparticles achieved significantly lower transfection levels. Previous studies have reported that molecular weight correlated positively with nanoparticle transfection efficacy in several polymeric nanoparticle systems.[35-36] This was not the case here as polymers 446 and 447 enabled significantly higher transfection than polymer 537 despite having a significantly lower molecular weight (**Table 4-S1**). The differential transfection levels also do not appear to be dependent on nanoparticle physical characteristics as 447 and 537 nanoparticles do not have statistically significant differences in hydrodynamic diameter or zeta potential (**Figure 4-1**).

Previous work suggests that this cell-type specificity may be in part due to the structure of polymer endgroups,[11, 37] which can lead to differential uptake pathways resulting from different nanoparticle-membrane interactions.[38] To test this hypothesis, we performed endocytosis pathway inhibition studies on nanoparticles formulated from polymers 446, 447, and 537. BT-12 cells were pre-treated with small molecule drugs to inhibit specific endocytosis pathways, and nanoparticles were added to cells to study the endocytosis pathways responsible for nanoparticle uptake and DNA transfection (**Figure 4-4B**). Compared to polymers end-capped with E7, uptake inhibition of 446 nanoparticles by methyl-β-cyclodextrin was significantly higher, indicating that lipid raft-mediated endocytosis was a major uptake pathway for this polymer structure. Across all three polymer structures, genistein caused very high levels of uptake inhibition without high levels of transfection inhibition, indicating that caveolin-mediated endocytosis was a rather wasteful endocytosis pathway through which nanoparticles were taken up but did not lead to transfection. Chlorpromazine inhibited 60-80% nanoparticle uptake, corresponding to 30-50% transfection inhibition. This indicates that clathrin-mediated endocytosis is a major pathway for leading to transfection. Taken together, our results demonstrate that subtle changes in PBAE polymer structure can lead to significant changes in the endocytosis and transfection behavior of nanoparticles. These results do not provide a conclusive explanation for how certain structures lead to higher transfection levels than others, however, suggesting that nanoparticle trafficking steps between endocytosis and gene expression such as endosomal escape, intracellular migration, and nuclear penetration should be further explored to elucidate the mechanisms behind biomaterial-mediated cell type specificity.

Furthermore, while BT-12 cells formed monolayers, D425 cells have been documented to grow as macrospheroids[39] and were transfected in suspension. Our results show that PBAE nanoparticles could be tailored for cell type-specific transfection as well as penetrate and transfect 3D cellular macrospheroids. This data suggest that certain nanomedicine formulations may be potentially useful for pediatric CNS malignancies in general (447 and 537), while other nanomedicine formulations may be able to further improve efficacy for patients with particular tumors (446 and 457). Of note, optimized PBAE formulations significantly outperformed leading commercially-available transfection reagents such as Lipofectamine 3000™.

In vitro assays showed robust and specific cell killing in cells treated with HSVtk nanoparticles and GCV prodrug. GCV treatment alone, with or without nanoparticle-mediated transfection of a reporter gene, did not result in appreciable levels of cytotoxicity. Interestingly, formulation 447 nanoparticles enabled 45% transfection in BT-12 (as assessed via GFP reporter gene screening) but resulted in >65% cell death when used to deliver HSVtk. This is due to a well-documented bystander effect in the HSVtk-GCV system, whereby a fraction of transfected cells can lead to cell death in the greater cell population by releasing activated GCV into the cell medium or through gap junctional intercellular communication.[39] This is an advantage of a suicide gene therapy approach, as the treatment does not rely on 100% transfection efficacy to have a broad effect on a tumor.

In vivo survival studies demonstrated the efficacy of using PBAE nanoparticles carrying HSVtk for treating MB and AT/RT. Of note, the increased median overall survival in mice with AT/RT or MB that were treated with PBAEs carrying HSVtk showed a more impressive therapeutic effect when compared to our previous studies on GBM in rat models.[10] Furthermore, in tumors like MB, which have since been characterized as having one of four possible molecular subtypes,[33] the customizability of PBAE formulations lends itself well to the optimization of personalized nanomedicine technology between these different tumor groups.

It should be noted that PBAEs are not restricted to delivering genes such as HSVtk, as they have been validated as vectors for the delivery of other nucleic acids such as siRNA[19] and miRNA[24] as well. Our data demonstrates proof of principle that PBAEs can be used to deliver genes of interest to MB and AT/RT tumors with significant therapeutic effect. This finding offers a promising alternative avenue to our current limited treatment modalities, with PBAE nanomedicine opening the door to safe and effective non-viral gene-based therapies for pediatric CNS malignancies.

Acknowledgements

The authors would like to thank the NIH (R01CA228133) for support of this work. The authors would also like to thank the Wilmer Equipment Core for use of Cellomics Arrayscan VTI for automated image

acquisition and quantification (Microscopy Core Grant EY001765). JC thanks the Johns Hopkins University Deans Research Fund for their fellowship support. YR (DGE-1232825) and DRW (DGE-0707427) thank the NSF for fellowship support, and JK thanks Samsung for scholarship support. JG thanks the Bloomberg~Kimmel Institute for Cancer Immunotherapy for support.

References:

1. Gondi V; Yock TI; Mehta MP. Proton Therapy for Paediatric Cns Tumours—Improving Treatment-Related Outcomes. *Nat Rev Neurol* 2016**; 12:** 334.

2. Smoll NR; Drummond KJ. The Incidence of Medulloblastomas and Primitive Neurectodermal Tumours in Adults and Children. *J Clin Neurosci* 2012**; 19:** 1541-1544.

3. Biswas A; Kashyap L; Kakkar A; Sarkar C; Julka PK. Atypical Teratoid/Rhabdoid Tumors: Challenges and Search for Solutions. *Cancer Manag Res* 2016**; 8:** 115.

4. Babgi M; Samkari A; Al-Mehdar A; Abdullah S. Atypical Teratoid/Rhabdoid Tumor of the Spinal Cord in a Child: Case Report and Comprehensive Review of the Literature. *Pediatr Neurosurg* 2018**; 53:** 254-262.

5. Ren Y; Tao C; Wang X; Ju Y. Identification of Rpl5 and Rpl10 as Novel Diagnostic Biomarkers of Atypical Teratoid/Rhabdoid Tumors. *Cancer Cell Int* 2018**; 18:** 190.

6. Duffner PK; Horowitz ME; Krischer JP; Burger PC; Cohen ME; Sanford RA, et al. The Treatment of Malignant Brain Tumors in Infants and Very Young Children: An Update of the Pediatric Oncology Group Experience. *Neuro-Oncology* 1999**; 1:** 152-161.

7. Tekautz TM; Fuller CE; Blaney S; Fouladi M; Broniscer A; Merchant TE, et al. Atypical Teratoid/Rhabdoid Tumors (Atrt): Improved Survival in Children 3 Years of Age and Older with Radiation Therapy and High-Dose Alkylator-Based Chemotherapy. *J Clin Oncol* 2005**; 23:** 1491-1499.

8. Dufour C; Beaugrand A; Le Deley MC; Bourdeaut F; André N; Leblond P, et al. Clinicopathologic Prognostic Factors in Childhood Atypical Teratoid and Rhabdoid Tumor of the Central Nervous System: A Multicenter Study. *Cancer* 2012**; 118:** 3812-3821.

9. Chi SN; Zimmerman MA; Yao X; Cohen KJ; Burger P; Biegel JA, et al. Intensive Multimodality Treatment for Children with Newly Diagnosed Cns Atypical Teratoid Rhabdoid Tumor. *J Clin Oncol* 2009**; 27:** 385.

10. Mangraviti A; Tzeng SY; Kozielski KL; Wang Y; Jin Y; Gullotti D, et al. Polymeric Nanoparticles for Nonviral Gene Therapy Extend Brain Tumor Survival in Vivo. *ACS Nano* 2015**; 9:** 1236-1249.

11. Sunshine J; Green JJ; Mahon KP; Yang F; Eltoukhy AA; Nguyen DN, et al. Small-Molecule End-Groups of Linear Polymer Determine Cell-Type Gene-Delivery Efficacy. *Adv Mater* 2009**; 21:** 4947-4951.

12. Sunshine JC; Sunshine SB; Bhutto I; Handa JT; Green JJ. Poly (B-Amino Ester)-Nanoparticle Mediated Transfection of Retinal Pigment Epithelial Cells in Vitro and in Vivo. *PloS one* 2012**; 7:** e37543.

13. Guerrero-Cázares H; Tzeng SY; Young NP; Abutaleb AO; Quiñones-Hinojosa A; Green JJ. Biodegradable Polymeric Nanoparticles Show High Efficacy and Specificity at DNA Delivery to Human Glioblastoma in Vitro and in Vivo. *ACS Nano* 2014**; 8:** 5141-5153.

14. Thomas CE; Ehrhardt A; Kay MA. Progress and Problems with the Use of Viral Vectors for Gene Therapy. *Nature Reviews Genetics* 2003**; 4:** 346-358.

15. Forbes DC; Peppas NA. Oral Delivery of Small Rna and DNA. *J Control Release* 2012**; 162:** 438-445.

16. Zhang T; Ma J; Li C; Lin K; Lou F; Jiang H, et al. Core-Shell Lipid Polymer Nanoparticles for Combined Chemo and Gene Therapy of Childhood Head and Neck Cancers. *Oncol Rep* 2017**; 37:** 1653-1661.

17. Lynn DM; Langer R. Degradable Poly (B-Amino Esters): Synthesis, Characterization, and Self-Assembly with Plasmid DNA. *J Am Chem Soc* 2000**; 122:** 10761-10768.

18. Sunshine JC; Peng DY; Green JJ. Uptake and Transfection with Polymeric Nanoparticles Are Dependent on Polymer End-Group Structure, but Largely Independent of Nanoparticle Physical and Chemical Properties. *Molecular Pharmaceutics* 2012**; 9:** 3375-3383.

19. Kozielski KL; Tzeng SY; Hurtado De Mendoza BA; Green JJ. Bioreducible Cationic Polymer-Based Nanoparticles for Efficient and Environmentally Triggered Cytoplasmic Sirna Delivery to Primary Human Brain Cancer Cells. *ACS Nano* 2014**; 8:** 3232-3241.

20. Tzeng SY; Higgins LJ; Pomper MG; Green JJ. Student Award Winner in the Ph. D. Category for the 2013 Society for Biomaterials Annual Meeting and Exposition, April 10–13, 2013, Boston, Massachusetts: Biomaterial-Mediated Cancer-Specific DNA Delivery to Liver Cell Cultures Using Synthetic Poly (Beta-Amino Ester) S. *J Biomed Mater Res A* 2013**; 101:** 1837-1845.

21. Zamboni CG; Kozielski KL; Vaughan HJ; Nakata MM; Kim J; Higgins LJ, et al. Polymeric Nanoparticles as Cancer-Specific DNA Delivery Vectors to Human Hepatocellular Carcinoma. *J Control Release* 2017**; 263:** 18-28.

22. Allard E; Passirani C; Benoit J-P. Convection-Enhanced Delivery of Nanocarriers for the Treatment of Brain Tumors. *Biomaterials* 2009**; 30:** 2302-2318.

23. Wilson DR; Routkevitch D; Rui Y; Mosenia A; Wahlin KJ; Quinones-Hinojosa A, et al. A Triple-Fluorophore-Labeled Nucleic Acid Ph Nanosensor to Investigate Non-Viral Gene Delivery. *Molecular Therapy* 2017**; 25:** 1697-1709.

24. Lopez-Bertoni H; Kozielski KL; Rui Y; Lal B; Vaughan H; Wilson DR, et al. Bioreducible Polymeric Nanoparticles Containing Multiplexed Cancer Stem Cell Regulating Mirnas Inhibit Glioblastoma Growth and Prolong Survival. *Nano Lett* 2018**; 18:** 4086-4094.

25. Serwer L; Hashizume R; Ozawa T; James CD. Systemic and Local Drug Delivery for Treating Diseases of the Central Nervous System in Rodent Models. *J Vis Exp* 2010.

26. Wilson DR; Mosenia A; Suprenant MP; Upadhya R; Routkevitch D; Meyer RA, et al. Continuous Microfluidic Assembly of Biodegradable Poly(Beta-Amino Ester)/DNA Nanoparticles for Enhanced Gene Delivery. *J Biomed Mater Res A* 2017**; 105:** 1813-1825.

27. Ivanov DP; Coyle B; Walker DA; Grabowska AM. In Vitro Models of Medulloblastoma: Choosing the Right Tool for the Job. *J Biotechnol* 2016**; 236:** 10-25.

28. Knipstein JA; Birks DK; Donson AM; Alimova I; Foreman NK; Vibhakar R. Histone Deacetylase Inhibition Decreases Proliferation and Potentiates the Effect of Ionizing Radiation in Atypical Teratoid/Rhabdoid Tumor Cells. *Neuro-Oncology* 2012**; 14:** 175-183.

29. D'cunja J; Shalaby T; Rivera P; von Büren A; Patti R; Heppner FL, et al. Antisense Treatment of Igf-Ir Induces Apoptosis and Enhances Chemosensitivity in Central Nervous System Atypical Teratoid/Rhabdoid Tumours Cells. *Euro J Cancer* 2007**; 43:** 1581-1589.

30. Narendran A; Coppes L; Jayanthan A; Coppes M; Teja B; Bernoux D, et al. Establishment of Atypical-Teratoid/Rhabdoid Tumor (at/Rt) Cell Cultures from Disseminated Csf Cells: A Model to Elucidate Biology and Potential Targeted Therapeutics. *J Neuro-Oncol* 2008**; 90:** 171-180.

31. Jayanthan A; Bernoux D; Bose P; Riabowol K; Narendran A. Multi-Tyrosine Kinase Inhibitors in Preclinical Studies for Pediatric Cns at/Rt: Evidence for Synergy with Topoisomerase-I Inhibition. *Cancer Cell Int* 2011**; 11:** 44-44.

32. Studebaker AW; Hutzen B; Pierson CR; Shaffer TA; Raffel C; Jackson EM. Oncolytic Measles Virus Efficacy in Murine Xenograft Models of Atypical Teratoid Rhabdoid Tumors. *Neuro-Oncology* 2015**; 17:** 1568-1577.

33. Studebaker AW; Hutzen BJ; Pierson CR; Haworth KB; Cripe TP; Jackson EM, et al. Oncolytic Herpes Virus Rrp450 Shows Efficacy in Orthotopic Xenograft Group 3/4 Medulloblastomas and Atypical Teratoid/Rhabdoid Tumors. *Mol Ther Oncolytics* 2017**; 6:** 22-30.

34. Fröhlich E. The Role of Surface Charge in Cellular Uptake and Cytotoxicity of Medical Nanoparticles. *Int J Nanomedicine* 2012**; 7:** 5577-5591.

35. Huang M; Khor E; Lim L-Y. Uptake and Cytotoxicity of Chitosan Molecules and Nanoparticles: Effects of Molecular Weight and Degree of Deacetylation. *Pharmaceutical Research* 2004**; 21:** 344-353.

36. Eltoukhy AA; Siegwart DJ; Alabi CA; Rajan JS; Langer R; Anderson DG. Effect of Molecular Weight of Amine End-Modified Poly(B-Amino Ester)S on Gene Delivery Efficiency and Toxicity. *Biomaterials* 2012**; 33:** 3594-3603.

37. Bhise NS; Gray RS; Sunshine JC; Htet S; Ewald AJ; Green JJ. The Relationship between Terminal Functionalization and Molecular Weight of a Gene Delivery Polymer and Transfection Efficacy in Mammary Epithelial 2-D Cultures and 3-D Organotypic Cultures. *Biomaterials* 2010**; 31:** 8088-8096.

38. Kim J; Sunshine JC; Green JJ. Differential Polymer Structure Tunes Mechanism of Cellular Uptake and Transfection Routes of Poly(B-Amino Ester) Polyplexes in Human Breast Cancer Cells. *Bioconjugate Chemistry* 2014**; 25:** 43-51.

39. Wikstrand CJ; Friedman HS; Bigner DD. Medulloblastoma Cell-Substrate Interaction in Vitro. *Invasion Metastasis* 1991**; 11:** 310-324.

Supporting Information

Polymer	M_N	M_W	PDI
446	5935	10817	1.82
447	7957	31963	4.02
456	5826	10836	1.86
457	12195	65421	5.36
536	6495	14446	2.22
537	14512	89602	6.17

Table 4-S1. Gel permeation chromatography (GPC) characterization of polymers. The number-average (M_N) weight-average (M_W) molecular weights and polydispersity index (PDI) are shown for each polymer.

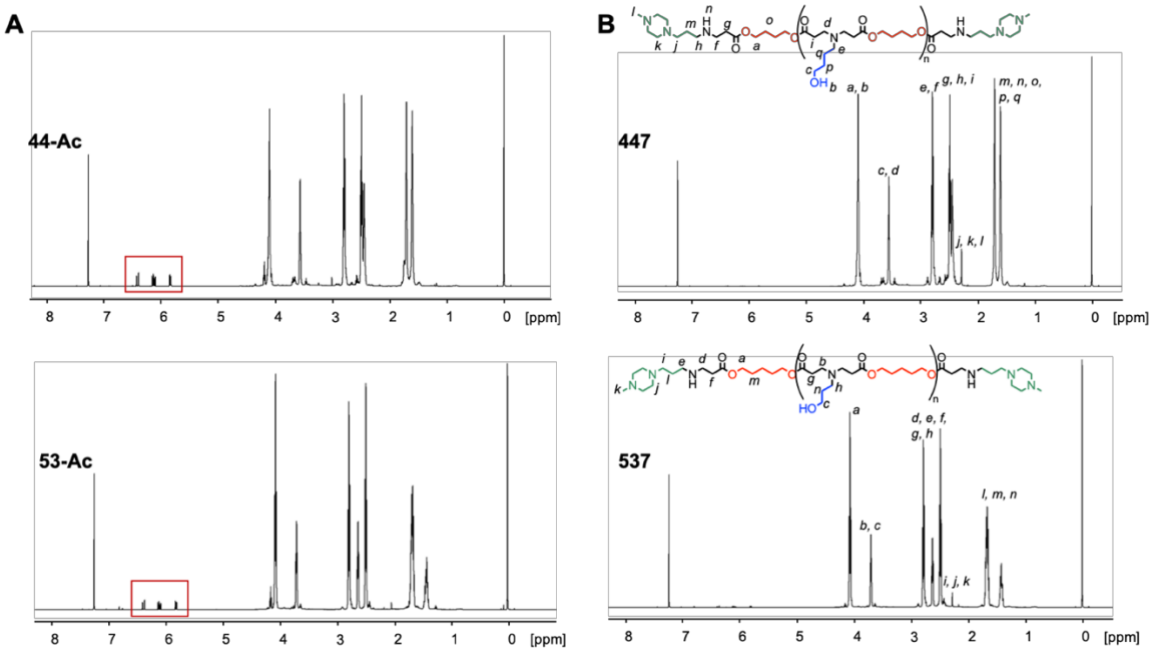

Figure 4-S1. ^{1}H NMR spectra of (A) acrylate-terminated and (B) end-capped polymers. Acrylate peaks (5.5-6.5 ppm) disappeared after end-capping. Polymer structures with labeled peaks are also shown.

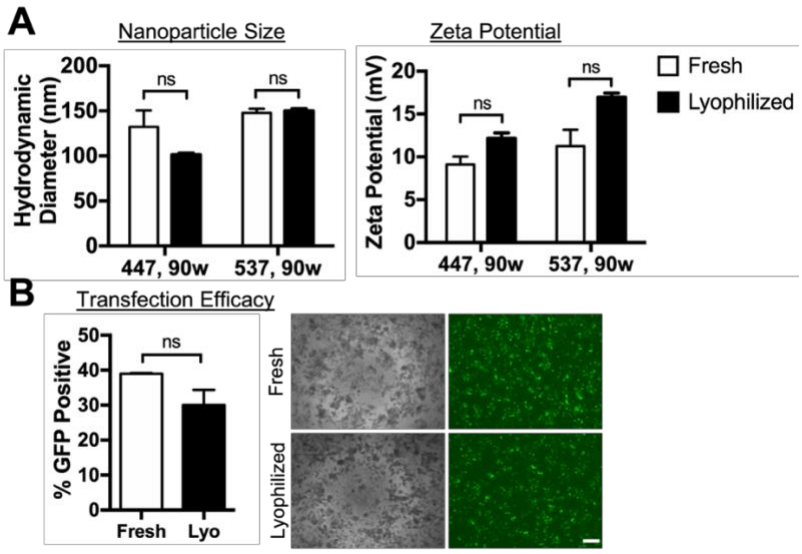

Figure 4-S2. Nanoparticle characterization before and after lyophilization. (A) Freshly prepared nanoparticles and nanoparticles resuspended in water after lyophilization were characterized for size and zeta potential using DLS (n = 3). **(B)** Functional performance of lyophilized nanoparticles were tested using lyophilized 447 nanoparticles to transfect BT-12 cells (n = 4); scale bar = 300 μm. Statistical significance determined using multiple t tests with Holm-Sidak corrections.

Chapter 5: Poly(beta-amino ester) nanoparticles enable non-viral delivery of CRISPR/Cas9 plasmids for gene knockout and gene deletion

Yuan Rui[1], Mahita Varanasi[1], Shanelle Mendes[1], Hannah M. Yamagata[1], David R. Wilson[1], and Jordan J. Green[1,2,3,*].

[1]Department of Biomedical Engineering, Institute for NanoBioTechnology, the Translational Tissue Engineering Center, [2]Departments of Ophthalmology, Oncology, Neurosurgery, Materials Science & Engineering, and Chemical & Biomolecular Engineering, [3]Bloomberg~Kimmel Institute for Cancer Immunotherapy, Johns Hopkins University School of Medicine, Baltimore, MD 21231, USA

Abstract

The CRISPR/Cas9 system is a powerful gene editing tool with wide-ranging applications, but the safe and efficient intracellular delivery of CRISPR components remains a challenge. In this study, we utilized biodegradable poly(beta-amino ester) nanoparticles to co-deliver plasmid DNA encoding Cas9 and sgRNA, respectively, to enable gene knockout following 1-cut edits as well as gene deletion following 2-cut edits. We designed a reporter system that allows for easy evaluation of both types of edits: gene knockout can be assessed by a decrease in iRFP fluorescence while deletion of an expression stop cassette turns on a red-enhanced nanolantern fluorescence/luminescence dual reporter. Nanoparticles enabled up to 70% gene knockout due to small indels as well as 45% gain-of-function expression after a 600-bp deletion edit. The efficiency of 2-cut edits is more sensitive than 1-cut edits to Cas9 and sgRNA expression level. We demonstrate promising biodegradable nanoparticle formulations for gene editing. Our findings also provide

new insights into the screening and transfection requirements for different types of gene edits, which are applicable for designing non-viral delivery systems for the CRISPR/Cas9 platform.

Introduction

The CRISPR/Cas9 gene editing system consists of a short guide RNA (sgRNA) conferring target sequence specificity which complexes with the Cas9 endonuclease to enable site-specific DNA cleavage.[1-3] This could result in gene knockout following non-homologous end joining (NHEJ) or, in the presence of a repair template, gene knock-in through homology-directed repair (HDR). Targeting sgRNAs to two sites flanking a genomic region of interest can result in the complete removal of the gene segment following NHEJ, which could be important in the silencing of genetic elements with no open reading frames such as microRNAs or long noncoding RNAs.[4, 5] CRISPR-mediated gene editing is contingent upon nuclear colocalization of both the Cas9 protein and sgRNA, and efficient intracellular delivery of CRISPR components remains a challenge.

Viral vectors have been demonstrated to be effective for delivery but are more challenging to produce for both pre-clinical and clinical studies and restricted in cargo size. This is problematic as the Cas9 gene is over 4 kb long, and delivery using adeno-associated viruses (AAVs; packaging capacity ~4.7 kb) sometimes require that different CRISPR components be packaged in separate viral particles, introducing complexity and potentially reducing efficacy.[6, 7] Synthetic vectors are largely agnostic to cargo size, and several recent reports have demonstrated strategies for non-viral intracellular delivery of the CRISPR/Cas9 gene editing platform. These include nanoparticle delivery of Cas9 and sgRNA as a ribonucleoprotein (RNP) complex [8-12] or in the form of Cas9 mRNA and sgRNA.[13, 14] Cas9 and sgRNA encoded in plasmid DNA is another delivery format for CRISPR gene editing. Plasmid DNA can be easily constructed using standard molecular cloning techniques to include different Cas9 structures,[15, 16] multiplex sgRNA,[17] and transcriptional targeting elements for cell type-specific editing.[18] Furthermore, large libraries of biomaterials previously used for plasmid DNA delivery can be screened for CRISPR gene editing in a high-throughput manner[19] to yield optimal formulations for gene editing in different applications.

It is important to note that delivery of CRISPR gene editing complexes in the form of plasmid DNA carries several potential safety concerns that must be taken into account when designing translationally relevant therapeutics. For example, there is a risk of plasmid DNA unintentionally integrating into the host genome, inducing insertional mutagenesis when highly active promoter elements are inserted into oncogenes or disrupt tumor suppressor genes.[20] Furthermore, plasmid DNA encoding Cas9 and sgRNA increases the persistence time of CRISPR RNPs inside the cell, which has been shown to increase off-target editing.[21] In this respect, delivery of CRISPR gene editing complexes in the form of mRNA or proteins has the benefit of low persistence time and reduced off-target editing. As effective non-viral delivery vehicles for mRNA or protein complexes are still somewhat lacking, however, CRISPR delivery in these formats can often suffer from low serum tolerance or poor *in vivo* efficacy.[22]

Although several studies have reported strategies for non-viral CRISPR plasmid delivery,[18, 23-26] most involve gene knockout applications using sgRNA designed to enable cleavage at a single site, and none to our knowledge have investigated the transfection requirements for gene deletion after cleavage at multiple sites. In this study, we designed a novel reporter system for easy detection of gene knockout following CRISPR-mediated cleavage at one genomic site (1-cut edit) as well as gene deletion following DNA cleavage at two sites flanking a region of interest (2-cut edit). We used poly(beta-amino ester)s (PBAEs), a class of biodegradable cationic polymers that has been shown to be effective at plasmid DNA delivery,[27] for intracellular delivery of plasmid DNA encoding both the Cas9 endonuclease and sgRNA, respectively, and demonstrate that these polymeric nanoparticles enable efficient 1-cut as well as 2-cut edits. Moreover, we systematically varied transfection parameters to probe the relationship between the expression of CRISPR components and the subsequent efficacy of different types of CRISPR-mediated edits. Our results provide important insights on the threshold gene expression levels required for 1- and 2-cut edits in easy-to-transfect as well as hard-to-transfect cell lines.

Results

Polymeric Nanoparticles for Gene Delivery

Polymer 446, which has been shown previously to be effective at plasmid DNA delivery to a variety of cells,[28, 29] was used to transfect HEK-293T cells (**Figure 5-1A**). The newly developed branched polymer 7,8-4-J11 enabled higher transfection efficacy in B16-F10 murine melanoma cells[30] (**Figure 5-S1**) and was used to transfect these cells. Both polymers formed nanoparticles 100-200 nm in diameter with positive zeta potentials (12-25 mV) (**Figure 5-1B**). Transfection efficacy as assessed with a GFP reporter plasmid showed that >80% cells were transfected in both cell lines (**Figure 5-1C**). However, when geometric mean fluorescence was used to quantify expression, 293T cells achieved expression that was nearly 1 order of magnitude higher than B16 cells.

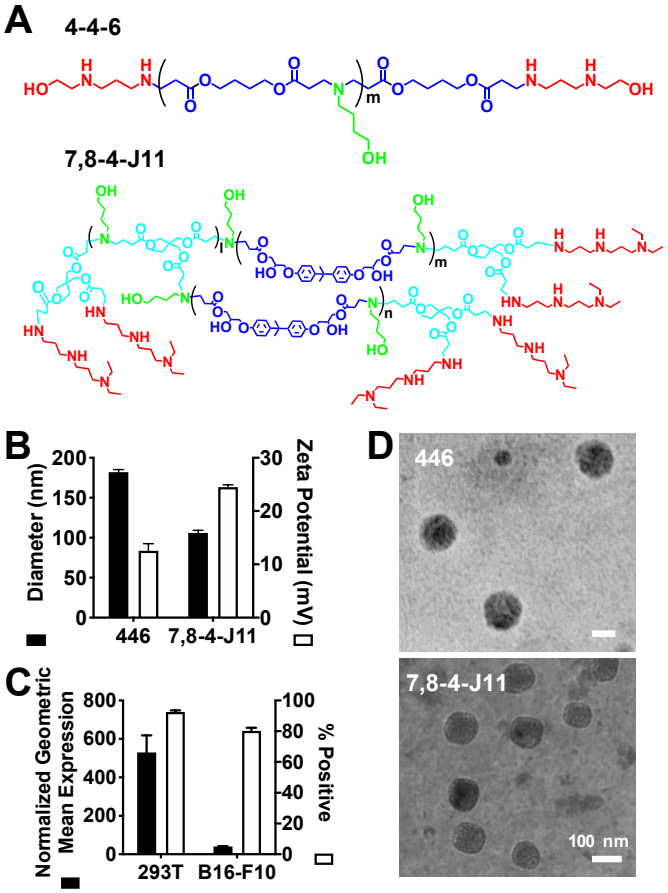

Figure 5-1. PBAEs form nanoparticles with plasmid DNA and enable transfection in HEK293T and B16-F10 cells. (A) Polymer structures for 446 and 7,8-4-J11, which were used to transfect HEK-293T and B16,F10 cells, respectively. **(B)** Nanoparticle hydrodynamic diameter and zeta potentials as measured by dynamic light scattering. 446 nanoparticles were formulated at 60 w/w while 7,8-4-J11 nanoparticles were

formulated at 30 w/w. **(C)** Transfection efficacy as measured by nanoparticles delivering GFP; 600 ng/well dose was used. Bars show average + SEM; *N* = 4. (D) TEM image of 7,8-4-J11 nanoparticles. Scale bar = 100 nm.

Gene Knockout Following 1-Cut Edits

The efficiency of 1-cut edits was assessed in 293T cells constitutively expressing a destabilized form of GFP (GFPd2). GFPd2 is ubiquitinylated for rapid degradation and has a half-life of around 2 hours (compared to a half-life of 26 hours for wildtype GFP).[31] This allows for rapid detection of gene knockout, which can be assessed by a decrease in GFP fluorescence following transfection with nanoparticles encapsulating two plasmids encoding the Cas9 endonuclease and a sgRNA targeting GFP, respectively. Nanoparticles co-delivering both plasmids enabled co-expression, generating 70% gene knockout as assessed by decrease in GFP fluorescence and 24% gene knockout as assessed by TIDE analysis of genomic DNA; formulations delivering either component alone had negligible effects (**Figure 5-2A**). A kinetic study revealed that gene knockout reached maximal levels on day 3 and was maintained for over 3 weeks (**Figure 5-2B**). The Surveyor® mutation detection assay was performed on cells treated with the combination nanoparticles or each component alone (**Figure 5-2C**) and confirmed that edits occurred only when both CRISPR components were delivered. Sanger sequencing revealed that most edits were single base-pair indels (**Figure 5-2D & 5-S2**), which likely caused frameshift mutations and subsequent gene silencing.

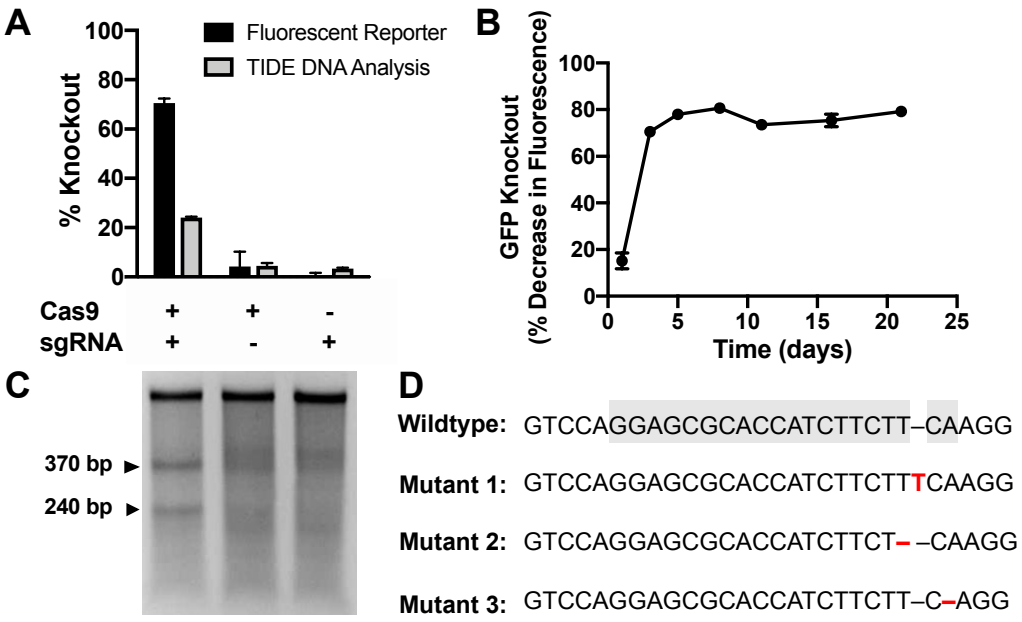

Figure 5-2. 446 nanoparticles enable sustained and robust gene knockout in HEK-293T cells. (A) GFP knockout experiments in HEK-GFPd2 cells showed gene knockout only when plasmids coding for both components were co-delivered. Gene knockout was assessed by flow cytometry analysis of loss of GFP fluorescence and using TIDE analysis of Sanger sequencing data of genomic DNA of treated cells. $N = 4$, data presented as mean + SEM. **(B)** Gene knockout was sustained over the 3-week experiment. $N = 4$. **(C)** Surveyor mutation detection assay confirms genomic DNA cleavage in Cas9+/sgRNA+ treatment group. (D) Sanger sequencing of edited cells suggest that all edits were small indels. sgRNA targeting region highlighted in grey; PAM site highlighted in red.

Gain-of-Function Edits after 2-Cut Stop Cassette Deletion

We designed a reporter system based on the Ai9 mouse[32] in which an expression stop cassette consisting of two SV40 terminators in series was placed upstream of a red-enhanced nanolantern (ReNL) fluorescence-luminescence dual reporter[33] (**Figure 5-3A**). This CRISPR-stop expression cassette was cloned into a piggyBac transposon plasmid to facilitate genomic integration at high efficiency after co-transfection with a piggyBac transposase plasmid.[34] A near-infrared fluorescent protein (iRFP670)[35] was also incorporated into the system as a selection marker for positively-expressing cells during fluorescence-activated cell sorting

(FACS). Thus, this system can be easily used to generate stably-expressing reporter cell lines for rapid read-out of knockout as well as deletion mutations.

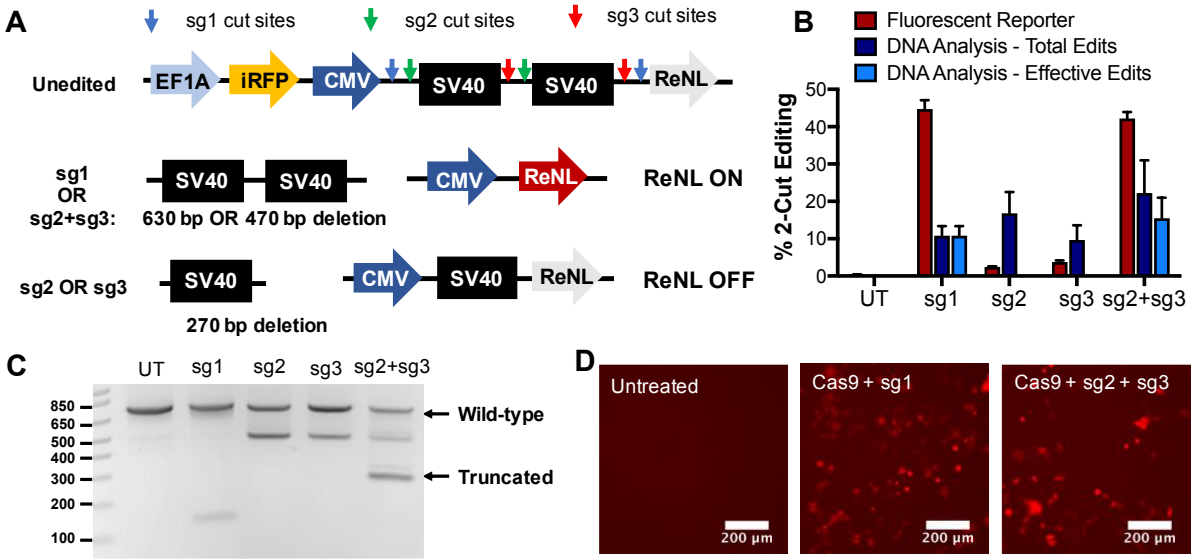

Figure 5-3. Deletion of an expression stop cassette following 2-cut edits result in gain-of-function ReNL expression. (A) Schematic demonstrating that complete removal of the dual-SV40 stop cassette results in turning on of ReNL. **(B)** 2-cut gene deletion efficiency in cells treated with Cas9 and different sgRNAs as assessed by flow cytometry for turning on of ReNL fluorescence reporter (fluorescent reporter), gel electrophoresis-based genomic DNA analysis for total % editing (total edits), and % editing leading to ReNL expression (effective edits). *N* = 4; data presented as mean + SEM. **(C)** Gel electrophoresis of PCR products of the genomic region surrounding the stop cassette show differential banding patterns in treated cells. (D) Fluorescence microscopy image of untransfected control cells and cells transfected with Cas9+sg1 or Cas9+sg2+sg3 plasmids, respectively. Scale bar = 200 µm.

The sgRNA sequence sg1, which was designed to remove both SV40 sequences (cut sites indicated by blue arrows in **Figure 5-3A**) via a 630 bp deletion, resulted in turning on of ReNL expression in nearly 50% of cells when co-transfected with Cas9 plasmid. In contrast, sgRNA sequences sg2 or sg3 were designed to only remove one SV40 sequence and yielded negligible levels of ReNL expression. A plasmid containing both sg2 and sg3 sequences governed by two U6 promoters (sg2+sg3) also resulted in turning on of expression through the deletion of both SV40 sequences (**Figure 5-3B**). Gain of ReNL fluorescence

increased steadily after nanoparticle transfection, reaching a plateau at 3 days (**Figure 5-S3**). Therefore all experiments assessing the efficacy of 2-cut edits were performed at 3 days post-transfection. Genomic DNA of cells treated with each sgRNA was PCR amplified for the 800 bp region immediately surrounding the stop cassette. Gel electrophoresis of the PCR products revealed unique banding patterns for each sgRNA (**Figure 5-3C**). For cells treated with sg1, a faint band around 150 bp corresponded to the deletion of around 630 bp and the complete removal of both SV40 sequences. The banding pattern for cells treated with sg2 or sg3 showed a band around 500 bp indicating the removal of only one SV40 sequence (270 bp deletion). As flow cytometry results showed negligible ReNL expression in these cells, this demonstrates that the remaining SV40 sequence was sufficient for blocking transcription of the downstream ReNL sequence and that removal of both SV40 sequences (>450 bp deletion) was necessary for gain-of-function ReNL expression. For cells treated with the combination sg2+sg3 plasmid, a faint band around 500 bp was observed, indicating that only one SV40 sequence was deleted in a fraction of edits, and a second band around 300 bp indicated that both SV40 sequences were deleted in other cells. Thus the level of editing that led to functional turning on of ReNL (termed Effective Edits in **Figure 5-3B**) was lower in these cells than the total editing level.

RT-qPCR of cells transfected with combination Cas9 and sg1 plasmids revealed that Cas9 mRNA levels stayed relatively constant throughout all time points evaluated (**Figure 5-4A**). Western blots over the same time course showed that Cas9 protein levels steadily accumulated after transfection; expression levels peaked at day 2 and became virtually undetectable after 11 days (**Figure 5-4B & 5-S6**). sgRNA levels plateaued after 48 hours (**Figure 5-4C**), and the same trend was observed in ReNL mRNA levels after stop cassette removal (**Figure 5-4D**).

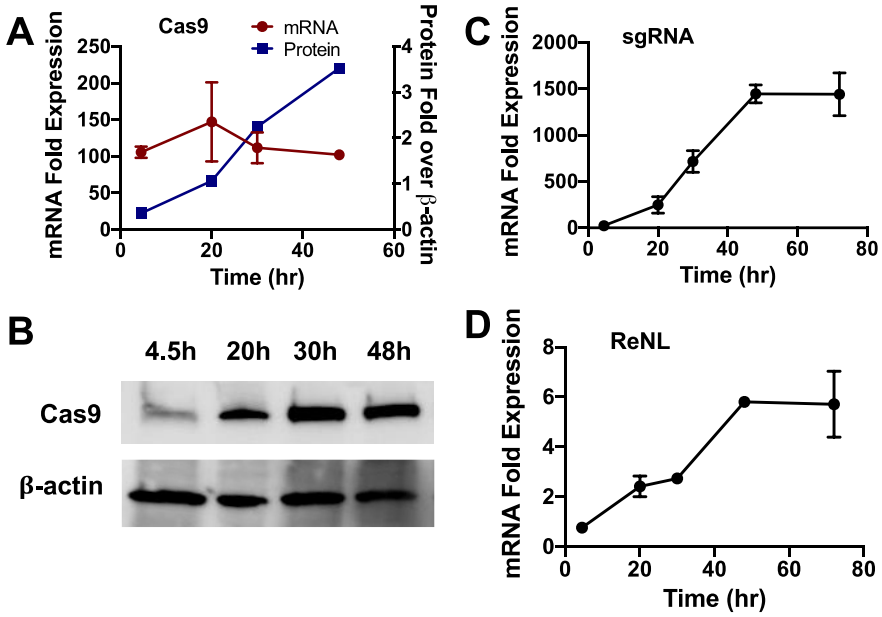

Figure 5-4. Expression kinetics of CRISPR components after co-delivery of Cas9 and sg1 plasmids in 293T cells. Cas9 mRNA **(A,** red curve**)** and protein expression **(A,** blue curve**; B)** were measured over time in HEK-293T cells. **(C)** sgRNA and (D) ReNL mRNA expression kinetics. *N* = 2 for qRT-PCR experiments; *N* = 1 for western blots.

Expression Thresholds for 1-Cut and 2-Cut Edits

In order to assess the expression levels necessary to achieve 1-cut knockout edits and 2-cut gain-of-function edits, respectively, we varied the dosage of plasmid DNA delivered in nanoparticles. In 293T cells engineered to express the CRISPR-stop gene construct, a GFP reporter was used to gauge transfection levels. Results showed that lowering the total DNA dose from 600 to 300 ng did not change the percentage of cells positively expressing GFP, but the geometric mean of fluorescence decreased by nearly 50% (**Figure 5-5A**). This effect can be observed in flow cytometry histograms as the 300 ng treatment yielded a larger population of cells with low GFP fluorescence compared to the 600 ng treatment (**Figure 5-5D, left panel**). Lowering total DNA dose significantly decreased levels of 2-cut deletion edits (**Figure 5-5B**) but did not significantly change the levels of 1-cut knockout edits (**Figure 5-5C**).

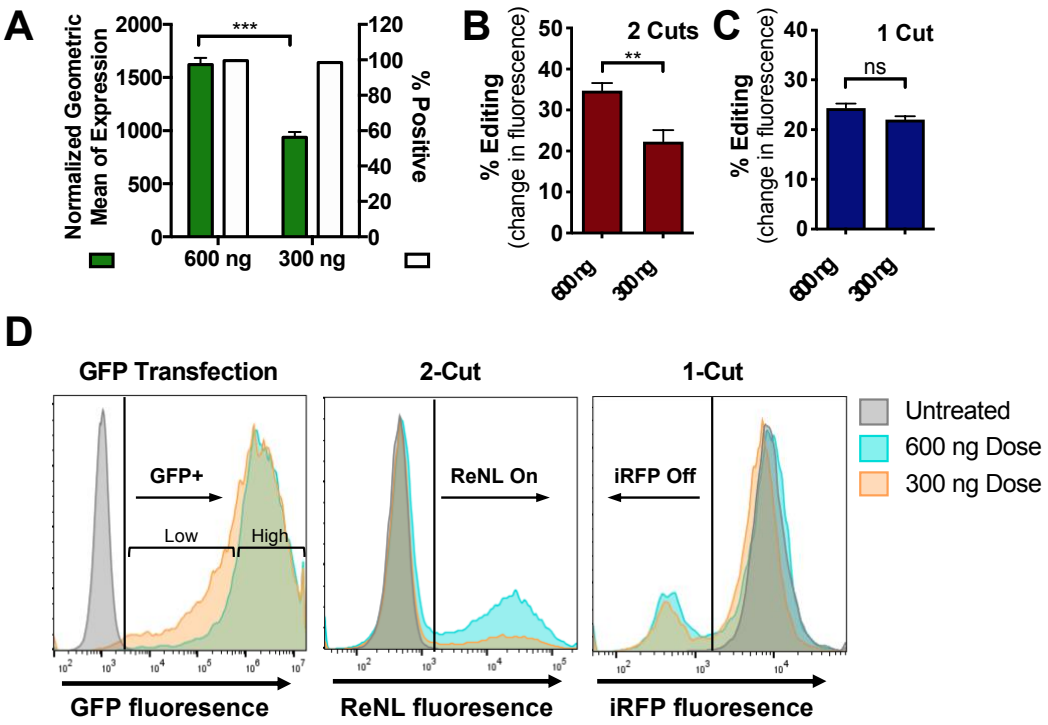

Figure 5-5. DNA dosage titration reveals different threshold expression requirements for 1-cut and 2-cut edits. (A) DNA dosage decrease from 600 ng to 300 ng did not change the overall percentage of GFP-positive cells but significantly decreased the geometric mean of expression. Dosage decrease significantly decreased the efficacy of 2-cut gene deletion edits **(B)** but not 1-cut iRFP knockout edits **(C)**. Statistical significance determined by Holm-Sidak corrected multiple t tests; **p < 0.01, ***p < 0.001. Data presented as mean + SEM; *N* = 4. **(D)** Flow cytometry plots of cells treated with different DNA doses.

We varied the total DNA dose delivered over a wider range in order to more thoroughly probe the effect of transfection efficacy on gene editing levels (**Figure 5-6A**). Plotting percent editing as a function of Cas9 mRNA expression levels revealed a logarithmic relationship for 1 cut edits (R^2 = 0.9550) and a linear relationship for 2-cut edits (R^2 = 0.9195). Transfection levels were further varied by manipulating cellular metabolic rates through incubation temperature variation (**Figure 5-6B**). Cells were transfected using the same nanoparticle formulation delivering the same DNA dose, after which they were either incubated at standard 37°C or treated with a transient "cold shock" via incubation at 30°C. Transfection efficacy, as

measured by Cas9 mRNA expression levels, increased significantly in cold-shocked cells; the same trend was observed for the level of 2-cut edits. Interestingly, cold shock treatment did not significantly change the level of 1-cut editing efficiency, which is consistent with the results from dose titration experiments.

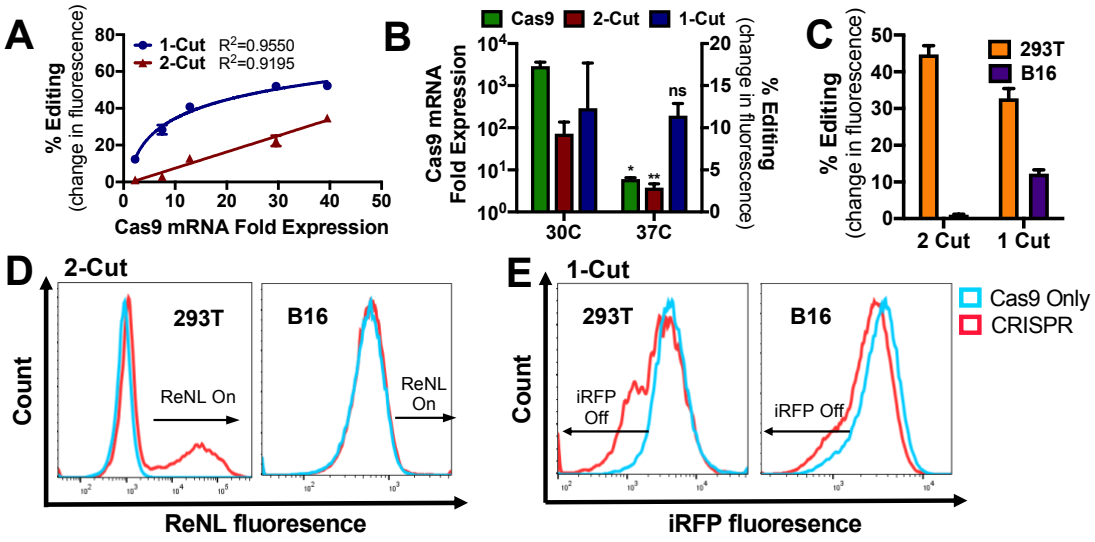

Figure 5-6. 1-cut and 2-cut edits in easy-to-transfect HEK-293T cells and hard-to-transfect B16-F10 cells. (A) 1-cut edit efficiency correlated logarithmically with level of transfection as indicated by qRT-PCR measurement of Cas9 mRNA expression while 2-cut edit efficiency correlated linearly in 293T cells. **(B**) In B16 cells, transient cold shock after transfection significantly increased transfection efficacy (measured by Cas9 mRNA expression levels) as well as 2-cut editing efficiency but no significant change was seen in 1-cut editing efficiency as assessed by Holm-Sidak corrected multiple t tests; *$p < 0.05$, **$p < 0.01$. **(C)** B16 cells achieved minimal levels of 2-cut edits; 1-cut edits were lower compared to 293T cells, but the difference is smaller. Data in **(B)** and **(C)** shown as mean + SEM; $N = 4$. Differences in editing are observed in flow cytometry histograms **(D-E)**.

1-cut knockout of iRFP expression and 2-cut gain-of-function edits were also performed on B16-F10 murine melanoma cells, which achieved lower levels of transfection compared to 293T cells. This was seen both when transfection was assessed using the geometric mean fluorescence of GFP expression when using a GFP reporter gene for nanoparticle screening (**Figure 5-1**) as well as the level of Cas9 mRNA expression

(**Figure 5-4 & 5-S5**). The lower transfection level in B16 cells was reflected most notably in the results for 2-cut editing, where the ReNL fluorescence observed in B16 cells was 1 order of magnitude lower than 293T cells (**Figure 5-6C & 5-6D**). Interestingly, the effect of lower transfection efficacy was less pronounced for 1-cut iRFP knockout experiments. Although lower knockout levels were observed in B16 compared to 293T cells, the difference was much smaller (12% for B16 and 33% for 293T). Representative flow cytometry histograms showed that in 293T cells, 1-cut editing produced a new iRFP-negative peak while no such peak was observed in B16 cells, which showed an overall population shift of iRFP expression (**Figure 5-6E**). Since each cell very likely contains several copies of iRFP integrated into the genome,[36] the peak in 293T cells indicates that 1-cut editing produced a small population of cells with complete iRFP knockout whereas the edited population in B16 cells lost some but not all copies of iRFP, and the incomplete iRFP knockout in this population resulted in a general shift in fluorescence. Combined, this validates results seen earlier with dose titration as well as temperature modulation experiments and confirms our hypothesis that 1-cut knockout edits require a lower expression threshold compared to 2-cut edits.

Standard transfection reagents were also used to assess 2-cut editing efficiency. For both cell lines, the commercially available cationic polymer transfection reagent jetPrime® resulted in significantly lower editing levels than PBAE nanoparticles (**Figure 5-S7**). The commercially available cationic lipid transfection reagent Lipofectamine™ 3000 enabled significantly higher editing than earlier generation linear PBAE polymer 446 in 293T cells but did not achieve significantly higher levels of editing than the newly developed next-generation branched PBAE polymer 7,8-4-J11in harder-to-transfect B16 cells. Notably, Lipofectamine™ 3000 caused significantly higher levels of cytotoxicity than both PBAE nanoparticle formulations, further demonstrating the advantage of using a biodegradable gene delivery system.

A multiplex tRNA-gRNA expression system

To facilitate a simpler method for multiplex CRISPR editing, we designed a tRNA-gRNA expression system[17] which utilizes the cell's endogenous tRNA processing machinery to generate multiple sgRNAs **(Figure 5-7A)**. Using a simple Golden Gate assembly strategy, we created a plasmid in which the targeting sequences and gRNA scaffolds of sg2 and sg3 are arrayed in tandem with pre-tRNA, with all components

governed by a single U6 promoter. Mature sgRNA is released after processing of the primary RNA transcript by tRNA-processing RNases. When transfected into cells alongside the Cas9 plasmid, this tRNA-gRNA plasmid enabled similar levels of 2-cut editing as the plasmid in which a U6 promoter governed each sgRNA **(Figure 5-7B)**. This demonstrates that the multiplex tRNA-gRNA expression system effectively expressed both sgRNAs required for 2-cut editing.

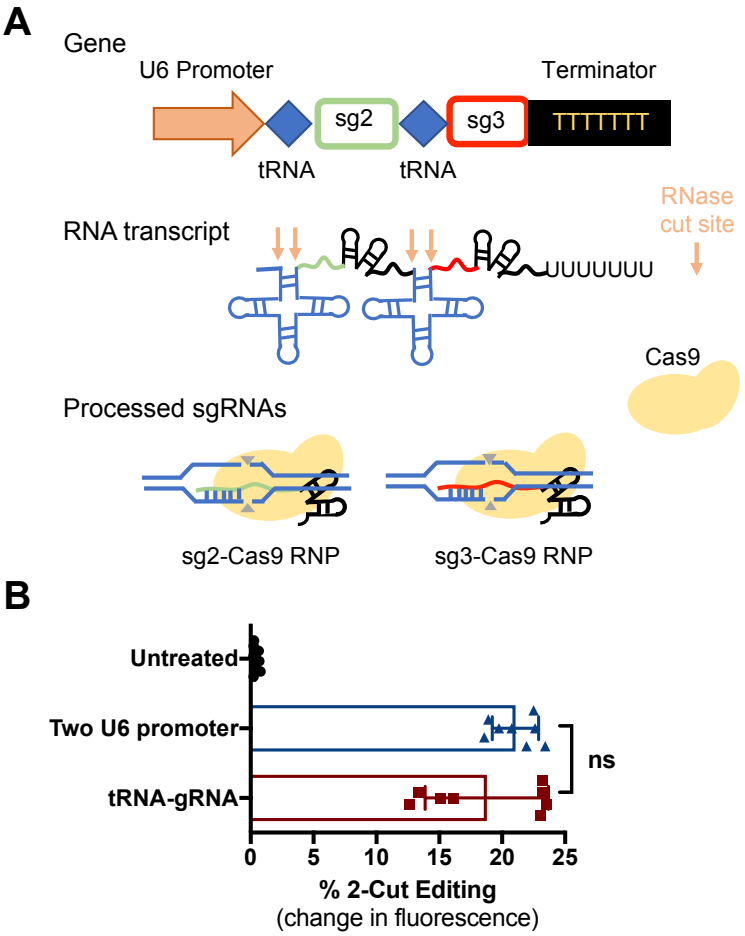

Figure 5-7. A tRNA-gRNA expression system for multiplex editing. (A) Schematic of a multiplex sgRNA expression system in which multiple tRNA-gRNA units are arrayed in tandem. The primary RNA transcript is processed by the endogenous tRNA machinery, releasing mature sgRNAs. **(B)** The tRNA-gRNA plasmid coding for sg2 and sg3 results in similar levels of 2-cut editing compared to a plasmid in which each sgRNA is governed by an individual U6 promoter (sg2+sg3). Statistical analysis was assessed by one-way ANOVA with Tukey post-hoc tests. Data presented as mean +/- SEM; $N = 4$.

Discussion

In this work, we demonstrated that both linear and branched PBAE nanoparticles co-delivering two DNA plasmids encoding Cas9 and sgRNA, respectively, can achieve efficient gene editing in both 1-cut knockout as well as 2-cut gene deletion applications. We created a novel CRISPR-stop reporter system that can be used to assess both types of edits: an iRFP fluorescent reporter can be silenced by indels after 1-cut edits while an expression stop cassette upstream of a ReNL reporter can be deleted using 2-cut edits for gain-of-function ReNL expression. This expression cassette was cloned into a piggyBac transposon system and can be used to generate stably-expressing cell lines to investigate gene editing efficacy *in vitro*, eliminating the need to culture primary cells from the Ai9 mouse,[37] on which our reporter system is based. This system further has the potential to be used as an *in vivo* reporter for live-animal imaging studies of effective 2-cut gain-of-function ReNL expression using the red-shifted luminescent properties of ReNL. Using two cell lines stably expressing this construct – easy-to-transfect HEK-293T and hard-to-transfect B16-F10 – we further investigated the transfection requirements for each type of gene editing.

Several recent studies have demonstrated the feasibility of using polymeric nanoparticles, including a different PBAE formulation,[38] to deliver CRISPR gene editing components in the form of plasmid DNA.[18, 23-25] All of these systems have exclusively investigated the use of 1-cut editing to achieve gene knockout, and none have presented a systematic study of the expression levels required for 1-cut and 2-cut edits. The removal of a gene segment requires sgRNA to target two sites flanking the region of interest and is significantly more difficult than 1-cut knockout edits.[5] To date, only 3 studies have reported the use of non-viral delivery vectors for 2-cut gene deletion by delivering Cas9 mRNA and sgRNA[14] or RNP complexes[12, 37], but plasmid delivery with polymeric nanoparticles to achieve this type of deletion has not been previously reported. The use of DNA plasmids to encode Cas9 overcomes the manufacturing challenges of producing large scales of Cas9 mRNA or Cas9 protein, but the intracellular delivery and expression of exogenous DNA can be more challenging than the delivery of its downstream products.

We evaluated two types of PBAE nanoparticles to encapsulate Cas9 and sgRNA plasmids for intracellular delivery of gene editing complexes. One of these was the well-published linear PBAE polymer

446 that has shown efficacy in multiple cell types and one was a newly developed branched PBAE polymer 7,8-4-J11, and both were found to be useful for developing efficacious biodegradable nanoparticles for gene editing. The cationic polymer and anionic DNA self-assembled into nanoparticles 100-200 nm in diameter with positive zeta potentials (12-25 mV) (**Figure 5-1**). Previous reports have shown that high levels of co-delivery can be achieved by pre-mixing plasmids prior to nanoparticle assembly.[39] Using this strategy, we showed successful co-delivery of CRISPR plasmids that enabled robust 1-cut gene knockout (**Figure 5-2**). More importantly, we demonstrated a versatile gene deletion platform in which a single sgRNA targeting sites flanking the region of interest or a combination of sgRNAs targeting sites throughout the region of interest both resulted in successful removal of the entire gene segment (**Figure 5-3**). Successful deletion of up to 630 bp could be easily visualized through the gain-of-function expression of a ReNL fluorescence/luminescence dual reporter.

Evaluation of the expression kinetics of Cas9 and sgRNA revealed that Cas9 mRNA maintained at high levels throughout the time period tested (4.5-48 hr), while sgRNA expression reached peak levels at 48 hr and plateaued out thereafter (**Figure 5-4**). The plateau observed in the expression of sgRNA (but not Cas9) in the short term is likely due to a difference in the expression kinetics of the U6 promoter driving sgRNA expression compared to the CMV promoter driving Cas9 expression. After a slower start, sgRNA rapidly accumulated inside the cell, eventually reaching a plateau at which point the expression of additional copies of sgRNA was likely balanced out by plasmid dilution through cellular division. This is a common pattern seen in transient gene expression induced by nanoparticle transfection,[40] and we would expect expression levels of both Cas9 and sgRNA to drop at longer time points. Indeed, when we evaluated Cas9 protein accumulation at longer time periods, we found that Cas9 protein levels declined steadily after 48 hours and was virtually undetectable at 11 days post transfection (**Figure 5-S6**). Compared to delivery of CRISPR components in mRNA or protein form, where Cas9 protein expression decreased to below levels of detection after 3 days,[21] the long Cas9 persistence time following plasmid DNA delivery raises concerns of off-target editing. It is important to note that the risk of off-target editing following synthetic nanoparticle delivery of CRISPR plasmids is significantly lower than when viral vectors are used for gene editing.

However, these risks can be further mitigated by using Cas9 variants[41, 42] that have been engineered to have enhanced proofreading and lower off-target editing rates compared to wildtype Cas9.

We further explored the transfection requirements for 1-cut and 2-cut edits by titrating the total DNA dose delivered. Interestingly, decreasing total DNA dose from 600 ng to 300 ng significantly decreased the level of 2-cut editing but did not affect the level of 1-cut edits (**Figure 5-5**). The same trend was observed when transfection efficiency was varied by treating transfected cells with a minor "cold shock" (**Figure 5-6**). A brief cold shock slowed the rate of cellular division, which enhanced protein accumulation in expressing cells and decreased the rate of plasmid DNA dilution in the cell population. This increased transfection efficiency and the level of 2-cut edits, which is consistent with previous reports using cold shock treatment to enhance the editing efficiency of ZFN-mediated gene disruption[43] or CRISPR-mediated homology-directed repair.[44] In contrast, cold shock treatment did not significantly change the efficiency of 1-cut edits. Recent studies on the enzyme kinetics of sgRNA-Cas9 RNPs have reported that while Cas9-sgRNA binding (k_b = 6.1 s^{-1}), target DNA binding ($t_{1/2}$ = 4-40 s), and DNA cleavage events (k_c = 25-90 s^{-1}) happen very quickly,[45] the release of DNA cleavage products is extremely slow ($t_{1/2}$ = 43-91 h),[46] causing Cas9 to be virtually a single turnover enzyme. Taken together with these results, our data suggest that 2-cut edits have a much higher expression threshold than 1-cut edits because twice the number of DNA cleavage events are required for successful edits to occur.

The expression thresholds of 1-cut and 2-cut edits have important implications on gene editing in different cell types. To demonstrate this, we compared the gene editing efficiency in easier-to-transfect HEK-293T and harder-to-transfect B16-F10 cells. HEK-293T cells were derived from the parent HEK-293 human embryonic kidney cell line and further modified with the SV40 large T antigen.[47] The SV40 large T antigen causes plasmid DNA containing the SV40 origin of replication to unwind inside HEK-293T cells, allowing for plasmid DNA replication and high levels of transfection.[48] HEK-293T cells are widely known to be an easy-to-transfect cell line and are commonly used for the production of recombinant proteins[49] and viral vectors[50] after transient plasmid DNA transfection using commercially-available transfection reagents. B16-F10 cells are a well-established murine melanoma cell line that are commonly used for tumor inhibition

studies.[51] B16-F10 cells have been reported to be much more difficult to transfect with non-viral vectors,[52] which is in part due to significantly lower nanoparticle uptake levels (**Figure 5-S8**).

Although the top nanoparticle formulation for each cell line achieved >80% transfection as assessed by percentage of total cells transfected, the level of expression, as assessed by the normalized geometric mean of expression of a GFP reporter, was 1 order of magnitude higher for 293T cells (**Figure 5-1**). This discrepancy was reflected in the level of 2-cut edits as B16 cells showed very minimal levels of ReNL expression after stop cassette deletion (**Figure 5-6**). In contrast, the difference in editing efficiency between the two cell lines was much smaller for 1-cut iRFP knockout (<3-fold difference compared to nearly 44-fold difference for 2-cut edits). These results further validate our hypothesis that the efficiency of 2-cut edits correlates more strongly with the level of DNA expression. Taken together, we have demonstrated that low levels of DNA transfection severely limit 2-cut editing efficiency. One solution for improving 2-cut editing efficiency is to deliver CRISPR components in RNP form, which we recently demonstrated enabled >40% 2-cut editing in B16 cells after nanoparticle delivery of CRISPR RNPs targeted to excise the transcription stop cassette.[53] This demonstrates that bypassing limits in DNA transfection altogether may be a viable way to achieve efficient 2-cut editing in hard-to-transfect cell lines such as B16 cells.

Finally, we designed and implemented a tRNA-gRNA plasmid in which the expression of multiplex sgRNAs is governed under a single U6 promoter. The expression of two sgRNAs required for turning on of ReNL fluorescence in these tRNA-gRNA tandem repeats enabled similar levels of editing compared to that of a plasmid in which each sgRNA is governed by its own U6 promoter (**Figure 5-7**). This expression system has the advantage of ease of synthesis as upwards of 6 sgRNAs can be arranged in tandem using a single Golden Gate assembly reaction.[17] More importantly, the tRNA-gRNA system reduces the need for repeating U6 promoters, enabling the use of a much smaller plasmid construct especially at high numbers of sgRNAs. Originally developed for use in rice plants,[17] this system has also been adapted for use in yeast[54] and zebrafish.[55] To our knowledge, this is the first time it has been adapted for gene editing in mammalian cells.

In summary, we have demonstrated that PBAE nanoparticles co-delivering plasmids encoding Cas9 and sgRNA can achieve 1-cut knockout as well as 2-cut deletion edits. We designed a novel reporter system

whereby both modes of edits can be easily evaluated. 2-cut deletion events required much higher levels of transfection than 1-cut gene knockout edits, which we demonstrated by titrating the DNA dosage delivered, treating transfected cells with a transient cold shock, and comparing editing efficiencies in two cell lines with different transfection efficacy. The PBAE/DNA nanoparticles optimized here are promising for DNA-based non-viral gene editing. Further, the results presented herein have implications on the design and screening of next-generation non-viral delivery vehicles broadly for CRISPR/Cas9 gene editing.

Materials and Methods

Materials

Small molecules used as monomers for polymer synthesis were obtained as follows: bisphenol A glycerolate (1 glycerol/phenol) diacrylate (B7; 411167), trimethylolpropane triacrylate (B8; 246808), 2-(3-aminopropylamino)ethanol (E6; 09293), and N,N-diethyldiethylenetriamine (J11; 518832)[56] were purchased from Sigma-Aldrich; 1,4-butanediol diacrylate (B4; 32780) and 4-amino-1-butanol (S4; A12680) were purchased from Alfa Aesar. The following plasmids were purchased from Addgene: hCas9 (41815),[3] gRNA_GFP-T2 (41820),[3] pCAG-GFPd2 (14760),[31] PBCAG-eGFP (40973),[57] piRFP670-N1 (45457),[35] tubulin-ReNL_pcDNA3 (89530).[58] PB-CMV-MCS-EF1a-RFP PiggyBac plasmid (PB512B-1) and PiggyBac transposase expression plasmid (PB200A-1) were purchased from System Biosciences. sgRNA gBlock sequences were purchased from IDT and the expression stop cassette was synthesized by SynBio-Tech (Monmouth Junction, NJ). Restriction enzymes and T4 DNA ligase for molecular cloning were purchased from New England BioLabs.

Polymer Synthesis

Polymer 446 was synthesized by reacting monomers B4 and S4 at a molar ratio of 1.1:1 at 90°C with stirring overnight. The B4-S4 polymer was dissolved in anhydrous THF at 167 mg/mL and added to monomer E6 (0.5 M in THF) at a 3:2 volume ratio and reacted at room temperature for 1 hour. The end-capped polymer was washed in diethyl ether twice to remove unreacted monomers and oligomers. Solvents were removed in a vacuum desiccant chamber and polymer was dissolved in DMSO at 100 mg/mL, then stored at -20°C with desiccant. Polymer 7,8-4-J11 was synthesized by reacting monomers B7, B8, and S4 at an

overall vinyl:amine ratio of 2.2:1 and monomer concentration of 200 mg/mL in anhydrous DMSO at 90°C with stirring overnight; the acrylate monomer composition was 80% B7 and 20% B8 by mole fraction. Polymer end-capping and purification were done following the same procedure as polymer 446 but using monomer J11.

Nanoparticle Characterization

Nanoparticle hydrodynamic diameter was measured via dynamic light scattering (DLS) using a Malvern Zetasizer NanoZS (Malvern Instruments). Samples were prepared in 25 mM sodium acetate (NaAc), pH 5.0, and then diluted 1:6 in 150 mM PBS to determine hydrodynamic diameter in neutral, isotonic buffer. Zeta potential was measured by electrophoretic light scattering on the same instrument. Transmission electron microscopy (TEM) images were captured using a Philips CM120 (Philips Research) on 400 square mesh carbon coated TEM grids. Samples were prepared at a polymer concentration of 1.8 mg/mL at 30 w/w in 25 mM NaAc and 30 μL were allowed to coat TEM grids for 20 minutes. Grids were then rinsed with ultrapure water and allowed to fully dry before imaging.

Cell Culture and Cell Line Preparation

HEK-293T and B16-F10 cells were cultured in Dulbecco's Modified Eagle Medium (DMEM; ThermoFisher) supplemented with 10% FBS and 1% penicillin/streptomycin. Cells were induced to constitutively express fluorescent protein constructs using the PiggyBac transposon/transposase system. The GFPd2 gene was cloned into the PB-CMV-MCS-EF1a-RFP plasmid using restriction enzyme cloning to create a PiggyBac transposon plasmid containing the GFPd2 gene. A sequence containing iRFP and transcription stop sequences was cloned into the PBCAG-eGFP plasmid backbone, and the ReNL gene was inserted into this plasmid using restriction enzyme cloning to create a PiggyBac transposon plasmid containing the iRFP-STOP-ReNL sequence (plasmid available on Addgene). Each transposon plasmid was co-transfected with the PiggyBac transposase plasmid into HEK-293T and/or B16-F10 cells using nanoparticles as described below. Fluorescent protein signal from DNA not integrated into the cell genome was allowed to fade over 5 passages, after which positive cells were isolated using fluorescence-assisted cell

sorting (FACS). Cells were further expanded for 3 more passages and sorted again to generate stably-expressing cell lines.

sgRNA Design and Preparation

Single guide RNAs were designed using the CRISPR.mit.edu platform and ordered as gBlocks containing the U6 promoter, a unique 20 bp targeting sequence, and the duplex optimized sgRNA scaffold from IDT.[5] The gBlocks were cloned into the pCAG-GFPd2 plasmid backbone using restriction enzyme cloning. sgRNA plasmids were transformed into DH5α competent *E. coli* (NEB), grown out overnight at 37°C in 5 mL LB broth liquid cultures, and plasmid DNA was harvested using QIAprep miniprep kit (Qiagen). Plasmid DNA was characterized using NanoDrop spetrophotomoter (ThermoFisher) and sequence confirmed via Sanger sequencing before use in transfections. All sgRNA target sequences are listed in Table S2 and plasmids are available on Addgene.

The gRNA-tRNA plasmid containing multiplex sgRNA constructs under a single U6 promoter was synthesized according to the protocol by Xie *et al.*[17] Briefly, the pGTR construct containing a sgRNA scaffold sequence fused to a tRNA fragment was synthesized as a gBlock from IDT and cloned into a plasmid via restriction enzyme cloning. This pGTR plasmid was used as the template DNA for PCR reactions which produced amplicons used in a hierarchical Golden Assembly process to generate a DNA fragment containing the tRNA-gRNA tandem arrays. This fragment was then cloned into a backbone plasmid containing a U6 promoter via restriction enzyme cloning. The sequences for the pGTR sequence and PCR primers used are listed in Table S3.

Transfection

Cells were plated at 15,000 cells per well (HEK-293T) or 10,000 cells per well (B16-F10) in 100 μL complete medium in CytoOne 96 well plates (USA Scientific) and allowed to adhere overnight. Polymers and DNA were dissolved separately in 25 mM NaAc at the desired concentrations and then mixed together via pipetting. Nanoparticles were allowed to self-assemble for 10 minutes and then 20 μL of the nanoparticle solution was added per well for a final volume of 120 μL and 600 ng DNA per well unless otherwise noted; for transfection experiments using the CRISPR/Cas9 system, the Cas9 and sgRNA plasmids were used at a

1:1 weight ratio. For example, in order to formulate nanoparticles that would deliver 600 ng DNA per well in 96 well plates at a polymer-to-DNA weight ratio of 60 (60 w/w), plasmid DNA was first dissolved in 25 mM NaAc at 0.06 mg/mL and polymer dissolved at 3.6 mg/mL. These two solutions were then mixed at a 1:1 volume ratio and allowed to self-assemble into nanoparticles. The N/P ratio is 34.5 for the 446 60 w/w formulation and 14.5 for the 7,8-4-J11 30 w/w formulation (**Calculation 5-S1**). Nanoparticles were incubated with cells for 2 hours at 37°C, at which point the media and nanoparticles were removed and replaced with fresh complete media. Commercially available transfection reagents jetPrime® (Polyplus) and Lipofectamine™ 3000 (ThermoFisher) were used as instructed by the manufacturer. For cold shock treatment, cells were transfected using standard transfection procedures and allowed to recover at 37°C after media change for 6 hours before being moved to 30°C. Cells were maintained at 30°C for 3 days, after which time they were moved back to 37°C.

Transfection and gene editing efficacies were evaluated via flow cytometry using a BD Accuri C6 flow cytometer (BD Biosciences). For nanoparticle screening experiments using a GFP reporter gene, transfection was quantified via two methods: 1) the percentage of cells positively expressing GFP when gated against untreated cells was reported as % positive expression; 2) the geometric mean fluorescence intensity in the FL1 channel (corresponding to GFP) for each treated well was normalized against that of untreated control wells, and the normalized geometric mean expression was reported. CRISPR knockout was quantified by normalizing the geometric mean fluorescence of treated wells to that of wells transfected with Cas9 plasmid only. Gain of fluorescence was quantified as the percentage of cells positively expressing the fluorescent protein when gated against untreated control. Gene editing in gene deletion experiments was also assessed by luminescence readings using Promega Nano-Glo® Luciferase assay system (Promega) measured with a Synergy2 plate reader (Biotek) with open optics and normalized to untreated control. Cell viability was assessed 24 hours post-transfection using MTS CellTiter 96 Aqueous One cell proliferation assay (Promega). (N = 4 ± SEM). Unless otherwise stated, flow cytometry to assess gene editing efficacy was performed on day 3 post-transfection.

Surveyor Assay

Genomic DNA from cells transfected with the combination Cas9-sgRNA plasmids and untransfected control were isolated using GeneJET genomic DNA purification kit (ThermoFisher). A 660 bp region flanking the predicted cut site was PCR amplified, and the PCR products were purified using QIAquick PCR purification kit. 400 ng of PCR amplicons were hybridized, and the Surveyor assay was performed using Surveyor® Mutation Detection Kit (IDT) following manufacturer's instructions. The uncut and cut DNA products were then run on a 2% agarose gel stained with ethidium bromide in tris/borate/EDTA (TBE) buffer and imaged under UV light.

TIDE Analysis to Assess 1-Cut Editing Efficiency

Sanger Sequencing was performed on purified PCR products from Surveyor assays. Sequencing data was uploaded to the online TIDE analysis tool (https://tide.deskgen.com/) to assess 1-cut editing efficiency.

Gel Electrophoresis Assay to Assess 2-Cut Editing Efficiency

Genominc DNA from 293T-CRISPR-stop cells transfected with Cas9 and sgRNA plasmids or untransfected controls were isolated as described above. An 800 bp region flanking the predicted cut sites was PCR amplified, and PCR products were purified as described above. Standard gel electrophoresis was performed on PCR products using 2% agarose gel stained with ethidium bromide in TBE buffer at 80V for 45 minutes and imaged under UV light to reveal unique banding patterns. Band intensities were quantified using ImageJ image processing software and % editing was calculated using the method reported by Schumann *et al.*[59] Edits where >450 bp were deleted were quantified as *Effective Edits* leading to gain-of-function ReNL expression while all deletion edits were quantified as *Total Edits* for each sample.

Sanger Sequencing to Detect Gene Editing

PCR products for the Surveyor assay were cloned into plasmid vectors using NEB PCR Cloning kit and transformed into DH5α competent *E. coli* (NEB). 30 colonies were grown out in 5 mL liquid cultures overnight and the plasmid DNA was isolated and characterized by Sanger sequencing.

qRT-PCR

Cells transfected with the combination Cas9-sgRNA plasmids in a 12-well plate were collected, and total RNA including small RNAs (<100 nt) were extracted using miRNeasy Mini kit (Qiagen). RNA was reverse transcribed using iScript cDNA synthesis kit (Bio-Rad), and qRT-PCR was run on a StepOnePlus Real-Time PCR system (ThermoFisher) using SYBR Green PCR Master Mix (ThermoFisher). The qPCR program is as follows: 95°C for 10 min.; 95°C 15 sec, 55°C 30 sec, and 60°C 30 sec for 40 cycles. Primers used for qRT-PCR are listed in Table S1. Results are shown as fold expression over β-actin.

Western Blotting

Transfected cells in 12-well plates were lysed in a solution of 1X RIPA buffer and 1X Protease/Phosphatase Inhibitor Cocktail (ThermoFisher). The lysate was cleared by centrifugation, protein concentration was determined using Pierce Micro BCA assay (ThermoFisher), and samples were denatured in Laemmli sample buffer (Bio-Rad) in the presence of DTT. 50 μg proteins were loaded into 4-15% TGX Precast Protein Gels (Bio-Rad). Proteins were then transferred to a PVDF membrane using a Pierce Power Blotter (ThermoFisher). Membranes were blocked in 5% non-fat milk for 1 hr at RT and probed with primary antibodies against Cas9 (Cell Signaling Technologies 14697; 1:500) or β-actin (Abcam ab8226; 1:10,000) at 4°C overnight. Secondary antibodies were applied at RT for 1 hr (m-IgGK BP-HRP; Santa-Cruz Sc-516102; 1:1000). The membrane was developed with Amersham ECL Western Blotting Detection Reagent (GE Healthcare) and imaged using an ImageQuant LAS 4000 CCD imager (GE Healthcare). Semi-quantitative analysis of Cas9 protein expression was done by calculating band intensities using ImageJ image analysis software and normalizing the intensity of Cas9 bands to that of β-actin.

Author Contributions

Conceptualization, Y.R., D.R.W. and J.J.G.; Methodology, Y.R., D.R.W. and J.J.G., Investigation Y.R., M.V., S.M., H.M.Y. and D.R.W.; Resources and funding acquisition, J.J.G.; Writing and editing, Y.R., M.V., S.M., H.M.Y. D.R.W. and J.J.G.; Supervision and administration, J.J.G.

Acknowledgments

The authors would like to thank the following organizations for financial support: NSF Graduate Research Fellowship DGE-0707427 (DRW) and DGE-1232825 (YR), Microscopy Core Grant (S10 OD016374) and the United States NIH grants R01EB016721 (JJG), and R01EB022148 (JJG), Wilmer Core Grant P30 EY001765. JJG thanks the Bloomberg~Kimmel Institute for Cancer Immunotherapy and the Research to Prevent Blindness James and Carole Free Catalyst Award for support.

References

1. Jinek, M.; Chylinski, K.; Fonfara, I.; Hauer, M.; Doudna, J. A.; Charpentier, E., A programmable dual-RNA–guided DNA endonuclease in adaptive bacterial immunity. *science* **2012**, 1225829.

2. Jinek, M.; East, A.; Cheng, A.; Lin, S.; Ma, E.; Doudna, J., RNA-programmed genome editing in human cells. *elife* **2013,** *2*.

3. Mali, P.; Yang, L.; Esvelt, K. M.; Aach, J.; Guell, M.; DiCarlo, J. E.; Norville, J. E.; Church, G. M., RNA-guided human genome engineering via Cas9. *Science* **2013,** *339* (6121), 823-826.

4. Ho, T.-T.; Zhou, N.; Huang, J.; Koirala, P.; Xu, M.; Fung, R.; Wu, F.; Mo, Y.-Y., Targeting non-coding RNAs with the CRISPR/Cas9 system in human cell lines. *Nucleic acids research* **2014,** *43* (3), e17-e17.

5. Dang, Y.; Jia, G.; Choi, J.; Ma, H.; Anaya, E.; Ye, C.; Shankar, P.; Wu, H., Optimizing sgRNA structure to improve CRISPR-Cas9 knockout efficiency. *Genome biology* **2015,** *16* (1), 280.

6. Yang, Y.; Wang, L.; Bell, P.; McMenamin, D.; He, Z.; White, J.; Yu, H.; Xu, C.; Morizono, H.; Musunuru, K., A dual AAV system enables the Cas9-mediated correction of a metabolic liver disease in newborn mice. *Nature biotechnology* **2016,** *34* (3), 334.

7. Yu, W.; Mookherjee, S.; Chaitankar, V.; Hiriyanna, S.; Kim, J.-W.; Brooks, M.; Ataeijannati, Y.; Sun, X.; Dong, L.; Li, T.; Swaroop, A.; Wu, Z., Nrl knockdown by AAV-delivered CRISPR/Cas9 prevents retinal degeneration in mice. *Nature Communications* **2017,** *8*, 14716.

8. Sun, W.; Ji, W.; Hall, J. M.; Hu, Q.; Wang, C.; Beisel, C. L.; Gu, Z., Self-assembled DNA nanoclews for the efficient delivery of CRISPR–Cas9 for genome editing. *Angewandte Chemie International Edition* **2015,** *54* (41), 12029-12033.

9. Zuris, J. A.; Thompson, D. B.; Shu, Y.; Guilinger, J. P.; Bessen, J. L.; Hu, J. H.; Maeder, M. L.; Joung, J. K.; Chen, Z.-Y.; Liu, D. R., Cationic lipid-mediated delivery of proteins enables efficient protein-based genome editing in vitro and in vivo. *Nature biotechnology* **2015,** *33* (1), 73.

10. Wang, M.; Zuris, J. A.; Meng, F.; Rees, H.; Sun, S.; Deng, P.; Han, Y.; Gao, X.; Pouli, D.; Wu, Q.; Georgakoudi, I.; Liu, D. R.; Xu, Q., Efficient delivery of genome-editing proteins using bioreducible lipid nanoparticles. *Proceedings of the National Academy of Sciences* **2016,** *113* (11), 2868.

11. Lee, K.; Conboy, M.; Park, H. M.; Jiang, F.; Kim, H. J.; Dewitt, M. A.; Mackley, V. A.; Chang, K.; Rao, A.; Skinner, C.; Shobha, T.; Mehdipour, M.; Liu, H.; Huang, W.-c.; Lan, F.; Bray, N. L.; Li, S.; Corn, J. E.; Kataoka, K.; Doudna, J. A.; Conboy, I.; Murthy, N., Nanoparticle delivery of Cas9 ribonucleoprotein and donor DNA in vivo induces homology-directed DNA repair. *Nature Biomedical Engineering* **2017,** *1* (11), 889-901.

12. Mout, R.; Ray, M.; Yesilbag Tonga, G.; Lee, Y.-W.; Tay, T.; Sasaki, K.; Rotello, V. M., Direct Cytosolic Delivery of CRISPR/Cas9-Ribonucleoprotein for Efficient Gene Editing. *ACS Nano* **2017,** *11* (3), 2452-2458.

13. Jiang, C.; Mei, M.; Li, B.; Zhu, X.; Zu, W.; Tian, Y.; Wang, Q.; Guo, Y.; Dong, Y.; Tan, X., A non-viral CRISPR/Cas9 delivery system for therapeutically targeting HBV DNA and pcsk9 in vivo. *Cell Research* **2017,** *27*, 440.

14. Miller, J. B.; Zhang, S.; Kos, P.; Xiong, H.; Zhou, K.; Perelman, S. S.; Zhu, H.; Siegwart, D. J., Non-Viral CRISPR/Cas Gene Editing In Vitro and In Vivo Enabled by Synthetic Nanoparticle Co-Delivery of Cas9 mRNA and sgRNA. *Angewandte Chemie International Edition* **2017,** *56* (4), 1059-1063.

15. Shen, B.; Zhang, W.; Zhang, J.; Zhou, J.; Wang, J.; Chen, L.; Wang, L.; Hodgkins, A.; Iyer, V.; Huang, X., Efficient genome modification by CRISPR-Cas9 nickase with minimal off-target effects. *Nature methods* **2014,** *11* (4), 399.

16. Konermann, S.; Brigham, M. D.; Trevino, A. E.; Joung, J.; Abudayyeh, O. O.; Barcena, C.; Hsu, P. D.; Habib, N.; Gootenberg, J. S.; Nishimasu, H.; Nureki, O.; Zhang, F., Genome-scale transcriptional activation by an engineered CRISPR-Cas9 complex. *Nature* **2014,** *517*, 583.

17. Xie, K.; Minkenberg, B.; Yang, Y., Boosting CRISPR/Cas9 multiplex editing capability with the endogenous tRNA-processing system. *Proceedings of the National Academy of Sciences* **2015,** *112* (11), 3570.

18. Luo, Y.-L.; Xu, C.-F.; Li, H.-J.; Cao, Z.-T.; Liu, J.; Wang, J.-L.; Du, X.-J.; Yang, X.-Z.; Gu, Z.; Wang, J., Macrophage-Specific in Vivo Gene Editing Using Cationic Lipid-Assisted Polymeric Nanoparticles. *ACS Nano* **2018**.

19. Steyer, B.; Carlson-Stevermer, J.; Angenent-Mari, N.; Khalil, A.; Harkness, T.; Saha, K., High content analysis platform for optimization of lipid mediated CRISPR-Cas9 delivery strategies in human cells. *Acta biomaterialia* **2016,** *34*, 143-158.

20. Yin, H.; Kanasty, R. L.; Eltoukhy, A. A.; Vegas, A. J.; Dorkin, J. R.; Anderson, D. G., Non-viral vectors for gene-based therapy. *Nature Reviews Genetics* **2014,** *15*, 541.

21. Liang, X.; Potter, J.; Kumar, S.; Zou, Y.; Quintanilla, R.; Sridharan, M.; Carte, J.; Chen, W.; Roark, N.; Ranganathan, S.; Ravinder, N.; Chesnut, J. D., Rapid and highly efficient mammalian cell engineering via Cas9 protein transfection. *Journal of Biotechnology* **2015,** *208*, 44-53.

22. Rui, Y.; Wilson, D. R.; Green, J. J., Non-Viral Delivery To Enable Genome Editing. *Trends in Biotechnology* **2019,** *37* (3), 281-293.

23. Liang, C.; Li, F.; Wang, L.; Zhang, Z.-K.; Wang, C.; He, B.; Li, J.; Chen, Z.; Shaikh, A. B.; Liu, J.; Wu, X.; Peng, S.; Dang, L.; Guo, B.; He, X.; Au, D. W. T.; Lu, C.; Zhu, H.; Zhang, B.-T.; Lu, A.; Zhang, G., Tumor cell-targeted delivery of CRISPR/Cas9 by aptamer-functionalized lipopolymer for therapeutic genome editing of VEGFA in osteosarcoma. *Biomaterials* **2017,** *147*, 68-85.

24. Kim, S. M.; Yang, Y.; Oh, S. J.; Hong, Y.; Seo, M.; Jang, M., Cancer-derived exosomes as a delivery platform of CRISPR/Cas9 confer cancer cell tropism-dependent targeting. *Journal of Controlled Release* **2017,** *266*, 8-16.

25. Timin, A. S.; Muslimov, A. R.; Lepik, K. V.; Epifanovskaya, O. S.; Shakirova, A. I.; Mock, U.; Riecken, K.; Okilova, M. V.; Sergeev, V. S.; Afanasyev, B. V.; Fehse, B.; Sukhorukov, G. B., Efficient gene editing via non-viral delivery of CRISPR–Cas9 system using polymeric and hybrid microcarriers. *Nanomedicine: Nanotechnology, Biology and Medicine* **2018,** *14* (1), 97-108.

26. Rui, Y.; Wilson, D. R.; Sanders, K.; Green, J. J., Reducible Branched Ester-Amine Quadpolymers (rBEAQs) Codelivering Plasmid DNA and RNA Oligonucleotides Enable CRISPR/Cas9 Genome Editing. *ACS Applied Materials & Interfaces* **2019,** *11* (11), 10472-10480.

27. Sunshine, J. C.; Peng, D. Y.; Green, J. J., Uptake and transfection with polymeric nanoparticles are dependent on polymer end-group structure, but largely independent of nanoparticle physical and chemical properties. *Molecular pharmaceutics* **2012,** *9* (11), 3375-3383.

28. Sunshine, J. C.; Akanda, M. I.; Li, D.; Kozielski, K. L.; Green, J. J., Effects of base polymer hydrophobicity and end-group modification on polymeric gene delivery. *Biomacromolecules* **2011,** *12* (10), 3592-600.

29. Wilson, D. R.; Mosenia, A.; Suprenant, M. P.; Upadhya, R.; Routkevitch, D.; Meyer, R. A.; Quinones-Hinojosa, A.; Green, J. J., Continuous microfluidic assembly of biodegradable poly(beta-amino ester)/DNA nanoparticles for enhanced gene delivery. *J Biomed Mater Res A* **2017,** *105* (6), 1813-1825.

30. Wilson, D. R.; Rui, Y.; Siddiq, K.; Routkevitch, D.; Green, J. J., Differentially Branched Ester Amine Quadpolymers with Amphiphilic and pH-Sensitive Properties for Efficient Plasmid DNA Delivery. *Molecular Pharmaceutics* **2019,** *16* (2), 655-668.

31. Matsuda, T.; Cepko, C. L., Controlled expression of transgenes introduced by in vivo electroporation. *Proceedings of the National Academy of Sciences* **2007,** *104* (3), 1027.

32. Madisen, L.; Zwingman, T. A.; Sunkin, S. M.; Oh, S. W.; Zariwala, H. A.; Gu, H.; Ng, L. L.; Palmiter, R. D.; Hawrylycz, M. J.; Jones, A. R.; Lein, E. S.; Zeng, H., A robust and high-throughput Cre reporting and characterization system for the whole mouse brain. *Nature neuroscience* **2010,** *13* (1), 133-140.

33. Suzuki, K.; Tsunekawa, Y.; Hernandez-Benitez, R.; Wu, J.; Zhu, J.; Kim, E. J.; Hatanaka, F.; Yamamoto, M.; Araoka, T.; Li, Z.; Kurita, M.; Hishida, T.; Li, M.; Aizawa, E.; Guo, S.; Chen, S.; Goebl, A.; Soligalla, R. D.; Qu, J.; Jiang, T.; Fu, X.; Jafari, M.; Esteban, C. R.; Berggren, W. T.; Lajara, J.; Nuñez-Delicado, E.; Guillen, P.; Campistol, J. M.; Matsuzaki, F.; Liu, G.-H.; Magistretti, P.; Zhang, K.; Callaway, E. M.; Zhang, K.; Belmonte, J. C. I., In vivo genome editing via CRISPR/Cas9 mediated homology-independent targeted integration. *Nature* **2016,** *540*, 144.

34. Yusa, K.; Zhou, L.; Li, M. A.; Bradley, A.; Craig, N. L., A hyperactive piggyBac transposase for mammalian applications. *Proceedings of the National Academy of Sciences* **2011,** *108* (4), 1531-1536.

35. Shcherbakova, D. M.; Verkhusha, V. V., Near-infrared fluorescent proteins for multicolor in vivo imaging. *Nature Methods* **2013,** *10*, 751.

36. Kettlun, C.; Galvan, D. L.; George, A. L., Jr.; Kaja, A.; Wilson, M. H., Manipulating piggyBac transposon chromosomal integration site selection in human cells. *Mol Ther* **2011,** *19* (9), 1636-1644.

37. Staahl, B. T.; Benekareddy, M.; Coulon-Bainier, C.; Banfal, A. A.; Floor, S. N.; Sabo, J. K.; Urnes, C.; Munares, G. A.; Ghosh, A.; Doudna, J. A., Efficient genome editing in the mouse brain by local delivery of engineered Cas9 ribonucleoprotein complexes. *Nature biotechnology* **2017,** *35* (5), 431.

38. Zhu, D.; Shen, H.; Tan, S.; Hu, Z.; Wang, L.; Yu, L.; Tian, X.; Ding, W.; Ren, C.; Gao, C.; Cheng, J.; Deng, M.; Liu, R.; Hu, J.; Xi, L.; Wu, P.; Zhang, Z.; Ma, D.; Wang, H., Nanoparticles based on poly (β-amino ester) and HPV16 targeting CRISPR/shRNA as potential drugs for HPV16 related cervical malignancy. *Molecular Therapy* **2018**.

39. Bhise, N. S.; Shmueli, R. B.; Gonzalez, J.; Green, J. J., A Novel Assay for Quantifying the Number of Plasmids Encapsulated by Polymer Nanoparticles. *Small* **2012,** *8* (3), 367-373.

40. Tzeng, S. Y.; Guerrero-Cázares, H.; Martinez, E. E.; Sunshine, J. C.; Quiñones-Hinojosa, A.; Green, J. J., Non-viral gene delivery nanoparticles based on Poly(β-amino esters) for treatment of glioblastoma. *Biomaterials* **2011,** *32* (23), 5402-5410.

41. Chen, J. S.; Dagdas, Y. S.; Kleinstiver, B. P.; Welch, M. M.; Sousa, A. A.; Harrington, L. B.; Sternberg, S. H.; Joung, J. K.; Yildiz, A.; Doudna, J. A., Enhanced proofreading governs CRISPR–Cas9 targeting accuracy. *Nature* **2017,** *550*, 407.

42. Kleinstiver, B. P.; Pattanayak, V.; Prew, M. S.; Tsai, S. Q.; Nguyen, N. T.; Zheng, Z.; Joung, J. K., High-fidelity CRISPR–Cas9 nucleases with no detectable genome-wide off-target effects. *Nature* **2016,** *529*, 490.

43. Doyon, Y.; Choi, V. M.; Xia, D. F.; Vo, T. D.; Gregory, P. D.; Holmes, M. C., Transient cold shock enhances zinc-finger nuclease–mediated gene disruption. *Nature Methods* **2010,** *7*, 459.

44. Guo, Q.; Mintier, G.; Ma-Edmonds, M.; Storton, D.; Wang, X.; Xiao, X.; Kienzle, B.; Zhao, D.; Feder, J. N., 'Cold shock' increases the frequency of homology directed repair gene editing in induced pluripotent stem cells. *Scientific Reports* **2018,** *8* (1), 2080.

45. Mekler, V.; Minakhin, L.; Semenova, E.; Kuznedelov, K.; Severinov, K., Kinetics of the CRISPR-Cas9 effector complex assembly and the role of 3'-terminal segment of guide RNA. *Nucleic acids research* **2016,** *44* (6), 2837-2845.

46. Raper, A. T.; Stephenson, A. A.; Suo, Z., Functional Insights Revealed by the Kinetic Mechanism of CRISPR/Cas9. *Journal of the American Chemical Society* **2018,** *140* (8), 2971-2984.

47. DuBridge, R. B.; Tang, P.; Hsia, H. C.; Leong, P. M.; Miller, J. H.; Calos, M. P., Analysis of mutation in human cells by using an Epstein-Barr virus shuttle system. *Mol Cell Biol* **1987,** *7* (1), 379-387.

48. Dean, F. B.; Bullock, P.; Murakami, Y.; Wobbe, C. R.; Weissbach, L.; Hurwitz, J., Simian virus 40 (SV40) DNA replication: SV40 large T antigen unwinds DNA containing the SV40 origin of replication. *Proceedings of the National Academy of Sciences* **1987,** *84* (1), 16.

49. Mancia, F.; Patel, S. D.; Rajala, M. W.; Scherer, P. E.; Nemes, A.; Schieren, I.; Hendrickson, W. A.; Shapiro, L., Optimization of Protein Production in Mammalian Cells with a Coexpressed Fluorescent Marker. *Structure* **2004,** *12* (8), 1355-1360.

50. Pear, W. S.; Nolan, G. P.; Scott, M. L.; Baltimore, D., Production of high-titer helper-free retroviruses by transient transfection. *Proc Natl Acad Sci U S A* **1993,** *90* (18), 8392-8396.

51. van Deventer, H. W.; Serody, J. S.; McKinnon, K. P.; Clements, C.; Brickey, W. J.; Ting, J. P. Y., Transfection of Macrophage Inflammatory Protein 1α into B16 F10 Melanoma Cells Inhibits Growth of Pulmonary Metastases But Not Subcutaneous Tumors. *The Journal of Immunology* **2002,** *169* (3), 1634.

52. Reynier, P.; Briane, D.; Coudert, R.; Fadda, G.; Bouchemal, N.; Bissieres, P.; Taillandier, E.; Cao, A., Modifications in the Head Group and in the Spacer of Cholesterol-based Cationic Lipids Promote Transfection in Melanoma B16-F10 Cells and Tumours. *Journal of Drug Targeting* **2004,** *12* (1), 25-38.

53. Rui, Y.; Wilson, D. R.; Choi, J.; Varanasi, M.; Sanders, K.; Karlsson, J.; Lim, M.; Green, J. J., Carboxylated branched poly(β-amino ester) nanoparticles enable robust cytosolic protein delivery and CRISPR-Cas9 gene editing. *Science Advances* **2019,** *5* (12), eaay3255.

54. Zhang, Y.; Wang, J.; Wang, Z.; Zhang, Y.; Shi, S.; Nielsen, J.; Liu, Z., A gRNA-tRNA array for CRISPR-Cas9 based rapid multiplexed genome editing in Saccharomyces cerevisiae. *Nature Communications* **2019,** *10* (1), 1053.

55. Shiraki, T.; Kawakami, K., A tRNA-based multiplex sgRNA expression system in zebrafish and its application to generation of transgenic albino fish. *Scientific Reports* **2018,** *8* (1), 13366.

56. Mishra, B.; Wilson, D. R.; Sripathi, S. R.; Suprenant, M. P.; Rui, Y.; Wahlin, K. J.; Berlinicke, C.; Green, J. J.; Zack, D. J., Combinatorial library of biodegradable polyesters enables delivery of plasmid DNA to polarized human RPE monolayers for retinal gene therapy. *bioRxiv* **2018**, 264390.

57. Chen, F.; LoTurco, J., A method for stable transgenesis of radial glia lineage in rat neocortex by piggyBac mediated transposition. *Journal of neuroscience methods* **2012,** *207* (2), 172-180.

58. Suzuki, K.; Kimura, T.; Shinoda, H.; Bai, G.; Daniels, M. J.; Arai, Y.; Nakano, M.; Nagai, T., Five colour variants of bright luminescent protein for real-time multicolour bioimaging. *Nature communications* **2016,** *7*

59. Schumann, K.; Lin, S.; Boyer, E.; Simeonov, D. R.; Subramaniam, M.; Gate, R. E.; Haliburton, G. E.; Chun, J. Y.; Bluestone, J. A.; Doudna, J. A., Generation of knock-in primary human T cells using Cas9 ribonucleoproteins. *Proceedings of the National Academy of Sciences* **2015,** *112* (33), 10437-10442.

Supporting Information

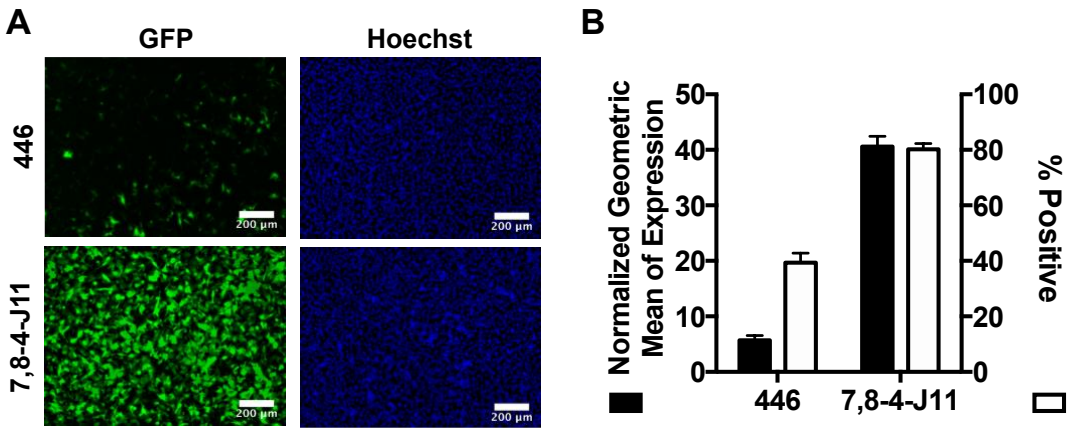

Figure 5-S1. GFP transfection screen results for B16-F10 cells. Fluorescence microscopy images **(A)** and flow cytometry results **(B)** show that branched PBAE polymer 7,8-4-J11 (30 w/w) transfects B16 cells more efficiently than canonical linear PBAE polymer 446 (60 w/w). Data presented as mean + SEM; *N* = 4. Scale bar = 200 µm.

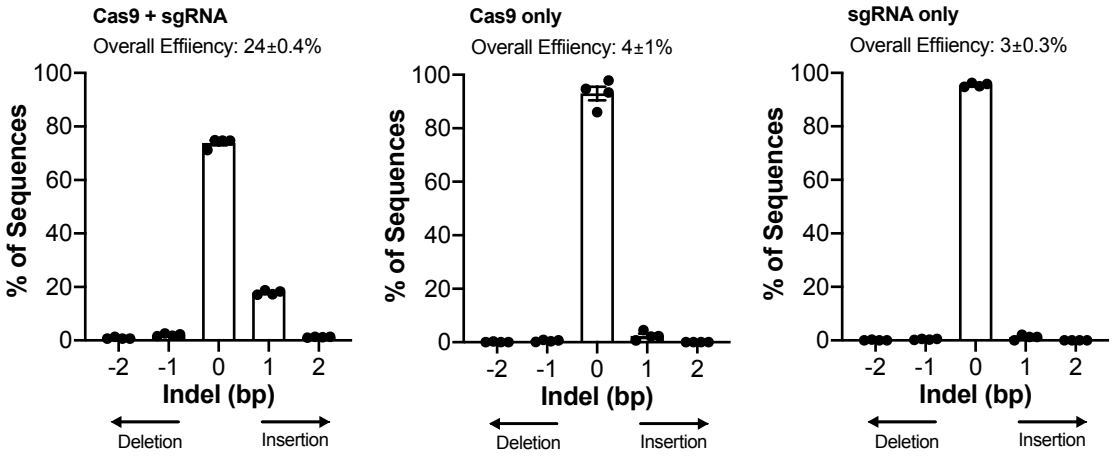

Figure 5-S2. TIDE quantification of indel frequencies. Sanger sequencing data of the genomic DNA of HEK-GFP cells treated with nanoparticles delivering CRISPR plasmids were quantified by TIDE analysis. *N* = 3, data presented as mean ± SEM.

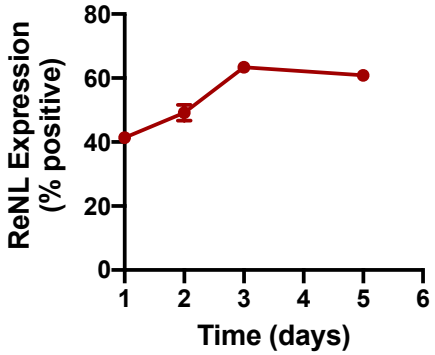

Figure 5-S3. ReNL expression time course after 2-cut edits in HEK cells. HEK cells were transfected on day 0 and gain of ReNL expression was monitored on selected days to determine the expression timeline for ReNL. *N* = 4, data presented as mean ± SEM.

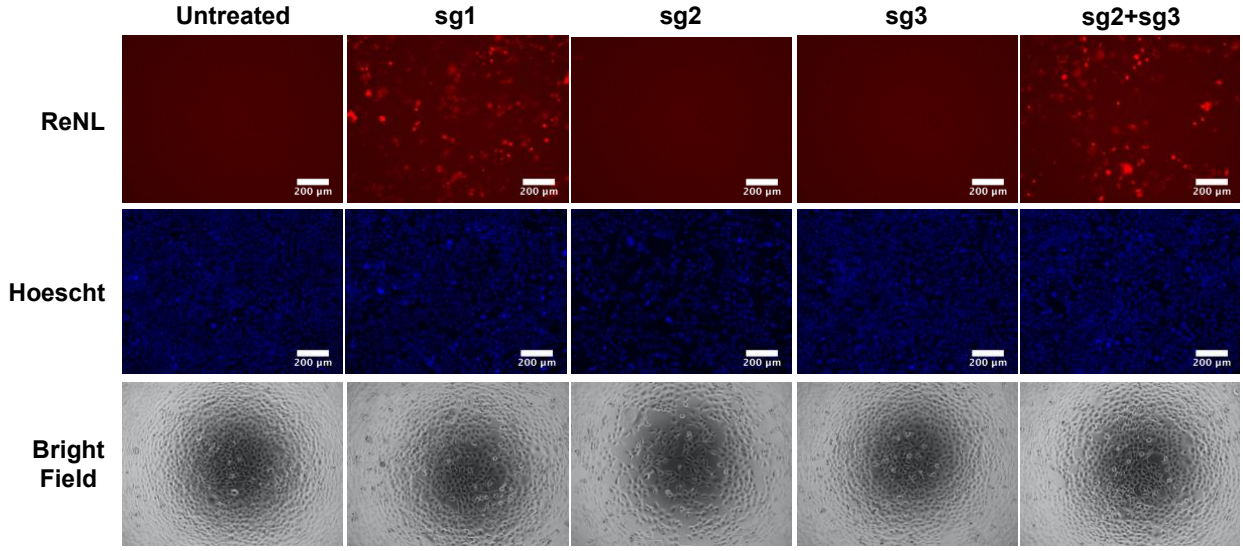

Figure 5-S4. Microscopy images of ReNL gain of expression. 2-cut CRISPR cleavage with sg1 or combination of sg2+sg3 turn on expression of ReNL by removal of two SV40 polyA sequences. Scale bar = 200 µm.

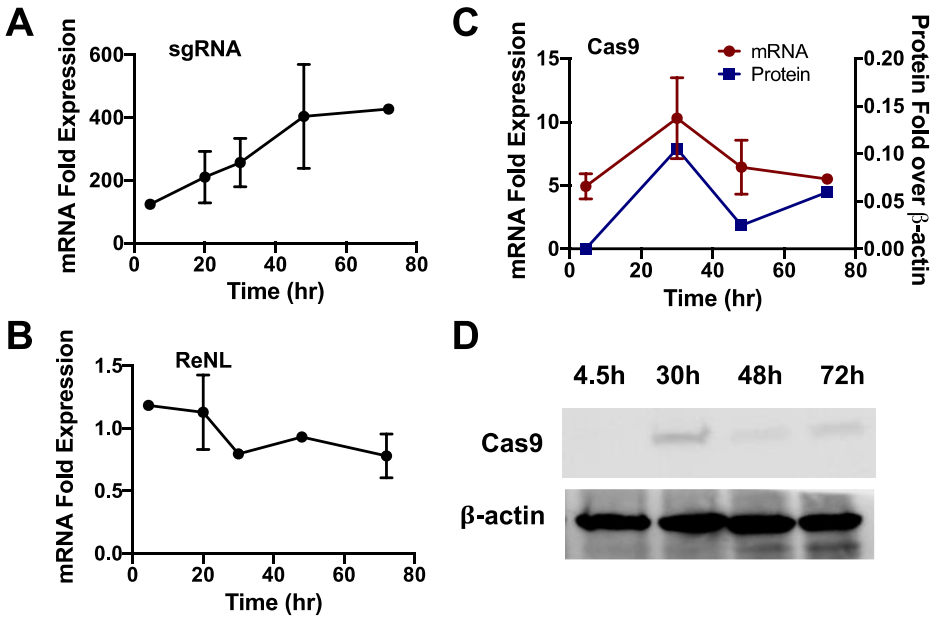

Figure 5-S5. Expression kinetics of CRISPR components in B16 cells. mRNA expression levels of sgRNA **(A)** and ReNL **(B)**. Cas9 mRNA **(C, red curve)** and protein **(C, blue curve; D)** expression levels over time. N = 2 (data shown as mean ± SEM) for qRT-PCR experiments; N=1 for western blots.

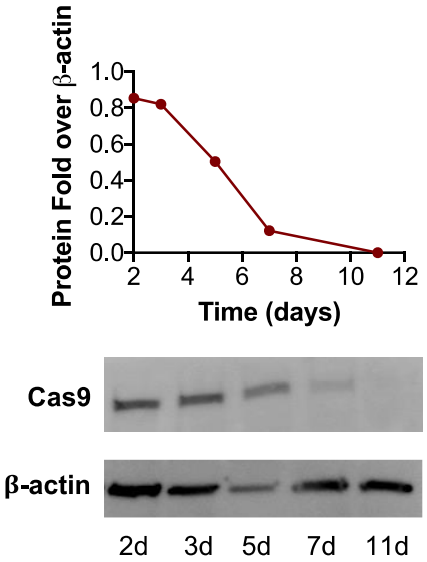

Figure 5-S6. Long-term Cas9 accumulation in 293T cells. Western blotting was performed on indicated days after transfection of Cas9 and sgRNA plasmids in HEK-293T cells and Cas9 protein expression levels were quantified as fold expression over **β**-actin based on image analysis of band intensities (n=1).

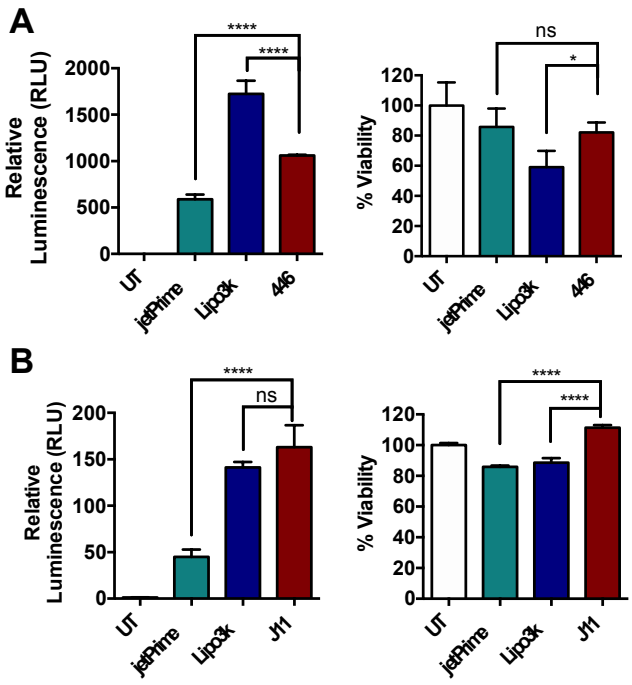

Figure 5-S7. Comparison to commercial transfection reagents. Gain of expression from 2-cut edits and viability of cells using commercial reagents and PBAEs in **(A)** 293T and **(B)** B16 cells as measured by ReNL luminescence. Data presented as mean + SEM; N=4. Statistical significance assessed by one-way ANOVA with Dunnett post-hoc tests as compared to the PBAE treated group (446 or J11, respectively); *****$p < 0.05$, ********$p < 0.0001$

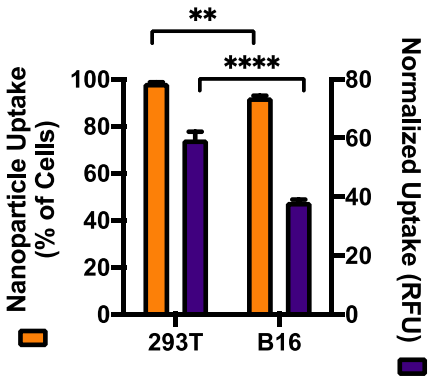

Figure 5-S8. Nanoparticle uptake analysis in B16 and 293T cells. Flow cytometry analysis of cellular uptake of nanoparticles encapsulating 20% Cy5-labeled DNA. Data shown as mean + SEM; N=4. Statistical significance assessed by one-way ANOVA with Sidak's post-hoc tests; **$p < 0.01$, **** $p < 0.0001$.

Target	Sequence	Notes
GFP	FWD: CTGGTCGAGCTGGACGGCGACG REV: CACGAACTCCAGCAGGACCATG	Amplicon size: 630 bp
2X-SV40 Stop Cassette	FWD: CGCAAATGGGCGGTAGGCGTG REV: GCCCTTGCTCACCATGAATT	Amplicon size: 755 bp
hCas9	FWD: GGAGTTGACGCCAAAGCAATCC REV: AGATTTAAAGTTGGGGGTCAGCC	Amplicon size: 150 bp
ReNL	FWD: ATCCCGTATGAAGGTCTGAGCG REV: GTCGATCATGTTCGGCGTAACC	Amplicon size: 147 bp
sgRNA1	FWD: ACATTATACGGTTTCAGAGC REV: GACTCGGTGCCACTTTTTCA	Amplicon size: 91 bp
β-actin (human)	FWD: CATGTACGTTGCTATCCAGGC REV: CTCCTTAATGTCACGCACGAT	Amplicon size: 250 bp Primerbank ID: 4501885a1
β-actin (mouse)	FWD: CTGTCCCTGTATGCCTCTG REV: ATGTCACGCACGATTTCC	Amplicon size: 218 bp

Table 5-S1. PCR primer sequences.

Plasmid Name	Addgene ID	Description
PB-iRFP-STOP-ReNL	113965	Piggybac transposon plasmid CRISPR gene deletion activatable fluorescence. Constitutive iRFP670 under EF1A promoter, CMV promoter with two SV40 polyA followed by red-enhanced nanolantern (ReNL)
sg1	113966	Single short guide RNA targeting GTATAGCATACATTATACG
sg2	133967	Single short guide RNA targeting TACCACATTTGTAGAGGTT
sg3	133968	Single short guide RNA targeting CAATGTATCTTATCATGTC
sg1+sg2+sg3	133969	Triple short guide RNA targeting GTATAGCATACATTATACG, TACCACATTTGTAGAGGTT & CAATGTATCTTATCATGTC
sg2+sg3	133970	Double short guide RNA targeting TACCACATTTGTAGAGGTT & CAATGTATCTTATCATGTC
sgiRFP1	133972	Single short guide RNA targeting GATCGAGTTCGAGCCTGCGG in iRFP670 sequence
sgiRFP2	133973	Single short guide RNA targeting GCGCGTTCTTTGGACGCGA in iRFP670 sequence
sgiRFP3	133974	Single short guide RNA targeting CGTGATGTTGTACCGCTTC in iRFP670 sequence

Table 5-S2. Plasmids deposited with Addgene

DNA Sequence	Description and notes
ATTATTGACTAGTAGTGGTTTTAGAGCTAGAAATAGCAAG TTAAAATAAGGCTAGTCCGTTATCAACTTGAAAAAGTGGC ACCGAGTCGGTGCAACAAAGCACCAGTGGTCTAGTGGTA GAATAGTACCCTGCCACGGTACAGACCCGGGTTCGATTCC CGGCTGGTGCAGCCAAGCTTGGCGTAA	pGTR sequence SpeI restriction enzyme site HindIII restriction enzyme site gRNA scaffold pre-tRNA
AGTTAGTTtctagaACAAAGCACCAGTGG	tRNA-start_F primer **XbaI restriction enzyme site**
GAACCTCTACAAATGTGGTA	sg2 protospacer sequence; overlapping base pairs used in Golden Gate primers
TAGGTCTCCACAAATGTGGTAGTTTTAGAGCTAGAA	sg2_F primer
ATGGTCTCATTGTAGAGGTTCTGCACCAGCCGGGAA	sg2_R primer
GCAATGTATCTTATCATGTC	sg3 protospacer sequence; overlapping base pairs used in Golden Gate primers
TAGGTCTCCTCTTATCATGTCGTTTTAGAGCTAGAA	sg3_F primer
ATGGTCTCAAAGATACATTGCTGCACCAGCCGGGAA	sg3_R primer
CAATGTAT**aagctt**AAAAAAAAAAGCACCGACTCG	gRNA-end_R primer **HindIII restriction enzyme site**

Table 5-S3. DNA and primer sequences used to generate multiplex tRNA-gRNA plasmid. The pGTR sequence was cloned into a backbone plasmid via restriction enzyme cloning using SpeI and HindIII. The pGTR plasmid was then used as the PCR template for amplifying gRNA-tRNA sequences for Golden Gate assembly. To synthesize a multiplex plasmid containing both sg2 and sg3, PCR amplicons were generated using the following pairs of primers: tRNA-start_F + sg2_R (amplicon 1); sg2_F + sg3_R (amplicon 2); sg3_F + gRNA-end_R (amplicon 3). Amplicons 1-3 were then purified, ligated by Golden Gate assembly, and cloned into a backbone vector containing a single U6 promoter using restriction enzyme cloning with XbaI and HindIII.

Calculation 5-S1. N-P ratios of PBAE/DNA nanoparticles. Gel permeation chromatography was used to measure the molecular weight of polymers 446 and 7,8-4-J11, respectively. The number averaged molecular weight (M_N) was 5935 Da for 446 and 6943 Da for 7,8-4-J11. Using polymer M_N and the molecular weight of individual monomers, the nitrogen (N) weight fraction was calculated to be 0.055 for 446 and 0.046 for 7,8-4-J11. The average phosphate (P) weight fraction for DNA was calculated to be 0.095. Taken together, 446

nanoparticles at 60 w/w had an N-P ratio of 34.5, and 7,8-4-J11 nanoparticles at 30 w/w had an N-P ratio of 14.5

Chapter 6: Reducible Branched Ester-Amine Quadpolymers (rBEAQs) Co-delivering Plasmid DNA and RNA Oligonucleotides Enable CRISPR/Cas9 Genome Editing

Yuan Rui[1], David R. Wilson[1], Katie Sanders[1], and Jordan J. Green[1,2,3,*].

[1]Department of Biomedical Engineering, Institute for NanoBioTechnology, and the Translational Tissue Engineering Center, Johns Hopkins University School of Medicine, [2]Departments of Ophthalmology, Oncology, Materials Science & Engineering, Chemical & Biomolecular Engineering, and Neurosurgery, Johns Hopkins University School of Medicine, [3]Bloomberg~Kimmel Institute for Cancer Immunotherapy, Johns Hopkins University School of Medicine.

Abstract

Functional co-delivery of plasmid DNA and RNA oligonucleotides in the same nanoparticle system is challenging due to differences in their physical properties as well as their intracellular locations of function. In this study, we synthesized a series of reducible branched ester-amine quadpolymers (rBEAQs) and investigated their ability to co-encapsulate and deliver DNA plasmids and RNA oligos. The rBEAQs are designed to leverage polymer branching, reducibility, and hydrophobicity to successfully co-complex DNA and RNA in nanoparticles at low polymer to nucleic acid w/w ratios and enable high delivery efficiency. We validate the synthesis of this new class of biodegradable polymers, characterize the self-assembled nanoparticles that these polymers form with diverse nucleic acids, and demonstrate that the nanoparticles enable safe, effective, and efficient DNA-siRNA co-delivery as well as non-viral CRISPR-mediated gene editing utilizing Cas9 DNA and sgRNA co-delivery.

1. Introduction

The introduction of exogenous genetic material into mammalian cells has been widely used in the laboratory to modulate gene expression and induce cellular reprogramming,[1] differentiation,[2-3] and programmed cell death.[4-6] Recently, these technologies have begun moving into the clinic and mark the beginning of a new paradigm for genetic medicine.[7-8] Traditional gene therapies involve the delivery of DNA, often in the form of plasmids or mini-circle DNA[9], into target cells. RNA oligonucleotides such as short interfering RNA (siRNA) can enable target-specific gene silencing,[10-11] and single guide RNAs (sgRNAs) complex with Cas9 endonucleases to achieve site-specific gene editing via the CRISPR/Cas9 system.[12-13] The biological functionality of these nucleic acids depend heavily on their successful intracellular delivery.[14]

Although non-viral vectors delivering either plasmid DNA or siRNA have been widely reported, very few studies have been able to functionally co-deliver both in the same nanoparticle system. This can be challenging as DNA and RNA oligonucleotides are vastly different in size (5,000 bp vs. 20 bp) and stiffness.[15-16] In this study, we synthesized a series of reducible branched ester-amine quadpolymers (rBEAQs) and investigated their ability to form nanoparticles that could functionally co-deliver plasmid DNA and RNA oligonucleotides. The rBEAQs were designed based on recent studies that have demonstrated that hyperbranched cationic polymers are superior than their linear counterparts at DNA[17-20] and oligonucleotide[21-22] delivery in multiple polymeric vector systems. The branched polymer architecture could increase the charge density of each polymer molecule, allowing for stronger nucleic acid binding affinity.[23] Disulfide bonds are another useful functionality as they can enable environmentally-triggered cargo release in the reducing cytosolic environment. They can be incorporated into delivery vectors as polymer side chains,[24] crosslinking moieties between polymer chains,[25] and part of the polymer backbone[26], and have been used successfully in several siRNA delivery systems. Finally, increasing polymer hydrophobicity has been shown to improve nanoparticle stability and increase DNA[27] as well as siRNA delivery efficacy.[28]

Using a facile one-pot Michael addition reaction, we were able to tune the reducibility and hydrophobicity of the polymers by simply adjusting the monomer ratios. We found that the nucleic acid binding affinity, release kinetics, nanoparticle uptake, and functional nucleic acid delivery could be modulated

in a highly controlled manner. Our nanoparticle system enabled up to 77% DNA transfection and 66% siRNA-mediated knockdown. More importantly, delivery of Cas9 DNA and sgRNA enabled 40% gene knockout, further highlighting the robustness of this co-delivery system.

2. Materials and Methods

2.1 Materials

2-Hydroxyethyl disulfide (CAS 1892291), triethylamine (CAS 121448), acryloyl chloride (CAS 814686), bisphenol A glycerolate (1 glycerol/phenol) diacrylate (B7; CAS 4687949), trimethylolpropane triacrylate (B8; CAS 15625895), 2-(3-aminopropylamino)ethanol (E6; CAS 4461396), L-buthionine-sulfoximine (CAS 83730534), and solvents were purchased from Sigma Aldrich (St. Louis, MO). 4-Amino-1-butanol (S4; CAS 133251005) was purchased from Alfa Aesar (Tewksbury, MA). Plasmids pCAG-GFPd2 (14760) and piRFP670-N1 (45457) were purchased from Addgene (Cambridge, MA). PB-CMV-MCS-EF1a-RFP PiggyBac plasmid (PB512B-1) and PiggyBac transposase expression plasmid (PB200A-1) were purchased from System Biosciences (Palo Alto, CA). Negative control siRNA (1027281) was purchased from Qiagen (Germantown, MD). GFP siRNA targeting the sequence 5'-GCA AGC TGA CCC TGA AGT TC-3' (P-002048-01) was purchased from Dharmacon (Lafayette, CO). Cy5-labeled siRNA (SIC005) was purchased from Sigma Aldrich.

2.2 Polymer Synthesis

Bioreducible monomer 2,2-disulfanediylbis(ethane-2,1-diyl) diacrylate (BR6) was synthesized using a method similar to Kozielski *et al.*[26] Briefly, 2-hydroxyethyl disulfide was acrylated with acryloyl chloride (1:1.1 molar ratio in dichloromethane) in the presence of excess triethylamine. After filtering out the precipitate, the product was washed with water, dried with sodium sulfate, and the solvent was removed by rotary evaporation.

For polymer synthesis, monomers BR6, B7, B8, and S4 were dissolved in anhydrous dimethylsulfoxide (DMSO) according to the B monomer molar ratios listed in Table S1 for an overall vinyl: amine ratio of 2.2:1 at a concentration of 150 mg/mL. After overnight reaction at 90°C with stirring, the

polymers were end-capped by reacting with monomer E6 (0.2 M final concentration in DMSO) at room temperature for 1 hr. The end-capped polymers were purified by 2 diethyl ether washes, after which remaining solvent was removed in a vacuum chamber. Polymers were dissolved in DMSO at 100 mg/mL and stored in aliquots at -20°C under desiccant.

2.3 Yo-Pro-1 Iodide Nucleic Acid Binding Assay

Yo-Pro-1 iodide fluorescent dye (Invitrogen) was mixed with siRNA at a final concentration of 0.5 μM Yo-Pro and 0.5 μM scRNA in 25 mM sodium acetate (NaAc, pH 5.0). Polymers were dissolved in NaAc, and 25 μL polymer solution was mixed with 75 μL RNA/Yo-Pro solution per well in 96 well black bottom plates. The solutions were incubated at 37°C for 20 minutes before fluorescence readings were taken on a fluorescence multiplate reader (Biotek Synergy 2). To measure siRNA binding in reducing conditions over time, polymer concentration was set at the lowest concentration at which each polymer achieved >80% quenching. The polymer/siRNA/Yo-Pro solution was mixed with 10 μL glutathione solution (final concentration 5 mM) and incubated at 37°C. Fluorescence readings were taken at the indicated time points.

2.4 Polymer Characterization: NMR and GPC

Polymer structure was characterized by nuclear magnetic resonance spectroscopy (NMR) via ^{1}H NMR in $CDCl_3$ (Bruker 500 MHz) and analyzed using TopSpin 3.5 software. To measure polymer molecular weight and polydispersity, polymers were dissolved in BHT-stabilized tetrahydrofuran with 5% DMSO and 1% piperidine, filtered through a 0.2 μm PTFE filter, and measured with gel permeation chromatography against linear polystyrene standards (Waters, Milford, MA).

2.5 Gel Retardation Assay

Nanoparticles were synthesized by dissolving polymer and siRNA separately in NaAc buffer at the desired concentrations. The solutions were mixed at a 1:1 volume ratio and nanoparticles were allowed to self-assemble at room temperature for 10 minutes, after which, nanoparticles were incubated in the presence of 5 mM glutathione or 150 mM PBS at 37°C. Samples were taken at various time points and frozen at -80°C to stop the reaction. For gel retardation assays of R6,7,8_64 nanoparticles co-encapsulating plasmid DNA

and siRNA, nucleic acids were first pre-mixed at 1:1 volume ratio and then mixed with polymer to allow for nanoparticle self-assembly. Polymer dosage was varied from 10 w/w to 0 w/w (free nucleic acids). Samples were loaded onto a 1% agarose gel using 30% glycerol as loading buffer. Gel electrophoresis was performed in TAE buffer at 100 V for 15 min, after which the gel was imaged under UV.

2.6 Nanoparticle Characterization

Nanoparticles were prepared as described above and diluted in 150 mM PBS to determine particle size and surface charge in neutral isotonic buffer. Hydrodynamic diameter was measured via nanoparticle tracking analysis at 1:500 dilution in PBS using a NanoSight NS300, while zeta potential was measured at 1:6 dilution in PBS via electrophoretic light scattering on a Malvern Zetasizer NanoZS (Malvern Panalytical). To characterize nanoparticle stability over time in physiological conditions, nanoparticle size was also measured at 1:6 dilution in 10% serum-containing cell culture medium once per hour for 9 hours using a Malvern Zetasizer Pro (Malvern Panalytical). Transmission electron microscopy (TEM) images were acquired with a Philips CM120 (Philips Research). Nanoparticles were prepared at a polymer concentration of 1.8 mg/mL in 25 mM NaAc, and 30 μL were added to 400-square mesh carbon coated TEM grids and allowed to coat grids for 20 min. Grids were then rinsed with ultrapure water, counterstained with uranyl acetate (0.5% in distilled water), and allowed to fully dry before imaging.

2.7 Cell Culture and Cell Line Preparation

HEK-293T human embryonic kidney and Huh7 human hepatocellular carcinoma cells were cultured in Dulbecco's Modified Eagle Medium (DMEM; ThermoFisher) supplemented with 10% FBS and 1% penicillin/streptomycin. A PiggyBac transponson/transposase system was used to generate cell lines constitutively expressing a destabilized form of GFP (GFPd2[29]). The GFPd2 PiggyBac transposon plasmid was created by inserting the GFPd2 gene into the PB-CMV-MCS-EF1a-RFP PiggyBac plasmid through standard restriction enzyme cloning. The transposon plasmid was then co-transfected with the PiggyBac transposase expression plasmid into cells using the method described below. Cells underwent 2 transfections and were then grown out for 5 passages to allow fluorescence signal from transient transfections to fade.

Positively-expressing cells were isolated via fluorescence-assisted cell sorting (FACS), and colonies grown from single cells were grown out to establish stably expressing cell lines.

2.8 Transfection

Cells were seeded onto 96 well tissue culture plates at a density of 15,000 cells per well in 100 μL complete medium and allowed to adhere overnight. Nanoparticles were formed immediately prior to transfection as described above. For experiments delivering siRNA only, each nanoparticle condition was formulated with a scrambled control RNA (scRNA) or an siRNA targeting GFP (siGFP) with a final RNA concentration of 100 nM per well. For experiments co-delivering siRNA and DNA, nanoparticles were formulated with a final dose of 200 ng DNA per well in addition to 100 nM scRNA or siGFP, respectively, for a final total nucleic acid dose of 400 ng per well. Nanoparticles co-encapsulating DNA and siRNA were formed by pre-mixing the nucleic acids at 1:1 volume ratio in NaAc buffer prior to mixing with polymer solution. Prior to the addition of nanoparticles, cell culture medium was replaced with 100 μL serum-free media. 20 μL of nanoparticles were added per well and incubated with cells for two hours, at which point the nanoparticle/media mixture was replaced with fresh complete media. Knockdown of GFPd2 fluorescence was assessed via flow cytometry one day post transfection using a BD Accuri C6 flow cytometer (BD Biosciences). Knockdown was quantified by normalizing the geometric mean of fluorescence of wells treated with siGFP to that of wells transfected using the same nanoparticle formulation delivering scRNA. For co-codelivery experiments, DNA transfection was quantified as the percentage of cells positively expressing iRFP when gated against untreated controls. (N = 4 +/- SEM.)

Transfections in which sodium bicarbonate ($NaHCO_3$) was used to increase nanoparticle pH were done by forming nanoparticles in acidic NaAc buffer as previously described and then mixing with 50 mg/mL $NaHCO_3$ buffer (pH 9) at 1:1 volume ratio before adding to cells. Transfections using commercially-available non-viral transfection reagents Lipofectamine 2,000™, Lipofectamine 3,000™ (ThermoFisher), and jetPrime® (Polyplus) were performed according to manufacturer instructions. 25 kD bPEI was used at 1 w/w in DNA-siRNA co-delivery experiments.

2.9 Cellular Uptake and Viability

Cy-5 labeled siRNA was diluted 1:5 in unlabeled siRNA and used to formulate nanoparticles as described above. Nanoparticles were added to cells in serum-free media and incubated for two hours, at which point cells were washed once with PBS and detached via trypsinization. Cells were further washed with heparin (50 μg/mL in PBS) to remove nanoparticles adhering to cells, resuspended in FACS buffer (2% FBS in PBS), and nanoparticle uptake was quantified by flow cytometry. Cell viability was assessed 24 hr post-transfection using MTS CellTiter 96 Aqueous One cell proliferation assay (Promega) following manufacturer's instructions. Cell viability of treated cells were normalized to that of untreated cells; N = 4 +/- SEM.

2.10 Glutathione Inhibition with L-buthionine-sulfoximine (BSO)

L-buthionine-sulfoximine (BSO) was dissolved in cell culture media at 2,000 μM. Cells were allowed to settle for three hours after plating, at which time 50 μL of media was replaced by 50 μL BSO solution for 1,000 μM final BSO concentration, which has been shown to effectively inhibit intracellular glutathione levels.[30] Cells were incubated for 24 hr with complete medium containing 1,000 μM BSO, which was replaced with serum-free BSO medium immediately before transfection. After two hours incubation with nanoparticles, cells were replenished with fresh BSO-containing complete medium and incubated for 24 hr, at which point cell viability and flow cytometry assays were performed.

2.11 Confocal Microscopy

HEK-293T cells were plated on Nunc Lab-Tek 8 chambered borosilicate coverglass well plates (155411; Thermo Fisher) at 30,000 cells/well one day prior to transfection in 300 μL phenol red free DMEM supplemented with 10% FBS and 1% penicillin/streptomycin. R6,7,8_64 nanoparticles were prepared as described above at 10 w/w ratio using pre-mixed Cy3 labeled siRNA and Cy5 labeled plasmid DNA at a 1 w/w ratio of nucleic acids. Cy5 labeled plasmid DNA was prepared as previously described[31-32] and mixed at 4 w/w ratio with unlabeled eGFP-N1 plasmid DNA. Nanoparticles were then diluted into media and added to cells at a total nucleic acid dose of 1,000 ng/well and incubated for two hours. Prior to imaging, cells were then stained with Hoechst 33342 at a 1:5,000 dilution for nuclei visualization. Images were acquired over a 19,660 μm area at Nyquist limit resolution using a Zeiss LSM 780 microscope with Zen Blue software and

63x oil immersion lens. Specific laser channels used were 405 nm diode, 488 nm argon, 561 nm solid-state, and 639 nm diode lasers. Laser intensity and detector gain settings were maintained across all image acquisition.

2.12 CRISPR Gene Editing

The template used for in vitro transcription of sgRNA targeting GFP was synthesized as a gBlock from IDT (sequence listed in Table S2). In vitro transcription was performed using a MEGAshortscript T7 Transcription kit (Invitrogen) according to manufacturer's instructions, and the sgRNA product was purified using MEGAclear Transcription Clean-up kit (Invitrogen). Cas9 plasmid DNA (41815)[12] was purchased from Addgene and amplified by Aldeveron (Fargo, ND). For co-delivery transfections, DNA and sgRNA were delivered using R6,7,8_64 nanoparticles as described above. Gene knockout was assessed using flow cytometry 5 days post-transfection unless otherwise noted.

2.13 Statistics

Prism 6 (Graphpad, La Jolla, CA) was used for all statistical analyses and curve plotting. Statistical tests were performed with a global alpha value of 0.05. Unless otherwise stated, absence of statistical significance markings where a test was stated to have been performed signified no statistical significance. The statistical test used and the number of experimental replicates were listed in the captions for each figure. Statistical significance was denoted as follows: *$p<0.05$; **$p<0.01$, ***$p<0.001$, ****$p<0.0001$.

3. Results and Discussion

3.1 Polymer Synthesis and Characterization

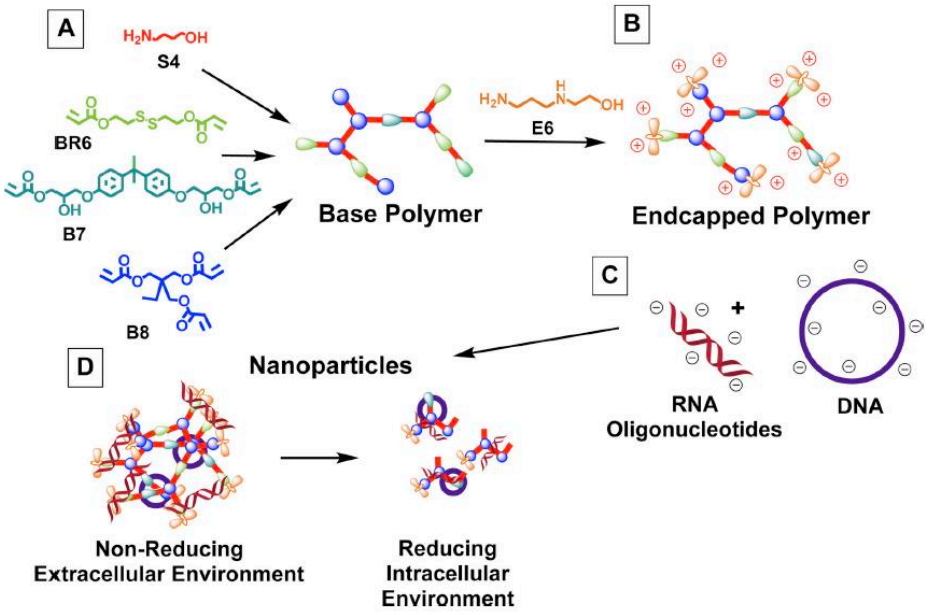

Figure 6-1. Monomer structures and proposed mechanism for polymer function. (A) B and S monomers were co-polymerized to form acrylate-terminated base polymers, which were then **(B)** end-capped with monomer E6. **(C)** These polymers self-assembled into nanoparticles with anionic nucleic acids and **(D)** partially degraded at reducible linkages in the reducing cytosolic environment, allowing for intracellular cargo release.

Polymers were synthesized following a facile one-pot Michael addition reaction in which acrylate monomers BR6 and B8 were copolymerized with amine-containing monomer S4 (**Scheme 6-1**). After end-capping with monomer E6, this class of polymers is referred to as R6,8_N, where N denotes the branching B8 monomer content in the polymer backbone (i.e. R6,8_20 contains 20% B8). In the polymer series containing the additional diacrylate monomer B7, polymers are referred to as R6,7,8_M, where M denotes the B7 monomer content in the polymer backbone. For acrylate-terminated base polymer synthesis, B and S monomers were dissolved in anhydrous DMSO at 150 mg/mL (monomer concentrations >400 mg/mL resulted in complete gelation), and step-wise polymerization reaction was allowed to proceed overnight at 90°C with stirring. The chemical structures of base polymers were determined via NMR spectroscopy, which verified that the polymers were acrylate terminated by three distinct acrylate peaks at 5.5-6.5 ppm (**Figure 6-S1**). Polymer end-capping with monomer E6 was performed at room temperature for 1 hr and confirmed by

the disappearance of these peaks. Molecular weight data was obtained from GPC analysis, which showed that with increasing B8 content, both M_n and M_w values generally increased (**Table 6-1**). For R6,7,8-4-6 polymers, for which B8 content was fixed at 20%, molecular weight did not change significantly with varying B7 content, suggesting that molecular weight is largely controlled by polymer branching and crosslinking effects contributed by triacrylate monomer B8.

	Polymer Name	M_n	M_w	PDI	Monomer Fraction in Polymer		
					BR6	B7	B8
R6,8-4-6	R6,8_0	2,224	2,682	1.21	1.00	--	--
	R6,8_20	3,168	4,038	1.27	0.75	--	0.25
	R6,8_40	4,050	5,896	1.46	0.54	--	0.46
	R6,8_60	4,943	9,949	2.01	0.36	--	0.64
	R6,8_80	4,675	8,728	1.87	0.23	--	0.77
R6,7,8-4-6 (20% B8)	R6,7,8_16	4,511	7,616	1.69	0.62	0.17	0.21
	R6,7,8_40	4,570	7,435	1.63	0.41	0.40	0.19
	R6,7-8_64	4,438	7,066	1.59	0.17	0.63	0.20

Table 6-1. Molecular weight data from GPC characterization and monomer composition calculated from ^{1}H NMR spectra.

3.2 siRNA Delivery: Gene Knockdown, Cellular Uptake, and Cytotoxicity

R6,8-4-6 polymers were used to deliver siRNA targeting GFP (siGFP) in HEK-293T cells stably expressing a destabilized form of GFP with short half-life (GFPd2).[29] At 100 nM siRNA dose and 180 polymer-siRNA w/w ratio, R6,8_20 achieved 75% knockdown with negligible cytotoxicity (**Figure 6-1A**). All branched polymers in the R6,8_N series with the exception of R6,8_80 achieved significantly higher knockdown than the linear polymer (R6,8_0). Knockdown levels peaked with R6,8_20 and R6,8_40 (**Figure 6-S2**), and the same trend was observed for nanoparticle uptake (**Figure 6-1B**). Previous studies have demonstrated that nanoparticle uptake and transfection efficacy increased with increasing polymer molecular weight.[33-34] This was not the case in our polymer system as R6,8_60 and R6,8_80 had the highest molecular weight but achieved relatively poor knockdown. This could in part be due to the fact that increasing polymer branching resulted in lower cell viability caused by decreasing reducible BR6 monomer content. Indeed, when

cells were pre-treated with L-buthionine-sulfoximine (BSO) to inhibit cellular production of glutathione, the main intracellular reducing agent,[35] nanoparticle-mediated cytotoxicity significantly increased (**Figure 6-1C**). This increased toxicity was beyond the additive effects of either nanoparticle or BSO treatment alone, indicating that the cell's inability to reduce disulfide bonds after glutathione blockade induced higher levels of cell death and confirming our hypothesis that polymer reducibility attenuated cytotoxicity by enabling them to rapidly degrade to relatively non-toxic oligomers. Thus, the bio-reducibility of the rBEAQ nanoparticles is designed to both enable environmentally-triggered release upon entering the cytosol and as a mechanism to limit potential cytotoxicity of the branched polymers by quickly breaking them down into smaller components once they reach their target inside the cell.

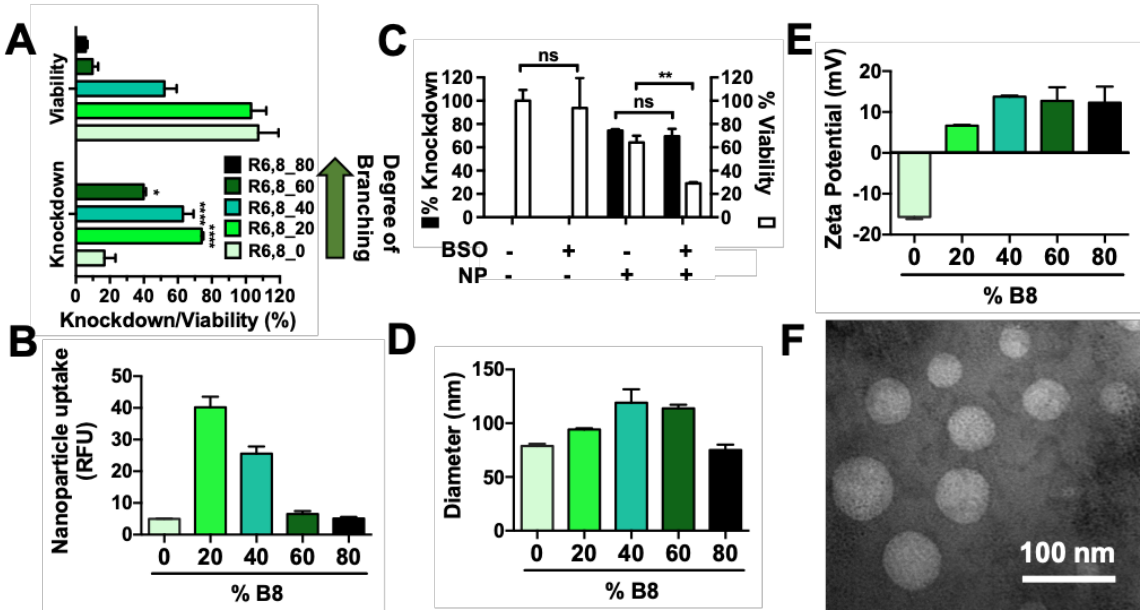

Figure 6-2. R6,8-4-6 polymers enable efficient intracellular siRNA delivery. (A) Gene knockdown and cytotoxicity of nanoparticles delivering 100 nM siRNA at 180 w/w. Statistical analysis was assessed by one-way ANOVA with Tukey post-hoc tests. N = 4. **(B)** Nanoparticle uptake measured by flow cytometry after treatment of nanoparticles containing Cy5-labeled siRNA. N = 4. **(C)** Pre-treatment with 1,000 μM L-buthionine-sulfoximine (BSO) shows that intracellular glutathione blockade did not change knockdown levels but significantly increased polymer-mediated cytotoxicity as assessed by Holm-Sidak corrected multiple t-tests; R6,8_20 nanoparticles (180 w/w) were used to deliver 100 nM siRNA. N = 4. **(D)** Nanoparticle

hydrodynamic diameter and **(E)** zeta potential measured using dynamic light scattering. Bars show average + SEM; N = 3. **(F)** Representative TEM image of R6,8_40 nanoparticles.

To elucidate the mechanism by which moderately branched polymers achieved the highest levels of knockdown, we assessed the physical characteristics of the nanoparticles. All polymers in the series formed nanoparticles with hydrodynamic diameters around 100 nm (**Figure 6-1D**). Nanoparticles formed with the linear polymer had negative surface charge, and zeta potential generally became increasingly positive with increased polymer branching (**Figure 6-1E**). This is likely due to the fact that increased branching resulted in increasing numbers of secondary amine-containing end-groups per polymer molecule, which are positively charged in pH 5 NaAc buffer. The increased cationic charge of moderately-branched polymer nanoparticles likely contributes to nanoparticle uptake and siRNA-mediated knockdown *in vitro*, which is consistent with many published reports.[36-38] This trend does not apply to very highly branched polymers, however, in part due to the high levels of cytotoxicity incurred by these nanoparticle formulations.

3.3 siRNA Binding and Environmentally-triggered Release

A competitive binding assay using Yo-Pro-1 iodide (Yo-Pro) was used to assess siRNA binding strength in R6,8-4-6 polymers. Yo-Pro dye fluoresces upon nucleic acid binding, and quenching of fluorescence after polymer outcompetes the dye for siRNA binding was used as a measure of binding strength. Increasing polymer branching increased siRNA binding strength, which was seen in both end-capped (**Figure 6-2A**) as well as acrylate-terminated polymers (**Figure 6-S3A**). Plotting knockdown as a function of the polymer EC_{50} w/w of siRNA binding (where lower EC_{50} w/w corresponds to tighter siRNA binding and higher degree of polymer branching) revealed a biphasic response (**Figure 6-2B**). Binding affinity and degree of knockdown both increased approximately 4-fold from R6,8_0 to R6,8_20 and decreased steadily when B8 content exceeded 40%. This suggests that an optimal range for siRNA binding affinity exists, and polymers that bind too tightly cannot release siRNA to achieve efficient knockdown while those that do not bind tightly enough cannot form nanoparticles that effectively promote nanoparticle internalization.[39-40] siRNA binding affinity, along with other nanoparticle biophysical and chemical properties

such as the size, surface charge, and bio-reducibility discussed earlier all contribute to the differential gene silencing effects seen here. For polymers with the same B8 content, end-capped polymers exhibited stronger binding than their acrylate-terminated counterparts (**Figure 6-S3B**). These results suggest that polymer branching increases siRNA binding via two mechanisms. The first is mediated by increased branching structure in the polymer backbone, which increases the molecular weight of the polymer and drives stronger binding through greater hydrophobic effects. The second is mediated by increased branching endpoints, which increases the number of end-capping molecules. As the secondary amines in the polymer end-groups are positively-charged in pH 5 NaAc buffer, they further increase siRNA binding through electrostatic interactions.

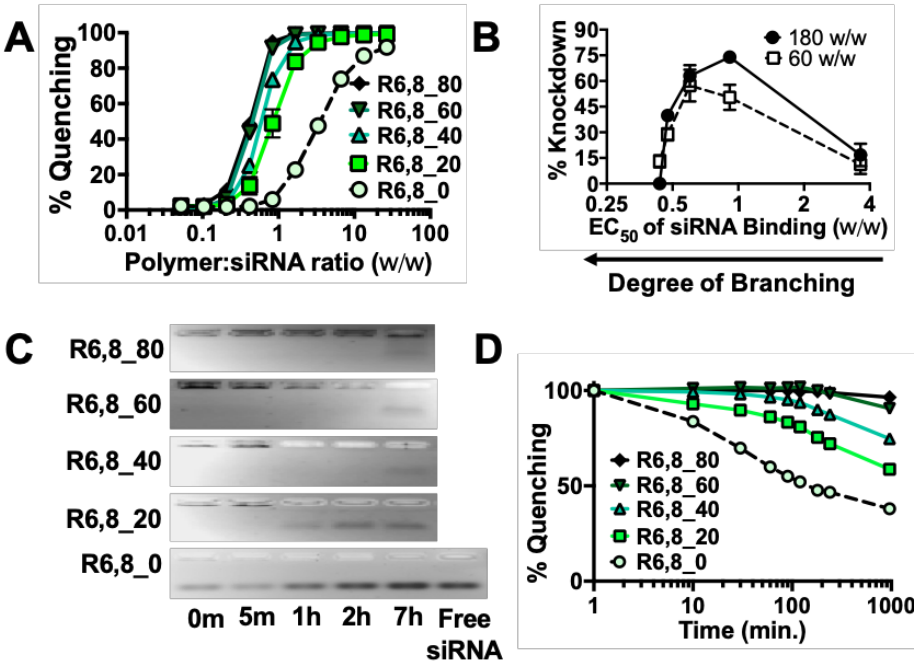

Figure 6-3. Polymer branching and reducibility can be modulated to control siRNA binding affinity and release kinetics. (A) Yo-Pro-1 iodide binding competition assay of R6,8-4-6 polymers to assess siRNA binding affinity. N = 4. **(B)** % knockdown plotted as a function of polymer EC_{50} w/w for siRNA binding. N = 4. **(C)** Gel retardation assays (N = 1) and **(D)** Yo-Pro binding assay (N = 4) were performed on nanoparticles incubated in 5 mM glutathione to mimic intracellular reducing environments and nucleic acid release slowed as the polymers became more branched with less frequent bio-reducible linkages.

We next investigated siRNA release kinetics of R6,8-4-6 nanoparticles in 5 mM glutathione to mimic the reducing intracellular environment.[35] Nanoparticles were sampled at specific time points and standard gel electrophoresis was performed to assess siRNA release (**Figure 6-2C**). The linear polymer released siRNA almost instantaneously, and release was complete by 1 hr. Increased polymer branching slowed siRNA release considerably, with R6,8_20 beginning release at 1 hr and higher branching polymers at 7 hr. The same trend was observed when a Yo-Pro binding assay was performed with nanoparticles incubated over time in reducing buffer conditions (**Figure 6-2D**). These results indicate that siRNA binding and release can be modulated in a highly controlled manner by changing the ratio between branching and reducible monomers and that siRNA release can be designed to occur in an environmentally-triggered manner via reduction of disulfide bonds. However, we have also shown that blocking intracellular glutathione levels did not significantly decrease the observed level of siRNA-mediated knockdown (**Figure 6-1C**), which suggests that other polymer degradation mechanisms such as the hydrolysis of ester bonds over a period of 4-6 hr[41] could also contribute to siRNA release from nanoparticles. Incorporation of disulfide linkages in the rBEAQ polymers helps ensure fragmentation of the polymers into small oligomers, reducing cytotoxicity, and enables higher doses, branching, or w/w formulation ratios of the polymers to be safely utilized.

3.4 Co-delivery of siRNA and DNA

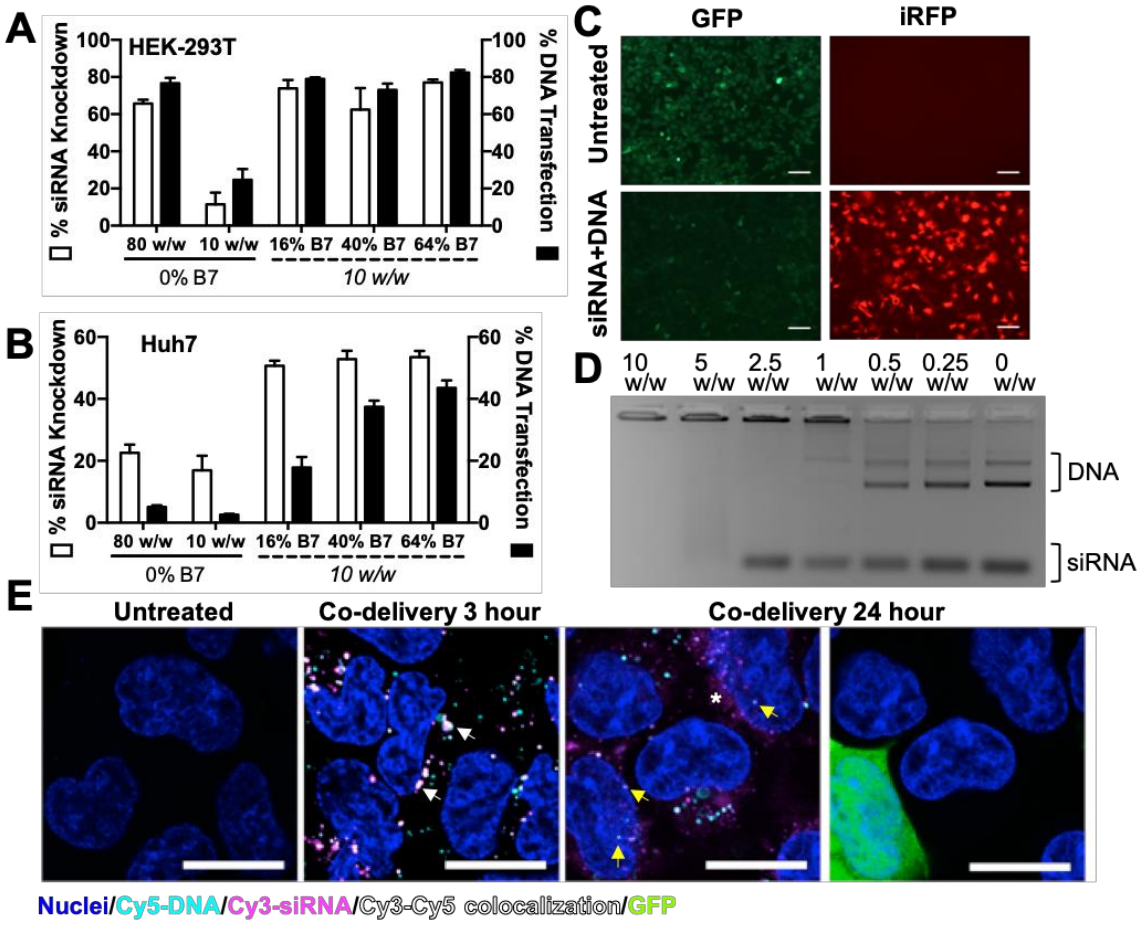

Figure 6-4. Hydrophobic R6,7,8-4-6 polymer series enables efficient co-delivery of DNA and siRNA. Co-delivery efficacy of R6,8-4-6 (0% B7) and R6,7,8-4-6 nanoparticles encapsulating 400 ng total nucleic acid in 293T **(A)** and Huh7 **(B)**. N = 4. **(C)** Fluorescence microscopy images of HEK-293T cells treated with R6,7,8_16 nanoparticles co-delivering 200 ng siRNA and 200 ng DNA (10 w/w formulation). Scale bar 100 μm. **(D)** R6,7,8_64 completely encapsulated plasmid DNA and siRNA at 10 w/w as seen by a gel retardation assay. **(E)** Confocal microscopy images of 293T cells treated with R6,7,8_64 nanoparticles co-delivering Cy3-siRNA, Cy5-DNA, and unlabeled GFP plasmid DNA (0.5:0.4:0.1 composition by weight) at 3 hr and 24 hr post-uptake. Cy3 and Cy5 signal colocalization could be seen at 3 hours post-uptake (white arrows). At 24 hours post-uptake, diffuse Cy3-siRNA signal could be seen in the cytosol (white asterisk) while some Cy5-DNA signal was detected in the nucleus (yellow arrows) and some cells were visibly expressing GFP. Scale bar 20 μm.

As moderately branched polymers have been shown to maintain strong nucleic acid binding affinity while effectively releasing siRNA cargo in the reducing cytosolic environment, we hypothesized that they may be suitable for the co-delivery of plasmid DNA and siRNA. R6,8_20 (the top polymer for siRNA delivery) was used to encapsulate 200 ng each of siGFP siRNA and a plasmid DNA encoding iRFP670. R6,8_20 nanoparticles enabled efficient co-delivery to HEK-293T cells (**Figure 6-3A**), resulting in 66% siRNA-mediated knockdown and 77% DNA transfection with negligible cytotoxicity (**Figure 6-S4A**). The same formulation achieved much lower delivery efficiency in harder-to-transfect Huh7 cells (23% knockdown and 5% transfection; **Figure 6-3B**), prompting the need to develop more effective polymers for co-delivery. To this end, we investigated the effect of polymer hydrophobicity by incorporating monomer B7 at ratios indicated in **Table 6-S1** to synthesize the R6,7,8-4-6 polymer series. B7 was chosen as it contains a bisphenol A group, which has been shown to bind DNA via hydrophobic effects[42] and enable high efficiency DNA transfection.[27, 43-44] B7-containing polymers effectively complexed nucleic acids at very low w/w, forming nanoparticles around 150 nm in diameter and +6 to +16 mV in zeta potential (**Figure 6-S5**). R6,7,8_64 nanoparticles at a 10 w/w ratio were quite stable in complete cell culture medium mimicking physiological conditions for several hours with a hydrodynamic diameter doubling time >4 hours as assessed by DLS (**Figure 6-S5D).** In contrast, R6,8-4-6 polymers with 0% B7 content formed much larger nanoparticles (270 nm) with -11 mV zeta potential at 10 w/w. B7-containing polymers were used at significantly lower w/w formulations compared to R6,8-4-6 polymers used for siRNA complexation earlier because R6,7,8-4-6 polymers incurred significantly higher cytotoxicity than the R6,8-4-6 polymers, limiting their use to very low w/w formulations (**Figure 6-S4B**). Nevertheless, B7-containing polymers enabled higher levels of knockdown and transfection at 10 w/w in HEK-293T cells (**Figure 6-3A and 6-3C**), though the difference was less notable when R6,8-4-6 polymers were used at higher w/w. More strikingly, R6,7,8-4-6 polymers enabled significantly higher co-delivery in Huh7 cells compared to R6,8-4-6 at all w/w formulations, with the best formulation achieving 53% knockdown and 37% transfection (**Figure 6-3B**). A gel retardation assay

demonstrated that R6,7,8_64 completely condensed both plasmid DNA and siRNA at 10 w/w, and decreasing polymer dose resulted in siRNA release at 5 w/w and DNA release at 1 w/w (**Figure 6-3D**).

We further explored the intracellular delivery location of siRNA and DNA using confocal laser scanning microscopy, which demonstrated different fates for internalized siRNA and DNA. At an early 3 hour timepoint following nanoparticle treatment, most endosomes possessed both siRNA and DNA, while at 24 hours post-treatment, diffuse cytosolic siRNA was detectable in most cells and the occasional z-slice revealed some Cy5 labeled plasmid DNA in the nucleus (**Figure 6-3E**). Using a mix of fluorescently labeled plasmid DNA and unlabeled plasmid DNA, we were also able to detect a fraction of the cells expressing a fluorescent reporter protein GFP at 24 hours post-transfection, which was undetectable in cells at 3 hours post-treatment (**Figure 6-S6**).

Studies have shown that polymers optimized for DNA delivery may not be optimal for siRNA and *vice versa*.[45] This may be due to the differences in size and charge density between DNA and siRNA as well as their intracellular sites of action. Bishop *et al.* approached this problem with a polymer-coated gold nanoparticle system where siRNA and DNA were adsorbed onto the nanoparticle using different polymers in a layer-by-layer synthesis scheme; the optimal formulation in this study resulted in 34% knockdown and 14% transfection in human brain cancer cells.[46] Another study using poly(L-lysine) polyplexes for co-delivery of siRNA and DNA to HEK-293T cells showed >80% knockdown but achieved <10% DNA transfection.[47] The delivery system reported herein achieved significantly higher co-delivery in both HEK-293T cells as well as harder-to-transfect Huh7 human liver cancer cells. These polymers are easy to formulate into nanoparticles via self-assembly in a single step, and enabled more efficient co-delivery of both DNA and siRNA compared to several leading commercially available non-viral transfection reagents (**Figure 6-S7**).

We further compared the DNA-siRNA co-delivery efficacy of the system presented herein with that of using nanoparticle formulations previously optimized for the delivery of each nucleic acid separately (**Figure 6-S8**). In the latter strategy, plasmid DNA was encapsulated using polymer 446 at 60 w/w (previously optimized for DNA delivery[48]) and siRNA was encapsulated using polymer R646 at 120 w/w (previously optimized for siRNA delivery[49]). The two nanoparticles were formulated separately and added to

cells after nanoparticle formation. In the single nanoparticle strategy, the same amount of nucleic acids was pre-mixed and co-encapsulated in R6,7,8_64 nanoparticles (10 w/w). Our results show that using the dual nanoparticle delivery strategy, siRNA knockdown levels were significantly lower than that achieved by the single nanoparticle co-delivery strategy while DNA transfection levels were similar. Furthermore, when polymers 446 and R646 were used to formulate nanoparticles at 10 w/w for direct comparison with polymer R6,7,8_64, both siRNA and DNA delivery levels were significantly lower. These results indicate that co-encapsulation of multiple nucleic acid cargo types in the same nanoparticle system has the advantages of higher transfection efficiency as well as greater simplicity in formulation; this is especially important for potential clinical translation as it could greatly simplify the synthesis and regulatory approval processes.

3.5 Co-delivery of Cas9 DNA and sgRNA for CRISPR-mediated Gene Editing

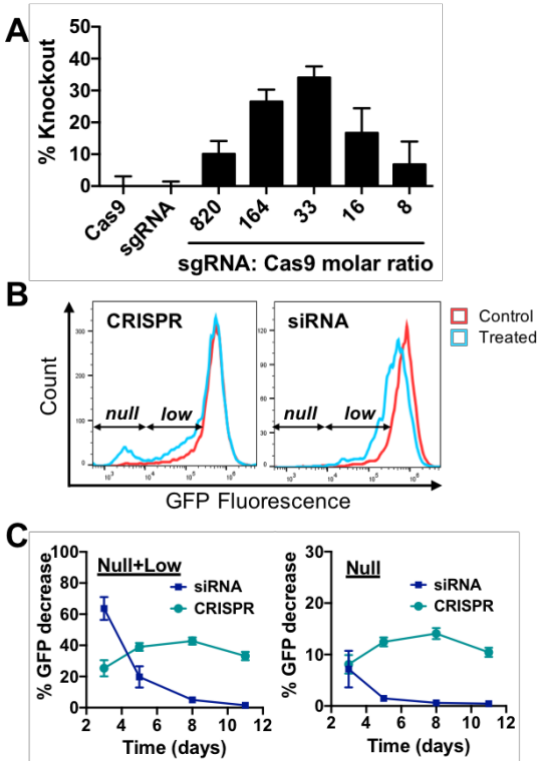

Figure 6-5. Co-delivery of anti-GFP sgRNA and Cas9 plasmid enables CRISPR-mediated gene knockout. (A) HEK-293T cells were transfected with R6,7,8_64 10 w/w nanoparticles encapsulating Cas9 DNA and sgRNA at the indicated nucleic acid molar ratios. N = 4. **(B)** Flow cytometry histograms of CRISPR- or siRNA-treated cells. CRISPR treatment produced a completely GFP-negative population (null)

while siRNA treatment mainly resulted in a general population shift to lower GFP fluorescence (low). **(C)** Gene suppression kinetics of CRISPR and siRNA treated cells. N = 4.

Next, we co-encapsulated Cas9 plasmid DNA and sgRNA targeting GFP in our nanoparticles for intracellular delivery of the CRISPR/Cas9 gene editing system within one biodegradable nanoparticle. Gene knockout, which can be assessed by a decrease in GFP fluorescence, is contingent upon co-delivery of both components as the Cas9 endonuclease must assemble with sgRNA to form a functional ribonucleoprotein (RNP) complex. This is a rigorous test of co-delivery as the two components must be present in the same cell as well as remain bioactive at the same time in order for editing to occur. Our results showed that R6,7,8_64 nanoparticles enabled 40% gene knockout in HEK-293T cells (**Figure 6-4A**). Delivery of either component alone did not result in appreciable levels of knockout, confirming the need for co-delivery. The optimal sgRNA-Cas9 molar ratio was 33. Interestingly, we saw a distinct GFP-negative population (GFP null) in CRISPR-treated cells which was not observed in cells treated with GFP siRNA (**Figure 6-4B**). siRNA-mediated gene silencing downshifted the GFP fluorescence of the entire population of treated cells while CRISPR-mediated knockout completely turned off GFP in a fraction of cells. Kinetic studies showed that siRNA-mediated gene silencing faded rapidly, and fluorescence returned to pre-treatment levels after 11 days (**Figure 6-4C**). In contrast, CRISPR-mediated silencing peaked after 5 days and remained constant for the entirety of the period tested. Our results suggest that gene silencing mediated by siRNA knockdown or CRISPR knockout could be suitable for different therapeutic goals. The former has a faster onset and results in significant but transient downregulation in the entire population of treated cells. The latter takes longer to reach peak levels but can produce a sustained and binary downregulation in a smaller fraction of the population.

It is important to note that all transfection experiments so far have been performed in serum-free medium. It has been widely reported that the presence of serum may decrease transfection efficacy by inducing polyplex disruption and aggregation.[50] On the contrary, some studies have also demonstrated that the presence of serum proteins may prevent disassembly of nanocomplexes.[51] To investigate the performance

of our nanoparticle system in serum conditions, R6,7,8_64 nanoparticles (10 w/w) were formulated with siRNA or Cas9 DNA and sgRNA and administered to cells in complete medium (10% serum). The presence of serum significantly reduced transfection efficacy in both cases (**Figure 6-S9**). However, when $NaHCO_3$ was added to the nanoparticle formulation to increase nanoparticle pH prior to addition to the cells, transfection in both cases increased back to similar levels as in serum-free conditions. The addition of anionic compounds to nanoparticles to increase transfection in serum conditions has been utilized in other delivery systems[52] and is a viable strategy to stabilize polymeric polyplexes.

4. Conclusions

We synthesized a new series of reducible branched ester-amine quadpolymers (rBEAQs) that enabled co-delivery of plasmid DNA and RNA oligonucleotides in the same biodegradable self-assembled nanoparticle system. Our best formulation achieved 77% DNA transfection and 66% siRNA-mediated knockdown in HEK-293T cells, and 37% transfection and 53% knockdown in Huh7 cells. More importantly, co-delivery of Cas9 DNA and sgRNA in the same non-viral nanoparticles enabled 40% CRISPR/Cas9-mediated gene knockout. To our knowledge, this is the first time that CRISPR-mediated gene editing has been achieved through the co-delivery of Cas9 plasmid and sgRNA. The effective co-delivery of plasmid DNA and RNA oligonucleotides reported here, as well as the ability to leverage bio-reducibility, hydrophobicity, and polymer branching to enable effective co-delivery in different cell types, may prove useful for applications such as novel combinatorial gene therapies and genome editing.

Author Contributions

Conceptualization, YR, DRW and JJG; Methodology, YR, DRW and JJG, Investigation YR, DRW, KS; Resources and funding acquisition, JJG; Writing and editing, YR, DRW, JJG; Supervision and administration, JJG.

Funding Sources

The authors would like to thank the following organizations for financial support: NSF Graduate Research Fellowship DGE-0707427 (DRW) and DGE-1232825 (YR), Microscopy Core Grant (S10 OD016374) and the United States NIH grants R01EB016721 (JJG), and R01EB022148 (JJG). JJG thanks the Bloomberg~Kimmel Institute for Cancer Immunotherapy and the Research to Prevent Blindness James and Carole Free Catalyst Award for support.

References

1. Bhise, N. S.; Wahlin, K. J.; Zack, D. J.; Green, J. J., Evaluating the Potential of Poly(Beta-Amino Ester) Nanoparticles for Reprogramming Human Fibroblasts to Become Induced Pluripotent Stem Cells. *International journal of nanomedicine* **2013,** *8*, 4641-58.

2. Warren, L.; Manos, P. D.; Ahfeldt, T.; Loh, Y.-H.; Li, H.; Lau, F.; Ebina, W.; Mandal, P. K.; Smith, Z. D.; Meissner, A., Highly Efficient Reprogramming to Pluripotency and Directed Differentiation of Human Cells with Synthetic Modified Mrna. *Cell stem cell* **2010,** *7* (5), 618-630.

3. Tzeng, S. Y.; Hung, B. P.; Grayson, W. L.; Green, J. J., Cystamine-Terminated Poly(Beta-Amino Ester)S for Sirna Delivery to Human Mesenchymal Stem Cells and Enhancement of Osteogenic Differentiation. *Biomaterials* **2012,** *33* (32), 8142-51.

4. Powers, M. V.; Clarke, P. A.; Workman, P., Dual Targeting of Hsc70 and Hsp72 Inhibits Hsp90 Function and Induces Tumor-Specific Apoptosis. *Cancer Cell* **2008,** *14* (3), 250-262.

5. Caldas, H.; Jaynes, F. O.; Boyer, M. W.; Hammond, S.; Altura, R. A., Survivin and Granzyme B–Induced Apoptosis, a Novel Anticancer Therapy. *Molecular cancer therapeutics* **2006,** *5* (3), 693-703.

6. Mangraviti, A.; Tzeng, S. Y.; Kozielski, K. L.; Wang, Y.; Jin, Y.; Gullotti, D.; Pedone, M.; Buaron, N.; Liu, A.; Wilson, D. R.; Hansen, S. K.; Rodriguez, F. J.; Gao, G.-D.; DiMeco, F.; Brem, H.; Olivi, A.; Tyler, B.; Green, J. J., Polymeric Nanoparticles for Nonviral Gene Therapy Extend Brain Tumor Survival in Vivo. *ACS Nano* **2015,** *9* (2), 1236-1249.

7. Ledford, H., Engineered Cell Therapy for Cancer Gets Thumbs up from Fda Advisers. *Nature* **2017,** *547* (7663), 270.

8. Fischer, A. Fda Approves Novel Gene Therapy to Treat Patients with a Rare Form of Inherited Vision Loss. FDA.gov.

9. Munye, M. M.; Tagalakis, A. D.; Barnes, J. L.; Brown, R. E.; McAnulty, R. J.; Howe, S. J.; Hart, S. L., Minicircle DNA Provides Enhanced and Prolonged Transgene Expression Following Airway Gene Transfer. *Sci. Rep.* **2016,** *6*, 23125.

10. Fire, A.; Xu, S. Q.; Montgomery, M. K.; Kostas, S. A.; Driver, S. E.; Mello, C. C., Potent and Specific Genetic Interference by Double-Stranded Rna in Caenorhabditis Elegans. *Nature* **1998,** *391* (6669), 806-811.

11. Hannon, G. J., Rna Interference. *nature* **2002,** *418* (6894), 244-251.

12. Mali, P.; Yang, L.; Esvelt, K. M.; Aach, J.; Guell, M.; DiCarlo, J. E.; Norville, J. E.; Church, G. M., Rna-Guided Human Genome Engineering Via Cas9. *Science* **2013,** *339* (6121), 823-826.

13. Cong, L.; Ran, F. A.; Cox, D.; Lin, S.; Barretto, R.; Habib, N.; Hsu, P. D.; Wu, X.; Jiang, W.; Marraffini, L. A.; Zhang, F., Multiplex Genome Engineering Using Crispr/Cas Systems. *Science* **2013,** *339* (6121), 819-823.

14. Kozielski, K. L.; Rui, Y.; Green, J. J., Non-Viral Nucleic Acid Containing Nanoparticles as Cancer Therapeutics. *Expert Opin Drug Deliv* **2016**, 1-13.

15. Kebbekus, P.; Draper, D. E.; Hagerman, P., Persistence Length of Rna. *Biochemistry-Us* **1995,** *34* (13), 4354-4357.

16. Hagerman, P. J., Flexibility of Rna. *Annu Rev Bioph Biom* **1997,** *26*, 139-156.

17. Tian, H.; Xiong, W.; Wei, J.; Wang, Y.; Chen, X.; Jing, X.; Zhu, Q., Gene Transfection of Hyperbranched Pei Grafted by Hydrophobic Amino Acid Segment Pblg. *Biomaterials* **2007,** *28* (18), 2899-2907.

18. Kadlecova, Z.; Rajendra, Y.; Matasci, M.; Baldi, L.; Hacker, D. L.; Wurm, F. M.; Klok, H.-A., DNA Delivery with Hyperbranched Polylysine: A Comparative Study with Linear and Dendritic Polylysine. *Journal of controlled release* **2013,** *169* (3), 276-288.

19. Zhao, T.; Zhang, H.; Newland, B.; Aied, A.; Zhou, D.; Wang, W., Significance of Branching for Transfection: Synthesis of Highly Branched Degradable Functional Poly (Dimethylaminoethyl Methacrylate) by Vinyl Oligomer Combination. *Angewandte Chemie International Edition* **2014,** *53* (24), 6095-6100.

20. Wilson, D. R.; Rui, Y.; Siddiq, K.; Routkevitch, D.; Green, J. J., Differentially Branched Ester Amine Quadpolymers with Amphiphilic and Ph Sensitive Properties for Efficient Plasmid DNA Delivery. *Molecular pharmaceutics* **2019**.

21. Rahbek, U. L.; Nielsen, A. F.; Dong, M.; You, Y.; Chauchereau, A.; Oupicky, D.; Besenbacher, F.; Kjems, J.; Howard, K. A., Bioresponsive Hyperbranched Polymers for Sirna and Mirna Delivery. *Journal of drug targeting* **2010,** *18* (10), 812-820.

22. Jia, H.-Z.; Zhang, W.; Zhu, J.-Y.; Yang, B.; Chen, S.; Chen, G.; Zhao, Y.-F.; Feng, J.; Zhang, X.-Z., Hyperbranched–Hyperbranched Polymeric Nanoassembly to Mediate Controllable Co-Delivery of Sirna and Drug for Synergistic Tumor Therapy. *Journal of Controlled Release* **2015,** *216*, 9-17.

23. Wilson, D. R.; Rui, Y.; Siddiq, K.; Routkevitch, D.; Green, J. J., Differentially Branched Ester Amine Quadpolymers with Amphiphilic and Ph-Sensitive Properties for Efficient Plasmid DNA Delivery. *Molecular Pharmaceutics* **2019,** *16* (2), 655-668.

24. Chen, G.; Wang, Y.; Xie, R.; Gong, S., Tumor-Targeted Ph/Redox Dual-Sensitive Unimolecular Nanoparticles for Efficient Sirna Delivery. *Journal of Controlled Release* **2017,** *259*, 105-114.

25. Tai, Z.; Wang, X.; Tian, J.; Gao, Y.; Zhang, L.; Yao, C.; Wu, X.; Zhang, W.; Zhu, Q.; Gao, S., Biodegradable Stearylated Peptide with Internal Disulfide Bonds for Efficient Delivery of Sirna in Vitro and in Vivo. *Biomacromolecules* **2015,** *16* (4), 1119-1130.

26. Kozielski, K. L.; Tzeng, S. Y.; Green, J. J., A Bioreducible Linear Poly(Beta-Amino Ester) for Sirna Delivery. *Chemical Communications* **2013,** *49* (46), 5319 - 5321.

27. Eltoukhy, A. A.; Chen, D.; Alabi, C. A.; Langer, R.; Anderson, D. G., Degradable Terpolymers with Alkyl Side Chains Demonstrate Enhanced Gene Delivery Potency and Nanoparticle Stability. *Advanced Materials* **2013,** *25* (10), 1487-1493.

28. Nelson, C. E.; Kintzing, J. R.; Hanna, A.; Shannon, J. M.; Gupta, M. K.; Duvall, C. L., Balancing Cationic and Hydrophobic Content of Pegylated Sirna Polyplexes Enhances Endosome Escape, Stability, Blood Circulation Time, and Bioactivity in Vivo. *ACS Nano* **2013,** *7* (10), 8870-8880.

29. Matsuda, T.; Cepko, C. L., Controlled Expression of Transgenes Introduced by in Vivo Electroporation. *Proceedings of the National Academy of Sciences* **2007,** *104* (3), 1027.

30. Yao, C.; Tai, Z.; Wang, X.; Liu, J.; Zhu, Q.; Wu, X.; Zhang, L.; Zhang, W.; Tian, J.; Gao, Y., Reduction-Responsive Cross-Linked Stearyl Peptide for Effective Delivery of Plasmid DNA. *International journal of nanomedicine* **2015,** *10*, 3403.

31. Wilson, D. R.; Mosenia, A.; Suprenant, M. P.; Upadhya, R.; Routkevitch, D.; Meyer, R. A.; Quinones-Hinojosa, A.; Green, J. J., Continuous Microfluidic Assembly of Biodegradable Poly(Beta-Amino Ester)/DNA Nanoparticles for Enhanced Gene Delivery. *J Biomed Mater Res A* **2017,** *105* (6), 1813-1825.

32. Wilson, D. R.; Routkevitch, D.; Rui, Y.; Mosenia, A.; Wahlin, K. J.; Quinones-Hinojosa, A.; Zack, D. J.; Green, J. J., A Triple-Fluorophore-Labeled Nucleic Acid Ph Nanosensor to Investigate Non-Viral Gene Delivery. *Molecular Therapy* **2017**.

33. Huang, M.; Khor, E.; Lim, L.-Y., Uptake and Cytotoxicity of Chitosan Molecules and Nanoparticles: Effects of Molecular Weight and Degree of Deacetylation. *Pharmaceutical Research* **2004,** *21* (2), 344-353.

34. Eltoukhy, A. A.; Siegwart, D. J.; Alabi, C. A.; Rajan, J. S.; Langer, R.; Anderson, D. G., Effect of Molecular Weight of Amine End-Modified Poly(B-Amino Ester)S on Gene Delivery Efficiency and Toxicity. *Biomaterials* **2012,** *33* (13), 3594-3603.

35. Griffith, O. W., Biologic and Pharmacologic Regulation of Mammalian Glutathione Synthesis. *Free Radical Biology and Medicine* **1999,** *27* (9-10), 922-935.

36. Yu, B.; Zhang, Y.; Zheng, W.; Fan, C.; Chen, T., Positive Surface Charge Enhances Selective Cellular Uptake and Anticancer Efficacy of Selenium Nanoparticles. *Inorg. Chem.* **2012,** *51* (16), 8956-8963.

37. Harush-Frenkel, O.; Debotton, N.; Benita, S.; Altschuler, Y., Targeting of Nanoparticles to the Clathrin-Mediated Endocytic Pathway. *Biochemical and biophysical research communications* **2007,** *353* (1), 26-32.

38. Liu, X.; Howard, K. A.; Dong, M.; Andersen, M. Ø.; Rahbek, U. L.; Johnsen, M. G.; Hansen, O. C.; Besenbacher, F.; Kjems, J., The Influence of Polymeric Properties on Chitosan/Sirna Nanoparticle Formulation and Gene Silencing. *Biomaterials* **2007,** *28* (6), 1280-1288.

39. Schaffer, D. V.; Fidelman, N. A.; Dan, N.; Lauffenburger, D. A., Vector Unpacking as a Potential Barrier for Receptor-Mediated Polyplex Gene Delivery. *Biotechnol. Bioeng.* **2000,** *67* (5), 598-606.

40. Bishop, C. J.; Ketola, T.-m.; Tzeng, S. Y.; Sunshine, J. C.; Urtti, A.; Lemmetyinen, H.; Vuorimaa-Laukkanen, E.; Yliperttula, M.; Green, J. J., The Effect and Role of Carbon Atoms in Poly(B-Amino Ester)S for DNA Binding and Gene Delivery. *Journal of the American Chemical Society* **2013,** *135* (18), 6951-7.

41. Sunshine, J. C.; Peng, D. Y.; Green, J. J., Uptake and Transfection with Polymeric Nanoparticles Are Dependent on Polymer End-Group Structure, but Largely Independent of Nanoparticle Physical and Chemical Properties. *Molecular pharmaceutics* **2012,** *9* (11), 3375-83.

42. Zhang, Y.-L.; Zhang, X.; Fei, X.-C.; Wang, S.-L.; Gao, H.-W., Binding of Bisphenol a and Acrylamide to Bsa and DNA: Insights into the Comparative Interactions of Harmful Chemicals with Functional Biomacromolecules. *J. Hazard. Mater.* **2010,** *182* (1-3), 877-885.

43. Cutlar, L.; Zhou, D.; Gao, Y.; Zhao, T.; Greiser, U.; Wang, W.; Wang, W., Highly Branched Poly (B-Amino Esters): Synthesis and Application in Gene Delivery. *Biomacromolecules* **2015,** *16* (9), 2609-2617.

44. Gao, Y.; Huang, J.-Y.; O'Keeffe Ahern, J.; Cutlar, L.; Zhou, D.; Lin, F.-H.; Wang, W., Highly Branched Poly (B-Amino Esters) for Non-Viral Gene Delivery: High Transfection Efficiency and Low Toxicity Achieved by Increasing Molecular Weight. *Biomacromolecules* **2016,** *17* (11), 3640-3647.

45. Tzeng, S. Y.; Green, J. J., Subtle Changes to Polymer Structure and Degradation Mechanism Enable Highly Effective Nanoparticles for Sirna and DNA Delivery to Human Brain Cancer. *Advanced Healthcare Materials* **2013,** *2* (3), 468-480.

46. Bishop, C. J.; Tzeng, S. Y.; Green, J. J., Degradable Polymer-Coated Gold Nanoparticles for Co-Delivery of DNA and Sirna. *Acta Biomaterialia* **2015,** *11*, 393-403.

47. Chang Kang, H.; Bae, Y. H., Co-Delivery of Small Interfering Rna and Plasmid DNA Using a Polymeric Vector Incorporating Endosomolytic Oligomeric Sulfonamide. *Biomaterials* **2011,** *32* (21), 4914-4924.

48. Wilson, D. R.; Mosenia, A.; Suprenant, M. P.; Upadhya, R.; Routkevitch, D.; Meyer, R. A.; Quinones-Hinojosa, A.; Green, J. J., Continuous Microfluidic Assembly of Biodegradable Poly(Beta-Amino Ester)/DNA Nanoparticles for Enhanced Gene Delivery. *Journal of Biomedical Materials Research Part A* **2017**, n/a-n/a.

49. Kozielski, K. L.; Tzeng, S. Y.; Mendoza, B. A. H. d.; Green, J. J., Bioreducible Cationic Polymer-Based Nanoparticles for Efficient and Environmentally Triggered Cytoplasmic Sirna Delivery to Primary Human Brain Cancer Cells. *ACS Nano* **2014,** *8* (4), 3232-3241.

50. Moore, T. L.; Rodriguez-Lorenzo, L.; Hirsch, V.; Balog, S.; Urban, D.; Jud, C.; Rothen-Rutishauser, B.; Lattuada, M.; Petri-Fink, A., Nanoparticle Colloidal Stability in Cell Culture Media and Impact on Cellular Interactions. *Chemical Society Reviews* **2015,** *44* (17), 6287-6305.

51. Pezzoli, D.; Zanda, M.; Chiesa, R.; Candiani, G., The Yin of Exofacial Protein Sulfhydryls and the Yang of Intracellular Glutathione in in Vitro Transfection with Ss14 Bioreducible Lipoplexes. *Journal of controlled release* **2013,** *165* (1), 44-53.

52. Guo, W.; Lee, R. J., Efficient Gene Delivery Via Non-Covalent Complexes of Folic Acid and Polyethylenimine. *Journal of controlled release : official journal of the Controlled Release Society* **2001,** *77* (1-2), 131-138.

	Polymer Name	Monomer Molar Ratios		
		BR6	B7	B8
R6,8-4-6	R6,8_0	100%	0%	0%
	R6,8_20	80%	0%	20%
	R6,8_40	60%	0%	40%
	R6,8_60	40%	0%	60%
	R6,8_80	20%	0%	80%
R6,7,8-4-6 (20% B8)	R6,7,8_16	64%	16%	20%
	R6,7,8_40	40%	40%	20%
	R6,7-8_64	16%	64%	20%

Table 6-S1. Backbone B monomer composition for R6,8-4-6 and R6,7,8-4-6 polymer series.

Sequence	Notes
GTTTTTTT***TAATACGACTCACTATA***ggagcgcaccatctt cttcagttttagagctagaaatagcaagttaaaataaggctagtccgttat caacttgaaaaagtggcaccgagtcggtgctttttt	***T7 promoter sequence*** GFP target sequence sgRNA scaffold

Table 6-S2.DNA sequence for sgRNA in vitro transcription template.

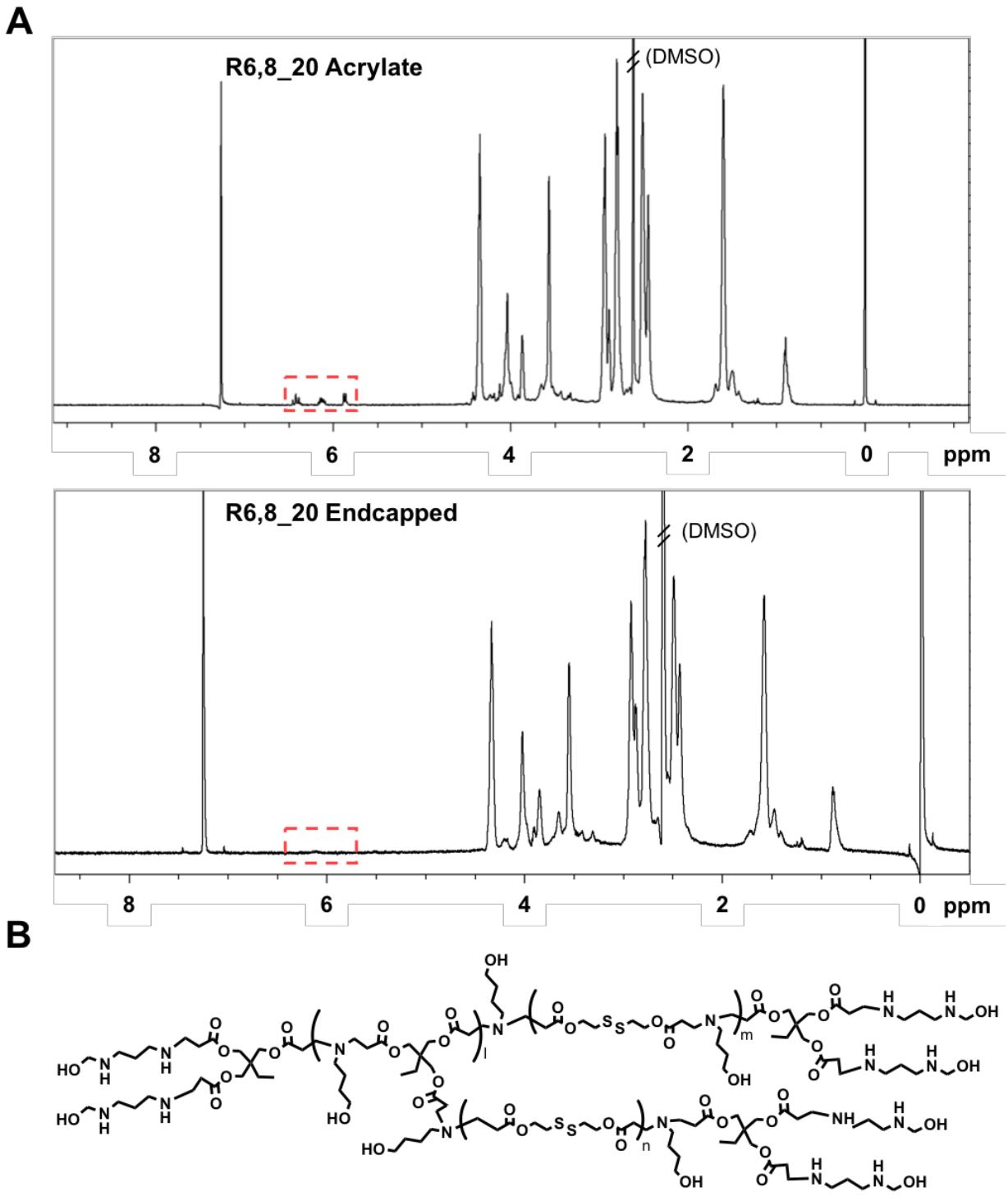

Figure 6-S1. Polymer structural information. (A) H^1-NMR spectra of acrylate-terminated and end-capped R6,8_20 polymer ($CDCl_3$, 500 MHz). Red box indicates the presence of acrylate peaks, which disappeared after end-capping. **(B)** Chemical structure of end-capped R6,8_20.

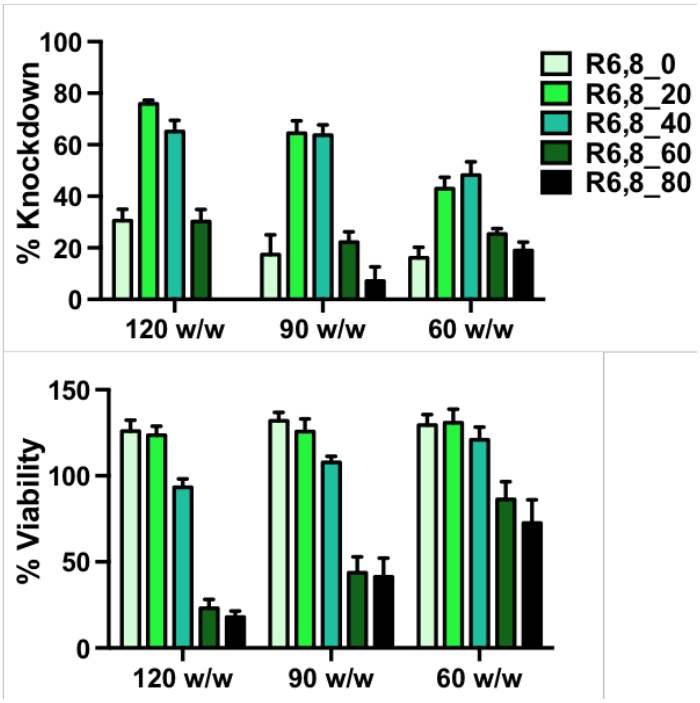

Figure 6-S2. Knockdown (A) and cytotoxicity (B) of R6,8-4-6 nanoparticles at lower w/w formulations. Nanoparticles encapsulated 100 nM siRNA dosage. Knockdown of GFP fluorescence was normalized against cells treated with non-targeting scrambled RNA (scRNA); n = 4.

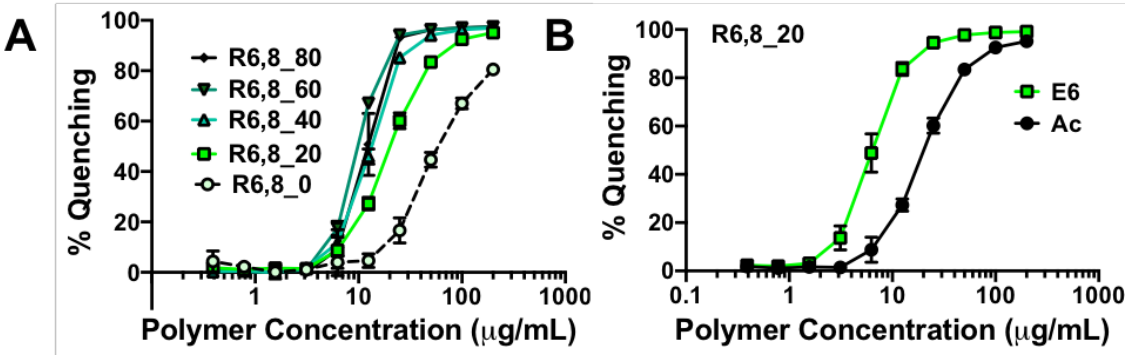

Figure 6-S3. Yo-Pro binding assay for acrylate-terminated polymers. (A) Increasing polymer branching increased binding affinity for acrylate-terminated polymers. **(B)** Endcapped polymers (E6) showed higher binding affinity than acrylate-terminated polymers (Ac). N = 4.

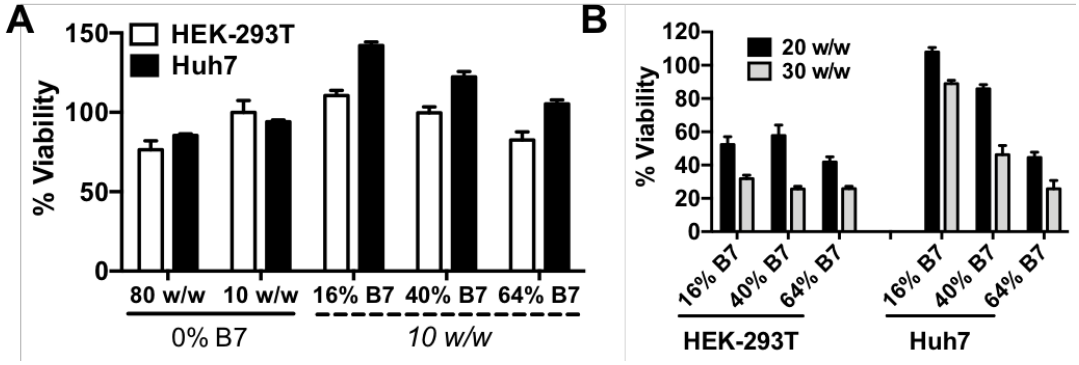

Figure 6-S4. Polymer-mediated cytotoxicity for R6,7,8-4-6 nanoparticles co-delivering DNA and siRNA in HEK-293T and Huh7 cells. (A) Cytotoxicity mediated by optimal formulations of R6,7,8-4-6 nanoparticles as well as R6,8-4-6 nanoparticles co-delivering 400 ng total nucleic acid. **(B)** R6,7,8-4-6 nanoparticles mediated high levels of toxicity at higher w/w formulations. N = 4.

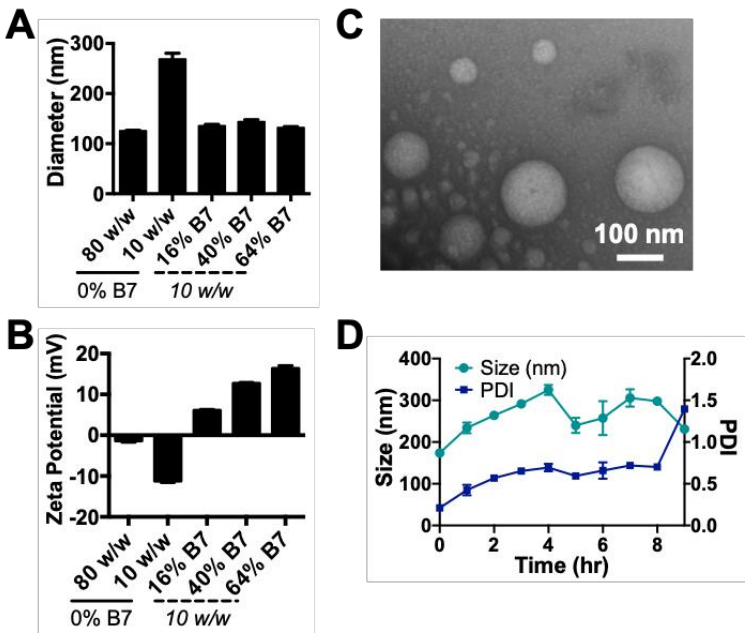

Figure 6-S5. Nanoparticle characterization. Hydrodynamic diameter **(A)** and zeta potential **(B)** confirm that B7-containing polymers formed smaller, more positively charged nanoparticles at low w/w formulations. Size and zeta potential measurements done via DLS using nanoparticles diluted in PBS. N = 3. **(C)** TEM image of R6,7,8_64 nanoparticles containing DNA and siRNA. **(D)** R6,7,8_64 nanoparticles (10 w/w) only moderately aggregated over the time-span of four hours in 10% serum-containing medium. N = 2.

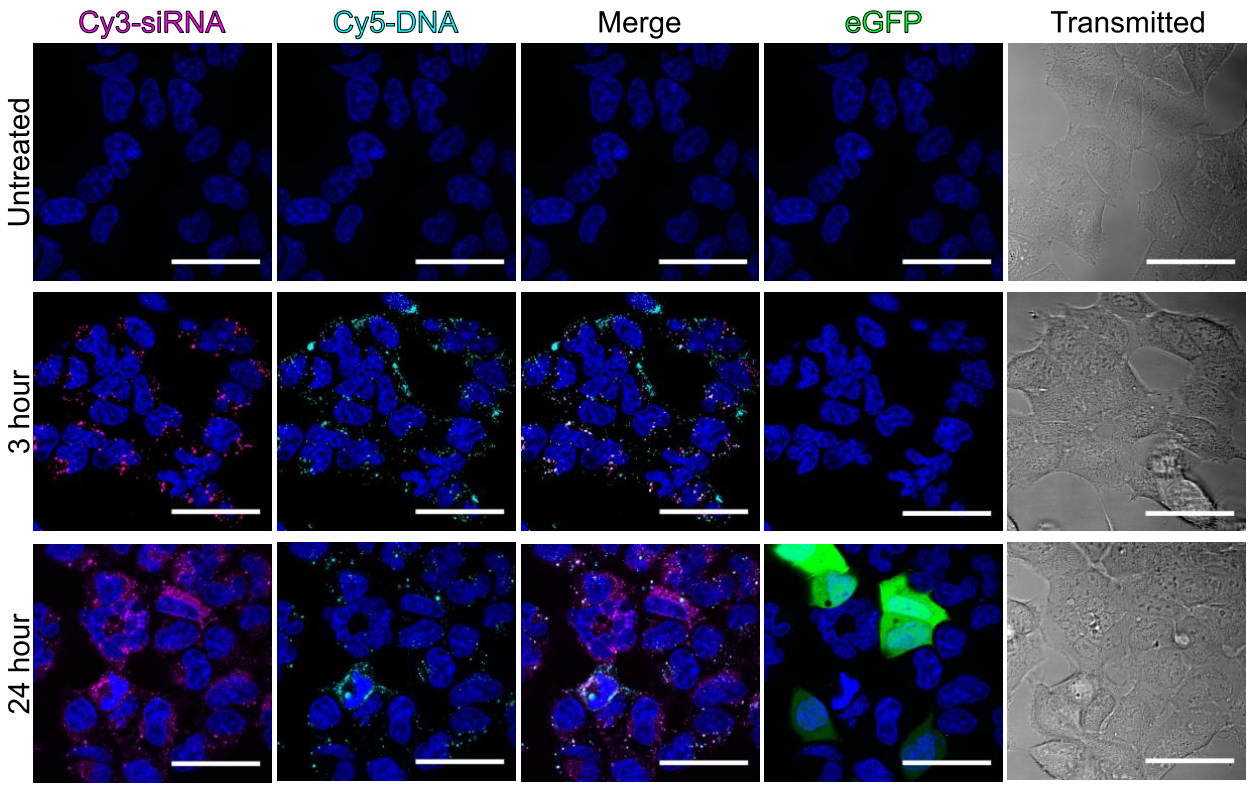

Figure 6-S6. Confocal microscopy of co-delivered DNA and siRNA. HEK-293T cells were transfected with polymer R6,7,8_64 nanoparticles formed at a 10 w/w ratio between polymer and nucleic acids. Cy3-siRNA, Cy5-DNA and eGFP-DNA were pre-mixed before nanoparticle encapsulation at a mass ratio of 50:40:10. At 3 hours after nanoparticle exposure, many endosomes visibly contain both Cy3 and Cy5 signal for siRNA and DNA respectively. At 24 hours post-treatment, diffuse Cy3-siRNA fluorescence is detectable while Cy5-DNA fluorescence is punctate and GFP is visibly being expressed by some cells. Scale bar 50 μm.

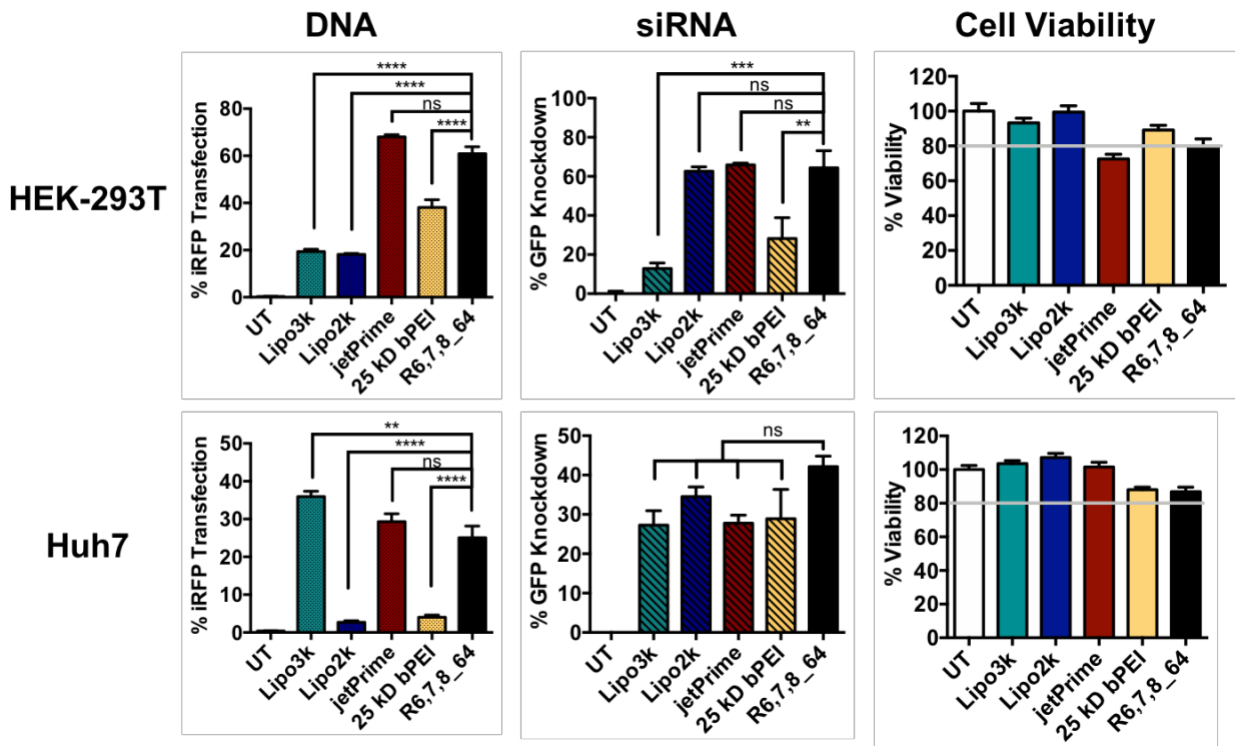

Figure 6-S7: DNA and siRNA co-delivery with leading commercially-available transfection reagents. R6,7,8_64 nanoparticles (10 w/w) and non-viral transfection reagents Lipofectamine 2,000™, Lipofectamine 3,000™, jetPrime®, and 25 kD bPEI (1 w/w) were used to co-deliver DNA and siRNA to HEK-293T and Huh7 cells. R6,7,8_64 nanoparticles generally performed better or as well as leading commercially-available reagents at co-delivery. N = 4. Statistical analysis was assessed by one-way ANOVA with Tukey post-hoc tests.

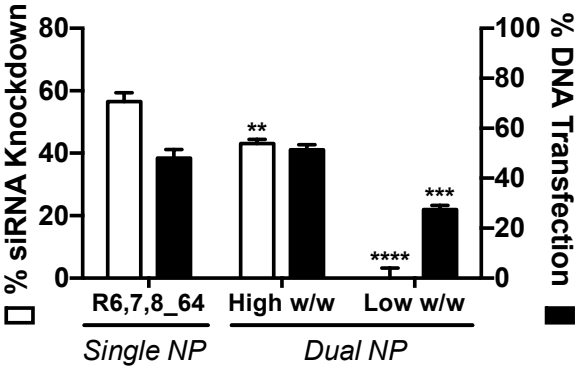

Figure 6-S8: Nucleic acid co-encapsulation outperforms DNA and siRNA delivery with their respective previously-optimized nanoparticle formulation. R6,7,8_64 nanoparticles were formulated with 200 ng each of pre-mixed plasmid DNA and siRNA at 10 w/w before nanoparticles were added to cells (Single NP). Polymer 446 (optimal for DNA delivery) and polymer R646 (optimal for siRNA delivery) were formulated separately with their respective cargos and each nanoparticle formulation was added separately to cells, with 200 ng of DNA and siRNA, respectively, delivered (dual NP). The single NP strategy outperformed the dual NP strategy when NPs were formulated at high w/w (60 w/w for 446 and 120 w/w for R646) as well as at low w/w (10 w/w for 446 and R646, respectively). R6,7,8_64 polymers were always used at 10 w/w, demonstrating its higher delivery efficiency. Huh 7 cells were used in this experiment. N = 4. Statistical analysis was assessed by one-way ANOVA with Tukey post-hoc tests.

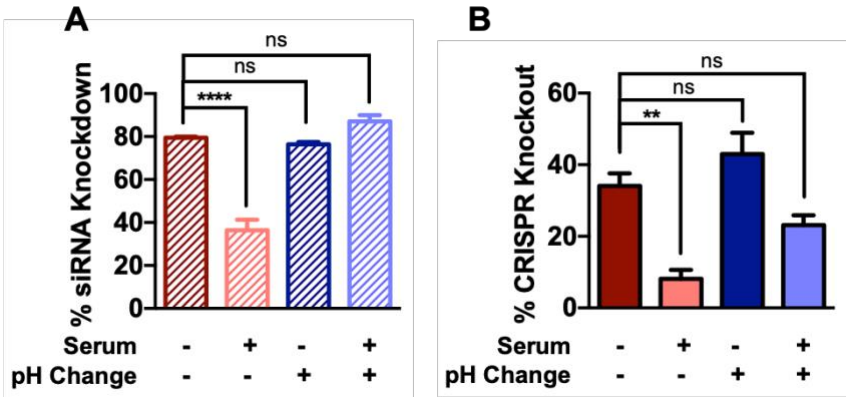

Figure 6-S9: R6,7,8_64 nanoparticle delivery efficacy in serum-containing medium. R6,7,8_64 nanoparticles (10 w/w) containing **(A)** siRNA or **(B)** Cas9 DNA and sgRNA were administered to cells in cell culture medium with or without 10% FBS. The presence of serum significantly decreased transfection in both cases. The addition of $NaHCO_3$ solution to increase the pH of nanoparticles prior to adding to cells led to recovery in transfection efficacy. N = 4 for all experiments. Statistical analysis was assessed by one-way ANOVA with Tukey post-hoc tests.

Chapter 7: Carboxylated branched poly(beta-amino ester) nanoparticles enable robust cytosolic protein delivery and CRISPR/Cas9 gene editing

Yuan Rui[1], David R. Wilson[1], John Choi[2], Mahita Varanasi[1], Katie Sanders[1], Johan Karlsson[1], Michael Lim[2], and Jordan J. Green[1, 2, 3, 4, *]

[1]Department of Biomedical Engineering, Institute for NanoBioTechnology, and the Translational Tissue Engineering Center, Johns Hopkins University School of Medicine.

[2]Department of Neurosurgery, Johns Hopkins University School of Medicine.

[3]Departments of Ophthalmology, Oncology, Materials Science & Engineering, and Chemical & Biomolecular Engineering, Johns Hopkins University.

[4]Bloomberg~Kimmel Institute for Cancer Immunotherapy, Johns Hopkins University School of Medicine.

Abstract

Efficient cytosolic protein delivery is necessary to fully realize the potential of protein therapeutics. Current methods of protein delivery often suffer from low serum tolerance and limited *in vivo* efficacy. Here, we report the synthesis and validation of a new class of carboxylated branched poly(beta-amino ester)s that can self-assemble into nanoparticles for efficient intracellular delivery of a variety of different proteins. *In vitro*, nanoparticles enabled rapid cellular uptake, efficient endosomal escape, and functional cytosolic protein release into cells in media containing 10% serum. Moreover, nanoparticles encapsulating CRISPR/Cas9 ribonucleoproteins (RNPs) induced robust levels of gene knock-in (4%) and gene knock-out (> 75%) in several cell types. A single intracranial administration of nanoparticles delivering a low RNP dose (3.5 pmol)

induced robust gene editing in mice bearing engineered orthotopic murine glioma tumors. This self-assembled polymeric nanocarrier system enables a versatile protein delivery and gene editing platform for biological research and therapeutic applications.

Introduction

Since the introduction of the first recombinant protein drug– human insulin[1] – in 1982, the number of therapeutic proteins and the frequency of their use have dramatically increased. These diverse and dynamic macromolecules have been used to treat diseases ranging from metabolic disorders to cancer[2] and are important in applications such as genome editing[3] and synthetic biology.[4] However, their high molecular weight and overall hydrophilicity render most proteins essentially membrane impermeable,[5] limiting most current protein therapeutics to extracellular targets. As proteins have the potential to target intracellular pathways with high specificity and fewer side effects,[6] it is imperative to develop novel strategies for efficient, functional, and cytosolic protein delivery.

Cytosolic protein delivery vehicles must overcome several barriers such as cargo encapsulation, cellular internalization, escape from endo/lysosomes, and cytosolic cargo release.[7] One well characterized approach is the covalent modification of the protein of interest with protein transduction domains (PTDs) such as the TAT protein from human immunodeficiency virus.[8] This strategy has been shown to enable rapid cellular internalization of a wide variety of proteins but requires chemical modifications that could alter the bioactivity of the native protein. More recently, several studies have reported the use of self-assembled protein delivery vehicles based on lipid-like,[9] polymeric,[10] or hybrid materials.[11-13] These methods still face limitations such as the need for purification steps, low protein loading efficiency, and limited applicability to certain cargo types, prompting the need for improved self-assembled protein delivery systems.

Hyperbranched cationic poly(β-amino ester)s (PBAEs) have recently generated interest as an efficient gene delivery material for highly negatively-charged nucleic acids.[14-16] These amphiphilic, pH-sensitive polymers are synthesized via facile Michael addition reactions and have been shown to possess robust transfection capabilities under challenging conditions as well as efficient endosomal escape properties.

However, cationic polymers such as PBAEs form self-assembled nucleic acid nanoparticles mainly through electrostatic interactions, which are generally insufficient to encapsulate proteins of diverse surface charge.

In this study, we synthesized and validated a new biomaterial class of hyperbranched PBAE containing both cationic and anionic charges. This was accomplished through polymer end-capping with carboxylate ligands derived from amino acid-like precursors. Polymers were assembled into nanoparticles with proteins by simple mixing in aqueous buffer. We hypothesized that the carboxylate ligands can enhance polymer-protein interactions for nanoparticle assembly via increased hydrogen bonding and hydrophobic effects in addition to electrostatic interactions. Furthermore, we found that differential polymer end-group hydrophobicity affected protein complexation capabilities as well as nanoparticle internalization and endosomal escape. Our delivery platform enabled functional cytosolic delivery of proteins ranging from 27 kD to 160 kD in molecular weight with varying surface charges. Encapsulation of Cas9 ribonucleoproteins (RNPs) enabled efficient gene editing *in vitro* and *in vivo*, further highlighting the robustness and therapeutic utility of these nanocarriers.

Results

Polymer synthesis and screening

Hyperbranched PBAEs were synthesized via a step-wise copolymerization reaction between acrylate-containing monomers bisphenol A glycerolate (1 glycerol/phenol) diacrylate (B7) and trimethylolpropane triacrylate (B8), and amino alcohol monomer 4-amino-1-butanol (S4). B monomers were added in molar excess to yield acrylate-terminated polymers, which were end-capped with the diamine-containing small molecule 1,3-diaminopropane (E1) to yield E1 base polymers (Figure 7-1A). These polymers underwent a second round of end-capping reactions with carboxylate ligands (Figure 7-S1), which were synthesized via reaction of a series of amino acid-like precursors with acryloyl chloride. Ligands were named according to the number of carbon atoms between the amide and carboxylic acid groups, with C1 deriving from the amino acid glycine (Figure 7-S2). Five carboxylate ligands ranging from C1 to C10 were synthesized to investigate the effect of end-cap hydrophobicity on the protein encapsulation and delivery capabilities of the polymers.

We hypothesized that the combination of the biodegradable and hyperbranched polymer backbone, which has been shown to be amphiphilic and pH sensitive,[15] and carboxylate end-capping ligands, capable of forming hydrogen bonds and salt bridges with proteins, would result in a versatile protein delivery polymer platform.

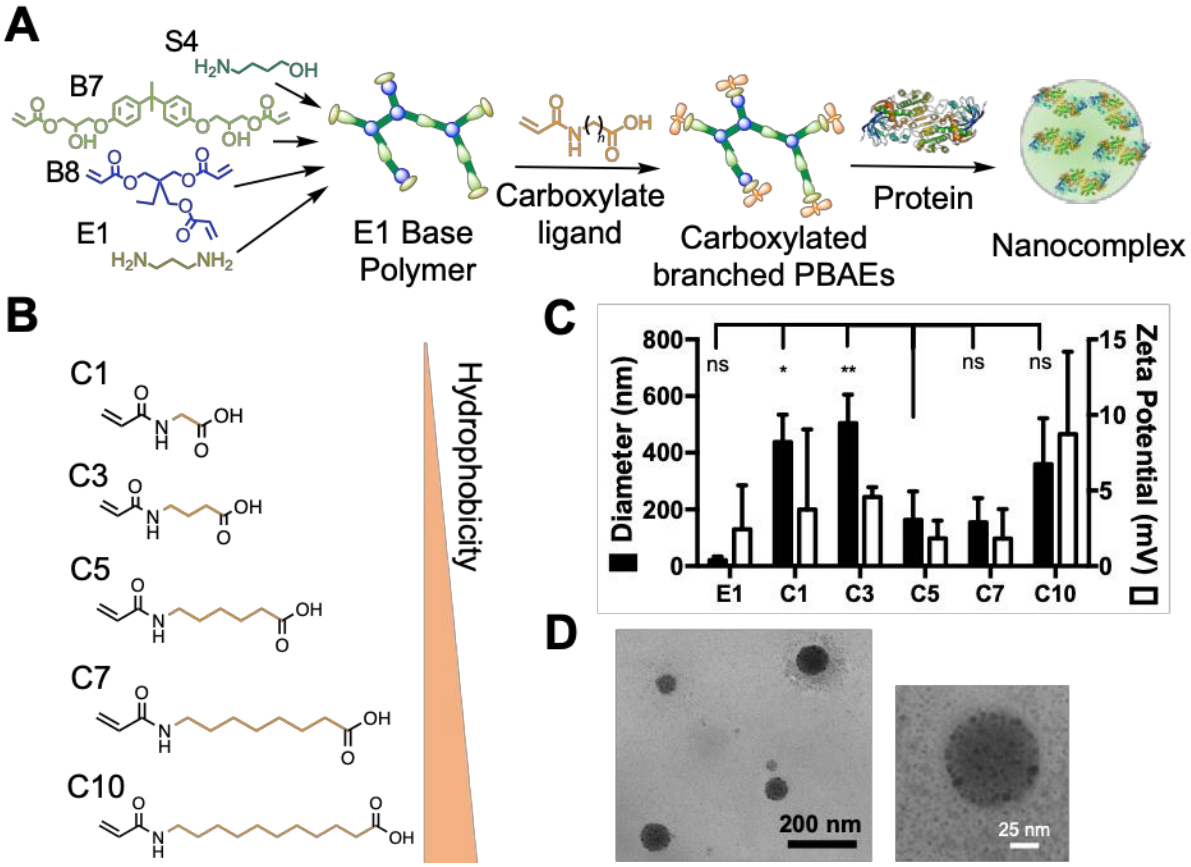

Figure 7-1. Design and characterization of self-assembled carboxylated branched PBAE protein nanoparticles. (A) Assembly of carboxylated branched PBAEs with proteins. **(B)** Structures of carboxylate ligands C1-C10, arranged in order of increasing hydrophobicity. **(C)** Hydrodynamic diameter and zeta potentials of nanoparticles formulated with BSA (30 w/w) as measured by DLS. Data presented as mean+SD (n=3). Statistical comparisons of nanoparticle diameter were performed with one-way ANOVA with Dunnett's post-hoc tests against the C5 group. *P<0.05, **P<0.01. Similar statistical comparisons were made with zeta potential data and no significant differences were observed. **(D)** Representative TEM images of C5/BSA nanoparticles.

To investigate the protein encapsulation capabilities of the polymers, we formulated self-assembled polymeric nanoparticles with bovine serum albumin (BSA). At a polymer-protein weight ratio (wt/wt) of 30, all carboxylate terminated polymers in the series formed nanoparticles ranging 200-500 nm in hydrodynamic diameter with surface charges close to neutral (Figure 7-1C), whereas the E1 terminated polymer, useful for self-assembly with nucleic acids,[17] failed to effectively form nanoparticles with BSA. The diameter of the nanoparticles formulated from carboxylated polymers had a biphasic response dependent on the number of carbon atoms between the amide and carboxylic acid groups. Polymers end-capped with ligands C5 and C7 formed the smallest nanoparticles, and polymers with lower or higher end-cap carbon length formed much larger nanoparticles. Moreover, the same biphasic response was observed functionally when these polymers were used to deliver FITC-labeled BSA intracellularly (Figure 7-2A). In all four cell lines evaluated (CT-2A murine glioma, HEK-293T human embryonic kidney, B16-F10 murine melanoma, and MSC-083 primary human adipose-derived mesenchymal stem cells), polymers surface engineered with C5 or C7 moieties enabled the highest levels of intracellular nanoparticle-mediated protein uptake. These data indicate that end-cap hydrophobicity and the spacing length between charges play a major role in the interactions between polymer and protein during nanoparticle self-assembly, which in turn affects interactions between nanoparticles and cells during cellular uptake. The high levels of protein nanoparticle uptake did not result in significant levels of cytotoxicity and the viability of cells treated with nanoparticles was >70% for all polymers and cell lines tested when polymers were used at standard conditions <0.15 mg/mL (Figure 7-S3).

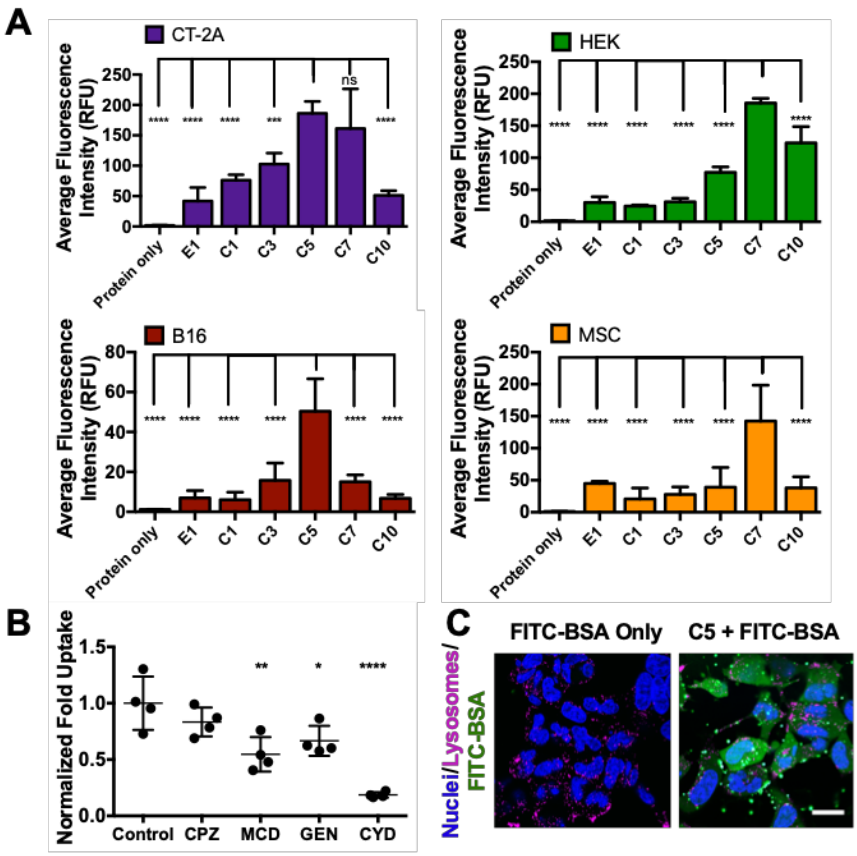

Figure 7-2. Carboxylated PBAE nanoparticles mediate cytosolic protein delivery. (A) Average fluorescence intensity of cells treated with carboxylated PBAE nanoparticles encapsulating FITC-BSA (300 ng FITC-BSA per well, 20 w/w). Data presented as mean+SD (n=4); statistical significance determined by one-way ANOVA with Dunnett's post-hoc tests comparing uptake levels to that of the nanoparticle formulation achieving the highest levels of FITC-BSA uptake in each cell line. ***P<0.001, ****P<0.0001. **(B)** Uptake by HEK cells in the presence of different endocytosis inhibitors; CPZ=chlorpromazine, MCD=methyl-β-cyclodextrin, GEN=genistein, CYD=cytochalasin-D. Data presented as mean±SD; statistical significance determined by one-way ANOVA with Dunnett's post-hoc tests as compared to the control group (n=4). *P<0.05, **P<0.01, ****P<0.0001. **(C)** Confocal images of HEK cells treated with C5/FITC-BSA nanoparticles or protein alone for 4 h. Scale bar = 10 μm.

When nanoparticle internalization pathways were probed by selectively inhibiting endocytosis pathways using small molecule drugs, we found that pre-treatment with cytochalasin-D decreased

nanoparticle uptake by over 80%, suggesting that nanoparticles were internalized primarily by macropinocytosis (Figure 7-2B). Methyl-β-cyclodextrin and genistein also significantly decreased cellular uptake while chlorpromazine had negligible effects, indicating that nanoparticles were also taken up through lipid raft- and caveolin-mediated endocytosis but not through clathrin-mediated endocytosis. Finally, confocal laser scanning microscopy images of cells after 4 h incubation with C5/FITC-BSA nanoparticles revealed diffuse FITC-BSA signal throughout the cytosol, indicating that nanoparticles successfully escaped degradative endo-lysosomes to enable cytosolic protein delivery (Figures 7-2C and 7-S4).

Endosomal disruption characterization via Gal8-GFP recruitment assay

We further characterized the endosomal escape capabilities of carboxylated branched PBAE nanoparticles using an assay based on the recruitment of galectin 8 (Gal8) to disrupted endosomal membranes similar to the method recently innovated by Kilchrist *et al.*[18] Gal8 is a cytosolic protein that binds to glycosylation moieties located selectively on the inner leaflets of endosomal membranes. Using a PiggyBac transposon, we created a cell line stably expressing a Gal8-GFP fusion protein. Endosomal rupture exposes Gal8 binding sites to cytosolic Gal8-GFP, and Gal8-GFP recruitment results in punctate fluorescent spots at disrupted endosomes (Figure 7-3A). After staining with Hoechst 33342 nuclear dye to allow for cell identification, automated high content imaging analysis can then be used to identify punctate Gal8-GFP spots and calculate the number of Gal8-GFP spots per cell as an indicator of the level of nanoparticle-mediated endosomal disruption (Figure 7-3B).

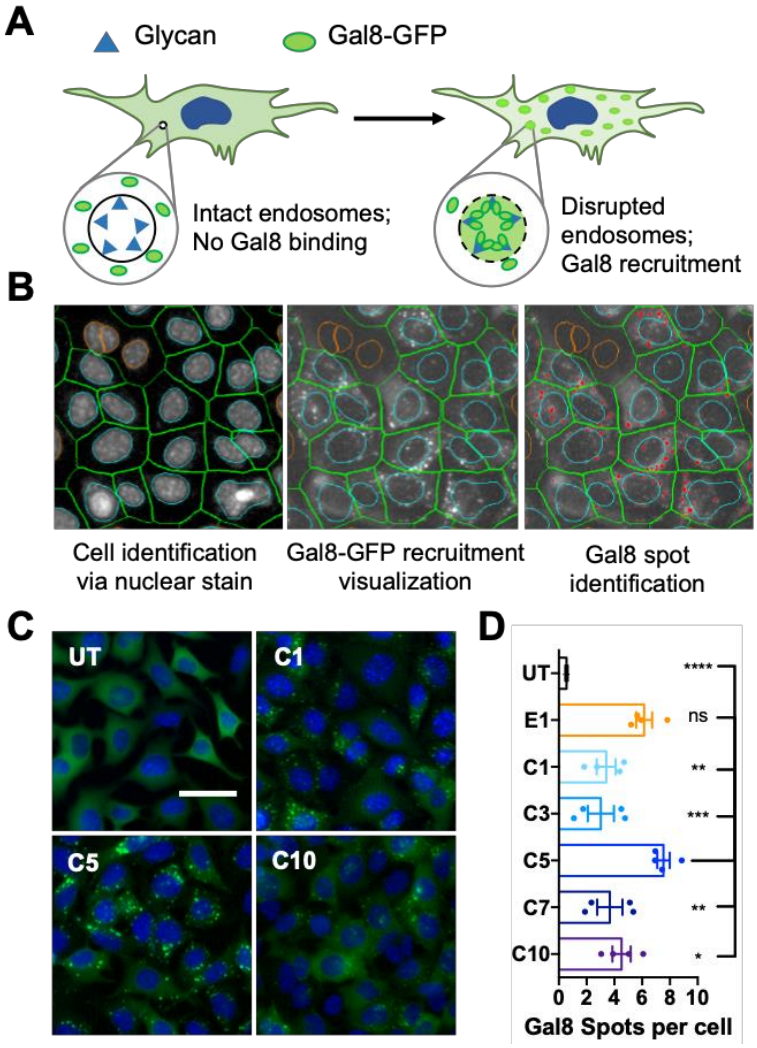

Figure 7-3. Gal8-GFP recruitment assay to assess nanoparticle-mediated endosomal disruption. (A) Gal8 recruitment overview; in cells with intact endosomes, Gal8-GFP is dispersed throughout endosomes with no interactions with intra-endosomal glycans. Gal8-GFP binds glycans in disrupted endosomes, resulting in punctate fluorescent dots. **(B)** Gal8–GFP recruitment were quantified by image-based analysis. Individual cells were identified through nuclear staining (left); Gal8-GFP recruitment could be visualized in the green fluorescence channel (center); punctate GFP+ spots were identified and counted (red dots). **(C)** Representative images of Gal8-GFP+ B16 cells treated with carboxylated PBAE/BSA nanoparticles (125 ng BSA per well, 25 w/w; scale bar = 50 μm). **(D)** Endosomal disruption level quantified by the number of Gal8-GFP spots per cell. Data presented as mean±SD; statistical significance determined by one-way

ANOVA with Dunnett's post-hoc tests as compared to the C5 group (n=4). *P<0.05, **P<0.01, ****P<0.0001.

Our results revealed that among the carboxylate end-capped polymers, polymer C5 enabled the highest level of endosomal disruption (Figure 7-3D). This was not due to the buffering capabilities of these polymers, as pH titration experiments showed that there was no significant difference in buffering capacity among the different carboxylated polymers (Figure 7-S5A). It is also important to note that there was no significant difference between the Gal8-GFP recruitment levels of nanoparticles formed with the E1 base polymer and those formed with polymer C5. In fact, polymer end-capping with carboxylate ligands of shorter chain lengths (e.g. C1 and C3) resulted in a decrease in endosomal disruption levels. This may be explained by the fact that the E1 monomer itself interacts with endosomal membranes in a way that causes disruption, as was demonstrated in previous reports using this molecule as an end-cap to efficiently deliver plasmid DNA.[17] Further end-capping with carboxylate ligands masked this effect, and endosomal disruption became dependent on hydrophobic chain length. PBAEs have also been shown to form polymer-only, micellar nanoparticles in the absence of nucleic acid or protein cargo due to their amphiphilic structure.[19] Thus, the paradoxical low FITC-BSA uptake and high Gal8-GFP recruitment observed in E1 nanoparticles could be explained by the fact that E1 base polymers could not adequately form protein-encapsulated nanoparticles and mainly formed polymer-only nanoparticles, which caused endosomal disruption after endocytosis. Taken together, our data indicate that polymer C5 clearly outperformed all other polymers in the series and was chosen for use in all subsequent experiments.

Robustness of C5-PBAE nanoparticles

We further examined the robustness of C5 end-capped polymers by utilizing them for cytosolic delivery of a variety of proteins. C5 polymers successfully encapsulated FITC-labeled human IgG (FITC-IgG) and GFP, respectively, and enabled diffuse cytosolic delivery of both (Figure 7-4). To investigate the capability for functional protein delivery, C5 polymers were further utilized to encapsulate the ribosome-

inactivating protein saporin, a potent toxin lacking cellular internalization domains[20] (Figure 7-4C). In all three cell lines tested, C5/saporin nanoparticles induced high levels of cell death even at very low saporin doses (EC_{50}<5 nM). This indicates that C5 nanoparticles enabled functionally intact saporin proteins to reach the ribosome, their intracellular sites of action, with high efficiency. In contrast, unencapsulated saporin could not be internalized on its own and resulted in negligible cytotoxicity even at high concentrations. Our data demonstrate that C5 end-capped branched PBAEs are a versatile and robust protein delivery platform, enabling cytosolic, functional protein delivery to a variety of cell lines. More importantly, the polymers are largely agnostic to the size and surface charge of the protein cargo that they carry (Figure 7-4E & Table 7-S1), unlike traditional PBAEs that depend on electrostatic interactions and can only encapsulate strongly negatively charged cargos such as nucleic acids.

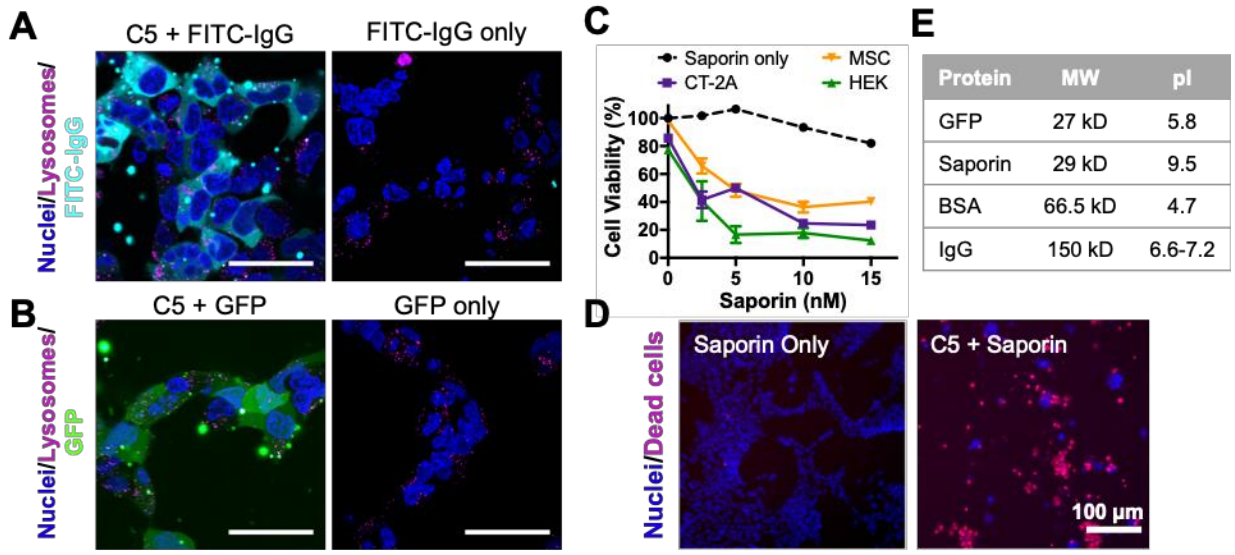

Figure 7-4. Carboxylated C5 polymeric nanoparticles for cytosolic delivery of different protein types. Confocal images of HEK cells treated with C5 nanoparticles encapsulating FITC-IgG **(A)** and GFP **(B)** for 4 h; 450 ng protein delivered per well at 30 w/w (scale bar = 50 µm). **(C)** Functional delivery of ribosome-inactivating protein saporin resulted in significant levels of cell death; the final polymer concentration per well was 0.075 µg/µL. Data presented as mean±SD (n=4). **(D)** Representative images of CT-2A cells treated with 10 nM naked saporin or C5/saporin nanoparticles. **(E)** Molecular weight and isoelectric point of proteins delivered by C5 nanoparticles.

CRISPR gene editing through RNP delivery in vitro

C5 polymers were also used to encapsulate and deliver Cas9 ribonucleoproteins (RNPs) to enable CRISPR gene editing *in vitro*. In these experiments, Cas9 protein and gene-targeting short guide RNA (sgRNA) were first incubated together at room temperature for 10 minutes to allow RNP self-assembly, then simply mixed with polymers to form nanoparticles. Delivery of RNPs targeting the GFP gene in cells constitutively expressing the GFP reporter resulted in 77% GFP knockout in HEK cells and 47% GFP knockout in GL261 murine glioma cells as quantified by flow cytometry (Figure 7-5B). Surveyor® mutation detection assay was also performed to verify that loss in GFP fluorescence was indeed due to perturbations in genomic DNA (Figure 7-5C). RNPs were membrane impermeable on their own and treatment with RNP alone yielded negligible levels of gene editing.

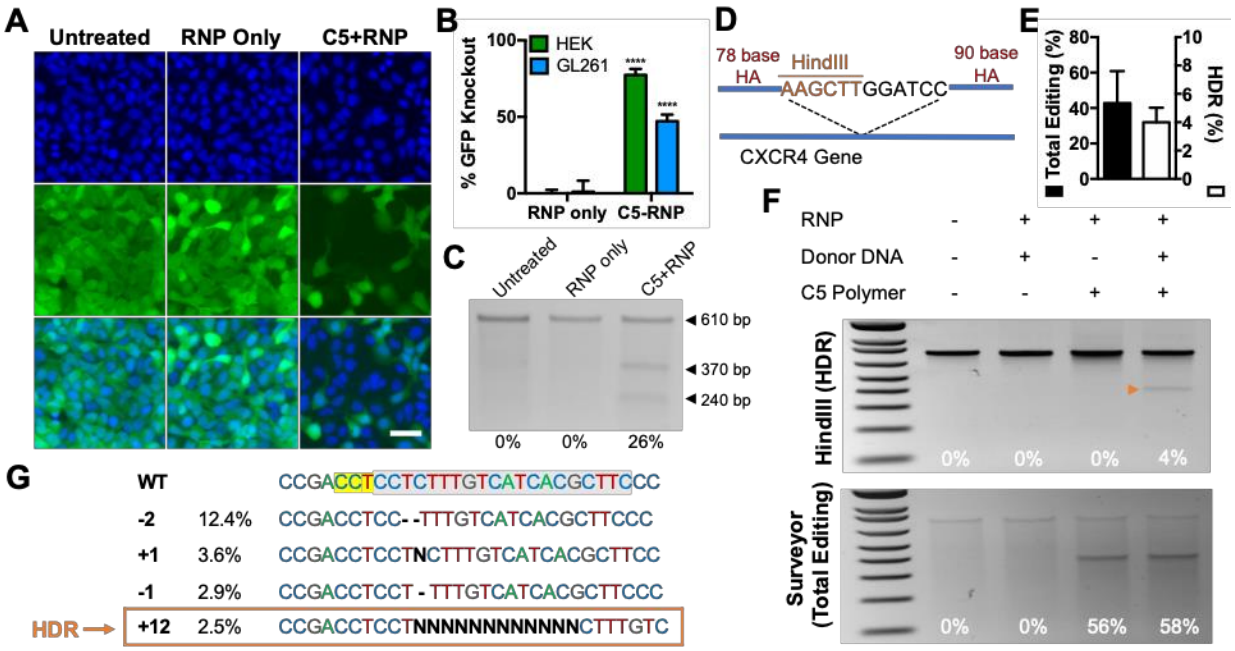

Figure 7-5. C5 nanoparticle delivery of Cas9 RNPs enable robust CRISPR gene editing *in vitro*. (A) Fluorescence microscopy images of HEK-GFPd2 cells treated with RNPs alone or C5+RNPs; C5+RNPs enabled knockout of GFP fluorescence. Scale bar = 50 μm. **(B)** Flow cytometry quantification of GFP knockout in HEK and GL261 cells. Data are mean+SD; *n*=4. Editing level of the C5-RNP group for each cell line was compared to that of the corresponding RNP only group using Holm-Sidak corrected multiple t

tests. ****P<0.0001. **(C)** Surveyor® mutation detector assay of GL261-GFPd2 cells treated with C5+RNP nanoparticles. **(D)** Experimental design of HDR assay in the *CXCR4* gene; knock-in of a 12-bp insert flanked by homology arms (HA) results in the addition of a HindIII restriction enzyme site. **(E)** Quantification of total editing (via Surveyor® assay) and HDR (via HindIII restriction digest) in HEK cells. Data are mean+SD; n=3. **(F)** HindIII restriction enzyme assay (top) and Surveyor® assay (bottom) of HEK cells treated with different C5/RNP/donor DNA combinations; orange arrow indicates HDR. **(G)** Inference of CRISPR Edits (ICE) analysis of Sanger sequencing data from C5+RNP+donor DNA treated cells provides a breakdown of different edits. Percentages indicate the percentage of the total DNA population with the indicated genotype. The targeted sequence is highlighted in grey and PAM sequence in yellow.

Next, we investigated the capability of C5/RNP nanoparticles to edit an endogenous gene through homology directed repair (HDR). Cas9 protein was first self-assembled into RNPs with sgRNA targeting the human *CXCR4* gene, and RNPs were further mixed with a single-stranded DNA (ssDNA) repair template before mixing with C5 polymer. The ssDNA repair template included ~80 base homology arms flanking a 12 base insert containing a HindIII restriction enzyme site (Figure 7-5D). Successful HDR was quantified by HindIII restriction digest of PCR amplicons of the genomic *CXCR4* site while total amount of editing (NHEJ and HDR) was quantified using the Surveyor® mutation detection assay. Our results indicate that C5 nanoparticles successfully delivered the combination of RNP+ssDNA into HEK-293T cells. Gel electrophoresis analysis of cleavage products indicate that 4% HDR was achieved while over 50% total editing was achieved (Figure 7-5E&5F). Inclusion of a ssDNA template into the nanoparticle self-assembly process did not change the total level of editing achieved. Inference of CRISPR Edits (ICE)[21] analysis of Sanger sequencing results confirmed the presence of a 12 bp insert in 2.5% of DNA sequences (Figure 7-5G).

Validation of CRISPR-stop reporter system to assess gene deletion

We engineered a CRISPR-stop reporter construct wherein a 630-bp stop-of-transcription cassette is placed upstream of a red-enhanced nanolantern (ReNL) fluorescent reporter (Figure 7-6A). This CRISPR-

stop construct was integrated into the genomic DNA of GL261 and B16-F10 cells via a PiggyBac transposon, and targeting CRISPR RNPs to regions flanking the stop cassette resulted in deletion of the stop cassette and turning on of ReNL fluorescence. We chose this system to evaluate *in vivo* gene editing as gain-of-function ReNL expression via dual-cut gene deletion could be easily and clearly detected.

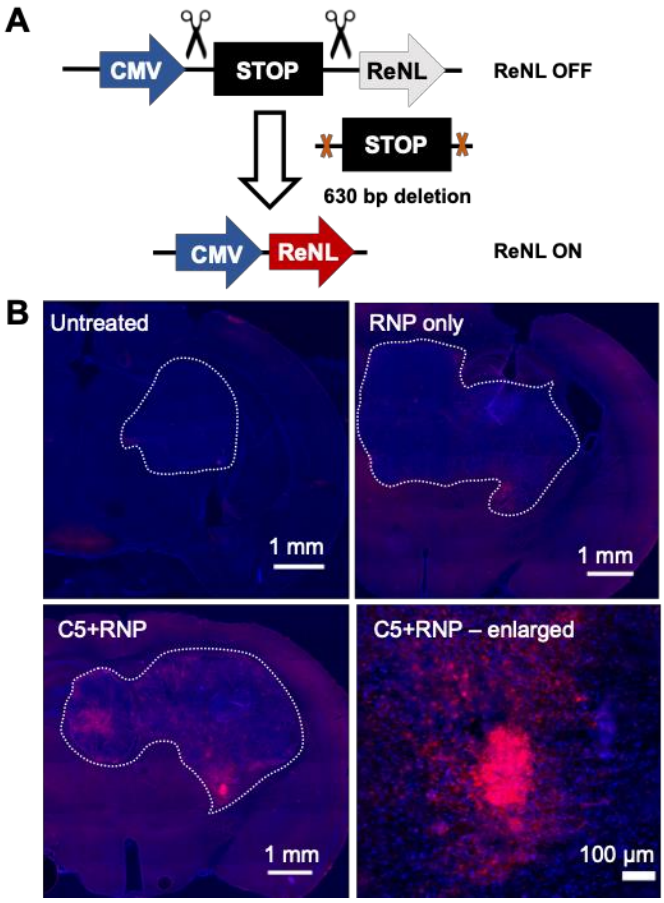

Figure 7-6. C5/RNP nanoparticles enable CRISPR editing *in vivo*. (A) Schematic of CRISPR-stop gene construct; deletion of a 630-bp expression stop cassette turns on downstream ReNL expression. **(B)** Direct intracranial administration of C5/RNP nanoparticles to an orthotopic GL261-stop-ReNL tumor enabled CRISPR editing *in vivo*. Nanoparticles were formulated at 3.5 pmol RNP with 15 w/w C5 polymer. Tumors boundary outlined in white.

In vitro assessment of this CRISPR-stop system using C5/RNP nanoparticles indicated that 16% and 43% editing were achieved in GL261 and B16 cells, respectively (Figure 7-S6A). Compared to commercially-

available CRISPR delivery agents, C5/RNP nanoparticles enabled significantly higher editing levels than Lipofectamine™ CRISPRMAX™ at all RNP doses tested and significantly higher editing levels than jetCRISPR™ at equimolar RNP doses tested (Figure 7-S6B). jetCRISPR™ enabled significantly higher levels of editing than C5/RNP nanoparticles only when twice the RNP dose was used, further demonstrating the robustness of our nanoparticle system in delivering CRISPR RNPs.

This reporter system also allowed us to easily assess the stability of our nanoparticles under physiological conditions. C5/RNP nanoparticles were pre-incubated in serum-containing complete cell culture media at 37°C for up to 4 h before adding to cells, and their ability to induce gain-of-function CRISPR-stop edits was assessed (Figure 7-S7A). Flow cytometry data revealed that no significant loss of nanoparticle efficacy was observed until pre-incubation time reached 4 h, at which time delivery efficacy dropped by 25%. This is likely due to PBAE hydrolysis and is consistent with previous reports of PBAE half-life in aqueous conditions of 4-6 hours, a benefit to facilitate fast biodegradation and minimized toxicity *in vivo*.[22] To achieve greater long-term stability of nanoparticles, as would be required for storage and supply chain management, we demonstrated that C5/RNP nanoparticles retain their efficacy following lyophilization with sucrose as a cryoprotectant, which may be the first documented case of a functional lyophilized RNP formulation (Figure 7-S7B).[23]

CRISPR editing in murine glioma tumors in vivo

Finally, we investigated the ability of C5/RNP nanoparticles to enable CRISPR gene editing *in vivo*. *In vivo* assessment of gene editing was performed following intracranial implantation of GL261 cells constitutively expressing the CRISPR-stop construct into C57BL/6J mice. C5/RNP nanoparticles were infused intracranially through convection-enhanced delivery (CED) 10 days post-tumor inoculation, and mice were euthanized and brains extracted 6 days after nanoparticle CED. Histological analysis of mouse brains treated with C5/RNP nanoparticles (3.5 pmol RNP dose with 15 w/w polymer) revealed bright ReNL fluorescence within the tumor bulk, which was not observed in mice that received naked RNP infusion only (Figures 7-6B and 7-S8). Although the brightest ReNL signal was localized in closest proximity to the

injection site, ReNL expression was detectable several millimeters away from the primary injection site. These results demonstrate proof-of-principle that C5/RNP nanoparticles can enable efficient localized CRISPR gene editing *in vivo*.

Discussion

Functional cytosolic protein delivery holds great value in biological research as well as therapeutic applications by enabling the perturbation of intracellular pathways previously undruggable by small molecule drugs. To overcome the intrinsic cell membrane impermeability of many proteins, we synthesized and validated a series of carboxylated branched PBAEs for the encapsulation of a variety of different protein types into self-assembled nanoparticles. Carboxylate ligand chain length and hydrophobicity played an important role in polymer-protein interactions as well as the ability for protein-encapsulated nanoparticles to interact with cellular and endosomal membranes. Polymers terminated with C5, a carboxylate ligand of moderate hydrophobicity, outperformed other ligands in the series both in the level of cellular internalization as well as endosomal disruption. The superior performance of C5 over end-caps of lesser hydrophobicity could be explained by the fact that increased hydrophobicity facilitates nanoparticle stabilization through hydrophobic effects. Furthermore, the hydrocarbon chains in the polymer end-group could also interact with membranes, facilitating cellular internalization as well as endosomal escape through transient membrane perturbations. A similar phenomenon has been extensively reported with lipid-like materials and may also be applicable here.[24] On the other hand, polymer end-groups such as C10 may be too hydrophobic, or else allow too long of a linker length, to efficiently interact with proteins. For example, a potential collapse of the hydrocarbon tail in aqueous buffer could obstruct interactions between the carboxylic acid functional group with proteins and cell membranes. This biphasic response is consistent with that reported by Ayala *et al* when similar amino acid analogs were utilized for hydrogel synthesis.[25]

We further demonstrated the robustness of our nanoparticle system by cytosolically delivering a variety of proteins of different size and surface charge. The ability to functionally deliver the ribosome-inactivating protein saporin, which has an isoelectric point of 9.5[20] and is thus strongly cationic at the pH of nanoparticle formation, validates our hypothesis that carboxylated PBAEs can rely on interactions beyond

purely electrostatic forces to complex protein cargo into nanoparticles. This is a significant innovation upon traditional gene delivery PBAEs engineered to complex only highly anionic nucleic acid cargos through charge interactions.[26]

Finally, we demonstrated that C5 polymers were capable of functional delivery of Cas9 RNPs to enable CRISPR gene editing. *In vitro* delivery of RNPs targeting a GFP reporter gene resulted in nearly 80% GFP knockout following NHEJ. This level of gene knockout is comparable to that achieved by the DNA nanoclew system developed by Sun *et al.*[27] and significantly higher than that reported by Alsaiari *et al.* using ZIF-8 metal-organic framework nanoparticles for CRISPR RNP delivery.[13] Compared to commercially-available CRISPR delivery reagents Lipofectamine™ CRISPRMax™ and jetCRISPR, C5/RNP nanoparticles enabled significantly higher levels of gene editing at manufacturer-recommended RNP doses. Further, co-delivery of RNPs targeting the human *CXCR4* gene and a ssDNA repair template in the same self-assembled nanoparticle enabled 4% HDR in HEK-293T cells, which is significantly higher than that achieved by the CRISPR-Gold system developed by Lee *et al.*[28] in the same cell line when scaled by the RNP dose delivered. For translation considerations, the C5/RNP+ssDNA encapsulated nanoparticles can be formulated by simple mixing with polymers while the aforementioned CRISPR-Gold requires a multistep synthesis scheme including covalent conjugation of DNA sequences.

C5/RNP nanoparticles induced CRISPR gene editing *in vivo* as well using a challenging reporter model requiring a 631 bp deletion for gain-of-function fluorescence. In a proof-of-principle study, we demonstrated that deletion of an expression stop cassette resulted in gain of function ReNL reporter fluorescence upon intracranial injection of C5/RNP nanoparticles in a mouse glioma model. The highest levels of editing occurred near the primary nanoparticle infusion site, covering a region in the brain approximately 0.4 mm^2 in area, which is comparable to that reported by Wang *et al.*,[9] who used bio-reducible lipids to deliver 5 pmol supercharged GFP-Cre to mouse brains containing a CRISPR-stop reporter system in which the stop cassette is flanked by LoxP sites. In another study, Staahl *et al.* utilized a protein engineering approach to enable cellular internalization by adding 4×NLS residues to the N-terminus of the Cas9 protein but required an order of magnitude higher RNP dose to achieve wide-spread editing.[29] Intracranial injection

of 4 pmol modified RNPs enabled gain-of-function tdTomato fluorescence in mouse brain regions similar in area to that observed by Wang *et al.*[9] In comparing *in vivo* editing efficiency, it is important to note that gene editing occurred in primary mouse neurons in the two abovementioned studies while our study investigated gene editing in orthotopic mouse brain tumors. However, the bright ReNL signal induced by the C5/RNP nanoparticles highlight their robust *in vivo* delivery capabilities.

A further advantage of our polymeric nanoparticle-based protein delivery system is its ability to potentially evade immune responses. It has been demonstrated that PBAE nanoparticles optimized for nucleic acid delivery could be administered repeatedly to immune-competent animals without a reduction in transfection efficacy,[30] indicating that neutralizing antibodies were not formed against the nanoparticles. We hypothesize that our protein delivery system would have similarly low levels of vector-mediated immune responses, which is a significant advantage over traditional viral delivery vectors for which immunogenicity is a serious concern. Immunogenicity to Cas9 protein cargo may be a concern for direct *in vivo* CRISPR editing in human patients as Charlesworth *et al.* recently reported that pre-existing immunity against spCas9 is likely to limit the editing efficacy of CRISPR RNPs delivered to human patients.[31] Polymeric nanoparticle encapsulation may attenuate immune responses against the protein cargo itself by protecting against circulating neutralizing antibodies, enabling CRISPR gene editing in patients with pre-existing immunity. This effect was not studied in this work but would be an interesting future direction to explore.

In summary, we have reported herein a polymeric nanoparticle system that can encapsulate and enable robust cytosolic delivery of a variety of different protein types, including potent cytotoxic agents as well as CRISPR/Cas9 RNPs. RNP delivery *in vitro* and *in vivo* induced high levels of gene editing at relatively low RNP doses. Biodegradable nanoparticles were formulated via a facile, highly scalable self-assembly process that is also amenable to lyophilization and storage. This versatile protein delivery platform provides a powerful tool for biological research as well as potential therapeutic applications for neurological disorders and beyond.

Materials and Methods

Materials

Acryloyl chloride (CAS 814686), glycine (CAS 56-40-6), 4-aminobutanoic acid (CAS 56-12-2), 6-aminocaproic acid (CAS 60-32-2), 8-aminooctanoic acid (CAS 1002-57-9), 11-aminoundecanoic acid (CAS 2432-99-7), bisphenol A glycerolate (1 glycerol/phenol) diacrylate (B7; CAS 4687949), trimethylolpropane triacrylate (B8; CAS 15625895), 1,3-diaminopropane (E1; CAS 109-76-2), FITC-BSA, saporin from *S. officinalis* seeds, FITC-IgG from human serum, and Cas9-NLS were purchased from Sigma-Aldrich (St. Louis, MO). 4-Amino-1-butanol (S4; CAS 133251005) was purchased from Alfa Aesar (Tewksbury, MA).

Carboxylate Ligand Synthesis

Carboxylate ligands were synthesized according to the method by Ayala *et al.*[25] Briefly, 0.1 mol carboxylate precursor molecule (listed in Figure 7-S2B) was added at a 1:1.1 molar ratio with NaOH and dissolved in 80 mL DI water with vigorous stirring in an ice bath. 0.11 mol acryloyl chloride in 15 mL THF was added drop-wise, and the pH of the reaction was maintained at 7.5-7.8 with 1M NaOH solution. The reaction was allowed to proceed overnight before being acidified to the pH listed in Figure 7- S2B with 1M HCl solution and extracted 3 times with ethyl acetate. The organic layer was collected, dried with sodium sulfate, and the solvent was removed with rotary evaporation to yield a white powder.

Polymer Synthesis

Monomers B7 and B8 were dissolved in anhydrous DMSO at 0.8:0.2 molar ratio, and monomer S4 was added at an overall vinyl: amine ratio of 2.2:1 to a final monomer concentration of 150 mg/mL. The reaction was allowed to proceed at 90°C with stirring overnight, at which point polymers were end-capped by reacting with monomer E1 (0.2 M final concentration in DMSO) at room temperature for 2 hr. The resulting E1 polymers were purified by 2 diethyl ether washes, after which polymers were dissolved at 200 mg/mL in DMSO and end-capped with carboxylate ligands (0.2 M final concentration in DMSO) at room temperature for 2 hr. The resulting carboxylated polymers were further purified by ether precipitation and remaining solvent was removed in a vacuum chamber. Polymers were dissolved in DMSO at 100 mg/mL and stored in single-use aliquots at -20°C with desiccant.

Polymer Characterization: NMR, GPC, and pH Titration

Polymer structure was characterized by nuclear magnetic resonance spectroscopy (NMR) via ^{1}H NMR in $CDCl_3$ (Bruker 500 MHz) and analyzed using TopSpin 3.5 software. Polymer molecular weight was characterized by gel permeation chromatography (GPC); polymers were dissolved in BHT-stabilized THF with 5% DMSO and 1% piperidine, filtered through a 0.2 μm PTFE filter, and characterized using GPC against linear polystyrene standards (Waters, Milford, MA). pH titrations were performed using a SevenEasy pH meter (Mettler Toledo) with 10 mg of polymer dissolved in 10 mL of 100 mM NaCl acidified with HCl as previously described.[15] Polymer was titrated from pH 3.0 to pH 11.0 using 100 mM NaOH added stepwise, and pH was recorded after each addition.

Nanoparticle Characterization

Nanoparticles were prepared by dissolving polymer and protein separately in 25 mM sodium acetate (NaAc, pH 5), mixing the two solutions at a 1:1 volume ratio, and allowing for nanoparticle self-assembly at room temperature for 10 minutes. To prepare nanoparticles encapsulating CRISPR ribonucleoproteins (RNPs), sgRNA and Cas9 protein were first mixed together at a 2:1 molar ratio to allow RNP assembly at room temperature for 10 minutes; RNPs were then mixed with polymers at a 1:1 volume ratio. Nanoparticles were diluted 1:5 in 150 mM PBS to determine particle size and zeta potential in neutral, isotonic buffer. Hydrodynamic diameter was measured via dynamic light scattering (DLS) on a Malvern Zetasizer Pro (Malvern Panalytical); zeta potential was measured via electrophoretic light scattering on the same instrument. Transmission electron microscopy (TEM) images were acquired with a Philips CM120 (Philips Research). Nanoparticles encapsulating BSA (30 w/w) were prepared at a polymer concentration of 1.8 mg/mL in 25 mM NaAc. 30 μL nanoparticles were added to 400-square mesh carbon coated TEM grids and allowed to adhere for 20 minutes. Grids were then rinsed with ultrapure water and allowed to fully dry before imaging.

sgRNA In Vitro Transcription

In vitro transcription was performed using a MEGAshortscript T7 Transcription kit (Invitrogen) and purified using a MEGAclear Transcription Clean-up kit (Invitrogen) following manufacturer's instructions. The DNA templates used for *in vitro* transcription were synthesized as gBlocks from IDT (sequences listed in Table 7-S2).

Cell Culture and Cell Line Preparation

HEK-293T human embryonic kidney cells, GL261 murine glioma cells, CT-2A murine glioma cells, B16-F10 murine melanoma cells, and MSC-083 human primary adipose-derived mesenchymal stem cells (hAMSCs) were cultured in Dulbecco's Modified Eagle Medium (DMEM; ThermoFisher) supplemented with 10% FBS and 1% penicillin/streptomycin. To generate reporter cell lines for CRISPR editing experiments, HEK-293T and GL261 cells were induced to constitutively express a destabilized form of GFP (GFPd2) via a PiggyBac transposon/transposase system as detailed previously.[16] Similarly, GL261 and B16-F10 cells were induced to constitutively express a construct where transcription of a red-enhanced nanolantern (ReNL) reporter gene is prevented by a dual-SV40 transcription stop cassette (CRISPR-stop). The PiggyBac transposon plasmids used to generate GFPd2+ and CRISPR-stop+ cell lines are available on Addgene as plasmids #115665 and #113965, respectively.

Transfection

Cells were plated at a density of 15,000 cells per well in 96 well tissue culture plates and allowed to adhere overnight. Protein-encapsulated nanoparticles were prepared as described above, and optimal nanoparticle formulations for each protein are listed in Table 7-S1. 20 μL nanoparticles were added per well into serum-containing complete cell culture media and incubated with cells for 4 hours. For FITC-BSA uptake experiments, the nanoparticle/media mixture was removed at 4 hours, and cells were washed 3 times with PBS and uptake was assessed via flow cytometry using a BD Accuri C6 flow cytometer (BD Biosciences). Nanoparticle uptake was quantified by normalizing the geometric mean fluorescence of treated wells to that of untransfected controls.

For all other transfection experiments, fresh complete medium was replenished after 4 hours incubation with nanoparticles. For saporin transfection experiments, cell killing was assessed 2 days post-transfection. Cells were stained with Hoechst 33342 nuclear stain (1:5000 dilution) and propidium iodide (1:500 dilution) for 20 minutes and imaged and analyzed using Cellomics Arrayscan VTI with live cell imaging module (ThermoFisher). Cell killing was calculated by normalizing live cell numbers in wells treated with C5/saporin nanoparticles to those in wells treated with matching nanoparticle formulations delivering non-toxic BSA. For CRISPR RNP transfection experiments, gene editing was assessed 3 days post-transfection. GFPd2 knockout and turning on of ReNL were assessed via flow cytometry. GFPd2 knockout was quantified by normalizing the GFP geometric mean fluorescence of C5/RNP treated wells to that of untransfected control wells; gain of ReNL fluorescence was quantified as the percentage of cells positively expressing ReNL when gated against untreated control.

For CRISPR HDR experiments, Cas9 and sgRNA targeting the *CXCR4* gene were first mixed at a 1:2 molar ratio and allowed to self-assemble into RNPs. The ssDNA repair template was then added at a 1:1 volume ratio to the RNPs, and the combined solution was mixed with C5 polymer to allow for nanoparticle self-assembly. Each well received a final dose of 300 ng sgRNA, 690 ng Cas9 protein, and 400 ng ssDNA repair template.

Commercial Reagent RNP Delivery

For CRISPR RNP delivery experiments using commercial reagents, B16-F10 cells expressing the PiggyBac CRISPR-stop+ cassette were plated in 96 well plates 24 hours prior. Lipofectamine™ CRISPRMax and jetCRISPR™ commercial reagents designed for RNP delivery were formulated with SpCas9 RNP nanoparticles according to manufacturer instructions and added to cells at the specified doses. Specifically, RNPs were formulated as recommended at 1:1 molar ratio of SpCas9 to sgRNA using the single guide CRISPR-stop sgRNA and complexed with commercial reagents prior to adding to cells and incubating 48 hours. Editing efficacy was assessed two days following RNP delivery using flow cytometry to assess percentage of cells expressing ReNL from the 630 bp deletion of the CRISPR-stop+ cassette.

Endocytosis Pathway Inhibition

HEK-293T cells were plated for transfection as described above and incubated for 1 hr with endocytosis inhibitors[32] in complete cell culture media immediately prior to transfection. Chlorpromazine (CPZ; 3 μg/mL) was used to inhibit clathrin-mediated endocytosis; methyl-β-cyclodextrin (MCD; 7.5 mg/mL) was used to inhibit lipid raft-mediated endocytosis; genistein (GEN; 10 μg/mL) was used to inhibit caveolin-mediated endocytosis; cytochalasin-D (CYD; 0.5 μg/mL) was used to inhibit actin polymerization and macropinocytosis. C5/FITC-BSA nanoparticles were formulated at 300 ng protein per well and 30 w/w. Nanoparticles were incubated with cells for 2 hr, at which time they were washed with PBS and analyzed via flow cytometry to assess nanoparticle uptake. Endocytosis inhibition was quantified by normalizing the geometric mean fluorescence of wells treated with inhibitor to that of untransfected control wells.

Gal8-GFP Recruitment Assay

The Gal8-GFP recruitment assay to assess endosomal disruption was based on methods previously reported by Kilchrist *et al.*[18] Briefly, B16-F10 cells were made to constitutively express a Gal8-GFP fusion protein using a PiggyBac transposon plasmid (Addgene 127191). Nanoparticles encapsulating BSA (125 ng BSA per well, 25 w/w) were incubated with cells for 4 hours, at which point cells were replenished with complete media and stained with Hoechst 33342 nuclear stain (1:5000 dilution). Gal8-GFP recruitment was imaged and analyzed with Cellomics Arrayscan VTI with live cell imaging module; cell count was generated using an algorithm to extrapolate area surrounding Hoechst-stained cell nuclei and endosomal disruption was reported as the average number of punctate Gal8-GFP spots per cell.

Cellular Viability

Cell viability was assessed 24 hours post-transfection using MTS CellTiter 96 Aqueous One cell proliferation assay (Promega) following manufacturer's instructions. Cell viability of treated cells were normalized to that of untreated controls; N = 4 +/- SEM.

Confocal Microscopy

HEK-293T or MSC-083 cells were plated on Nunc Lab-Tek 8 chambered borosilicate coverglass well plates (155411; ThermoFisher) at 30,000 cells/well in 250 μL phenol red free DMEM supplemented with 10% FBS and 1% penicillin/streptomycin one day prior to transfection. C5 nanoparticles were prepared at 30 w/w with the indicated proteins and 50 μL nanoparticles were administered per well for a total dose of 300 ng protein. Nanoparticles were incubated with cells for 4 hours, at which time cells were replenished with fresh complete medium and stained with Hoechst 33342 nuclear stain at a 1:5000 dilution and Cell Navigator Lysosome Staining dye (AAT Bioquest). Excess stain was washed away and cells were imaged in live cell imaging solution at 37°C in 5% CO_2. Images were acquired at Nyquist limit resolution using a Zeiss LSM 780 microscope with Zen Blue software and 63x oil immersion lens. Specific laser channels used were 405 nm diode, 488 nm argon, 561 nm solid-state, and 639 nm diode lasers. Laser intensity and detector gain settings were maintained across all image acquisition for each experiment.

Indel Quantification via Surveyor® Assay

Genomic DNA from cells treated with C5/RNP nanoparticles and untransfected controls were isolated using a GeneJET genomic DNA purification kit (ThermoFisher). A 660 bp region flanking the predicted cut site was PCR amplified (primers listed in Table 7-S2), and PCR products were purified using a QIAquick PCR purification kit (Qiagen). 400 ng of PCR amplicons were hybridized in the presence of 50 mM KCl, and the Surveyor® mutation detection assay (IDT) was performed following manufacturer's instructions. The DNA products were then run on a 2% agarose gel stained with ethidium bromide in TBE buffer (80 V for 50 minutes) and imaged under UV light. DNA band intensity was quantified using ImageJ image analysis software and indel rate was calculated based on the method by Schumann *et al.*[33]

HDR Quantification via Restriction Enzyme Digest

A restriction enzyme-based assay to quantify HDR rates was adapted from methods reported by Lee *et al.*[28] Briefly, a HDR repair template was designed to insert a 12-bp region that includes the HindIII

restriction site into the *CXCR4* gene, with 78 base homology arm upstream and 90 base homology arm downstream of the insert site. The repair template was synthesized as a single-stranded DNA oligo from IDT (sequence listed in Table 7-S2). Genomic DNA of cells treated with C5/RNP+ssDNA nanoparticles or control nanoparticles was harvested 5 days post-transfection. A 770 bp region surrounding the edit site was PCR amplified, and the PCR amplicon was digested with HindIII (0.01 enzyme units/ng DNA) for 1 hr at 37°C prior to standard gel electrophoresis as described above. Percent HDR was calculated by dividing the band intensity of the digested fragment (approximately 400 bp) by the band intensity of all bands in the lane.

GL261-CRISPR-stop Tumor Implantation

All animal work was done in strict adherence of the policies and guidelines of the Johns Hopkins University Animal Care and Use Committee. For intracranial tumor implantations, 6-8 week old female C57BL/6J mice (Jackson Laboratory) were anesthetized using a 10 mg/kg ketamine (100 mg/kg)/Xylazine (10 mg/kg) cocktail and mounted on a stereotaxic frame. A rostro-caudal incision was made with a scalpel, the surface of the skull was exposed and cleaned with 100% ethanol, and a small burr hole was made in the skull 4 mm posterior to the coronal suture and 2 mm lateral to the sagittal suture using an electric drill. 130,000 GL261 murine glioma cells engineered to constitutively express the CRISPR-stop construct were implanted into mouse brain parenchyma through the burr hole using a 10 μL Hamilton syringe (Hamilton Company); the injection volume was 2 μL.

Intratumoral C5/RNP Nanoparticle Injection

Tumors were allowed to form for 10 days, at which time C5/RNP nanoparticle administration began. Nanoparticles were formed in PBS buffer at a final polymer concentration of 0.86 mg/mL and 3.5 pmol RNPs (15 w/w) immediately prior to injection. Mice were anesthetized with a 10 mg/kg ketamine cocktail as described earlier, and the original incision was opened. Convection-enhanced delivery (CED) was performed using a 26 gauge Hamilton needle stereotaxically placed at a depth of 3 mm and an UltraMicroPump (UMP3) with SYS-Micro4 Controller (World Precision Instruments, Sarasota, FL) was used

to infuse nanoparticles at a rate of 0.5 μL/min.[34] 10 μL of nanoparticles were injected per animal, after which the needle was left at the injection site for 5 min to mitigate backflow. Following needle removal, the incision was closed with 4-0 silk sutures and the animal was allowed to awaken and recover.

In Vivo Visualization of ReNL Reporter

For ReNL reporter analysis, 6-d post-injection mice were anesthetized and perfused with 4% paraformaldehyde. Brains were extracted, post-fixed overnight, and soaked in 30% sucrose for 24 h. Brains were frozen on dry ice and mounted onto a cryostat sample holder using Optimal Cutting Temperature compound (OCT), cryosectioned (coronal plane sections) using a Leica CM 3050 S cryostat (Leica Biosystem), and the prepared 40 μm sections were mounted onto glass slides with Hoechst nuclear stain (1:4000 dilution) and SlowFade® Gold Antifade Reagent (ThermoFisher). Mounted sections were stored at -80°C and protected from light until use. Sections were imaged by fluorescence microscopy using a Zeiss Apotome.2 microscope with Zen Blue software. Microscope settings were maintained across all image acquisition.

Nanoparticle Stability

To characterize nanoparticle stability over time in physiological conditions, C5/RNP nanoparticles were incubated in serum-containing complete cell culture medium at 37°C and added to GL261-CRISPR-stop cells at designated time points up to 4 h. C5/RNP nanoparticles were also lyophilized with 30 mg/mL sucrose as cryoprotectant following previously-reported protocols[35] and stored at -20°C for 4 days before adding to cells. Cells were incubated with nanoparticles for 3 h and the level of gene editing was analyzed via flow cytometry 3 days post-transfection.

Statistics

Prism 6 (Graphpad, La Jolla, CA) was used for all statistical analyses and curve plotting. Statistical tests were performed with a global alpha value of 0.05. Unless otherwise stated, absence of statistical significance

markings where a test was stated to have been performed signified no statistical significance. The statistical test used and the number of experimental replicates were listed in the captions for each figure. Statistical significance was denoted as follows: *P<0.05, **P<0.01, ***P<0.001, ****P<0.0001.

Acknowledgments

Funding: The authors would like to thank the following organizations for financial support: NSF Graduate Research Fellowship DGE-0707427 (DRW) and DGE-1232825 (YR), Microscopy Core Grant (S10 OD016374) and the United States NIH grants R01CA228133 (JJG), and R01EB022148 (JJG), Wilmer Core Grant P30 EY001765. JJG thanks the Bloomberg~Kimmel Institute for Cancer Immunotherapy and the Research to Prevent Blindness James and Carole Free Catalyst Award for support. JC thanks the Johns Hopkins University Deans Research Fund for their fellowship support. **Author contributions:** Conceptualization, YR, DRW, and JJG; Methodology, YR, DRW, JC, JK, and JJG; Investigation, YR, DRW, JC, MV, KS, and JK; Resources and funding acquisition, JJG; Writing and editing, YR, DRW, JC, MV, KS, JK, ML, and JJG; Supervision and administration, ML, JJG. **Competing interests:** The authors declare that they have no competing interests. **Data and materials availability:** All data needed to evaluate the conclusions in the paper are present in the paper and/or Supplementary Materials. Additional data related to this paper may be requested from the authors.

References

1. Clark, A. L.; Knight, G.; Wiles, P.; Keen, H.; Ward, J.; Cauldwell, J.; Adeniyi-Jones, R.; Leiper, J.; Jones, R.; Maccuish, A., Biosynthetic human insulin in the treatment of diabetes: a double-blind crossover trial in established diabetic patients. *The Lancet* **1982,** *320* (8294), 354-357.

2. Leader, B.; Baca, Q. J.; Golan, D. E., Protein therapeutics: a summary and pharmacological classification. *Nature Reviews Drug Discovery* **2008,** *7*, 21.

3. Paschon, D. E.; Lussier, S.; Wangzor, T.; Xia, D. F.; Li, P. W.; Hinkley, S. J.; Scarlott, N. A.; Lam, S. C.; Waite, A. J.; Truong, L. N.; Gandhi, N.; Kadam, B. N.; Patil, D. P.; Shivak, D. A.; Lee, G. K.; Holmes, M.

C.; Zhang, L.; Miller, J. C.; Rebar, E. J., Diversifying the structure of zinc finger nucleases for high-precision genome editing. *Nature Communications* **2019,** *10* (1), 1133.

4. Lienert, F.; Lohmueller, J. J.; Garg, A.; Silver, P. A., Synthetic biology in mammalian cells: next generation research tools and therapeutics. *Nature reviews Molecular cell biology* **2014,** *15* (2), 95.

5. Postupalenko, V.; Desplancq, D.; Orlov, I.; Arntz, Y.; Spehner, D.; Mely, Y.; Klaholz, B. P.; Schultz, P.; Weiss, E.; Zuber, G., Protein Delivery System Containing a Nickel-Immobilized Polymer for Multimerization of Affinity-Purified His-Tagged Proteins Enhances Cytosolic Transfer. *Angewandte Chemie International Edition* **2015,** *54* (36), 10583-10586.

6. Southwell, A. L.; Khoshnan, A.; Dunn, D. E.; Bugg, C. W.; Lo, D. C.; Patterson, P. H., Intrabodies binding the proline-rich domains of mutant huntingtin increase its turnover and reduce neurotoxicity. *The Journal of neuroscience : the official journal of the Society for Neuroscience* **2008,** *28* (36), 9013-9020.

7. Rui, Y.; Wilson, D. R.; Green, J. J., Non-Viral Delivery To Enable Genome Editing. *Trends in Biotechnology* **2019,** *37* (3), 281-293.

8. Schwarze, S. R.; Ho, A.; Vocero-Akbani, A.; Dowdy, S. F., In Vivo Protein Transduction: Delivery of a Biologically Active Protein into the Mouse. *Science* **1999,** *285* (5433), 1569.

9. Wang, M.; Zuris, J. A.; Meng, F.; Rees, H.; Sun, S.; Deng, P.; Han, Y.; Gao, X.; Pouli, D.; Wu, Q.; Georgakoudi, I.; Liu, D. R.; Xu, Q., Efficient delivery of genome-editing proteins using bioreducible lipid nanoparticles. *Proceedings of the National Academy of Sciences* **2016,** *113* (11), 2868.

10. Zhang, Z.; Shen, W.; Ling, J.; Yan, Y.; Hu, J.; Cheng, Y., The fluorination effect of fluoroamphiphiles in cytosolic protein delivery. *Nature Communications* **2018,** *9* (1), 1377.

11. Cheng, G.; Li, W.; Ha, L.; Han, X.; Hao, S.; Wan, Y.; Wang, Z.; Dong, F.; Zou, X.; Mao, Y., Self-Assembly of Extracellular Vesicle-like Metal–Organic Framework Nanoparticles for Protection and Intracellular Delivery of Biofunctional Proteins. *Journal of the American Chemical Society* **2018**.

12. Chen, T.-T.; Yi, J.-T.; Zhao, Y.-Y.; Chu, X., Biomineralized Metal-Organic Framework Nanoparticles Enable Intracellular Delivery and Endo-Lysosomal Release of Native Active Proteins. *Journal of the American Chemical Society* **2018**.

13. Alsaiari, S. K.; Patil, S.; Alyami, M.; Alamoudi, K. O.; Aleisa, F. A.; Merzaban, J. S.; Li, M.; Khashab, N. M., Endosomal Escape and Delivery of CRISPR/Cas9 Genome Editing Machinery Enabled by Nanoscale Zeolitic Imidazolate Framework. *Journal of the American Chemical Society* **2017,** *140* (1), 143-146.

14. Gao, Y.; Huang, J.-Y.; O'Keeffe Ahern, J.; Cutlar, L.; Zhou, D.; Lin, F.-H.; Wang, W., Highly Branched Poly(β-amino esters) for Non-Viral Gene Delivery: High Transfection Efficiency and Low Toxicity Achieved by Increasing Molecular Weight. *Biomacromolecules* **2016,** *17* (11), 3640-3647.

15. Wilson, D. R.; Rui, Y.; Siddiq, K.; Routkevitch, D.; Green, J. J., Differentially Branched Ester Amine Quadpolymers with Amphiphilic and pH-Sensitive Properties for Efficient Plasmid DNA Delivery. *Mol Pharm* **2019,** *16* (2), 655-668.

16. Rui, Y.; Wilson, D. R.; Sanders, K.; Green, J. J., Reducible Branched Ester-Amine Quadpolymers (rBEAQs) Codelivering Plasmid DNA and RNA Oligonucleotides Enable CRISPR/Cas9 Genome Editing. *ACS Applied Materials & Interfaces* **2019,** *11* (11), 10472-10480.

17. Shmueli, R. B.; Sunshine, J. C.; Xu, Z.; Duh, E. J.; Green, J. J., Gene delivery nanoparticles specific for human microvasculature and macrovasculature. *Nanomedicine: Nanotechnology, Biology and Medicine* **2012,** *8* (7), 1200-1207.

18. Kilchrist, K. V.; Dimobi, S. C.; Jackson, M. A.; Evans, B. C.; Werfel, T. A.; Dailing, E. A.; Bedingfield, S. K.; Kelly, I. B.; Duvall, C. L., Gal8 Visualization of Endosome Disruption Predicts Carrier-Mediated Biologic Drug Intracellular Bioavailability. *ACS Nano* **2019,** *13* (2), 1136-1152.

19. Wilson, D. R.; Mosenia, A.; Suprenant, M. P.; Upadhya, R.; Routkevitch, D.; Meyer, R. A.; Quinones-Hinojosa, A.; Green, J. J., Continuous microfluidic assembly of biodegradable poly(beta-amino ester)/DNA nanoparticles for enhanced gene delivery. *J Biomed Mater Res A* **2017,** *105* (6), 1813-1825.

20. Lombardi, A.; Marshall, R. S.; Savino, C.; Fabbrini, M. S.; Ceriotti, A., Type I Ribosome-Inactivating Proteins from Saponaria officinalis. In *Toxic Plant Proteins*, Lord, J. M.; Hartley, M. R., Eds. Springer Berlin Heidelberg: Berlin, Heidelberg, 2010; pp 55-78.

21. Hsiau, T.; Maures, T.; Waite, K.; Yang, J.; Kelso, R.; Holden, K.; Stoner, R., Inference of crispr edits from sanger trace data. *BioRxiv* **2018**, 251082.

22. Sunshine, J. C.; Peng, D. Y.; Green, J. J., Uptake and transfection with polymeric nanoparticles are dependent on polymer end-group structure, but largely independent of nanoparticle physical and chemical properties. *Mol Pharm* **2012,** *9* (11), 3375-3383.

23. Guerrero-Cázares, H.; Tzeng, S. Y.; Young, N. P.; Abutaleb, A. O.; Quiñones-Hinojosa, A.; Green, J. J., Biodegradable polymeric nanoparticles show high efficacy and specificity at DNA delivery to human glioblastoma in vitro and in vivo. *ACS Nano* **2014,** *8* (5), 5141-5153.

24. Rehman, Z. u.; Hoekstra, D.; Zuhorn, I. S., Mechanism of Polyplex- and Lipoplex-Mediated Delivery of Nucleic Acids: Real-Time Visualization of Transient Membrane Destabilization without Endosomal Lysis. *ACS Nano* **2013,** *7* (5), 3767-3777.

25. Ayala, R.; Zhang, C.; Yang, D.; Hwang, Y.; Aung, A.; Shroff, S. S.; Arce, F. T.; Lal, R.; Arya, G.; Varghese, S., Engineering the cell–material interface for controlling stem cell adhesion, migration, and differentiation. *Biomaterials* **2011,** *32* (15), 3700-3711.

26. Rui, Y.; Quiñones, G.; Green, J. J., Biodegradable and bioreducible poly(beta-amino ester) nanoparticles for intracellular delivery to treat brain cancer. *AIChE Journal* **2017,** *63* (5), 1470-1482.

27. Sun, W.; Ji, W.; Hall, J. M.; Hu, Q.; Wang, C.; Beisel, C. L.; Gu, Z., Self-Assembled DNA Nanoclews for the Efficient Delivery of CRISPR–Cas9 for Genome Editing. *Angewandte Chemie International Edition* **2015,** *54* (41), 12029-12033.

28. Lee, K.; Conboy, M.; Park, H. M.; Jiang, F.; Kim, H. J.; Dewitt, M. A.; Mackley, V. A.; Chang, K.; Rao, A.; Skinner, C.; Shobha, T.; Mehdipour, M.; Liu, H.; Huang, W.-C.; Lan, F.; Bray, N. L.; Li, S.; Corn, J. E.; Kataoka, K.; Doudna, J. A.; Conboy, I.; Murthy, N., Nanoparticle delivery of Cas9 ribonucleoprotein and donor DNA in vivo induces homology-directed DNA repair. *Nature biomedical engineering* **2017,** *1*, 889-901.

29. Staahl, B. T.; Benekareddy, M.; Coulon-Bainier, C.; Banfal, A. A.; Floor, S. N.; Sabo, J. K.; Urnes, C.; Munares, G. A.; Ghosh, A.; Doudna, J. A., Efficient genome editing in the mouse brain by local delivery of engineered Cas9 ribonucleoprotein complexes. *Nature Biotechnology* **2017,** *35*, 431.

30. Patel, A. K.; Kaczmarek, J. C.; Bose, S.; Kauffman, K. J.; Mir, F.; Heartlein, M. W.; DeRosa, F.; Langer, R.; Anderson, D. G., Inhaled Nanoformulated mRNA Polyplexes for Protein Production in Lung Epithelium. *Adv Mater* **2019,** *31* (8), 1805116.

31. Charlesworth, C. T.; Deshpande, P. S.; Dever, D. P.; Camarena, J.; Lemgart, V. T.; Cromer, M. K.; Vakulskas, C. A.; Collingwood, M. A.; Zhang, L.; Bode, N. M.; Behlke, M. A.; Dejene, B.; Cieniewicz, B.; Romano, R.; Lesch, B. J.; Gomez-Ospina, N.; Mantri, S.; Pavel-Dinu, M.; Weinberg, K. I.; Porteus, M. H., Identification of preexisting adaptive immunity to Cas9 proteins in humans. *Nature Medicine* **2019,** *25* (2), 249-254.

32. dos Santos, T.; Varela, J.; Lynch, I.; Salvati, A.; Dawson, K. A., Effects of Transport Inhibitors on the Cellular Uptake of Carboxylated Polystyrene Nanoparticles in Different Cell Lines. *PLOS ONE* **2011,** *6* (9), e24438.

33. Schumann, K.; Lin, S.; Boyer, E.; Simeonov, D. R.; Subramaniam, M.; Gate, R. E.; Haliburton, G. E.; Ye, C. J.; Bluestone, J. A.; Doudna, J. A.; Marson, A., Generation of knock-in primary human T cells using Cas9 ribonucleoproteins. *Proceedings of the National Academy of Sciences* **2015,** *112* (33), 10437.

34. Serwer, L.; Hashizume, R.; Ozawa, T.; James, C. D., Systemic and local drug delivery for treating diseases of the central nervous system in rodent models. *Journal of visualized experiments : JoVE* **2010,** (42), 1992.

35. Lopez-Bertoni, H.; Kozielski, K. L.; Rui, Y.; Lal, B.; Vaughan, H.; Wilson, D. R.; Mihelson, N.; Eberhart, C. G.; Laterra, J.; Green, J. J., Bioreducible Polymeric Nanoparticles Containing Multiplexed Cancer Stem Cell Regulating miRNAs Inhibit Glioblastoma Growth and Prolong Survival. *Nano Lett* **2018,** *18* (7), 4086-4094.

Supporting Information

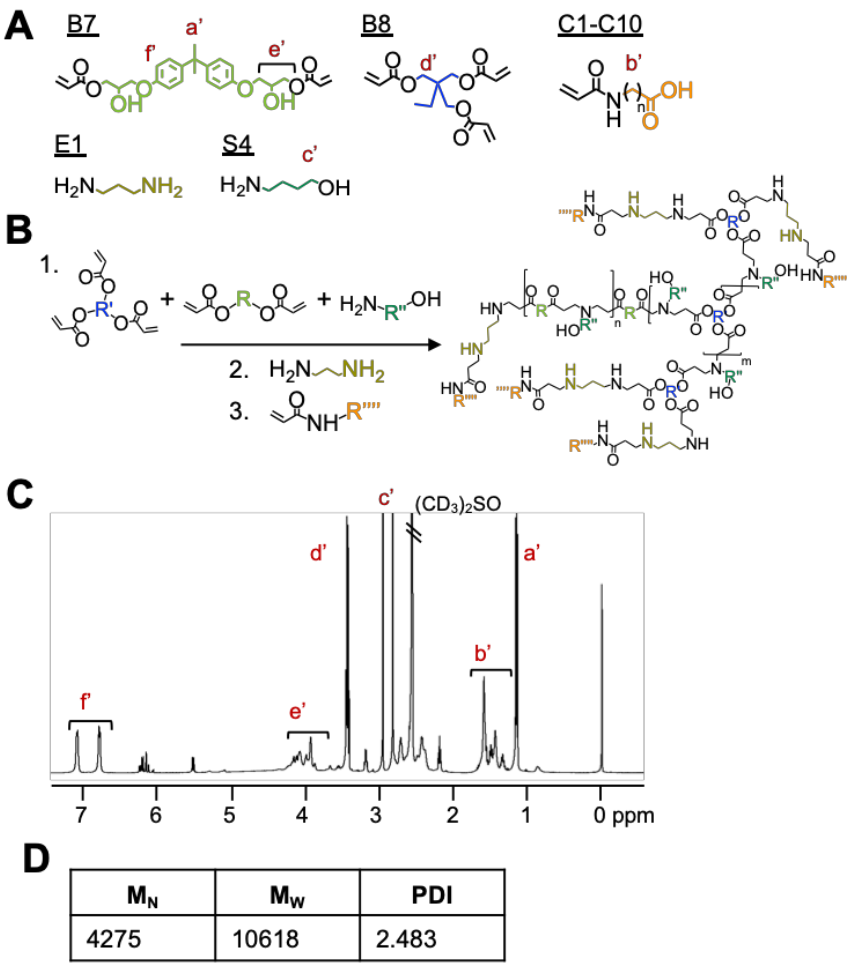

D

M_N	M_W	PDI
4275	10618	2.483

Figure 7-S1. Synthesis and characterization of carboxylated branched PBAE polymers. (A) Monomer structures. **(B)** Reaction scheme for branched polymers. (1) Acrylate-terminated branched PBAE is synthesized via Michael addition of B and S monomers; (2) polymer end-capping with monomer E1 results in amine-terminated polymers; (3) further end-capping with carboxylate ligands yields final polymer products. **(C)** ^{1}H NMR spectrum of polymer C5; distinctive peaks from each monomer are labeled according to chemical structures shown in **(A). (D)** Molecular weight data of polymer C5 obtained via GPC.

A

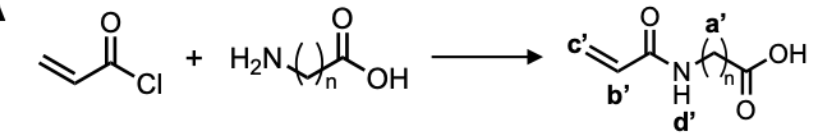

Acryloyl chloride | Carboxylate precursor | Carboxylate ligand

B

Ligand	Carboxylate precursor	Extraction pH
C1	Glycine	2.0
C3	4-aminobutyric acid	2.0
C5	6-aminocaproic acid	3.0
C7	8-amino-caprylic acid	5.0
C10	11-aminoundecanoic acid	5.0

C

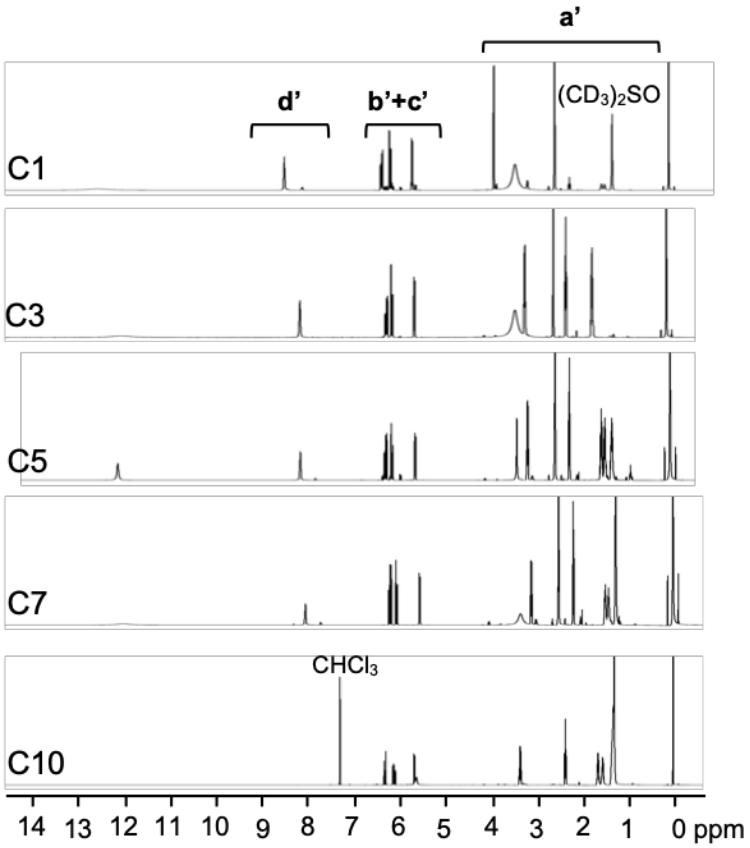

Figure 7-S2. Synthesis and characterization of carboxylate ligands. (A) Reaction route schematic. **(B)** Acidification pH for extraction of each ligand. **(C)** ^{1}H NMR spectrum of each ligand; peaks labeled according to the chemical structure shown in **(A)**.

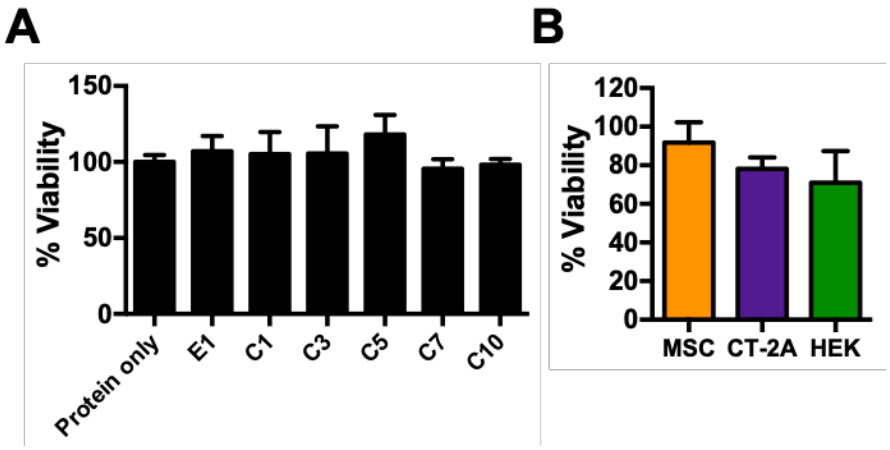

Figure 7-S3. Cell viability after treatment with carboxylated branched PBAE protein nanoparticles. **(A)** Cell viability of CT-2A murine glioma cells treated with E1-C10 nanoparticles encapsulating BSA. **(B)** Cell viability of other cell types treated with C5/BSA nanoparticles. Nanoparticle formulation used in both experiments is 300 ng protein per well at 20 w/w. Cell viability measured using MTT assay. Data presented as mean+SD; *n*=4.

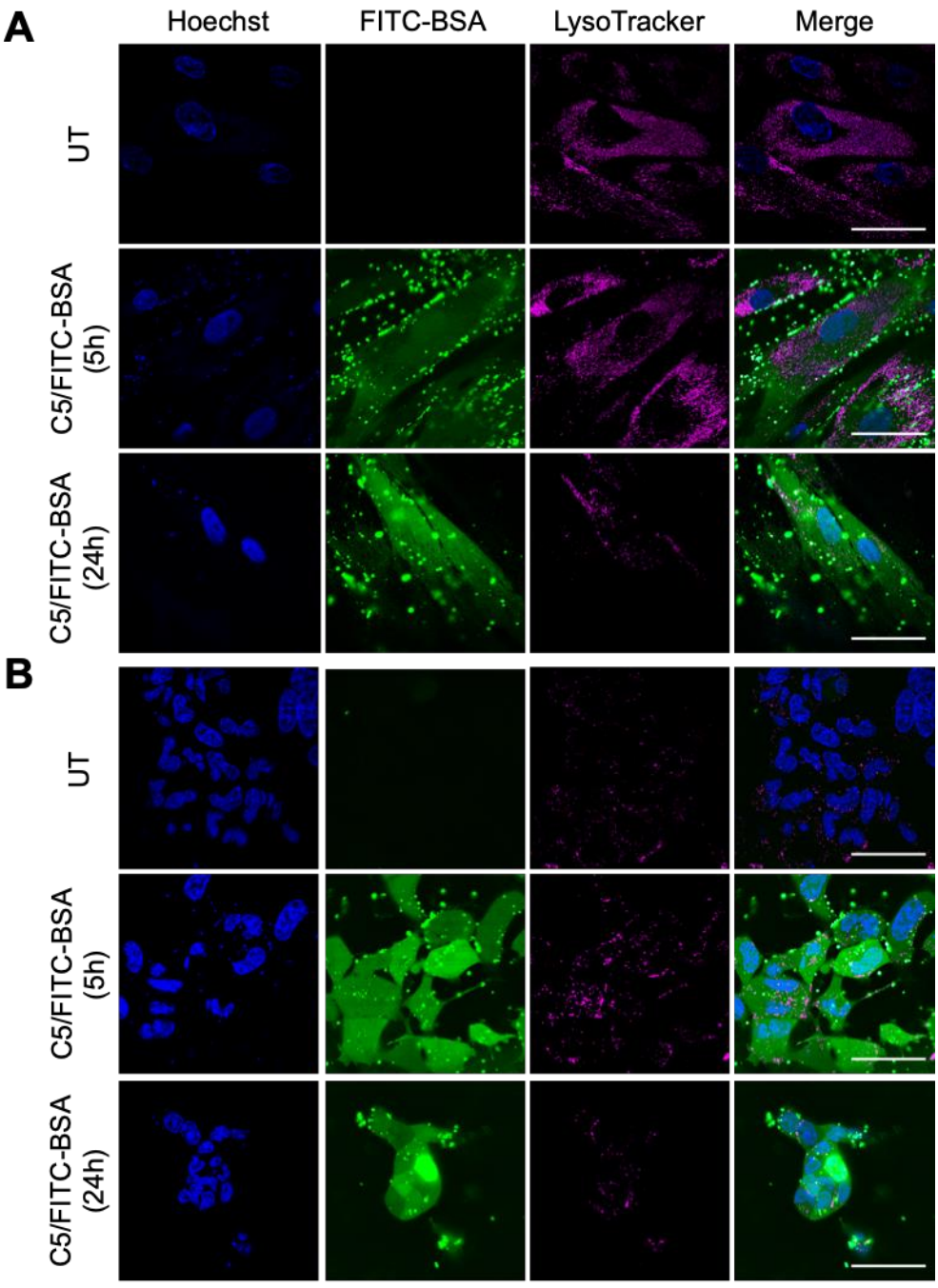

Figure 7-S4. Confocal images of cells treated with C5/FITC-BSA nanoparticles. (A) Human adipose-derived mesenchymal stem cells and **(B)** HEK-293T cells were treated with C5/FITC-BSA nanoparticles (300 ng protein dose, 30 w/w) and imaged at 5 and 24 hours post-transfection. Untreated cells (UT) were also imaged as controls. Scale bar = 10 μm.

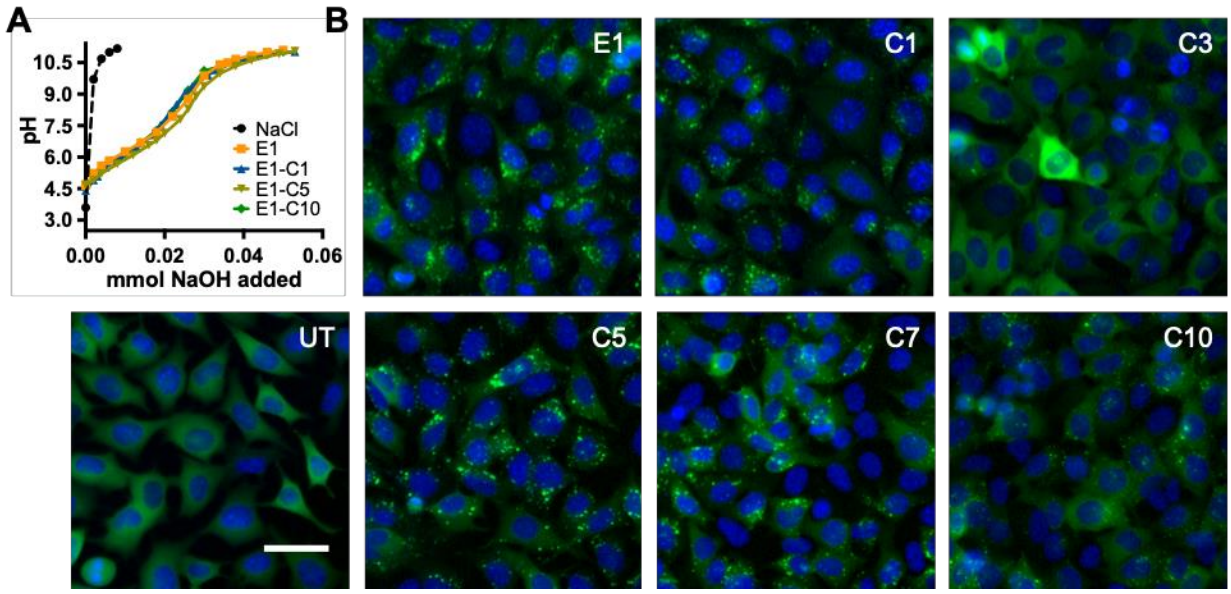

Figure 7-S5. Characterization of polymer pH buffering and endosomal disruption capabilities. (A) pH titration curve of several polymers in the series. Sigmoidal curve fit of the titration curves and comparison via sum-of-squares F-test statistically demonstrated that there was no significant difference between buffering in the range of pH 4.5-8 for carboxylate ligands ($P = 0.062$). **(B)** Representative images from high content imaging of B16-F10/Gal8-GFP cells treated with nanoparticles encapsulating BSA (125 ng BSA per well, 25 w/w; scale bar = 50 μm).

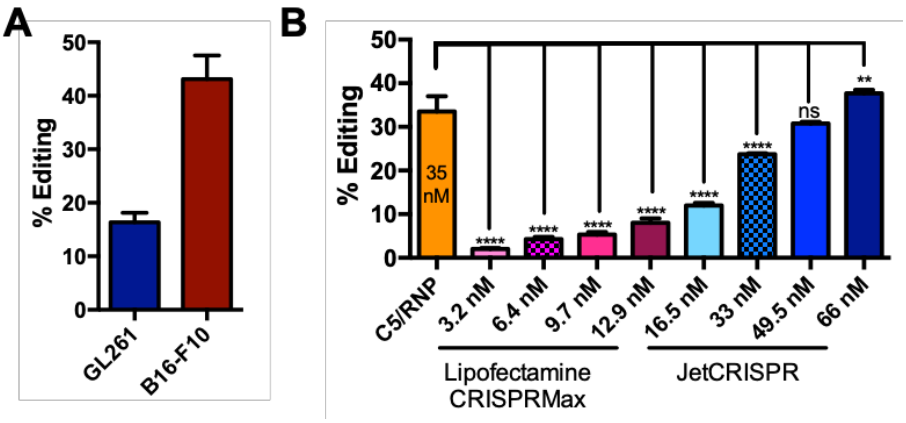

Figure 7-S6. C5/RNP nanoparticles enable *in vitro* gene deletion. (A) C5/RNP deletion of stop cassette *in vitro* in 2 murine cancer cell lines resulted in turning on of ReNL fluorescence as detected by flow cytometry. Data are mean+SD; *n*=4. **(B)** Comparison in gene editing performance with commercially-available CRISPR transfection reagents in B16-F10 cells. C5/RNP nanoparticles were administered at an RNP dose of 35 nM per well; RNP dose for commercial reagents are indicated. For each commercial reagent, the manufacturer recommended RNP dose is indicated by checkerboard pattern. Turning on of ReNL fluorescence was quantified by flow cytometry. Data are mean+SD; *n*=4. Statistical analysis performed using one-way ANOVA with Dunnett's post-hoc tests compared against the C5/RNP group; ***P*<0.01, *****P*<0.0001.

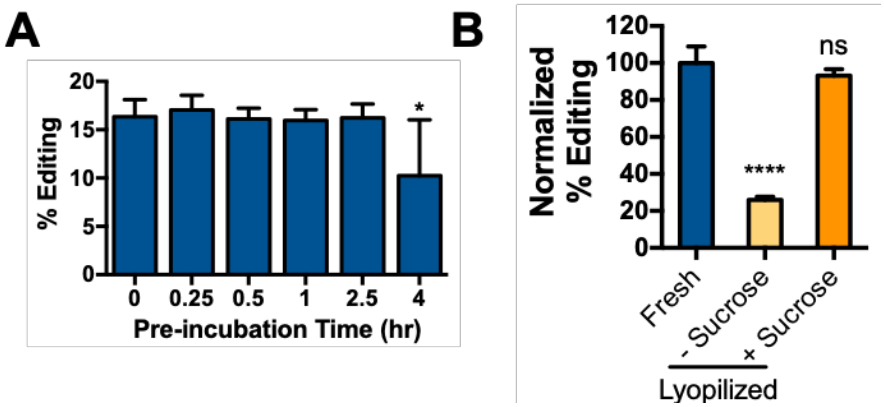

Figure 7-S7. C5/RNP nanoparticles are stable in serum-containing media and in lyophilized form. **(A)** % Editing observed in GL261-CRISPR-stop cells after treatment with nanoparticles pre-incubated in

serum-containing complete medium at 37°C for the designated times. Statistical significance determined by one-way ANOVA with Dunnett's post-hoc tests as compared to time = 0 . Data presented as mean+SD; (n=4). *P<0.05. **(B)** Nanoparticles lyophilized with or without 30 mg/mL sucrose and stored at -20°C prior to being added to cells. Percent editing normalized to fresh nanoparticles. Data presented as mean+SD; n=4. Statistical significance determined by one-way ANOVA with Dunnett's post-hoc tests as compared to fresh nanoparticles; (n=4). *P<0.05, ****P<0.0001.

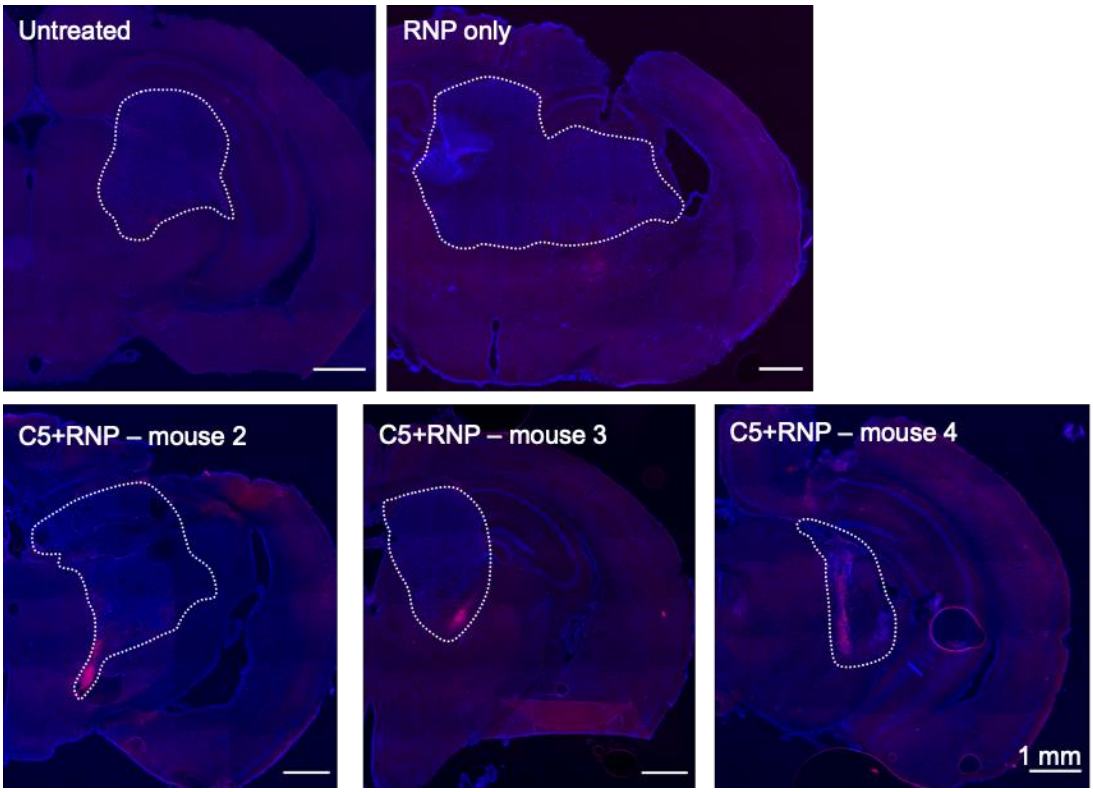

Figure 7-S8. C5/RNP nanoparticle-enabled *in vivo* CRISPR editing is reproducible. Red ReNL fluorescent signal can be detected in 3 additional mice treated with C5/RNP nanoparticles while untreated and RNP only groups showed no signal. Nanoparticles were formulated at 3.5 pmol RNP with 15 w/w C5 polymer. Tumors boundary outlined in white.

Protein	Protein Characteristics		Nanoparticle Characteristics				
	MW	pI	Size (nm)	Zeta (mV)	Optimal Protein Dose	Optimal Polymer Dose (mg/mL)	Equivalent w/w
GFP	27 kD	5.8	150±50	9.9±0.7	300 ng	0.075	30
Saporin	29 kD	9.5	120±30	8.7±0.4	2.5-15 nM	0.075	2600-175
BSA	66.5 kD	4.7	160±60	5±1	300 ng	0.075	30
IgG	150 kD	6.6-7.2	120±20	-1±1	300 ng	0.075	30
Cas9	163 kD	9	180±10	12.3±0.2	690 ng	0.1	22

Table 7-S1. Characteristics of proteins and encapsulated C5 nanoparticles and optimal nanoparticle formulations used in this study.

		Sequences	Notes
Target Sequences	GFP	GGAGCGCACCATCTTCTTCAAGG	PAM; Positive strand
	CRISPR-stop	GTATAGCATACATTATACGAGG	PAM; Negative strand
	CXCR4	GAAGCGTGATGACAAAGAGGAGG	PAM; Negative strand
sgRNA IVT Template	GFP	*GTTTTTAATACGACTCACTATA*GGAGCGCACCATCTTCTTCAGTTTTAGAGCTAGAAATAGCAAGTTAAAATAAGGCTAGTCCGTTATCAACTTGAAAAAGTGGCACCGAGTCGGTGCTTTTTTT	*T7 promoter* Target sequence gRNA scaffold
	CRISPR-stop	*GTTTTTAATACGACTCACTATA*GGTATAGCATACATTATACGGTTTTAGAGCTAGAAATAGCAAGTTAAAATAAGGCTAGTCCGTTATCAACTTGAAAAAGTGGCACCGAGTCGGTGCTTTTTTT	
	CXCR4	*GTTTTTAATACGACTCACTATA*GAAGCGTGATGACAAAGAGGGTTTTAGAGCTAGAAATAGCAAGTTAAAATAAGGCTAGTCCGTTATCAACTTGAAAAAGTGGCACCGAGTCGGTGCTTTTTTT	
Primers for Surveyor® Assay	GFP_FWD	CTGGTCGAGCTGGACGGCGACG	Amplicon size: 630 bp
	GFP_REV	CACGAACTCCAGCAGGACCATG	
	CXCR4_FWD	TTAATTCTCTTGTGCCCTTAGCCCACTACTTCAG	Amplicon size: 770 bp
	CXCR4_REV	GGACAGGATGACAATACCAGGCAGGATAAGGCC	
HDR Donor Template	CXCR4	CCTGGTCATGGGTTACCAGAAGAAACTGAGAAGCATGACGGACAAGTACAGGCTGCACCTGTCAGTGGCCGACCTCCTAAGCTTGGATCCCTTTGTCATCACGCTTCCCTTCTGGGCAGTTGATGCCGTGGCAAACTGGTACTTTGGGAACTTCCTATGCAAGGCAGTCCATGTCATCTA	Inserted region Homology arms HindIII restriction site

Table 7-S2. DNA sequences.

Chapter 8: Poly(beta-amino ester) Quadpolymer Structure Tunes Endosomal Escape, Cellular Uptake, and *In Vivo* Delivery of mRNA Nanoparticles

Yuan Rui[1,#], David R. Wilson[1,#], Stephany Y. Tzeng[1,#], Hannah M. Yamagata[1], Deepti Sudhakar[1], Marranne Conge[1, 2], Cynthia A. Berlinicke[3], Donald J. Zack[3, 4], Anthony Tuesca[5], and Jordan J. Green[1, 3, 6, 7, 8, *]

[1]Department of Biomedical Engineering, Institute for NanoBioTechnology, and the Translational Tissue Engineering Center, Johns Hopkins University School of Medicine.

[2]Department of Biology, Berea College

[3]Department of Ophthalmology, Johns Hopkins University School of Medicine

[4]Departments of Neuroscience, Molecular Biology & Genetics, and Genetic Medicine, Johns Hopkins University School of Medicine

[5]AstraZeneca, Dosage Form and Design Development, BioPharmaceutical Development, BioPharmaceuticals R&D, Gaithersburg, MD

[6]Department of Neurosurgery and Oncology, Johns Hopkins University School of Medicine.

[7]Departments of Materials Science & Engineering, and Chemical & Biomolecular Engineering, Johns Hopkins University.

[8]Bloomberg~Kimmel Institute for Cancer Immunotherapy, Johns Hopkins University School of Medicine.

[#] These authors contributed equally

Abstract

Nanoparticle-based mRNA therapeutics hold great promise for the treatment of a variety of diseases. However, cellular internalization and endosomal escape remain key barriers in functional, cytosolic mRNA delivery. To facilitate *in vitro* identification of potent mRNA nanoparticle formulations, we developed a dual nanoparticle uptake and endosomal disruption assay using high throughput and high content image-based screening. Using a genetically encoded Galectin 8 fluorescent fusion protein sensor (Gal8-mRuby), endosomal disruption could be detected 6 hours after nanoparticle treatment via Gal8-mRuby clustering on

damaged endosomal membranes. Simultaneously, nucleic acid endocytosis was quantified using fluorescently-tagged mRNA. We used a series of biodegradable poly(beta-amino ester)s as well as Lipofectamine and PEI to demonstrate that this assay has higher predictive capacity for *in vitro* mRNA delivery compared to conventional polymer and nanoparticle physiochemical characteristics. Top nanoparticle formulations enabled safe and efficacious mRNA expression following intravenous injection, demonstrating that this *in vitro* screening method is also predictive of *in vivo* performance. Efficacious non-viral systemic delivery of mRNA with biodegradable particles opens up new avenues for genetic medicine and human health.

Introduction

Recent advances in the synthesis of *in vitro* transcribed (IVT) mRNA[1, 2] has spurred a vast amount of research into mRNA-based gene therapies including the development of next generation vaccines.[3] Compared to their plasmid DNA counterparts, mRNA offers safer and more controlled gene expression by virtually eliminating the risk for integration into the host genome.[4] mRNA delivery could also lead to more potent expression in cell populations that are largely refractory to DNA transfection, such as T cells, which have been shown to mount immune responses against foreign cytosolic DNA.[5, 6] However, due to their size and hydrophilicity, mRNA molecules are membrane-impermeable, making safe and efficient cytosolic mRNA delivery a major obstacle to their clinical utility.

Non-viral nanoparticle (NP) formulations have emerged as promising mRNA delivery vehicles. Many lipid-based[7] and several polymeric[8] mRNA NP systems have recently been reported for protein replacement,[9, 10] immune modulation,[11, 12] and gene editing applications.[13, 14] To fully realize the promise of mRNA therapeutics, NP systems must be engineered to overcome intracellular barriers, such as cellular internalization and escape from endosomal sequestration.[15] A study of lipid NPs encapsulating siRNA showed that only an estimated 1-2%[16] of internalized siRNA reaches the cytosol, highlighting the need for improved nanomaterials as well as quantitative high-throughput *in vitro* assays that can measure NP performance at key delivery bottlenecks and improve NP design.

Several image-based methods for quantifying the ability of NPs to overcome endosomal entrapment have been reported. The most common method is assessing the lack of co-localization of fluorescently labeled NPs with the pH-sensitive Lysotracker dye,[17, 18] which selectively accumulates in the acidic environment of endosomes. This approach is easy to use and applicable to a wide variety of materials, but only provides an indirect assessment, as it does not indicate effective endosomal escape or disruption. Transmission electron microscopy (TEM) imaging is another widely accepted method for confirming endosomal disruption and escape.[16, 19] However, this method is not amenable to high-throughput analysis, cannot be done on living cells, and requires electron-dense labels such as gold NPs, which could alter the properties of the native NP system. More recently, several groups have reported the use of advanced imaging approaches such as high-dynamic-range confocal microscopy[20] or super-resolution stochastic optical reconstruction microscopy (STORM),[21] which have yielded important mechanistic data for the intracellular fate of the materials being studied, but lack the high-throughput screening capacity required to evaluate arrays of nanomaterials.

In this study, we used Galectin 8 (Gal8) tracking for high-throughput image-based quantification of endosomal disruption. Gal8 is a β-galactoside carbohydrate-binding protein that selectively binds to glycans found on the inner leaflet of endosomal membranes.[22, 23] Using cells genetically engineered to constitutively express a Gal8-mRuby fusion protein, we characterized the endosomal disruption capabilities of nanocarriers by quantifying the fluorescent puncta that formed following Gal8-mRuby clustering on damaged endosomal membranes, building upon the Gal8 recruitment assay using PEG-(DMAEMA-*co*-BMA) siRNA NPs by Kilchrist et al.[24] We adapted this approach to a high-throughput, widefield imaging assay to simultaneously study how cellular internalization and endosomal disruption correlated with nucleic acid delivery efficacy of biodegradable poly(beta-amino ester)s (PBAEs) and other common materials for nucleic acid delivery. For PBAEs specifically, we systematically varied polymer backbone hydrophobicity as well as polymer end-cap structure to probe structure-function relationships. The predictive capacity of this dual cellular uptake and endosomal disruption assay was compared to that of several polymer and NP physiochemical properties such as polymer nucleic acid binding strength, pH buffering capacity, predicted LogP value, NP hydrodynamic

diameter, and zeta potential. The effects of nucleic acid cargo type as well as cell type for *in vitro* transfection were investigated. In total, a library of 22 PBAEs with unique chemical structures were screened as well as widely used commercially available transfection reagents such as Lipofectamine™ 3000, polyethyleneimine (PEI), and poly-L-lysine (PLL). Finally, we examined whether our new *in vitro* screening assays correlated with systemic *in vivo* delivery efficacy of polymeric NPs encapsulating mRNA upon tail-vein injection in mice. The data presented here demonstrate the robustness of this image-based dual NP uptake and endosomal disruption NP screening system across a broad range of materials for mRNA delivery efficacy *in vitro* as well as *in vivo*. Such a quantitative, high-throughput screening platform with high predictive capacity for delivery efficacy has important implications for the standardization of the optimization and testing of novel materials for non-viral gene delivery and genetic medicine.

Results

High-Content Imaging of NP Uptake and Endosomal Disruption

We engineered B16-F10 murine melanoma cells to genetically encode a Gal8-mRuby endosomal disruption sensor to facilitate simultaneous characterization of NP uptake and endosomal disruption. NP uptake was measured by quantifying Cy5 puncta resulting from intracellular delivery of NPs carrying Cy5-labeled nucleic acids; endosomal disruption was measured by quantifying mRuby puncta resulting from Gal8-mRuby clustering at damaged endosomal membranes (**Figure 8-1A**). This dual NP uptake and endosomal disruption assay was performed in a high-throughput manner using a CellInsight CX7 LZR high content imager capturing 20 fields of view per well of a 96-well plate at 20X magnification. An image analysis algorithm was then optimized and used to identify cells by extrapolating the cell body surrounding Hoechst 33342-stained cell nuclei and provide puncta counts per cell (**Figure 8-1B**). On average, intracellular puncta count was collected for over 15,000 cells per NP formulation.

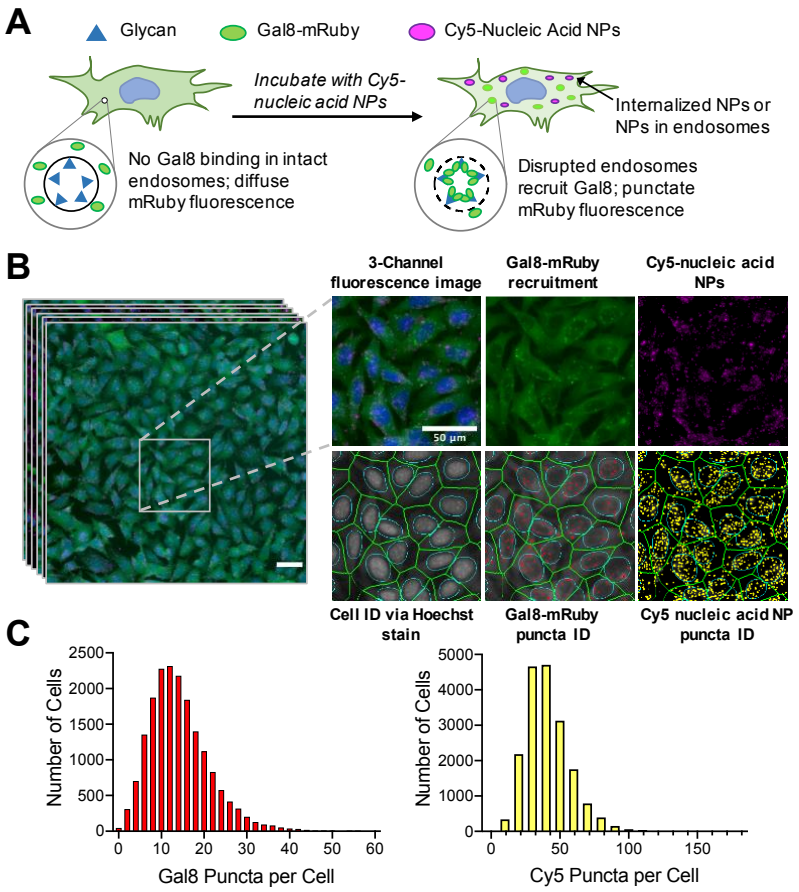

Figure 8-1. Image-based analysis of NP uptake and Gal8 endosomal disruption assay. (A) Assay overview: cells genetically encoding a Gal8-mRuby fusion fluorescence protein exhibited diffuse cytosolic mRuby signal in the absence of endosomal disruption. Endosomal disruption caused by NPs carrying Cy5-labeled nucleic acid NPs allow Gal8-mRuby to bind to intra-endosomal glycans, resulting in punctate fluorescent spots. **(B)** A typical field-of-view (taken from 80 per NP formulation) imaged by high-throughput fluorescence microscopy of B16-F10 murine melanoma cells after 6 h exposure to PBAE NPs carrying Cy5-mRNA. Cell identification was done using Hoechst 33342 staining of cell nuclei. Identification of Gal8-mRuby puncta and Cy5 puncta were used to quantify endosomal disruption and NP uptake, respectively. Scale bars = 50 □ m. **(C)** Representative distributions of the Gal8 puncta or Cy5 puncta count per cell obtained from image analysis data.

To identify the optimal time point to conduct the assay, we performed a time course experiment in which B16-mRuby-Gal8 cells were incubated with PBAE NPs for up to 30 h and imaged at select time points. We found that the Cy5 and Gal8 puncta counts both peaked at 6 h post-transfection for most nucleic acid cargo types and generally decreased thereafter (**Figure 8-S1**), guiding us to perform this assay at 6 h for all remaining experiments. The decreases in Gal8 and Cy5 puncta over time are consistent with expected autophagy timelines for damaged endocytic vesicles.[25]

Effects of PBAE Backbone Hydrophobicity

We synthesized two series of PBAE polymers with varying hydrophobic monomer content to investigate the effects of polymer backbone hydrophobicity on NP uptake, endosomal disruption, and transfection capabilities. These were first synthesized as lipophilic PBAE terpolymers consisting of a linear diacrylate (B7) copolymerized with a hydrophilic amine (S90) and a hydrophobic amine (ScX) synthesized via Michael Addition reactions (**Figure 8-2**). Polymer hydrophobicity was varied in one series by incorporating hydrophobic amines of varying lipid tail length at 30 mol % and in a second series by varying the molar content of the Sc12 monomer. Polymers in both series were then end-capped with monomer E63 to create PBAE quadpolymers and molecular weight was found to be in the range of 4-10 kDa. All polymers were found to rapidly self-assemble into NPs with plasmid DNA, mRNA, and siRNA after simple pipette-mixing in aqueous buffer. NPs encapsulating nucleic acid cargo were 100-400 nm in diameter with positive zeta potential in the range of 30-60 mV (**Figure 8-S2**).

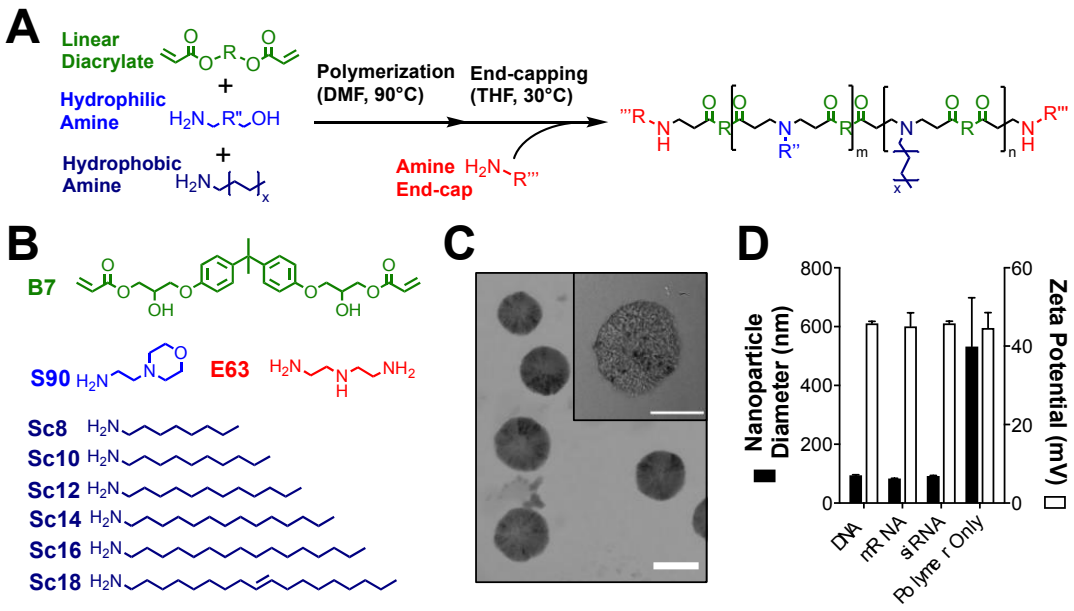

Figure 8-2. Chemical structure and characterization of PBAE NPs. (A) PBAE synthesis via 2-step Michael Addition reactions for linear, end-capped polymers **(B)** Structures of diacrylate (B), hydrophilic side chain (S), hydrophobic side chain (Sc), and endcap (E) monomers used in the synthesis of backbone hydrophobicity variation polymer series. **(C)** Representative TEM image of 7-90,c12-63, 50%-Sc12, mRNA NPs formulated at 60 w/w with 10% DMG-PEG2k and dialyzed into PBS. Scale bar = 100 nm. **(D)** DLS measurements of z-average NP hydrodynamic diameter and zeta potential of 7-90,c12-63, 50%-Sc12 NPs formed at 60 w/w and diluted into PBS. Data shown as mean + SD; n = 3.

We next assessed NP uptake, endosomal disruption, and gene delivery efficacy. In both PBAE polymer series, increasing polymer backbone hydrophobicity generally increased nucleic acid uptake and transfection in all three nucleic acid modalities (**Figure 8-3A**). The opposite was true for Gal8 endosomal disruption, where the polymer containing 100% Sc12 (most hydrophobic) resulted in half of the Gal8-mRuby puncta count compared to the polymer containing 0% Sc12 (least hydrophobic). Commercially available gene delivery materials were used to provide a benchmark for the bioassays. Of the five commercially available materials tested, Lipofectamine™ 3000 enabled the highest transfection across all nucleic acid types, followed by 25 kD branched PEI. Transfection by siRNA NPs was assessed by siRNA mediated GFP knockdown in

cells engineered to be GFP+, while transfection by DNA and mRNA NPs was assessed by GFP expression resulting from functional delivery of DNA or mRNA encoding the GFP gene in non-GFP+ cells. Transfection with these commercially available materials correlated positively with endosomal disruption (Spearman's coefficient of 0.68), and no significant correlation with NP uptake was observed. The Gal8 puncta counts for these materials were much lower than those achieved by PBAE NPs even when transfection efficacy was similar, suggesting that the two classes of materials utilize different mechanisms to enable endosomal disruption.

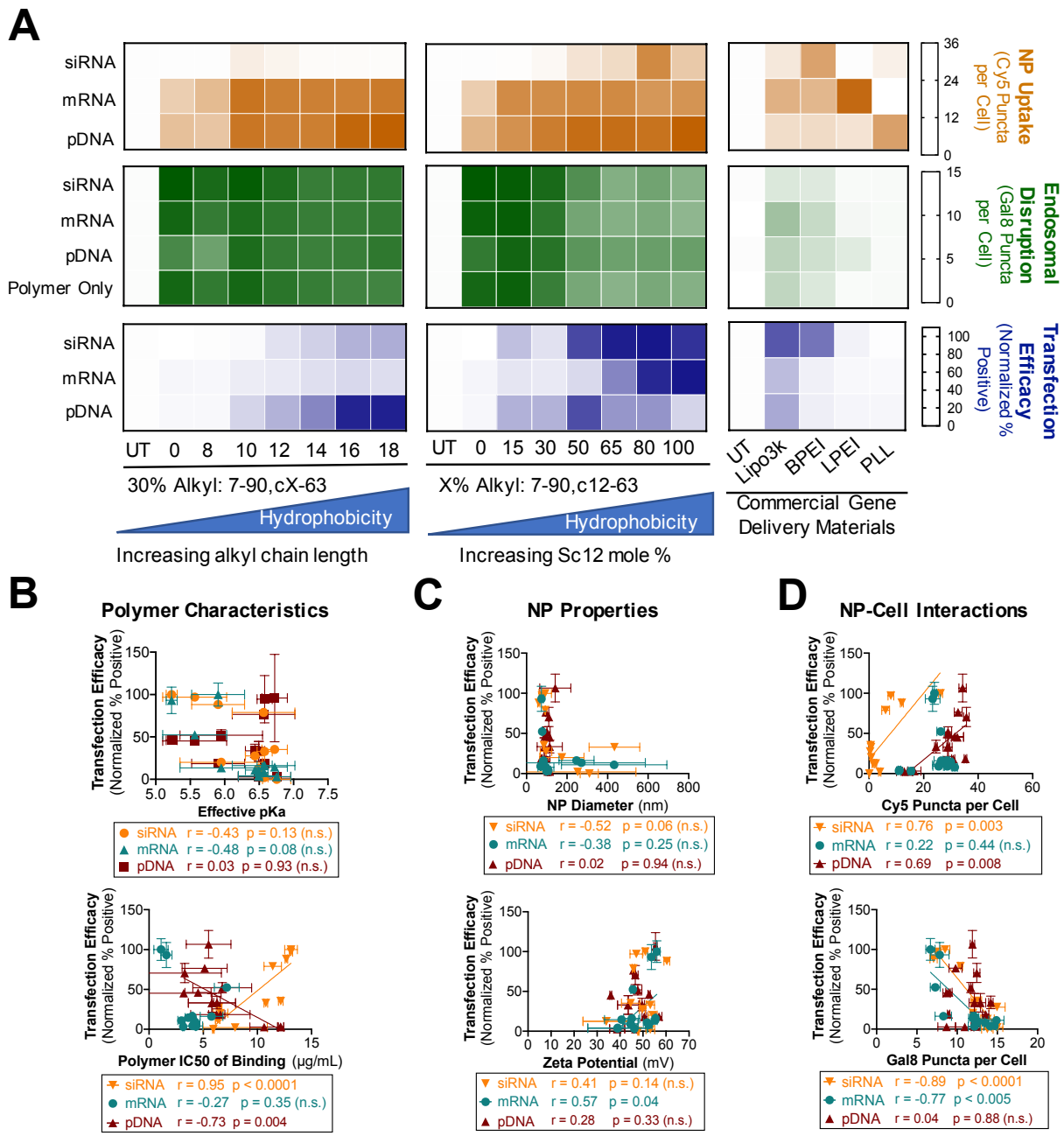

Figure 8-3. Validation of dual nanoparticle uptake/Gal8 endosomal disruption assay in PBAE nanoparticles and commercial reagents delivering different nucleic acid cargos to B16-F10 cells. (A) Heatmaps summarizing nanoparticle uptake, Gal8 endosomal disruption, and transfection efficacy data. Uptake and Gal8 data were obtained from high-throughput imaging analysis. Transfection efficacy was assessed by flow cytometry. For DNA and mRNA delivery, GFP fluorescence intensity for each formulation

was normalized to the max fluorescence intensity across all treatment conditions. siRNA-mediated GFP knockdown was quantified by normalizing the percent GFP+ cells for siGFP treated wells to the corresponding formulation delivering scRNA control. Data presented as the mean of 4 replicate wells. Transfection efficacy of nanoparticles formed with PBAE polymers encapsulating all nucleic acid types was plotted against common predictor readouts such as **(B)** various polymer characteristics, **(C)** nanoparticle properties, and **(D)** nanoparticle-cell interactions. Correlation significance was assessed for PBAE nanoparticles using Spearman's method, and data sets with statistically significant correlations were indicated with fitted lines. Data presented as mean ± SD, N=4.

We further assessed the predictive capacity of various polymer and NP properties on transfection efficacy. The polymer IC50 of nucleic acid binding, with larger values indicating weaker nucleic acid binding affinity, correlated negatively with DNA transfection but positively with siRNA knockdown. This may be due to the different intracellular sites of action for each nucleic acid. Plasmid DNA needs to reach the nucleus and strong initial binding could facilitate nuclear trafficking and maximize likelihood of transfection in each cell. On the other hand, siRNA needs to only be released to the cytosol to be active, and thus weaker polymer-nucleic acid binding could enable quicker and more effective cargo release and activity. mRNA transfection was not observed to correlate significantly with nucleic acid binding affinity in these experiments (**Figures 8-3B and 8-S4**). Standard biophysical characterization measurements of NP size and zeta potential showed no significant correlations with transfection efficiency (**Figure 8-3C**). The NP-cell interactions quantified by our new high-throughput and high-content imaging-based assay showed that PBAE transfection generally correlated positively with NP uptake and negatively with Gal8 endosomal disruption (**Figure 8-3D**). The negative correlation between transfection and endosomal disruption levels in this series of PBAE NPs was surprising, although, even at their lowest, the endosomal disruption levels achieved with the PBAE NPs were significantly higher than those induced by the commercial gene delivery materials. Thus, all PBAE NPs evaluated may be above a critical threshold of endosomal disruption capacity necessary to enable functional nucleic acid delivery that is at least equal to or greater than the endosomal disruption

capacity achieved by commercial gene delivery materials. The data indicated that in these experiments endosomal disruption was not a major transfection bottleneck for PBAEs. Interestingly, empty PBAE polymeric NPs in the absence of nucleic acids resulted in equivalent levels of endosomal disruption as NPs loaded with nucleic acids (**Figure 8-3A)**. This may explain why certain PBAE NP formulations less effective at transfection nonetheless exhibited high levels of endosomal disruption as these polymers may have formed a larger fraction of empty NPs. Such empty PBAE NPs could lead to a high Gal8 puncta count, indicating endosomal disruption, but would do so in a non-productive manner as no nucleic acids would be delivered to the cytosol. Interestingly, PBAE transfection with this series of polymers also did not correlate significantly with the polymers' effective pKa, as quantified in the physiologically relevant pH range (**Figures 8-3B, 8-S3, and 8-S5A**), which also reinforces that endosomal disruption is not a rate-limiting step for these PBAE NPs to achieve intracellular delivery under these conditions. Other polymer properties such as the predicted LogP value, which is a measure of polymer hydrophobicity, showed strong positive correlations with transfection for all three cargo types (**Figure 8-S5B**), further confirming our hypothesis that increased backbone hydrophobicity improves polymeric gene delivery efficacy.

Effects of Polymer End-groups

We next investigated the effects of polymer end-group structure on NP uptake and endosomal disruption by synthesizing an end-group variation polymer series by utilizing a moderately hydrophobic PBAE terpolymer backbone (7-90,c12-X, 50%-Sc12) and then independently conjugating 11 different end group monomers to it (**Figure 8-4A**). Previous work by our lab has shown that polymer end-group structure can play an important role in imparting biomaterial-mediated, selective transfection in certain cell types over others[26, 27] and that these effects may be due to changes in NP uptake pathways.[28] We hypothesized that our dual NP uptake/endosomal escape assay could be useful in further ascertaining how polymer end-group structure affect NP function in different cell types. To test this hypothesis, and to further evaluate the robustness of our new high-throughput and high-content bioassay, we evaluated these polymers on 3 different cell types induced to express the Gal8-mRuby construct: B16-F10 murine melanoma cells, RAW

264.7 murine macrophages, and NIH/3T3 murine fibroblasts. Our results showed highest mRNA transfection levels in B16-F10 cells, medium transfection in RAW 264.7 macrophages, and lowest transfection levels in NIH/3T3 fibroblasts (**Figure 8-4A**). Endosomal disruption showed positive correlations with mRNA transfection levels in RAW and 3T3 cells but not B16 cells, with a significant positive correlation when all three cell lines were evaluated together (**Figure 8-4B**). This effect is particularly striking for more difficult-to-transfect cell types such as RAW 264.7 and NIH/3T3 cells (Spearman's coefficient of 0.92 and 0.67, respectively), which suggests that mRNA transfection efficacy in difficult-to-transfect cells may largely be attributable to barriers in endosomal escape. Interestingly, the highest NP uptake levels were observed in NIH/3T3 cells, which demonstrated the lowest levels of mRNA transfection, and in general mRNA transfection did not show significant correlations with PBAE NP uptake among these cell types (**Figure 8-4C**). Collectively, these results suggest that for PBAEs with the same polymer backbone (and similar hydrophobicity), end-group structure plays an important role in endosomal disruption. These results also indicate that for these PBAEs, endosomal disruption, rather than NP uptake, is acting as a greater bottleneck for effective mRNA delivery. Differing levels of resistance to endosomal disruption among different cell types may also at least partially explain the differential transfection levels observed among these cells.

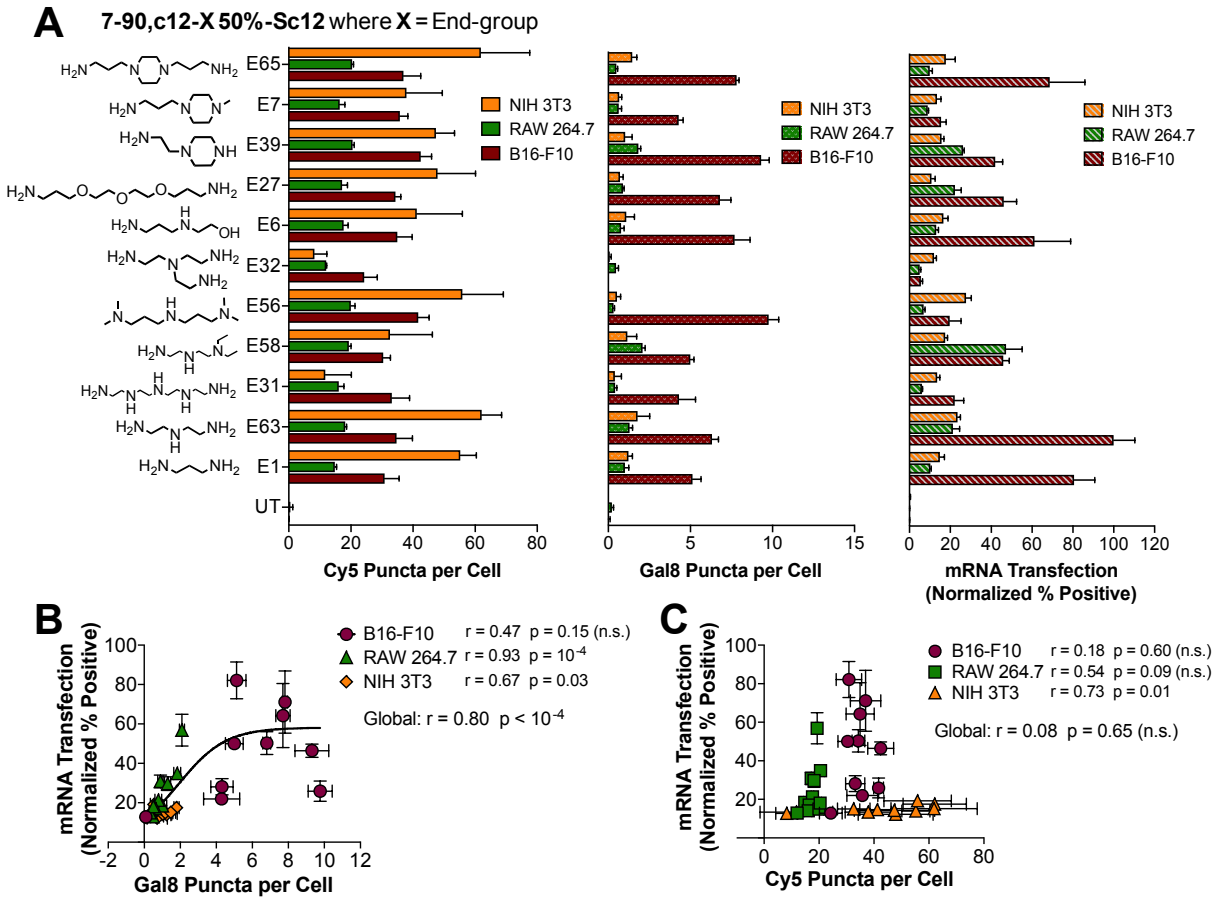

Figure 8-4. Effects of polymer end-group structure on mRNA transfection efficacy in multiple cell lines. (A) NP uptake, Gal8 puncta count, and mRNA delivery efficacy of polymer end-group variation PBAE library on three different cell lines. Transfection efficacy was plotted against **(B)** Gal8 puncta count indicating endosomal disruption or **(C)** Cy5 puncta count indicating NP uptake. Data presented as mean ± SD, $n = 4$. Correlation significance in **(B)-(C)** were calculated using Spearman's method; a hyperbolic curve was fitted in **(B)** to indicate a statistically significant correlation.

In Vivo mRNA Delivery: Whole-Body and Organ Level Expression

We next characterized the *in vivo* mRNA delivery capabilities of PBAE NPs after intravenous administration of NPs encapsulating mRNA encoding firefly luciferase (fLuc) to mice. For these experiments, NPs were formulated with the PEG-lipid DMG-PEG2k and dialyzed in PBS. Previous incorporation of

PEG-lipids into related PBAE NPs has been shown to enhance serum stability and *in vivo* mRNA expression.[29, 30] Incorporation of DMG-PEG2k into the PBAE quadpolymers was observed to decrease NP size and neutralize surface charge (**Figure 8-S8**). Dialysis and PEG-lipid coating did not significantly change transfection efficacy or endosomal disruption *in vitro*, though NP uptake was reduced. Upon *in vivo* administration, PEG-coated and dialyzed NPs enabled significantly higher mRNA expression compared to NPs without PEG coating, and this increased expression was predominately due to increased expression in the liver (**Figure 8-S8F-G**).

Four polymers with 0-80% Sc12 content in the polymer backbone and five polymers with different polymer end-groups were chosen to assess the effects of polymer backbone and end-group structure on *in vivo* expression. On the whole-body level, increased backbone hydrophobicity generally resulted in increased mRNA expression (**Figures 8-5B-C and 8-S6**) while polymer end-group variation resulted in differential *in vivo* expression levels (**Figures 8-5D and 8-S7**). Interestingly, overall *in vivo* expression correlated positively with *in vitro* transfection of B16-F10 cells (**Figure 8-5E**), indicating that *in vitro* screening had predictive capacity for *in vivo* performance with these nanomaterials. At the level of individual organs, increasing backbone hydrophobicity increased expression in all of the organs evaluated (**Figure 8-5F**), while polymer end-group played a major role in targeting NP expression to specific organs (**Figure 8-5G**). Indeed, when expression in the lungs and spleen was normalized to that in the liver, polymer E1 showed preferential expression in the spleen, polymer E63 in the liver, polymer E58 in the lungs, and polymer E39 was almost equally split between the lungs and spleen (**Figure 8-5H**).

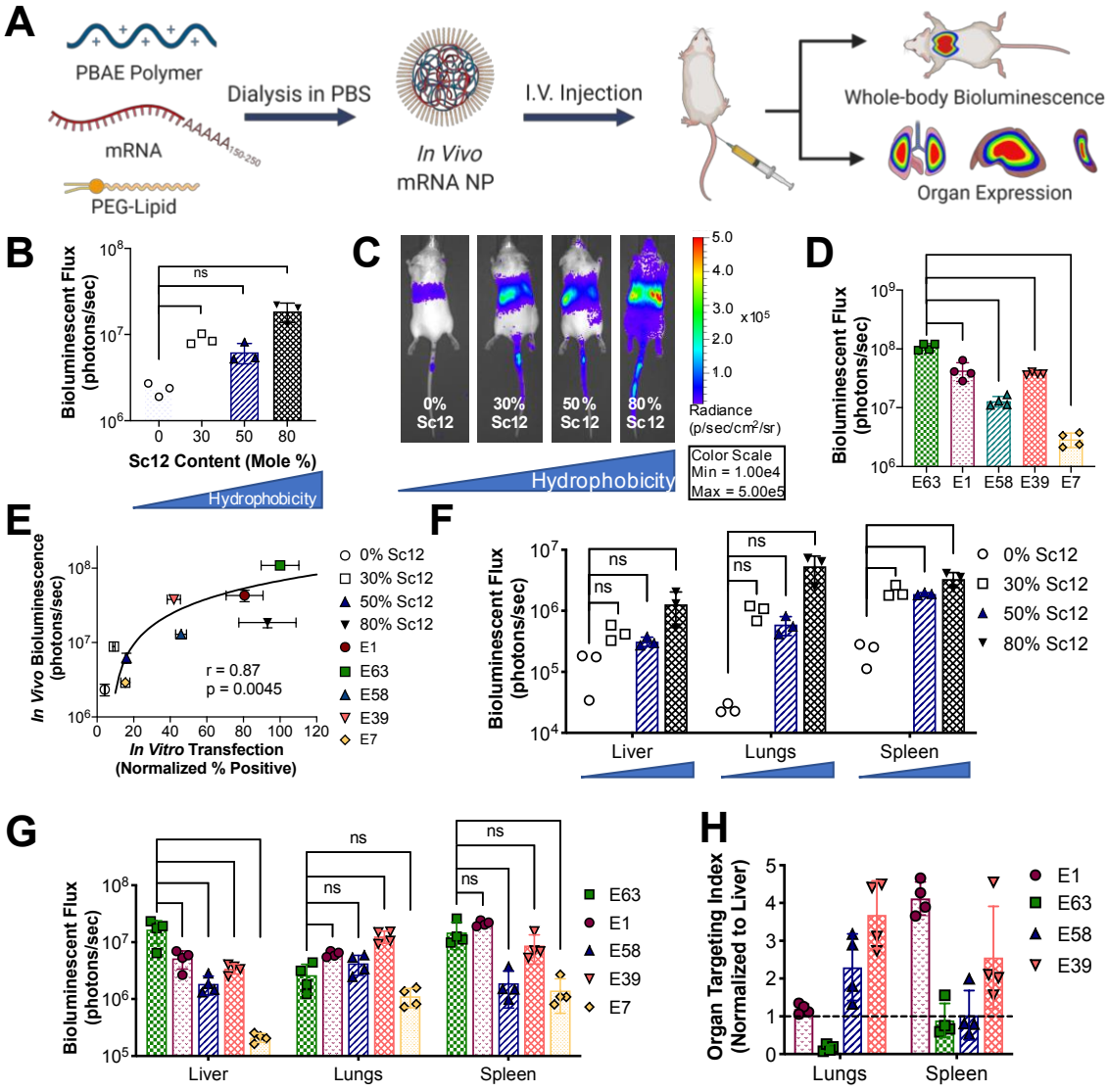

Figure 8-5. ***In vivo*** **validation of PEG-coated PBAE NPs delivering mRNA. (A)** Schematic depicting the experimental workflow. PBAE polymers were dialyzed with fLuc mRNA and the PEG-lipid DMG-PEG2k in PBS to form PEG-coated mRNA NPs, which were administered intravenously. fLuc expression was assessed 24 h after NP injection. **(B)** Whole body bioluminescence was assessed for NPs formulated with PBAEs with differential backbone hydrophobicity and **(C)** representative IVIS images (N = 3). **(D)** Whole body bioluminescence quantification for NPs formulated with 50%-Sc12 PBAEs with different end-groups (N = 4). **(E)** *In vivo* transfection efficacy (from **(B)** and **(D)**) was plotted against *in vitro* transfection in B16 cells. Spearman's correlation was used to measure the strength of association between the two variables. Organ bioluminescence in the most highly expressing organs when varying **(F)** polymer backbone

hydrophobicity (blue triangles below organ labels indicate increasing backbone hydrophobicity) and **(G)** polymer end-group structure. Statistical significance was determined using one-way ANOVA with Dunnett's post-hoc analysis comparing against the least hydrophobic polymer (0% Sc12) in **(B**) and (**F)** and against end-group E63 in **(D)** and **(G)**. *$P < 0.05$, **$P < 0.01$, ***$P < 0.001$, and ****$P < 0.0001$. ns, not significant. **(H)** The organ targeting index as calculated by normalizing bioluminescent flux in each non-liver organ against that of the liver was calculated for the lungs and spleen in high-expressing polymers of the polymer end-group variation series (E7 was excluded due to minimal expression observed). Dotted black line indicates liver expression level. $N = 4$. Data presented as mean ± SD in all bar graphs.

In Vivo mRNA Delivery: Expression in Different Cell Types

We further probed the cell populations that were transfected in each organ using the Ai9 mouse model, which contains a floxed expression stop cassette upstream of a tdTomato reporter gene. NPs encapsulating Cre mRNA were administered via tail vein injection into Ai9 mice, and transfected cells underwent Cre-Lox recombination, resulting in tdTomato expression that was measured by flow cytometry 3 d post-injection (**Figure 8-6A**). For this study, we used 7-90,c12-63, 80%-Sc12 NPs as they were found to enable high *in vivo* mRNA expression levels from fLuc mRNA experiments. We found that 7-90,c12-63, 80%-Sc12 NPs systemically administered transfected nearly 0.2% of the cells in the spleen, 2% of the cells in the liver, and 4% of the cells in the lungs, with minimal transfection levels seen in any of the other organs evaluated (**Figure 8-6B**). Over 20% of endothelial cells in the lungs were transfected following systemic injection, which is consistent with previous reports for related PBAE structures,[29] in addition to significant populations of macrophages and dendritic cells in the lungs (**Figure 8-6C**). Endothelial cells also made up a large fraction of the transfected cells in the liver (33%) and spleen (23%) (**Figure 8-6D**).

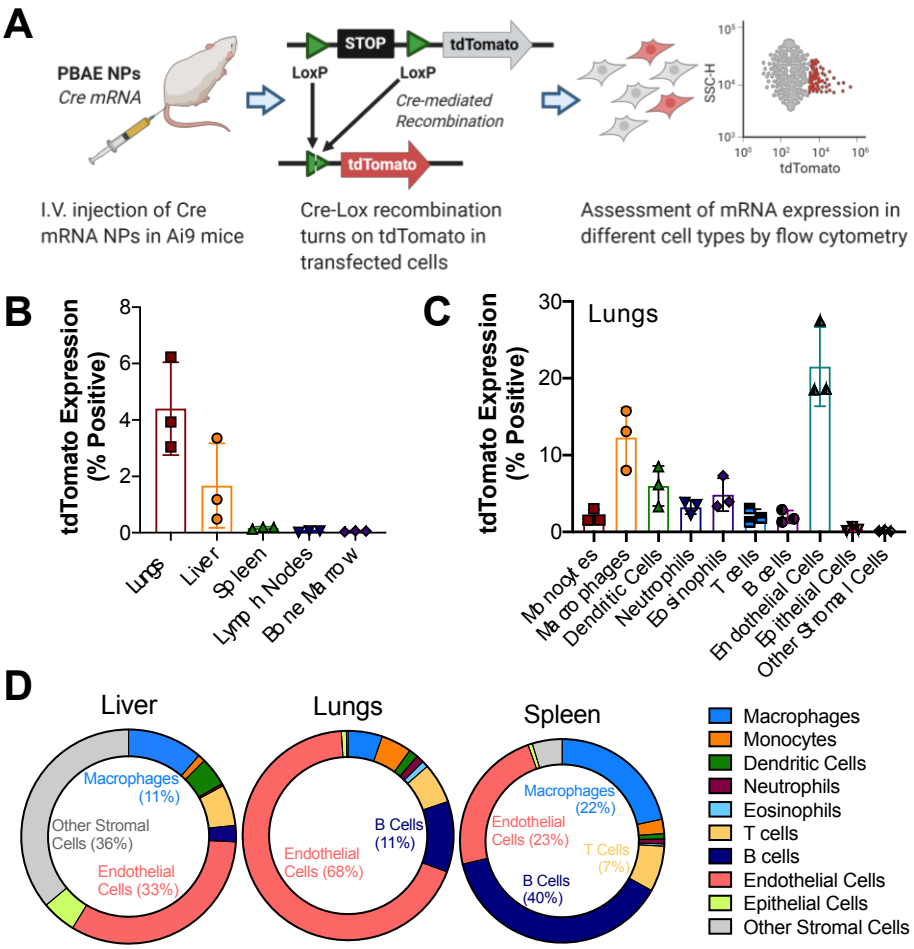

Figure 8-6. Assessment of *in vivo* mRNA transfection in different cell types. (A) Experimental workflow: Ai9 mice were injected with PEG-coated 7-90,c12-63, 80%-Sc12 NPs encapsulating Cre mRNA and single cell level transfection could be detected by tdTomato expression, which was quantified 3 days post-injection using flow cytometry. **(B)** tdTomato+ cells as a percentage of the total cell population in each of several major organs. **(C)** tdTomato expression in the lungs in different cell types (tdTomato+ cells as a percentage of the overall population of each cell type). **(D)** Distribution of tdTomato+ cells across different cell types in liver, lungs, and spleen. $N = 3$. Data presented as mean ± SD in bar graphs.

Discussion

To realize the full therapeutic potential of mRNA therapeutics, a high-throughput, standardized NP screening platform capable of quantitatively evaluating intracellular delivery steps with great predictive

capacity for transfection efficacy is needed. In this study, we developed a high-throughput, high content, imaging-based screening platform designed to simultaneously assess the cellular internalization and endosomal disruption capabilities of nucleic acid delivery NPs, requiring only wide-field, epifluorescence microscopy to enable full assessment of the cytosolic compartment. This bioassay was developed to be implemented in multiwell plates, enabling the evaluation of many intracellular events per cell, in thousands of replicate cells per condition, with up to 96 conditions per plate. Endosomal sequestration has long been identified as a major bottleneck to functional RNA delivery in multiple NP systems,[31, 32] but quantitative evaluation of endosomal disruption has been limited to low-throughput imaging methods requiring specialized microscopy modalities.[16, 21] We utilized a genetically encoded endosomal disruption sensor based on the natural clustering of Gal8 molecules at damaged endosomal membranes to detect NP induced endosomal disruption quantified at the level of intracellular events within single cells. Simultaneously, cellular internalization of NPs could be tracked by delivering nucleic acids labeled with a different fluorophore. We hypothesized that this dual NP uptake and endosomal disruption assay could provide useful information on structure-function relationships when used to screen several NP gene delivery systems.

We used two series of PBAE quadpolymers to validate this screening platform. PBAEs are cationic, biodegradable polymers that have been shown to be highly effective at *in vitro* delivery of plasmid DNA,[33] siRNA,[34] mRNA,[29] and protein cargos.[35] The highly modular nature of these polymers facilitate combinatorial library synthesis via Michael Addition of small molecule precursors, making it possible to systematically vary polymer backbone or end-group characteristics to directly probe the effects of incremental differential polymer structural changes on downstream nucleic acid delivery efficacy. The PBAE quadpolymer is the majority component of all our NP delivery formulations, including systemically administered *in vivo* formulations, which have 10% PEG-lipid incorporated as a second component, without the presence of other lipids or cholesterol. This approach differs significantly from many previously studied lipid-based NP systems, in which the NP formulation was changed primarily by varying the ratios of incorporated lipids[36] or the structure of the ionizable lipid in a NP system consisting of multiple lipid components.[11]

Two polymer series in which polymer backbone hydrophobicity were modulated by varying the content of lipophilic side chain monomers were synthesized to probe the effect of polymer backbone structure on cellular interactions of polymeric NPs. Traditional metrics of predicting NP function, such as polymer nucleic acid binding affinity, endosomal pH buffering potential, NP hydrodynamic diameter, and zeta potential, generally correlated poorly with functional delivery efficacy of multiple nucleic acid cargos, highlighting the need for new metrics for rapid and meaningful NP screening. The dual NP uptake and endosomal disruption assay presented here showed significant correlations with transfection efficacy for all nucleic acid cargos tested. NP uptake correlated positively with transfection (global $r = 0.55$, $p < 0.001$). Endosomal disruption correlated negatively with transfection for these PBAE NPs (that each had greater endosomal disruption capacity than that achieved by the commercial gene delivery materials) ($r = -0.57$, $p < 0.0001$). The negative correlation with endosomal disruption is surprising, but may be attributed to the formation of polymer-only NPs that do not contain nucleic acid cargo. Amphiphilic PBAEs like the ones presented in this study have been reported to form polymer-only micellar NPs without any nucleic acid.[37] Thus, PBAEs that are effective at endosomal disruption, but not efficient at leading to transfection, may be forming large populations of polymer-only NPs empty of nucleic acid cargo. When these polymer-only NPs are internalized by cells, they could enable endosomal disruption, resulting in high Gal8 counts but low transfection. When this dual NP uptake/Gal8 endosomal disruption assay was applied to commercial gene delivery materials such as Lipofectamine 3000, branched and linear PEI, and PLL, endosomal disruption as indicated by Gal8 puncta count was significantly lower for all of these commercial materials than the PBAE NPs, which for the most part also resulted in lower transfection efficacy compared to PBAE NPs. Transfection of these positive control materials correlated positively with endosomal disruption for all cargo types (global $r = 0.68$, $p = 0.02$). Taken together, our data show that a threshold for endosomal disruption, as defined by the amount achieved by the most effective commercial transfection reagent Lipofectamine 3000 ($\geq$ 2 Gal8 puncta per cell in B16-F10 cells), must be reached in order for gene delivery to efficiently occur. PBAE NPs generally enabled endosomal disruption levels significantly above this threshold in the B16-F10 cells evaluated here and resulted in generally high transfection levels, while commercial materials such as

linear PEI and PLL enabled endosomal disruption levels below this threshold and consequently showed negligible transfection levels. The lack of high transfection of PBAE NPs across the board indicates that delivery obstacles further downstream (such as intracellular trafficking or cargo release) may pose significant delivery challenges for some of these materials.

Previous studies have shown that the structure of PBAE polymer end-groups can significantly alter the transfection efficacy of the backbone polymer as well as impart biomaterial-mediated selectivity in transfection of certain cell types.[26-28] We synthesized a polymer series with a common backbone but varying end-group structure and evaluated mRNA delivery efficacy on three cell lines. The endosomal disruption levels of these polymers had positive correlations with transfection efficacy, which were strongest in more difficult-to-transfect cell lines as indicated by Spearman's coefficients (r) that are closer to 1; $r = 0.93$ for difficult-to-transfect RAW 264.7 cells but $r = 0.47$ for easier-to-transfect B16-F10 cells. Differences observed in transfection efficacy were not attributable to polymers' pH buffering capabilities, which varied with backbone structure but were generally unaffected by end-group structure. Even in the 7-90,c12-63 X% alkyl side chain polymer series, in which the effective pKa decreased with increasing hydrophobic Sc12 content in the polymer backbone, the correlation between pH buffering and transfection efficacy was poor. This is in contrast to an observation recently reported by our group with hyperbranched PBAEs, where increasing polymer branching by incorporation of a triacrylate monomer in the backbone increased both effective pKa and transfection[33] suggesting that different classes of PBAE polymer structures can enable endosomal escape via differing mechanisms. In the case of the linear lipophilic PBAE quadpolymers, the endosomal disruption mechanism may rely on the lipophilicity of the polymers causing them to associate with and directly interact with the endosomal membrane, where the charged polymer end-groups may cause transient pore formation that leads to NP leakage out of damaged endosomes, similar to that observed with lipid materials,[16, 32] rather than acidic buffering-induced complete endosomal rupture as proposed by the proton sponge hypothesis.[21] NP uptake of the end-modified linear PBAEs did not correlate significantly with mRNA transfection efficacy ($r = 0.22$, $p = 0.44$), although a significant positive correlation was observed when PBAE NPs carrying each of the three nucleic acid cargos were analyzed globally (global $r = 0.55$, $p < 0.001$). Collectively, our data

suggest that endosomal escape is the primary barrier in mRNA delivery to more difficult-to-transfect cells and that the differential gene delivery efficacy mediated by polymer end-groups is largely due to their ability to facilitate endosomal disruption.

Finally, we validated these PBAE NPs for *in vivo* mRNA expression following tail vein injection into mice. NPs formulated by simple mixing of mRNA and polymer in aqueous buffer yielded significantly lower transfection, particularly in the liver, than similar formulations with 10% PEG-lipid dialyzed into the NPs. Using dialyzed PEG-coated formulations, we saw that *in vivo* mRNA expression levels correlated strongly with *in vitro* transfection efficacy in B16-F10 cells, indicating a predictive capacity that is rare in large library screens.[38] Increasing polymer backbone hydrophobicity increased whole-body mRNA expression in general, following trends that we observed *in vitro*, and which could also be due in part to improved incorporation of PEG-lipid in hydrophobic formulations which could lead to more stable NPs in the blood.[30] Similar to differential transfection of various cell types *in vitro*, polymer end-group variation also led to tuning of organ tropism *in vivo*. Unlike most lipid NP formulations which have been demonstrated to predominantly target liver hepatocytes,[39, 40] the four top performing NP formulations from the *in vitro* mRNA transfection screens in the end-group variation polymer series exhibited alternative patterns of expression in non-liver organs, with preferential transfection in the lungs and/or spleen. Particularly high expression was seen in the lungs for most formulations, which is consistent with previous reports by Kaczmarek *et al.* utilizing related PBAE lipid-polymer NP formulations for mRNA delivery.[29] Within each organ, multiple cell types were transfected, including endothelial cells, B cells, and macrophages, all of which have distinct clinical relevance. The lipophilic side chains of the polymers enabled the PEG-lipid DMG-PEG2k to be easily incorporated into NP formulations via dialysis, which increased *in vivo* expression by an order of magnitude compared to NPs without PEG-lipid coating despite slightly lowering *in vitro* transfection. Cheng *et al.* recently reported that incorporation of selective organ targeting (SORT) molecules at defined ratios enabled highly targeted mRNA expression in select organs and that these molecules maintained their organ targeting capabilities across multiple lipid NP platforms.[41] This suggests intriguing future directions where an innate organ tropism of

PBAE NP formulations could perhaps be combined with other technologies to enhance selective organ targeting, and potentially cell-type specific targeting.

In summary, we have reported a high content high throughput quantitative imaging assay capable of simultaneously quantifying NP uptake and endosomal disruption. This assay is robust, has higher predictive capacity for *in vitro* mRNA delivery efficacy compared to conventionally used metrics of polymer or NP properties, and can be performed with ~100 nanoparticle formulations in a few hours. Assay validation using PBAE NPs elucidated structure-function relationships through incremental changes in both the polymer backbone and end-groups for these highly modular polymers. Moreover, we showed that this assay is generally applicable across all major nucleic acid types, several different cell lines, and multiple gene delivery systems. The NP screening platform presented herein can be a useful tool for high-throughput identification of promising candidates for gene delivery and further elucidation of structure/function relationships for the delivery of DNA, siRNA, and mRNA. Lead nanomaterials composed of PBAE quadpolymers demonstrated safe and effective delivery of mRNA *in vivo*, including organ-targeted expression based on polymer structure. PEGylated PBAE NPs enabled significant exogenous mRNA expression differentially to the liver, lung, and spleen. Critically, nanomaterial formulations identified as lead candidates *in vitro* also performed well for *in vivo* mRNA delivery following systemic intravenous injection. Such a broadly applicable screening method provides a new metric for nanomaterial characterization, which is important for directly comparing and contextualizing the myriad NP systems that have been reported in the burgeoning field of intracellular gene delivery. With further study, the PBAE-based materials investigated here may be promising for mRNA delivery to promote human health.

Materials and Methods

Materials

Bisphenol A glycerolate (1 glycerol/phenol) diacrylate (B7; CAS 4687949), 4-(2-aminoethyl)morpholine (S90; CAS 2038-031), octylamine (Sc8; CAS 111-86-4), 1-decylamine (Sc10; CAS 2016-57-1), oleylamine (Sc18; CAS 112-90-3), 1,3-diaminopropane (E1; CAS 109-76-2),

tetraethylenepentamine (E31; CAS 1112-57-2), N,N-diethyldiethylenetriamine (E58; CAS 24426-16-2), tris(2-aminoethyl)amine (E32; CAS 4097-89-6), 2-(3-Aminopropylamino)ethanol (E6; CAS 4461-39-6), 4,7,10-trioxa-1,13-tridecanediamine (E27; CAS 4246-51-9), and 1-(2-aminoethyl)piperazine (E39; CAS 140-31-8) were purchased from Sigma-Aldrich (St. Louis, MO). 1-Dodecylamine (Sc12; CAS 124-22-1) and 1-(3-aminopropyl)-4-methylpiperazine (E7; CAS 4572-031) were purchased from Alfa Aesar (Tewksbury, MA). Tetradecylamine (Sc14; CAS 2016-42-4) and hexadecylamine (Sc16; CAS 143-27-1) were purchased from Acros Organics (Pittsburgh, PA). Diethylentriamine (E63; CAS 111-40-0) was purchased from EMD Millipore (Burlington, MA). 3,3'-Iminobis(N,N-dimethylpropylamine) (E56; CAS 6711484) was purchased from Sant Cruz Biotechnology (Dallas, TX). 1,4-Bis(3-aminopropyl)piperazine (E65; CAS 7209-38-3) was purchased from MP Biomedicals (Solon, OH).

Plasmid eGFP-N1(Addgene 2491) was purchased from Elim Biopharmaceuticals (Hayward, CA) and amplified by Aldevron (Fargo, ND). Cy5-labeled plasmid DNA was synthesized following a method reported by Wilson et al.[42] 5-methoxyuridine-modified CleanCap® eGFP mRNA (L-7201), fLuc mRNA (L-7202), and Cy5-labeled mRNA (L-7702) were purchased from TriLink Biotechnologies (San Diego, CA). Negative control siRNA (1027281) was purchased from Qiagen (Germantown, MD). GFP siRNA targeting the sequence 5'-GCA AGC TGA CCC TGA AGT TC-3' (P-002048-01) was purchased from Dharmacon (Lafayette, CO). Cy5-labeled siRNA (SIC005) was purchased from Sigma Aldrich (St. Louis, MO). Plasmid DNA encoding a Gal8 fluorescent fusion protein was a generous gift from the lab of Dr. Craig Duvall and cloned into a PiggyBac transposon vector (PB-mRuby3-Gal8, Addgene #150815) for stable integration into mammalian chromosomal DNA.

Polymer Synthesis

Polymers were synthesized using previously reported protocols.[33] Briefly, diacrylate monomer B7 and side chain monomers (S90 and combinations of ScX monomers) were dissolved at 600 mg/mL in dimethylformamide (DMF) and reacted with stirring for 48 h at 90°C to allow polymerization via step-wise Michael Addition reactions. Monomers were reacted at an overall vinyl:amine ratio of 2.3 to allow acrylate-

terminated polymers to form. Polymers were end-capped by further reaction with primary amine-containing E monomers at room temperature for 2 h [200 mg/mL polymer and 0.3 M E monomer in tetrahydrofuran (THF)] and purified by 2 diethyl ether washes. Diethyl ether was decanted, dried thoroughly under vacuum, and polymers were dissolved in dimethyl sulfoxide (DMSO) at 100 mg/mL and stored at -20°C with desiccant in single-use aliquots.

Polymer Characterization

Polymer molecular weight was characterized using gel permeation chromatography (GPC) against linear polystyrene standards (Waters, Milford, MA). Polymers were dissolved in BHT-stabilized THF and filtered through 0.2-μm PTFE filters prior to GPC measurements. Predicted polymer LogP values were calculated using the online cheminformatics software molinspiration.com.

Polymer Buffering Capacity and Determination of Effective pKa

pH titrations were performed using a SevenEasy pH meter (Mettler Toledo, Columbus, OH) as previously described.[33] Briefly, 10 mg polymer was dissolved in 10 mL of 100 mM NaCl acidified with HCl and titrated from pH 3.0 to pH 11.0 via stepwise addition of 100 mM NaOH. To calculate the effective pKa of the polymer in the physiologically relevant pH range (pH 5-8), normalized buffering capacity was calculated from titration data as $\Delta(\text{-OH})/\Delta(\text{pH})$ for each titration point. Effective pKa was defined as the pH point corresponding to the maximum normalized buffering capacity.

Nucleic Acid Binding Assays

Ribogreen nucleic acid binding dye (Invitrogen, Carlsbad, CA) was mixed with nucleic acids in 25 mM magnesium acetate buffer ($MgAc_2$, pH 5.0) at a final nucleic acid concentration of 5 μg/mL (siRNA), 2.5 μg/mL (mRNA), or 1 μg/mL (pDNA) and a final 1:2000 RiboGreen dilution. Polymers were dissolved and serially diluted to a range of concentrations in $MgAc_2$, and 25 μL polymer solution was mixed with 75 μL nucleic acid/RiboGreen solution per well in 96-well black bottom assay plates. The solutions were incubated

at 37□ C for 20 minutes before fluorescence readings were taken on a Biotek Synergy 2 fluorescence multiplate reader (BioTek, Winooski, VT). To characterize nucleic acid binding affinity, the polymer IC50 of binding (polymer concentration at which 50% of RiboGreen fluorescence is quenched by RiboGreen displacement from polymer binding to nucleic acids) was calculated by plotting % fluorescence quenching as a function of polymer concentration and fitting a sigmoidal curve to the data. Polymer IC50 of binding varies inversely with binding affinity; lower IC50 values indicate higher binding affinity.

NP Formulation and Characterization

For *in vitro* studies, NPs were formulated in 25 mM magnesium acetate buffer ($MgAc_2$, pH 5) and added directly to cells without the addition of PEG lipids or dialysis. Polymers and nucleic acids (plasmid DNA, mRNA, or siRNA) were dissolved separately in 25 mM $MgAc_2$ at concentrations of 0.83 ng/μL for nucleic acids and 50 ng/μL for polymers, and mixed together via pipetting at a 1:1 volume ratio. NPs were allowed to self-assemble for 10 minutes at room temperature; the polymer-to-nucleic acid ratio was 60 by weight (60 w/w) for all experiments.

NP hydrodynamic diameter was measured via dynamic light scattering (DLS) using a Malvern Zetasizer Pro with universal dip cell (Malvern Panalytical, Malvern, United Kingdom). Samples were prepared in 25 mM $MgAc_2$ and diluted 1:6 in 150 mM PBS to determine NP characteristics in neutral, isotonic buffer. Zeta potential was measured by electrophoretic light scattering on the same instrument. Transmission electron microscopy (TEM) images were captured using a Philips CM120 transmission electron microscope (Philips Research, Cambridge, MA). 30 μL NP samples were allowed to coat 400-square mesh carbon coated TEM grids for 20 minutes. Grids were then rinsed with ultrapure water and allowed to fully dry before imaging.

Cell Culture and Cell Line Preparation

B16-F10 murine melanoma and RAW 264.7 murine macrophage cells were cultured in Dulbecco's Modified Eagle Medium (DMEM; ThermoFisher, Waltham, MA) supplemented with 10% FBS and 1%

penicillin/streptomycin. GFPd2+ B16-F10 cells used in siRNA knockdown experiments were established previously[35] and cultured using the same medium. NIH/3T3 murine fibroblasts were cultured in DMEM supplemented with 10% bovine calf serum and 1% penicillin/streptomycin. Cells were induced to constitutively express the Gal8-mRuby fusion fluorescent protein construct using the PiggyBac transposon/transposase system. The PiggyBac transposon plasmid carrying the Gal8-mRuby gene was created using restriction enzyme cloning and is available on Addgene (plasmid #150815). The transposase expression plasmid (PB200A-1) was purchased from System Biosciences (Palo Alto, CA). The transposon plasmid was co-transfected with the PiggyBac transposase plasmid using PBAE NPs as described below. mRuby+ cells were isolated using at least two rounds of fluorescence assisted cell sorting using a Sony SH800 Cell Sorter (Sony Biotechnology, San Jose, CA) to generate stably expressing cell lines.

Transfection

Cells were plated at 10,000 cells per well in 100 μL complete medium in CytoOne 96 well plates (USA Scientific, Ocala, FL) and allowed to adhere overnight. NPs were formulated following the *in vitro* transfection formulation described above; 20 μL NP solution was added to 100 μL fresh complete medium, and 120 μL per well of the NP medium mixture was used to replace the culture medium. For all *in vitro* transfections, NPs were formulated at 60 w/w delivering 50 ng nucleic acids per well. For cellular uptake experiments, 20% of the total nucleic acid drugs were replaced with Cy5-labeled nucleic acids prior to mixing with polymers. NPs were incubated with cells at 37°C for the appropriate duration, depending on assay conditions (6 h for dual uptake/Gal8 assay, 24 h for mRNA and siRNA transfections, and 48 h for DNA transfections).

For transfections using commercially available reagents, Lipofectamine™ 3000 (ThermoFisher) was used as instructed by the manufacturer. 25 kD branched polyethylenimine (BPEI), 2.5 kD linear polyethylenimine (LPEI), and 15 kD poly-L-lysine (PLL) were used at the highest concentrations that did not cause significant cytotoxicity (15 w/w for BPEI, 60 w/w for LPEI, and 30 w/w for PLL). PEI NPs were

formulated in 150 mM NaCl solution, and PLL NPs were formulated in 10 M HEPES buffer (pH 7); all formulations delivered 50 ng nucleic acids to match the dose delivered by PBAE NPs.

Transfection efficacy was evaluated via flow cytometry using a BD Accuri C6 flow cytometer (BD Biosciences, East Rutherford, NJ). For plasmid DNA and mRNA transfections, the expression of a GFP reporter gene was quantified by normalizing the geometric mean fluorescence intensity of each NP treatment to that of the formulation achieving maximum expression. Cells previously engineered to constitutively express GFP[43] were used siRNA knockdown transfections, and the percentage of cells positively expressing GFP when gated against untreated cells in wells treated with siRNA targeting GFP was normalized against that of wells treated with non-coding control siRNA.

Dual NP Uptake and Gal8 Endosomal Disruption Assay

NPs of matching formulation as those used for transfection experiments were used to deliver nucleic acids cargo containing 20% Cy5-labeled nucleic acids to enable visualization of NP uptake. NPs were incubated with Gal8-mRuby+ cells for 6 h (assay time point optimized in **Figure 8-S2**), at which point NPs and cell culture medium were removed, cells were washed with PBS, and fixed with 10% formalin for 10 minutes at room temperature. The formalin was then removed, cells washed with PBS, and Hoechst nuclear stain (1:5000 in PBS) was applied for 10 minutes. NP uptake and Gal8-mRuby endosomal escape were then quantified by high-content imaging analysis of Cy5 and mRuby puncta per cell, respectively, using a CellInsight CX7 LZR high-content imager (ThermoFisher) with HCS Studio analysis software.

NP Formulation for In Vivo Studies

NPs for *in vivo* mRNA delivery were formulated at 30 w/w. mRNA was dissolved in $MgAc_2$, while polymer and the PEG-lipid 1,2-dimyristoyl-rac-glycero-3-methoxypolyethylene glycol-2000 (DMG-PEG2k, 10% by mass) were dissolved in 100% ethanol. The mRNA and polymer-PEG lipid solutions were mixed via pipetting at 1:1 volume ratio, and NPs were allowed to self-assemble at room temperature for 10 minutes. NPs were then dialyzed against cold PBS at 4°C for 75 minutes using Spectra/Por Float-A-Lyzer G2 dialysis

devices (Repligen, Waltham, MA) with 50 kD molecular weight cut-off. NP volume post-dialysis was adjusted with PBS for final mRNA concentration of 0.1 mg/mL. NPs were administered to animals via 100 μL tail vein injections for a final dose of 10 μg mRNA per animal.

To investigate the effects of PEGylation and dialysis on *in vivo* mRNA expression, NPs with no PEG lipid and no dialysis were formulated in 25 mM $MgAc_2$ at the same final mRNA concentration and w/w ratio as above. 500 mg/mL sucrose solution was used to bring the mixture to isotonicity.

fLuc mRNA In Vivo Bioluminescence

NPs encapsulating fLuc mRNA were formulated as described above and administered to 6-7 week old male BALB/c mice via lateral tail vein injection. Whole-body bioluminescence was assessed 24 h post-injection. D-luciferin potassium salt solution (25 mg/mL in PBS; Cayman Chemical Company, Ann Arbor, MI) was administered to mice via 150 μL intraperitoneal injection, and mice were imaged using an IVIS Spectrum Imager (Perkin Elmer, Waltham, MA) 10 minutes later. The same animals were euthanized immediately after whole-body imaging via cervical dislocation, and select organs were extracted, submerged in 250 □g/mL D-luciferin solution, and imaged with IVIS.

Cre mRNA Delivery to Ai9 Mice

NPs encapsulating Cre mRNA were formulated with DMG-PEG2k and dialyzed in PBS as described above. NPs were administered to 6-week old male Ai9 mice via tail vein injection, and tdTomato expression following Cre-Lox recombination was allowed to accumulate for 3 days, at which point animals were euthanized via cervical dislocation. Select organs were extracted and dissociated by a 1 hr incubation in 2 mg/mL collagenase at 37°C followed by mechanical pressing through a 70-μm cell strainer. Cells were pelleted by centrifugation, the supernatant was removed, and red blood cells in the cell pellet were lysed by incubating in ACK lysing buffer (Quality Biological, Gaithersburg, MD) for 1 min at room temperature. Cells were diluted in PBS, passed through a 100-μm cell strainer, pelleted by centrifugation, and resuspended in FACS buffer (2% FBS in PBS with 0.02% sodium azide). Surface staining of cells with fluorescent antibodies

was then performed using the antibodies and dilutions listed in **Table 8-S1** in FACS buffer for 30 min at 4°C, at which time cells were washed twice and resuspended in FACS buffer for further analysis. FACS experiments were performed using an Attune NxT flow cytometer (ThermoFisher) and analyzed using FlowJo software (FlowJo, Ashland, OR). Gating strategies to identify cell populations are provided in **Figure 8-S9**.

Data Analysis and Statistics

Curve plotting and statistical analysis were performed using Prism 8 (Graphpad, La Jolla, CA). Data are shown as mean ± SD for groups of three or more replicates or as individual values with the mean indicated. Unless otherwise stated, absence of statistical significance markings where a test was stated to have been performed signify no statistical significance. The statistical tests used for each figure are indicated in the figure captions. Statistical significance is denoted as follows: *$p < 0.05$; **$p < 0.01$, ***$p < 0.001$, ****$p < 0.0001$. ns = not significant.

Graphical Illustrations

Graphical illustrations were created using BioRender (https://biorender.com/).

Acknowledgments

Funding: The authors would like to thank the following organizations for financial support: NSF Graduate Research Fellowship DGE-0707427 (DRW) and DGE-1232825 (YR); the Wilmer Core Grant (P30EY001765); and the NIH R01CA228133 (JJG), R01EY031097 (JJG), P41EB028239 (JJG), and F31CA250319 (YR). AstraZeneca is thanked for support in part for this research. JJG thanks the Bloomberg~Kimmel Institute for Cancer Immunotherapy and the Research to Prevent Blindness James and Carole Free Catalyst Award for support. *Author contributions:* Conceptualizations, YR, DRW, SYT, and JJG; Methodology, YR, DRW, SYT, CAB, DJZ, and JJG; Investigation, YR, DRW, SYT, HMY, DS, and MC; Resources and funding acquisition, AT and JJG; Writing and editing, YR, DRW, SYT, HMY, DS, MC, CAB,

DJZ, AT, and JJG; Supervision and administration, DJZ and JJG. *Competing interests:* The authors declare that they have no competing interests. *Data and materials availability:* All data needed to evaluate the conclusions in the paper are present in the paper and/or Supplementary Materials. Additional data related to this paper may be requested from the authors.

References

1. Karikó, K.; Muramatsu, H.; Welsh, F. A.; Ludwig, J.; Kato, H.; Akira, S.; Weissman, D., Incorporation of pseudouridine into mRNA yields superior nonimmunogenic vector with increased translational capacity and biological stability. *Molecular therapy* **2008,** *16* (11), 1833-1840.

2. Thess, A.; Grund, S.; Mui, B. L.; Hope, M. J.; Baumhof, P.; Fotin-Mleczek, M.; Schlake, T., Sequence-engineered mRNA without chemical nucleoside modifications enables an effective protein therapy in large animals. *Molecular Therapy* **2015,** *23* (9), 1456-1464.

3. Corbett, K. S.; Edwards, D. K.; Leist, S. R.; Abiona, O. M.; Boyoglu-Barnum, S.; Gillespie, R. A.; Himansu, S.; Schäfer, A.; Ziwawo, C. T.; DiPiazza, A. T.; Dinnon, K. H.; Elbashir, S. M.; Shaw, C. A.; Woods, A.; Fritch, E. J.; Martinez, D. R.; Bock, K. W.; Minai, M.; Nagata, B. M.; Hutchinson, G. B.; Wu, K.; Henry, C.; Bahi, K.; Garcia-Dominguez, D.; Ma, L.; Renzi, I.; Kong, W.-P.; Schmidt, S. D.; Wang, L.; Zhang, Y.; Phung, E.; Chang, L. A.; Loomis, R. J.; Altaras, N. E.; Narayanan, E.; Metkar, M.; Presnyak, V.; Liu, C.; Louder, M. K.; Shi, W.; Leung, K.; Yang, E. S.; West, A.; Gully, K. L.; Stevens, L. J.; Wang, N.; Wrapp, D.; Doria-Rose, N. A.; Stewart-Jones, G.; Bennett, H.; Alvarado, G. S.; Nason, M. C.; Ruckwardt, T. J.; McLellan, J. S.; Denison, M. R.; Chappell, J. D.; Moore, I. N.; Morabito, K. M.; Mascola, J. R.; Baric, R. S.; Carfi, A.; Graham, B. S., SARS-CoV-2 mRNA vaccine design enabled by prototype pathogen preparedness. *Nature* **2020**.

4. Pardi, N.; Hogan, M. J.; Porter, F. W.; Weissman, D., mRNA vaccines — a new era in vaccinology. *Nature Reviews Drug Discovery* **2018,** *17* (4), 261-279.

5. Mandal, P. K.; Ferreira, L. M. R.; Collins, R.; Meissner, T. B.; Boutwell, C. L.; Friesen, M.; Vrbanac, V.; Garrison, B. S.; Stortchevoi, A.; Bryder, D., Efficient ablation of genes in human hematopoietic stem and effector cells using CRISPR/Cas9. *Cell stem cell* **2014,** *15* (5), 643-652.

6. Monroe, K. M.; Yang, Z.; Johnson, J. R.; Geng, X.; Doitsh, G.; Krogan, N. J.; Greene, W. C., IFI16 DNA sensor is required for death of lymphoid CD4 T cells abortively infected with HIV. *Science* **2014,** *343* (6169), 428-432.

7. Sabnis, S.; Kumarasinghe, E. S.; Salerno, T.; Mihai, C.; Ketova, T.; Senn, J. J.; Lynn, A.; Bulychev, A.; McFadyen, I.; Chan, J., A novel amino lipid series for mRNA delivery: improved endosomal escape and sustained pharmacology and safety in non-human primates. *Molecular Therapy* **2018,** *26* (6), 1509-1519.

8. Patel, A. K.; Kaczmarek, J. C.; Bose, S.; Kauffman, K. J.; Mir, F.; Heartlein, M. W.; DeRosa, F.; Langer, R.; Anderson, D. G., Inhaled Nanoformulated mRNA Polyplexes for Protein Production in Lung Epithelium. *Advanced Materials* **2019,** *31* (8), 1805116.

9. Cheng, Q.; Wei, T.; Jia, Y.; Farbiak, L.; Zhou, K.; Zhang, S.; Wei, Y.; Zhu, H.; Siegwart, D. J., Dendrimer-Based Lipid Nanoparticles Deliver Therapeutic FAH mRNA to Normalize Liver Function and Extend Survival in a Mouse Model of Hepatorenal Tyrosinemia Type I. *Advanced Materials* **2018,** *30* (52), 1805308.

10. Cao, J.; An, D.; Galduroz, M.; Zhuo, J.; Liang, S.; Eybye, M.; Frassetto, A.; Kuroda, E.; Funahashi, A.; Santana, J.; Mihai, C.; Benenato, K. E.; Kumarasinghe, E. S.; Sabnis, S.; Salerno, T.; Coughlan, K.; Miracco, E. J.; Levy, B.; Besin, G.; Schultz, J.; Lukacs, C.; Guey, L.; Finn, P.; Furukawa, T.; Giangrande, P. H.; Saheki, T.; Martini, P. G. V., mRNA Therapy Improves Metabolic and Behavioral Abnormalities in a Murine Model of Citrin Deficiency. *Molecular Therapy* **2019,** *27* (7), 1242-1251.

11. Billingsley, M. M.; Singh, N.; Ravikumar, P.; Zhang, R.; June, C. H.; Mitchell, M. J., Ionizable Lipid Nanoparticle-Mediated mRNA Delivery for Human CAR T Cell Engineering. *Nano Letters* **2020,** *20* (3), 1578-1589.

12. Miao, L.; Li, L.; Huang, Y.; Delcassian, D.; Chahal, J.; Han, J.; Shi, Y.; Sadtler, K.; Gao, W.; Lin, J.; Doloff, J. C.; Langer, R.; Anderson, D. G., Delivery of mRNA vaccines with heterocyclic lipids increases anti-tumor efficacy by STING-mediated immune cell activation. *Nature Biotechnology* **2019,** *37* (10), 1174-1185.

13. Liu, J.; Chang, J.; Jiang, Y.; Meng, X.; Sun, T.; Mao, L.; Xu, Q.; Wang, M., Fast and efficient CRISPR/Cas9 genome editing in vivo enabled by bioreducible lipid and messenger RNA nanoparticles. *Advanced Materials* **2019,** *31* (33), 1902575.

14. Miller, J. B.; Zhang, S.; Kos, P.; Xiong, H.; Zhou, K.; Perelman, S. S.; Zhu, H.; Siegwart, D. J., Non-viral CRISPR/Cas gene editing in vitro and in vivo enabled by synthetic nanoparticle co-delivery of Cas9 mRNA and sgRNA. *Angewandte Chemie International Edition* **2017,** *56* (4), 1059-1063.

15. Rui, Y.; Wilson, D. R.; Green, J. J., Non-Viral Delivery To Enable Genome Editing. *Trends in Biotechnology* **2019,** *37* (3), 281-293.

16. Gilleron, J.; Querbes, W.; Zeigerer, A.; Borodovsky, A.; Marsico, G.; Schubert, U.; Manygoats, K.; Seifert, S.; Andree, C.; Stöter, M.; Epstein-Barash, H.; Zhang, L.; Koteliansky, V.; Fitzgerald, K.; Fava, E.; Bickle, M.; Kalaidzidis, Y.; Akinc, A.; Maier, M.; Zerial, M., Image-based analysis of lipid nanoparticle–mediated siRNA delivery, intracellular trafficking and endosomal escape. *Nature Biotechnology* **2013,** *31* (7), 638-646.

17. Tamura, A.; Oishi, M.; Nagasaki, Y., Enhanced Cytoplasmic Delivery of siRNA Using a Stabilized Polyion Complex Based on PEGylated Nanogels with a Cross-Linked Polyamine Structure. *Biomacromolecules* **2009,** *10* (7), 1818-1827.

18. Akita, H.; Kogure, K.; Moriguchi, R.; Nakamura, Y.; Higashi, T.; Nakamura, T.; Serada, S.; Fujimoto, M.; Naka, T.; Futaki, S.; Harashima, H., Nanoparticles for ex vivo siRNA delivery to dendritic cells for cancer vaccines: Programmed endosomal escape and dissociation. *Journal of Controlled Release* **2010,** *143* (3), 311-317.

19. Kilchrist, K. V.; Evans, B. C.; Brophy, C. M.; Duvall, C. L., Mechanism of Enhanced Cellular Uptake and Cytosolic Retention of MK2 Inhibitory Peptide Nano-polyplexes. *Cell Mol Bioeng* **2016,** *9* (3), 368-381.

20. Wittrup, A.; Ai, A.; Liu, X.; Hamar, P.; Trifonova, R.; Charisse, K.; Manoharan, M.; Kirchhausen, T.; Lieberman, J., Visualizing lipid-formulated siRNA release from endosomes and target gene knockdown. *Nature biotechnology* **2015,** *33* (8), 870-876.

21. Wojnilowicz, M.; Glab, A.; Bertucci, A.; Caruso, F.; Cavalieri, F., Super-resolution Imaging of Proton Sponge-Triggered Rupture of Endosomes and Cytosolic Release of Small Interfering RNA. *ACS Nano* **2019,** *13* (1), 187-202.

22. Hadari, Y. R.; Paz, K.; Dekel, R.; Mestrovic, T.; Accili, D.; Zick, Y., Galectin-8: A NEW RAT LECTIN, RELATED TO GALECTIN-4. *Journal of Biological Chemistry* **1995,** *270* (7), 3447-3453.

23. Thurston, T. L. M.; Wandel, M. P.; von Muhlinen, N.; Foeglein, Á.; Randow, F., Galectin 8 targets damaged vesicles for autophagy to defend cells against bacterial invasion. *Nature* **2012,** *482* (7385), 414-418.

24. Kilchrist, K. V.; Dimobi, S. C.; Jackson, M. A.; Evans, B. C.; Werfel, T. A.; Dailing, E. A.; Bedingfield, S. K.; Kelly, I. B.; Duvall, C. L., Gal8 Visualization of Endosome Disruption Predicts Carrier-Mediated Biologic Drug Intracellular Bioavailability. *ACS Nano* **2019,** *13* (2), 1136-1152.

25. Wittrup, A.; Ai, A.; Liu, X.; Hamar, P.; Trifonova, R.; Charisse, K.; Manoharan, M.; Kirchhausen, T.; Lieberman, J., Visualizing lipid-formulated siRNA release from endosomes and target gene knockdown. *Nature Biotechnology* **2015,** *33* (November 2014), 1-9.

26. Mishra, B.; Wilson, D. R.; Sripathi, S. R.; Suprenant, M. P.; Rui, Y.; Wahlin, K. J.; Berlinicke, C. A.; Green, J. J.; Zack, D. J., A Combinatorial Library of Biodegradable Polyesters Enables Non-viral Gene Delivery to Post-Mitotic Human Stem Cell-Derived Polarized RPE Monolayers. *Regenerative Engineering and Translational Medicine* **2019**.

27. Sunshine, J. C.; Peng, D. Y.; Green, J. J., Uptake and Transfection with Polymeric Nanoparticles Are Dependent on Polymer End-Group Structure, but Largely Independent of Nanoparticle Physical and Chemical Properties. *Molecular Pharmaceutics* **2012,** *9* (11), 3375-3383.

28. Kim, J.; Sunshine, J. C.; Green, J. J., Differential Polymer Structure Tunes Mechanism of Cellular Uptake and Transfection Routes of Poly(β-amino ester) Polyplexes in Human Breast Cancer Cells. *Bioconjugate Chemistry* **2014,** *25* (1), 43-51.

29. Kaczmarek, J. C.; Kauffman, K. J.; Fenton, O. S.; Sadtler, K.; Patel, A. K.; Heartlein, M. W.; DeRosa, F.; Anderson, D. G., Optimization of a Degradable Polymer–Lipid Nanoparticle for Potent

Systemic Delivery of mRNA to the Lung Endothelium and Immune Cells. *Nano Letters* **2018,** *18* (10), 6449-6454.

30. Eltoukhy, A. A.; Chen, D.; Alabi, C. A.; Langer, R.; Anderson, D. G., Degradable Terpolymers with Alkyl Side Chains Demonstrate Enhanced Gene Delivery Potency and Nanoparticle Stability. *Advanced Materials* **2013,** *25* (10), 1487-1493.

31. Sahay, G.; Querbes, W.; Alabi, C.; Eltoukhy, A.; Sarkar, S.; Zurenko, C.; Karagiannis, E.; Love, K.; Chen, D.; Zoncu, R.; Buganim, Y.; Schroeder, A.; Langer, R.; Anderson, D. G., Efficiency of siRNA delivery by lipid nanoparticles is limited by endocytic recycling. *Nature Biotechnology* **2013,** *31* (7), 653-658.

32. Rehman, Z. u.; Hoekstra, D.; Zuhorn, I. S., Mechanism of Polyplex- and Lipoplex-Mediated Delivery of Nucleic Acids: Real-Time Visualization of Transient Membrane Destabilization without Endosomal Lysis. *ACS Nano* **2013,** *7* (5), 3767-3777.

33. Wilson, D. R.; Rui, Y.; Siddiq, K.; Routkevitch, D.; Green, J. J., Differentially Branched Ester Amine Quadpolymers with Amphiphilic and pH-Sensitive Properties for Efficient Plasmid DNA Delivery. *Molecular Pharmaceutics* **2019,** *16* (2), 655-668.

34. Karlsson, J.; Rui, Y.; Kozielski, K. L.; Placone, A. L.; Choi, O.; Tzeng, S. Y.; Kim, J.; Keyes, J. J.; Bogorad, M. I.; Gabrielson, K.; Guerrero-Cazares, H.; Quiñones-Hinojosa, A.; Searson, P. C.; Green, J. J., Engineered nanoparticles for systemic siRNA delivery to malignant brain tumours. *Nanoscale* **2019,** *11* (42), 20045-20057.

35. Rui, Y.; Wilson, D. R.; Choi, J.; Varanasi, M.; Sanders, K.; Karlsson, J.; Lim, M.; Green, J. J., Carboxylated branched poly(β-amino ester) nanoparticles enable robust cytosolic protein delivery and CRISPR-Cas9 gene editing. *Science Advances* **2019,** *5* (12), eaay3255.

36. Sago, C. D.; Lokugamage, M. P.; Paunovska, K.; Vanover, D. A.; Monaco, C. M.; Shah, N. N.; Gamboa Castro, M.; Anderson, S. E.; Rudoltz, T. G.; Lando, G. N.; Munnilal Tiwari, P.; Kirschman, J. L.; Willett, N.; Jang, Y. C.; Santangelo, P. J.; Bryksin, A. V.; Dahlman, J. E., High-throughput in vivo screen of functional mRNA delivery identifies nanoparticles for endothelial cell gene editing. *Proceedings of the National Academy of Sciences* **2018,** *115* (42), E9944.

37. Wilson, D. R.; Mosenia, A.; Suprenant, M. P.; Upadhya, R.; Routkevitch, D.; Meyer, R. A.; Quinones-Hinojosa, A.; Green, J. J., Continuous microfluidic assembly of biodegradable poly(beta-amino ester)/DNA nanoparticles for enhanced gene delivery. *Journal of Biomedical Materials Research Part A* **2017,** *105* (6), 1813-1825.

38. Paunovska, K.; Sago, C. D.; Monaco, C. M.; Hudson, W. H.; Castro, M. G.; Rudoltz, T. G.; Kalathoor, S.; Vanover, D. A.; Santangelo, P. J.; Ahmed, R.; Bryksin, A. V.; Dahlman, J. E., A Direct Comparison of in Vitro and in Vivo Nucleic Acid Delivery Mediated by Hundreds of Nanoparticles Reveals a Weak Correlation. *Nano Letters* **2018,** *18* (3), 2148-2157.

39. Akinc, A.; Maier, M. A.; Manoharan, M.; Fitzgerald, K.; Jayaraman, M.; Barros, S.; Ansell, S.; Du, X.; Hope, M. J.; Madden, T. D.; Mui, B. L.; Semple, S. C.; Tam, Y. K.; Ciufolini, M.; Witzigmann, D.; Kulkarni, J. A.; van der Meel, R.; Cullis, P. R., The Onpattro story and the clinical translation of nanomedicines containing nucleic acid-based drugs. *Nature Nanotechnology* **2019,** *14* (12), 1084-1087.

40. Ramaswamy, S.; Tonnu, N.; Tachikawa, K.; Limphong, P.; Vega, J. B.; Karmali, P. P.; Chivukula, P.; Verma, I. M., Systemic delivery of factor IX messenger RNA for protein replacement therapy. *Proceedings of the National Academy of Sciences* **2017,** *114* (10), E1941.

41. Cheng, Q.; Wei, T.; Farbiak, L.; Johnson, L. T.; Dilliard, S. A.; Siegwart, D. J., Selective organ targeting (SORT) nanoparticles for tissue-specific mRNA delivery and CRISPR–Cas gene editing. *Nature Nanotechnology* **2020,** *15* (4), 313-320.

42. Wilson, D. R.; Routkevitch, D.; Rui, Y.; Mosenia, A.; Wahlin, K. J.; Quinones-Hinojosa, A.; Zack, D. J.; Green, J. J., A Triple-Fluorophore-Labeled Nucleic Acid pH Nanosensor to Investigate Non-viral Gene Delivery. *Molecular Therapy* **2017,** *25* (7), 1697-1709.

43. Rui, Y.; Wilson, D. R.; Sanders, K.; Green, J. J., Reducible Branched Ester-Amine Quadpolymers (rBEAQs) Codelivering Plasmid DNA and RNA Oligonucleotides Enable CRISPR/Cas9 Genome Editing. *ACS Applied Materials & Interfaces* **2019,** *11* (11), 10472-10480.

Supporting Information

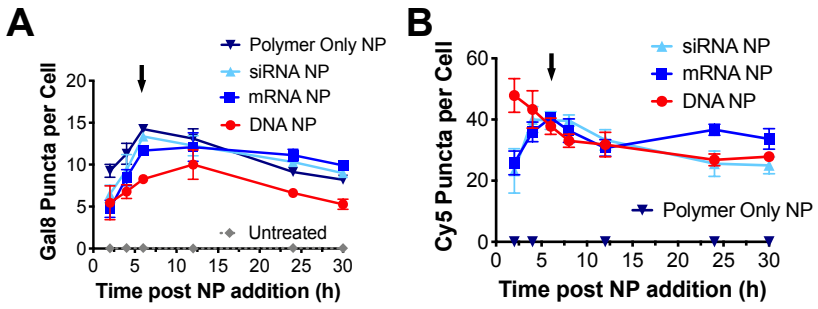

Figure 8-S1. Time course optimization for dual NP uptake/Gal8 endosomal disruption assay. (A) Gal8 puncta count and **(B)** Cy5 puncta count for 7-90,c12-63, 50%-Sc12 NPs delivering various nucleic acid cargos to B16-F10 cells after different incubation times. Black arrow indicates the 6 h time point, which was chosen as the NP incubation time for this assay. Data presented as mean ± SD, $n = 4$.

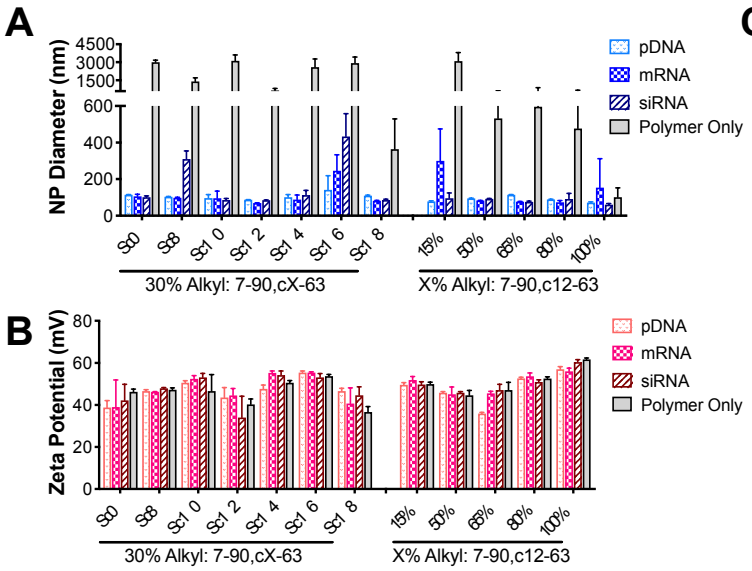

C

	Polymer ID	Alkyl Amine Content (mol %)	Number Average Molecular Weight (Da)	MW PDI
30% Alkyl: 7-90,cX-63	Sc0	None	7277	2.20
	Sc8	30% Sc8	4358	1.15
	Sc10	30% Sc10	9330	3.05
	Sc12	30% Sc12	4446	2.66
	Sc14	30% Sc14	7578	2.05
	Sc16	30% Sc16	8774	3.07
	Sc18	30% Sc18	8759	3.03
X% Alkyl: 7-90,c12-63	15%	15% Sc12	7473	1.62
	50%	50% Sc12	4464	2.66
	65%	65% Sc12	5820	2.50
	80%	80% Sc12	7217	2.38
	100%	100% Sc12	5083	1.80

Figure 8-S2. Polymer and nanoparticle characteristics for the polymer backbone hydrophobicity variation series. (A) Z-average hydrodynamic diameter and **(B)** zeta potential for polymers encapsulating plasmid DNA, mRNA, siRNA, or polymer only nanoparticles (no nucleic acids). Data shown as mean ± SD, $n = 3$. **(C)** Polymer molecular weight as determined by GPC.

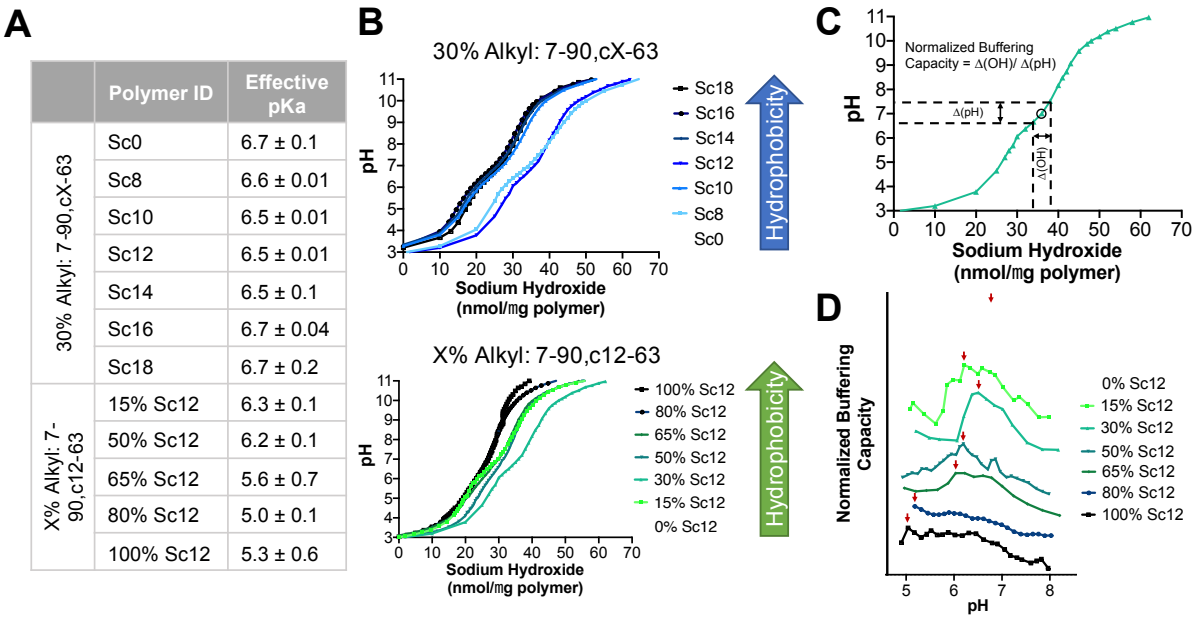

Figure 8-S3. Polymer effective pKa and pH titration curves. (A) Effective pKa in the physiologically relevant pH range for polymers in the backbone variation series. **(B)** Representative pH titration curves. **(C)** Normalized buffering capacity was calculated from pH titration data as Δ(OH)/ Δ(pH) at each titration point (pH 5-8). **(D)** Effective pKa value of each polymer was determined as the pH point of the maximum normalized buffering capacity (indicated by red arrows in representative curves).

A

	Polymer ID	Polymer IC50 of Binding (μg/mL)		
		pDNA	mRNA	siRNA
30% Alkyl: 7-90,cX-63	Sc0	12.2 ± 0.2	4.0 ± 0.7	5.8 ± 0.1
	Sc8	10.6 ± 0.9	3.15 ± 0.04	5.9 ± 0.1
	Sc10	6.3 ± 0.5	4.3 ± 0.3	6.2 ± 0.4
	Sc12	6 ± 2	4.23 ± 0.03	6.3 ± 0.1
	Sc14	7 ± 2	4.03 ± 0.01	6.6 ± 0.4
	Sc16	6 ± 1	3.99 ± 0.06	10.8 ± 0.1
	Sc18	3 ± 2	3.6 ± 0.2	12.2 ± 0.1
X% Alkyl: 7-90,c12-63	15% Sc12	6.3 ± 0.2	3.0 ± 0.2	6.5 ± 0.2
	50% Sc12	5 ± 1	5.8 ± 0.7	11.4 ± 0.5
	65% Sc12	3 ± 2	7.1 ± 0.8	13.1 ± 0.1
	80% Sc12	4.5 ± 0.9	1.6 ± 0.4	13.1 ± 0.3
	100% Sc12	7 ± 2	1.1 ± 0.5	12.7 ± 0.1

B

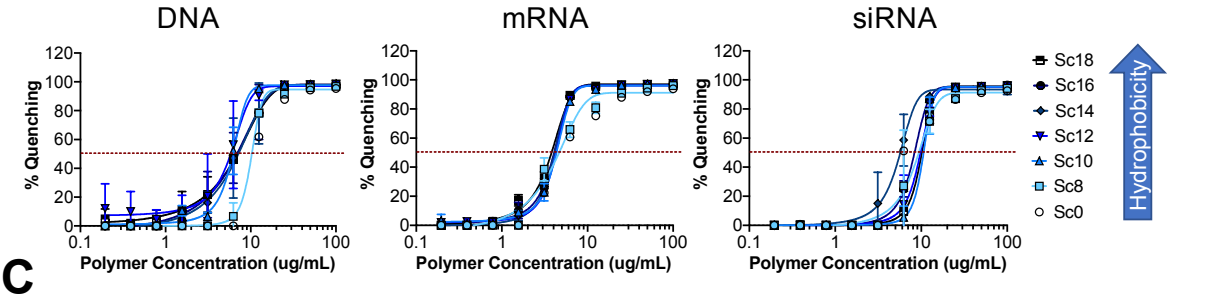

C

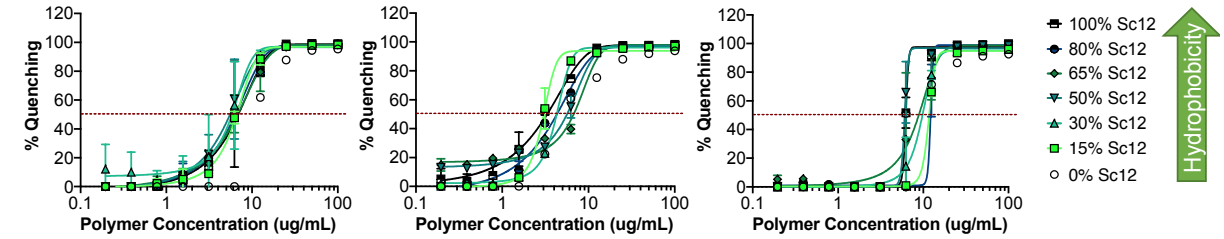

Figure 8-S4. RiboGreen nucleic acid binding data. (A) Tabulated polymer IC50 of binding for polymers in the backbone variation series assessed with plasmid DNA, mRNA, and siRNA. **(B)** RiboGreen fluorescence quenching competitive binding curves for polymers in the alkyl chain length variation series. **(C)** Binding curves for polymers in the alkyl fraction variation series. Red line indicates 50% fluorescence quenching. Data shown as mean ± SD, $n = 2$.

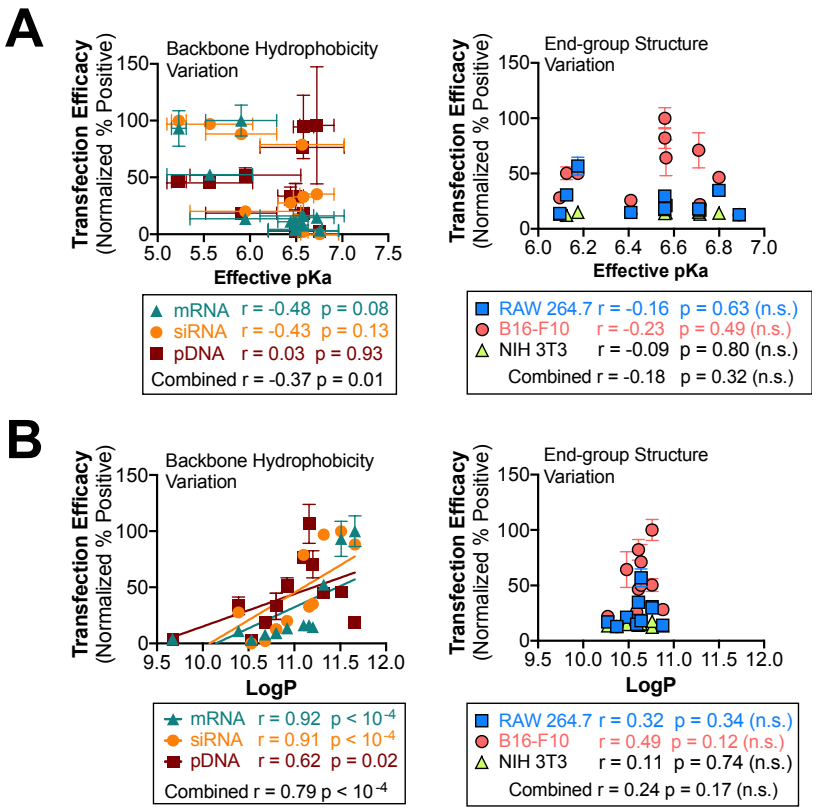

Figure 8-S5. Correlations *in vitro* transfection efficacy and polymer buffering capacity and hydrophobicity, respectively. Correlations between transfection efficacy and **(A)** polymer effective pKa in the physiological pH range or **(B)** predicted polymer LogP values of nanoparticles from backbone hydrophobicity variation polymers delivering different nucleic acid cargo (left) or end-group variation polymers delivering mRNA to different cell lines (right). Spearman's correlation was calculated to assess the strength of association between variable groups, and a line of best fit is shown for data sets with significant levels of correlation. Data shown as mean ± SD, $N = 4$.

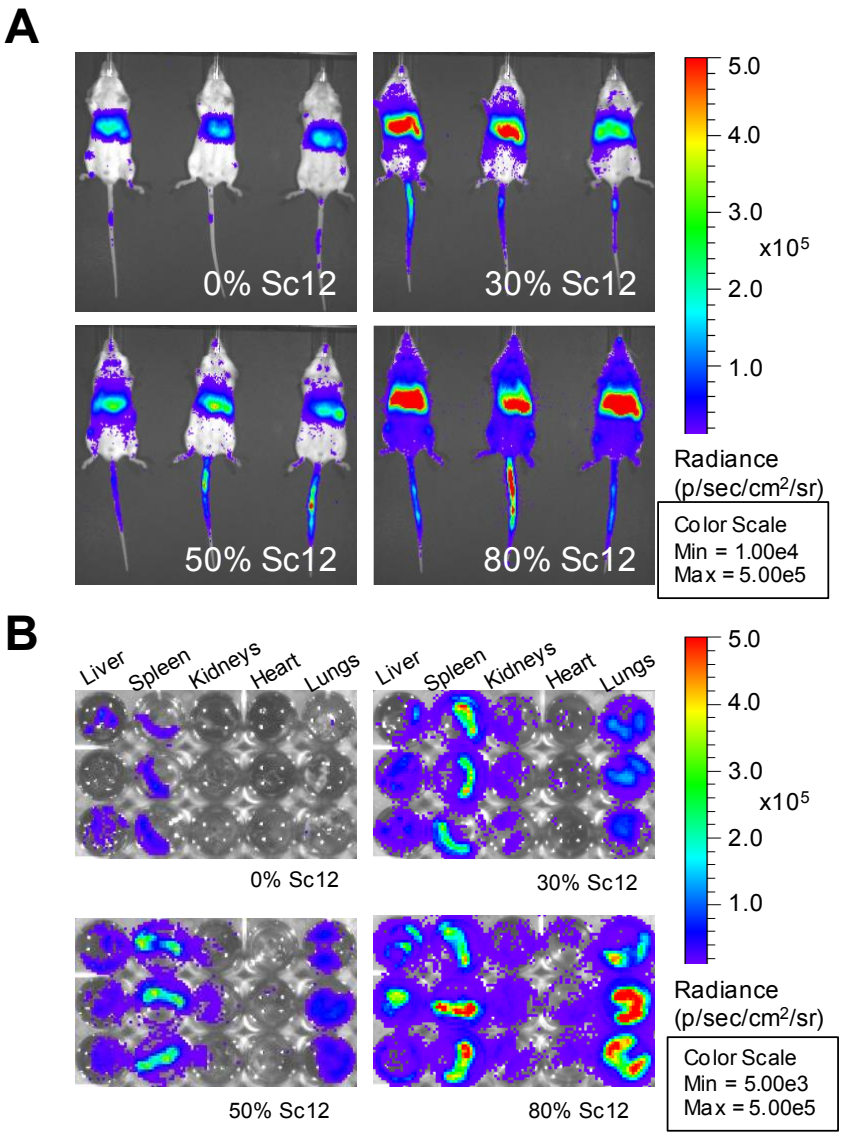

Figure 8-S6. IVIS images of BALB/c mice treated with NPs formulated with fLuc mRNA and select polymers from the backbone hydrophobicity variation series. (A) Whole-body, live animal bioluminescence imaging. **(B)** Bioluminescence imaging of select organs. Readings taken 24 h after NP injection. (n = 3).

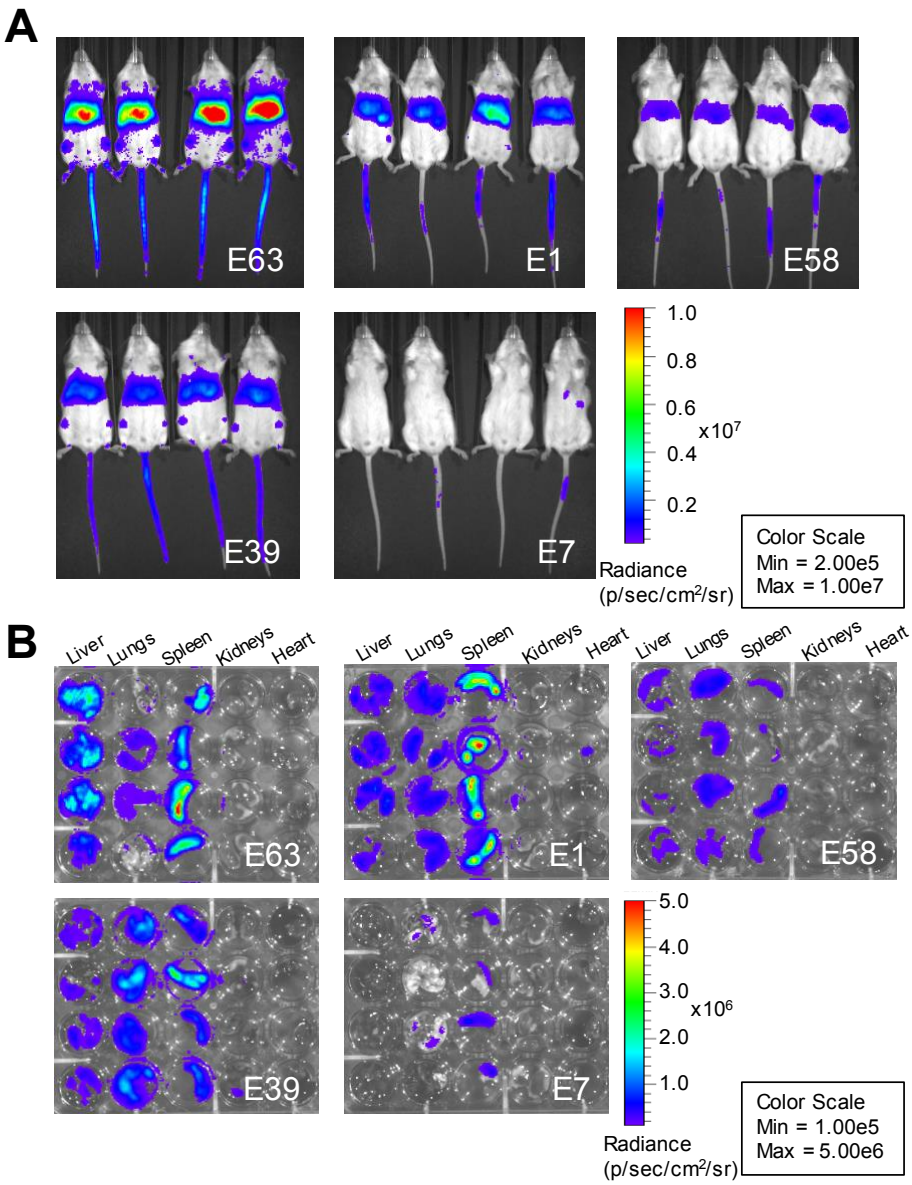

Figure 8-S7. IVIS images of BALB/c mice treated with NPs formulated with fLuc mRNA and select polymers from the end-group variation series. (A) Whole-body, live animal bioluminescence imaging. **(B)** Bioluminescence imaging of select organs. Readings taken 24 h after NP injection. (n = 4).

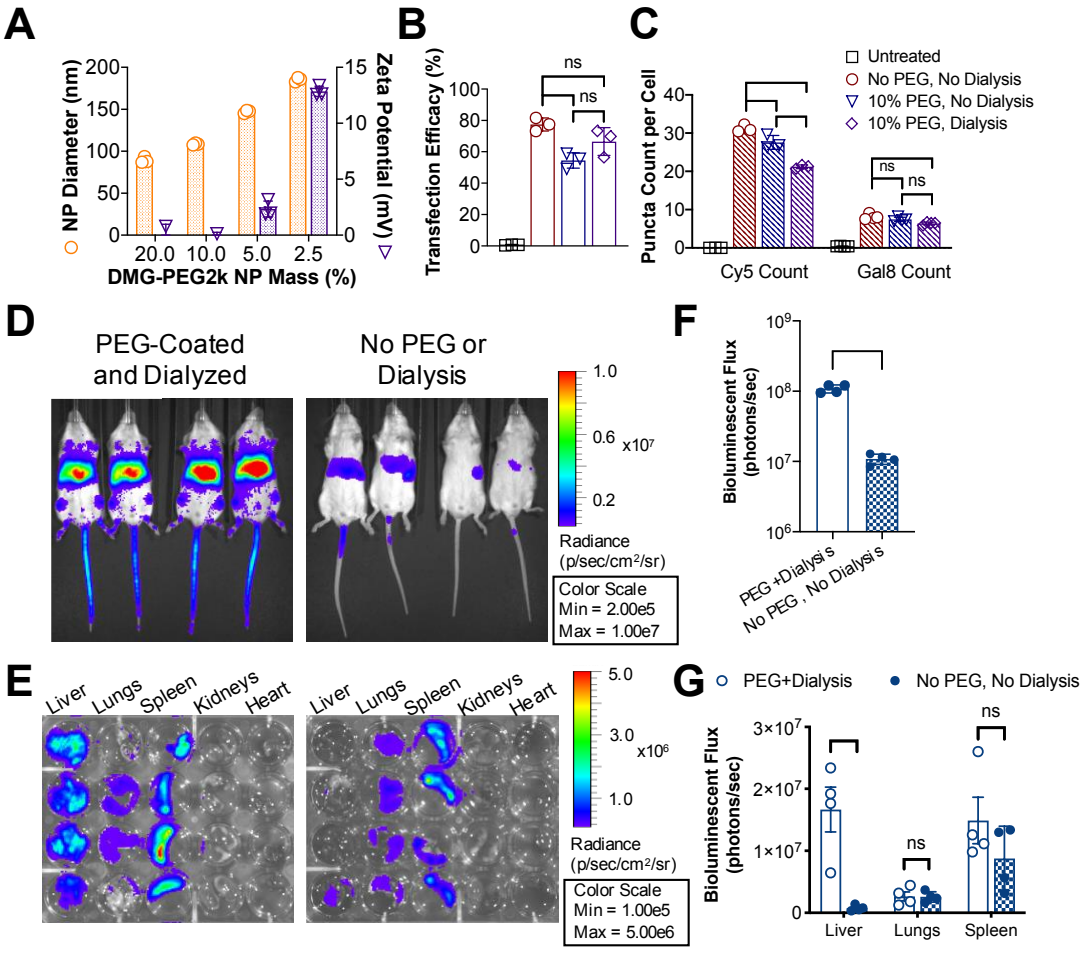

Figure 8-S8. Effect of PEG-coating and dialysis on mRNA transfection. (A) DLS NP measurements of dialyzed, PEG-coated PBAE mRNA NPs with increasing lipid-PEG content. **(B)** Transfection efficacy and **(C)** Cy5 and Gal8 puncta count for NPs with various combinations of PEG-coating and dialysis (assay performed using B16-F10 cells and delivering 50 ng mRNA per 96-well). Data presented as mean ± SD, n = 3. Statistical significance calculated using one-way ANOVA with Tukey's post-hoc analysis. *$P < 0.05$, **$P < 0.01$, and ***$P < 0.001$. ns, not significant. IVIS bioluminescence imaging for **(D)** whole-body, live animals and **(E)** select organs in animals injected with dialyzed and PEG-coated or non-dialyzed and non-PEG-coated NPs. Readings taken 24 h after NP injection. Quantification of luminescence from **(F)** whole-body or **(G)** organ level images. Statistical significance calculated using Student's t-test with Welch's correction for **(F)** and 2-way ANOVA with Sidak's post-hoc analysis for **(G)**. ***$P < 0.001$. ns, not significant. (n = 4).

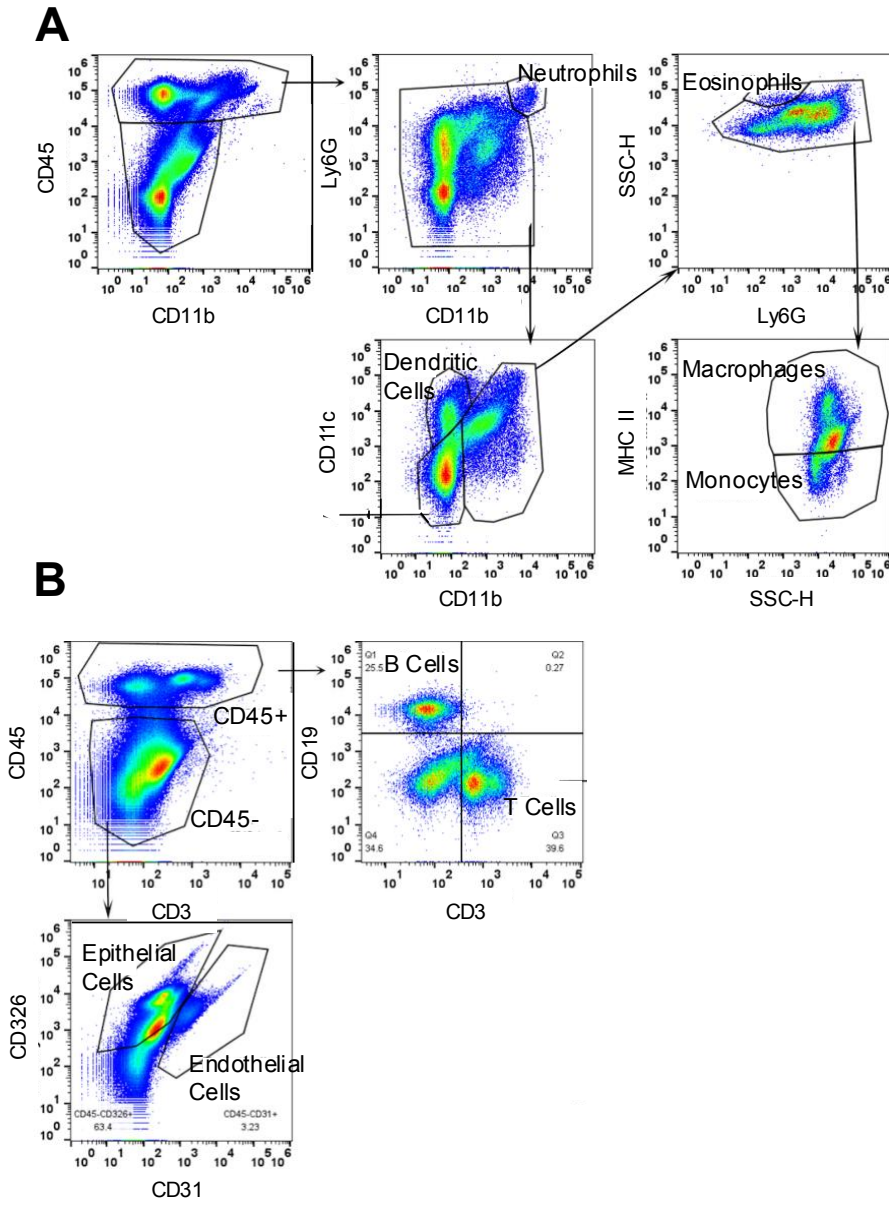

Figure 8-S9. Flow cytometry gating strategies to identify cell type expression in Ai9 mice.

Representative flow cytometry histograms to identify **(A)** various immune cell populations (panel 1) or **(B)** immune and non-immune cells (panel 2) in the liver.

Antigen	Color	Supplier	Clone	Dilution	Catalog No.	Lot No.
CD45	Brilliant Violet 421	Biolegend	30-F11	1:100	103134	B287242
CD11b	Alexa Fluor 488	Biolegend	M1/70	1:100	101217	B254608
CD11c	Allophycocyanin (APC)	Biolegend	N418	1:100	117310	B278343
I-A/I-E	Alexa Fluor 700	Biolegend	M5/114.14.2	1:100	107622	B264454
Ly6G	APC/Cyanine7 (Cy7)	Biolegend	1A8	1:100	127624	B264760
CD3	Alexa Fluor 488	Biolegend	17A2	1:80	100210	B284975
CD19	APC	Biolegend	6D5	1:100	115512	B284257
CD31/PECAM	Alexa Fluor 700	Biolegend	390	1:100	102443	B303280
CD326/EpCAM	APC/Cy7	Biolegend	G8.8	1:80	118218	B266989

Table 8-S1. Antibody information for Ai9 flow cytometry experiments.

Chapter 9: Future perspectives in the field of non-viral gene delivery

9.A: Recent advances with high potential to redefine the field

In the twenty-five years since polyethylenimine was first reported as a delivery vector for plasmid DNA, the field of non-viral gene delivery has moved forward by leaps and bounds, with large numbers of papers published on polymeric or lipid-based systems each year. What follows is a brief selection of advances during my PhD years (2015-2021) that I found particularly interesting.

On the materials chemistry side, I found the work coming out of Dr. Daniel Siegwart's lab very exciting. Their 2016 paper using asymmetrical linkages to synthesize modular degradable polyester dendrimers enabled structural variations in core/shell chemical structures as well as dendrimer generation for small RNA delivery.[1] Their work using zwitterionic amino lipids for co-delivery of Cas9 mRNA and sgRNA to enable gene editing was also very informative both on the materials side as well as on gene editing assays,[2] and the Ai9 mouse model for detecting *in vivo* transfection or gene editing is an assay that the Green lab has since started using broadly. Most recently, their work demonstrating that altering the biophysical properties of a supplemental component of lipid nanoparticles (NPs) which they termed SORT molecules precisely targeted *in vivo* RNA delivery to highly specific, non-hepatocyte tissues[3] touched on the very exciting idea of highly controlled, biomaterial-based tissue targeting and could be applied to many different delivery systems.

Another rapidly advancing area is non-viral delivery of CRISPR gene editing systems, which has seen a veritable explosion of publications during my PhD. One of the first papers to apply non-viral vectors to CRISPR delivery and was also a favorite read during my first year came out of Dr. Zhen Gu's lab, where rolling circle amplification was used to synthesize DNA nanoclews which encapsulated and enabled intracellular delivery of CRISPR ribonucleoproteins (RNPs).[4] Although this system was rather complex and the efficacy reported has since been far outstripped by other delivery systems, the idea of non-viral CRISPR delivery was so new at the time that this paper provided much of the groundwork for me as I first approached this field. Another paper worth mentioning involves the CRISPR-Gold system, which used a gold NP core with a DNA and polymer coated shell for CRISPR RNP delivery.[5] While this was a rather complex hybrid NP system, their demonstration of *in vivo* homology-directed repair to enable genotypic and

functional correction of a mouse model of Duchenne muscular dystrophy was very exciting. Finally, the work coming out of Dr. Alexander Marson's group using electroporation, a process where an electrical field is applied to cause transient permeabilization of the cell membrane, to deliver CRISPR RNPs to primary human T cells is potentially very close to clinical utilization as it facilitates efficient *ex vivo* generation of immune cells that could be infused into patients. As immune cells are notoriously difficult to transfect using chemical delivery systems, the reported gene knock-in efficiency of up to 20% using this method[6] is truly astonishing. Recent reports using the two-pronged strategy of modified repair templates and polymer coating for CRISPR RNPs further enhanced editing efficiencies by upwards of fourfold;[7] this has major implications for CRISPR editing for adaptive cell therapies.

Finally, it's worth mentioning recent advances in assay development to characterize non-viral delivery as these innovations play a major role in standardizing delivery technologies and moving the field forward. As described previously, the Ai9 mouse is a valuable tool for determining specific cell types being transfected after intravenous administration of gene delivery or gene editing NPs. This transgenic mouse model contains a transcription STOP cassette flanked by two LoxP sites that's situated directly upstream of a tdTomato fluorescent reporter.[8] Excision of the Lox-STOP-Lox sequence by introducing Cre recombinase or Cas9 RNPs targeting the LoxP sites result in turning on of the previously silenced tdTomato signal, and the cells expressing Cre or Cas9 RNPs could be identified through flow cytometry. This is useful for quantifying the percentage of cells transfected in a specific tissue as well as identifying the cell populations transfected after IV administration of NP systems carrying nucleic acids coding for Cre[9] or CRISPR RNPs.[2, 3] Another very exciting technology for detecting tissue and cellular level NP transfection *in vivo* utilizes high-throughput DNA barcoding to simultaneously measure the distribution of thousands of NP formulations and was pioneered by Dahlman *et al.*[10] In this method, chemically distinct NPs are formulated to carry specific nucleic acid barcodes. After the pooled NPs are administered to animals, NP distribution into organs and tissues are quantified using deep sequencing. This method of high throughput NP screening *in vivo* is superior to the traditional paradigm of *in vivo* testing of the handful of top formulations from large library *in vitro* NP screens as it has been shown that the correlation between *in vitro* and *in vivo* nucleic acid delivery is often very weak.[11]

It enables identification of NP formulations for delivery to specific tissues and cell types such as endothelial cells[12] and bone marrow[13] and is further advantageous in that it allows rapid testing of very large NP libraries with relatively few animals.

9.B: Future perspectives on where the field is heading

Although non-viral delivery of gene therapy or gene editing has great potential to treat (and even cure) a large variety of diseases, only a few delivery systems have a realistic chance of reaching the clinic in the next ten years. Most of the non-viral delivery systems being published are extremely difficult for clinical implementation as many are complex, multi-component hybrid systems that would be almost impossible to reliably synthesize at scale. Many systems would also not be able to reach efficacy levels necessary to treat human patients without the need to use unreasonably high doses that could cause high levels of vector-mediated toxicity. Nevertheless, recent publications point to a few areas in which bench-to-bedside translation could happen reasonably soon.

The most exciting recent development in non-viral gene delivery is the rapid development, widespread use, and astonishing efficacy of lipid NP-based mRNA vaccines for COVID-19. The fact that it took less than a year between the first identification of the disease to producing viable vaccines for shots in arms showcases the flexibility in design and ease of manufacturing of nucleic acid vaccines.[14] Several issues with the Pfizer-BioNTech and Moderna vaccines currently approved by the FDA under emergency use authorization such as severe allergic reactions and even cases of anaphylaxis against vaccine components[15, 16] and the need for ultralow storage temperatures[17] may limit their ability to gain full regulatory approval or achieve widespread use for future non-emergency vaccination campaigns. Nevertheless, mRNA COVID vaccines are still a major success story for nucleic acid vaccines and I very much look forward to seeing non-viral mRNA vaccines in regular rotation for diseases such as the seasonal flu in the near future.

Immuno-oncology is another area where I would expect rapid growth and clinical application of non-viral delivery. Recent work by Dr. Steph Tzeng in the Green lab showed that intratumoral administration of polymeric NPs delivering plasmid DNA encoding costimulatory molecule 4-1BBL and immunostimulatory

cytokine IL-12 enabled *in situ* reprogramming of tumor cells into antigen-presenting cells to significantly reduce tumor growth in combination with immune checkpoint blockade.[18] Similarly, Moderna published a study using mRNA NPs encoding OX40L, IL-36γ, and IL-23 lead to tumor regression and systemic immunity in several mouse models of cancer.[19] This strategy is particularly advantageous in that it does not require prior knowledge of the patient's tumor neo-antigen profile and could be an off-the-shelf cancer gene therapy for several types of solid tumors.

In the area of non-viral delivery of CRISPR gene editing, I would expect the earliest FDA approval to occur for disease treated by infusing patients with cells edited *ex vivo*. This is due to the still widely debated issue of off-target editing, which, despite new iterations of higher fidelity Cas9 being published regularly,[20-22] still has a high likelihood of occurring, leading to potentially deleterious edits that limit applications of *in vivo* CRISPR delivery. In contrast, *ex vivo* editing offers the advantage of quality controlling the edited cells prior to administration into patients, and a small clinical study has already been reported using mainly electroporation of CRISPR RNPs into hematopoietic stem cells to create cell therapies for diseases such as sickle cell anemia and β-thalassemia with functionally active edits observed more than a year after treatment.[23] A similar strategy could be applied to HIV treatment by creating CCR5 knockout hematopoietic stem cells that are resistant to HIV cellular entry, and CCR5 targeting with zinc finger nucleases (another gene editing modality) is currently in phase II clinical trials for HIV/AIDS treatment.[24]

Although I think IV administration of gene editing molecules is still far off due to concerns of off-target editing mentioned above, diseases related to the liver will likely be the first candidates when this application does eventually happen. Lipid NPs, a non-viral delivery system in clinical utilization, overwhelmingly target the liver.[25] It's no surprise that Alnylam's Patisiran (Onpattro), which uses lipid NPs to deliver siRNA to treat transthyretin-mediated amyloidosis, is the first non-viral gene therapy approved by the FDA.[26] Indeed, Intellia Therapeutics reported that a single administration of lipid NPs delivering Cas9 mRNA and a chemically modified sgRNA enabled >97% reduction in serum protein levels of mouse transtheyretin for at least 12 months after gene editing in the liver.[27] For these applications, I predict that CRISPR gene editing complexes will likely be delivered in mRNA or RNP form to reduce the risk of off-

target editing due to prolonged RNP persistence.[28] Other liver diseases amenable to CRISPR editing and are also currently in the Intellia pipeline include transthyretin amyloidosis, hereditary angioedema, and hemophilia A and B.[29]

References:

1. Zhou, K.; Nguyen, L. H.; Miller, J. B.; Yan, Y.; Kos, P.; Xiong, H.; Li, L.; Hao, J.; Minnig, J. T.; Zhu, H.; Siegwart, D. J., Modular degradable dendrimers enable small RNAs to extend survival in an aggressive liver cancer model. *Proceedings of the National Academy of Sciences* **2016,** *113* (3), 520.

2. Miller, J. B.; Zhang, S.; Kos, P.; Xiong, H.; Zhou, K.; Perelman, S. S.; Zhu, H.; Siegwart, D. J., Non-Viral CRISPR/Cas Gene Editing In Vitro and In Vivo Enabled by Synthetic Nanoparticle Co-Delivery of Cas9 mRNA and sgRNA. *Angewandte Chemie International Edition* **2017,** *56* (4), 1059-1063.

3. Cheng, Q.; Wei, T.; Farbiak, L.; Johnson, L. T.; Dilliard, S. A.; Siegwart, D. J., Selective organ targeting (SORT) nanoparticles for tissue-specific mRNA delivery and CRISPR–Cas gene editing. *Nature Nanotechnology* **2020,** *15* (4), 313-320.

4. Sun, W.; Ji, W.; Hall, J. M.; Hu, Q.; Wang, C.; Beisel, C. L.; Gu, Z., Self-assembled DNA nanoclews for the efficient delivery of CRISPR-Cas9 for genome editing. *Angew Chem Int Ed Engl* **2015,** *54* (41), 12029-33.

5. Lee, K.; Conboy, M.; Park, H. M.; Jiang, F.; Kim, H. J.; Dewitt, M. A.; Mackley, V. A.; Chang, K.; Rao, A.; Skinner, C.; Shobha, T.; Mehdipour, M.; Liu, H.; Huang, W.-c.; Lan, F.; Bray, N. L.; Li, S.; Corn, J. E.; Kataoka, K.; Doudna, J. A.; Conboy, I.; Murthy, N., Nanoparticle delivery of Cas9 ribonucleoprotein and donor DNA in vivo induces homology-directed DNA repair. *Nature Biomedical Engineering* **2017,** *1* (11), 889-901.

6. Schumann, K.; Lin, S.; Boyer, E.; Simeonov, D. R.; Subramaniam, M.; Gate, R. E.; Haliburton, G. E.; Ye, C. J.; Bluestone, J. A.; Doudna, J. A.; Marson, A., Generation of knock-in primary human T cells using Cas9 ribonucleoproteins. *Proceedings of the National Academy of Sciences* **2015,** *112* (33), 10437.

7. Nguyen, D. N.; Roth, T. L.; Li, P. J.; Chen, P. A.; Apathy, R.; Mamedov, M. R.; Vo, L. T.; Tobin, V. R.; Goodman, D.; Shifrut, E.; Bluestone, J. A.; Puck, J. M.; Szoka, F. C.; Marson, A., Polymer-stabilized Cas9 nanoparticles and modified repair templates increase genome editing efficiency. *Nature Biotechnology* **2020,** *38* (1), 44-49.

8. Madisen, L.; Zwingman, T. A.; Sunkin, S. M.; Oh, S. W.; Zariwala, H. A.; Gu, H.; Ng, L. L.; Palmiter, R. D.; Hawrylycz, M. J.; Jones, A. R.; Lein, E. S.; Zeng, H., A robust and high-throughput Cre reporting and characterization system for the whole mouse brain. *Nat Neurosci* **2010,** *13* (1), 133-40.

9. Kaczmarek, J. C.; Kauffman, K. J.; Fenton, O. S.; Sadtler, K.; Patel, A. K.; Heartlein, M. W.; DeRosa, F.; Anderson, D. G., Optimization of a Degradable Polymer–Lipid Nanoparticle for Potent Systemic Delivery of mRNA to the Lung Endothelium and Immune Cells. *Nano Letters* **2018,** *18* (10), 6449-6454.

10. Dahlman, J. E.; Kauffman, K. J.; Xing, Y.; Shaw, T. E.; Mir, F. F.; Dlott, C. C.; Langer, R.; Anderson, D. G.; Wang, E. T., Barcoded nanoparticles for high throughput in vivo discovery of targeted therapeutics. *Proceedings of the National Academy of Sciences* **2017,** *114* (8), 2060.

11. Paunovska, K.; Sago, C. D.; Monaco, C. M.; Hudson, W. H.; Castro, M. G.; Rudoltz, T. G.; Kalathoor, S.; Vanover, D. A.; Santangelo, P. J.; Ahmed, R.; Bryksin, A. V.; Dahlman, J. E., A Direct Comparison of in Vitro and in Vivo Nucleic Acid Delivery Mediated by Hundreds of Nanoparticles Reveals a Weak Correlation. *Nano Letters* **2018,** *18* (3), 2148-2157.

12. Sago, C. D.; Lokugamage, M. P.; Paunovska, K.; Vanover, D. A.; Monaco, C. M.; Shah, N. N.; Gamboa Castro, M.; Anderson, S. E.; Rudoltz, T. G.; Lando, G. N.; Munnilal Tiwari, P.; Kirschman, J. L.; Willett, N.; Jang, Y. C.; Santangelo, P. J.; Bryksin, A. V.; Dahlman, J. E., High-throughput in vivo screen of functional mRNA delivery identifies nanoparticles for endothelial cell gene editing. *Proceedings of the National Academy of Sciences* **2018,** *115* (42), E9944.

13. Sago, C. D.; Lokugamage, M. P.; Islam, F. Z.; Krupczak, B. R.; Sato, M.; Dahlman, J. E., Nanoparticles That Deliver RNA to Bone Marrow Identified by in Vivo Directed Evolution. *Journal of the American Chemical Society* **2018,** *140* (49), 17095-17105.

14. Polack, F. P.; Thomas, S. J.; Kitchin, N.; Absalon, J.; Gurtman, A.; Lockhart, S.; Perez, J. L.; Pérez Marc, G.; Moreira, E. D.; Zerbini, C.; Bailey, R.; Swanson, K. A.; Roychoudhury, S.; Koury, K.; Li, P.; Kalina, W. V.; Cooper, D.; Frenck, R. W.; Hammitt, L. L.; Türeci, Ö.; Nell, H.; Schaefer, A.; Ünal, S.; Tresnan, D. B.; Mather, S.; Dormitzer, P. R.; Şahin, U.; Jansen, K. U.; Gruber, W. C., Safety and Efficacy of the BNT162b2 mRNA Covid-19 Vaccine. *New England Journal of Medicine* **2020,** *383* (27), 2603-2615.

15. Shimabukuro, T. T.; Cole, M.; Su, J. R., Reports of Anaphylaxis After Receipt of mRNA COVID-19 Vaccines in the US—December 14, 2020-January 18, 2021. *JAMA* **2021,** *325* (11), 1101-1102.

16. Sellaturay, P.; Nasser, S.; Islam, S.; Gurugama, P.; Ewan, P. W., Polyethylene glycol (PEG) is a cause of anaphylaxis to the Pfizer/BioNTech mRNA COVID-19 vaccine. *Clinical & Experimental Allergy* **2021,** *n/a* (n/a).

17. Crommelin, D. J. A.; Anchordoquy, T. J.; Volkin, D. B.; Jiskoot, W.; Mastrobattista, E., Addressing the cold reality of mRNA vaccine stability. *Journal of Pharmaceutical Sciences* **2021,** *110* (3), 997-1001.

18. Tzeng, S. Y.; Patel, K. K.; Wilson, D. R.; Meyer, R. A.; Rhodes, K. R.; Green, J. J., In situ genetic engineering of tumors for long-lasting and systemic immunotherapy. *Proceedings of the National Academy of Sciences* **2020,** *117* (8), 4043.

19. Hewitt, S. L.; Bai, A.; Bailey, D.; Ichikawa, K.; Zielinski, J.; Karp, R.; Apte, A.; Arnold, K.; Zacharek, S. J.; Iliou, M. S.; Bhatt, K.; Garnaas, M.; Musenge, F.; Davis, A.; Khatwani, N.; Su, S. V.; MacLean, G.; Farlow, S. J.; Burke, K.; Frederick, J. P., Durable anticancer immunity from intratumoral administration of IL-23, IL-36γ, and OX40L mRNAs. *Science Translational Medicine* **2019,** *11* (477), eaat9143.

20. Slaymaker, I. M.; Gao, L.; Zetsche, B.; Scott, D. A.; Yan, W. X.; Zhang, F., Rationally engineered Cas9 nucleases with improved specificity. *Science* **2016,** *351* (6268), 84-88.

21. Kleinstiver, B. P.; Pattanayak, V.; Prew, M. S.; Tsai, S. Q.; Nguyen, N. T.; Zheng, Z.; Joung, J. K., High-fidelity CRISPR–Cas9 nucleases with no detectable genome-wide off-target effects. *Nature* **2016,** *529* (7587), 490-495.

22. Chen, J. S.; Dagdas, Y. S.; Kleinstiver, B. P.; Welch, M. M.; Sousa, A. A.; Harrington, L. B.; Sternberg, S. H.; Joung, J. K.; Yildiz, A.; Doudna, J. A., Enhanced proofreading governs CRISPR–Cas9 targeting accuracy. *Nature* **2017,** *550* (7676), 407-410.

23. Frangoul, H.; Altshuler, D.; Cappellini, M. D.; Chen, Y.-S.; Domm, J.; Eustace, B. K.; Foell, J.; de la Fuente, J.; Grupp, S.; Handgretinger, R.; Ho, T. W.; Kattamis, A.; Kernytsky, A.; Lekstrom-Himes, J.; Li, A. M.; Locatelli, F.; Mapara, M. Y.; de Montalembert, M.; Rondelli, D.; Sharma, A.; Sheth, S.; Soni, S.; Steinberg, M. H.; Wall, D.; Yen, A.; Corbacioglu, S., CRISPR-Cas9 Gene Editing for Sickle Cell Disease and β-Thalassemia. *New England Journal of Medicine* **2020,** *384* (3), 252-260.

24. Hofer, U.; Henley, J. E.; Exline, C. M.; Mulhern, O.; Lopez, E.; Cannon, P. M., Pre-clinical Modeling of CCR5 Knockout in Human Hematopoietic Stem Cells by Zinc Finger Nucleases Using Humanized Mice. *The Journal of Infectious Diseases* **2013,** *208* (suppl_2), S160-S164.

25. Witzigmann, D.; Kulkarni, J. A.; Leung, J.; Chen, S.; Cullis, P. R.; van der Meel, R., Lipid nanoparticle technology for therapeutic gene regulation in the liver. *Advanced Drug Delivery Reviews* **2020**.

26. Adams, D.; Gonzalez-Duarte, A.; O'Riordan, W. D.; Yang, C.-C.; Ueda, M.; Kristen, A. V.; Tournev, I.; Schmidt, H. H.; Coelho, T.; Berk, J. L.; Lin, K.-P.; Vita, G.; Attarian, S.; Planté-Bordeneuve, V.; Mezei, M. M.; Campistol, J. M.; Buades, J.; Brannagan, T. H.; Kim, B. J.; Oh, J.; Parman, Y.; Sekijima, Y.; Hawkins, P. N.; Solomon, S. D.; Polydefkis, M.; Dyck, P. J.; Gandhi, P. J.; Goyal, S.; Chen, J.; Strahs, A. L.; Nochur, S. V.; Sweetser, M. T.; Garg, P. P.; Vaishnaw, A. K.; Gollob, J. A.; Suhr, O. B., Patisiran, an RNAi Therapeutic, for Hereditary Transthyretin Amyloidosis. *New England Journal of Medicine* **2018,** *379* (1), 11-21.

27. Finn, J. D.; Smith, A. R.; Patel, M. C.; Shaw, L.; Youniss, M. R.; van Heteren, J.; Dirstine, T.; Ciullo, C.; Lescarbeau, R.; Seitzer, J.; Shah, R. R.; Shah, A.; Ling, D.; Growe, J.; Pink, M.; Rohde, E.; Wood, K. M.; Salomon, W. E.; Harrington, W. F.; Dombrowski, C.; Strapps, W. R.; Chang, Y.; Morrissey, D. V., A Single Administration of CRISPR/Cas9 Lipid Nanoparticles Achieves Robust and Persistent *In Vivo* Genome Editing. *Cell Reports* **2018,** *22* (9), 2227-2235.

28. Rui, Y.; Wilson, D. R.; Green, J. J., Non-Viral Delivery To Enable Genome Editing. *Trends in Biotechnology* **2019,** *37* (3), 281-293.

29. Intellia Therapeutics, I. In Vivo Therapies. https://www.intelliatx.com/in-vivo-therapies/ (accessed June 1).

Vita

Yuan Rui was born in Kunming, China on November 28, 1992 to Ping Zhang and Changxiang Rui. She moved to the US when she was eight years old and lived in Arkansas, Minnesota, Michigan, and Oklahoma during her formative years. Following graduation from Norman High School in Norman, OK, she attended the University of Oklahoma, graduating with a B.S. in chemical engineering in 2015. During her undergraduate studies, Yuan worked in the lab of Dr. Brian P. Grady, who introduced her to polymeric material research and encouraged her to apply to doctoral programs.

Yuan switched to the field of biomedical engineering for her PhD studies and joined the lab of Dr. Jordan J. Green in August 2015 at Johns Hopkins. In the Green lab, Yuan developed polymeric materials for intracellular delivery of nucleic acids and proteins, with special emphasis on brain cancer and gene editing applications. Her doctoral work has resulted in the publication of several research articles that are loosely interconnected under the giant umbrella of biomaterial-based non-viral delivery. While at Hopkins, Yuan met and married former lab mate and fellow nerd, David Wilson, with whom she formed very successful collaborations in science and in life. In addition to several co-authored manuscripts, Yuan and David share three children – cats Mavid and Dorkin, and baby human Alice Marie.

Yuan Rui

7587 Hearthside Way
Elkridge, MD 21075

yrui2@jhmi.edu
405-314-1916
Google Scholar: https://bit.ly/2RkixWz

Education

Johns Hopkins University, Baltimore, MD — 2015 – May 2021 (expected)
School of Medicine, Biomedical Engineering, PhD Program
Translational Tissue Engineering Center
Institute for Nanobiotechnology
Advisor: Dr. Jordan Green

University of Oklahoma, Norman, OK — 2015
Gallogly College of Engineering
B.S. in Chemical Engineering
GPA: 3.98

Awards

- Siebel Scholar — 2020
- NIH NCI F31 Pre-Doctoral Fellow — 2020
- Institute for NanoBioTechnology (INBT) Nano-Bio Symposium, Poster Competition, 3rd Place — 2019
- NSF Graduate Research Fellow — 2016
- Barry M. Goldwater Scholar — 2014
- Department of Chemical Engineering Outstanding Junior Researcher — 2014
- President's Honor Roll — 2011-2015
- National Merit Scholar — 2011

Leadership / Professional Membership / Service

- Translational Tissue Engineering Center (TTEC) Student Council. President: coordinated career transition talks by TTEC alumni, monthly journal club, and community building events. — 2019 - Present
- BME Edge (Extramural Development in Graduate Education). Co-Chair (2019-2020); Director of Public Relations (2018-2019): organized biomedical industry affiliated speaker series and professional development workshops for BME PhD students. — 2018 - Present
- American Society of Gene & Cell Therapy (ASGCT) — 2018 - Present
- Society for Biomaterials (SFB) — 2018 - Present
- Biomedical Engineering Society (BMES) — 2016 - Present
- MERIT Volunteer, Baltimore City high school summer research mentor — 2019
- Thread Volunteer, Baltimore City high school student mentor — 2015-2016

Publications

Research Articles

1. Karlsson J, Tzeng SY, Hemmati S, Luly KM, Choi O, **Rui Y**, Wilson DR, Kozielski KL, Quiñones - Hinojosa A, Green JJ. Photocrosslinked bioreducible polymeric nanoparticles for enhanced systemic siRNA delivery as cancer therapy. *Advanced Functional Materials*. pp 2009768 (**2021**).
2. **Rui Y**, Varanasi M, Mendes S, Yamagata HM, Wilson DR, Green JJ. Poly(beta-amino ester) nanoparticles enable non-viral delivery of CRISPR/Cas9 plasmids for gene knockout and gene deletion. *Molecular Therapy: Nucleic Acids*. 20, pp 661-672 (**2020**).
3. Lopez-Bertoni H, Kotchetkov IS, Mihelson N, Lal B, **Rui Y**, Ames H, Lugo-Fagundo M, Guerrero-Cazares H, Quiñones -Hinojosa A, Green JJ, Laterra J. A Sox2/miR-486-5p axis regulates survival of GBM cells by inhibiting tumor suppressor networks. *Cancer Research*. 80 (8), pp 1644-1655 (**2020**).
4. Kim J, Mondal SK, Tzeng SY, **Rui Y**, Al-kharboosh R, Kozielski KL, Bhargav AG, Garcia CA, Quiñones-Hinojosa A, Green JJ. Poly(ethylene glycol)-poly(beta-amino ester)-based nanoparticles for suicide gene therapy enhance brain penetration and extend survival in a preclinical human glioblastoma orthotopic xenograft model. *ACS Biomaterials Science & Engineering*. 6 (5), pp 2943-2955 (**2020**).
5. Choi J*, **Rui Y*,** Kim J*, Gorelick N, Wilson DR, Kozielski K, Mangraviti A, Sankey E, Brem H, Tyler B, Green JJ, Jackson EM. Nonviral polymeric nanoparticles for gene therapy in pediatric CNS malignancies. *Nanomedicine: Nanotechnology, Biology and Medicine*. 23 (**2020**). *These authors contributed equally.
6. **Rui Y**, Wilson DR, Choi J, Varanasi M, Sanders K, Karlsson J, Lim M, Green JJ. Carboxylated branched poly (B-amino ester) nanoparticles enable robust cytosolic protein delivery and CRISPR-Cas9 gene editing. *Science Advances*. 5 (12) (**2019**).
7. Mathios D, Hwang T, Xia Y, Phallen J, **Rui Y**, See AP, Maxwell R, Belcaid Z, Casaos J, Burger P, McDonald KL, Gallia G, Cope L, Kai M, Brem H, Pardoll D, Ha P, Green JJ, Velculescu V, Bettegowda C, Park CK, Lim M. Genome-wide investigation of intragenic DNA methylation identifies *ZMIZ1* gene as a prognostic marker in glioblastoma and multiple cancer types. *International Journal of Cancer*. 145, pp 3425-3435 (**2019**).
8. Karlsson J, **Rui Y**, Kozielski K, Placone A, Choi O, Tzeng S, Kim J, Keyes J, Bogorad M, Gabrielson K, Guerrero-Cazares H, Quinones-Hinojosa A, Searson P, Green JJ. Engineered nanoparticles for systemic siRNA delivery to malignant brain tumors. *Nanoscale*. 11 (42), pp 20045-20057 (**2019**).
9. Mishra B, Wilson DR, Sripathi SR, Suprenant MP, **Rui Y**, Wahlin KJ, Berlinicke CA, Green JJ, Zack DJ. A combinatorial library of biodegradable polyesters enables non-viral gene delivery to post-mitotic human stem cell-derived polarized RPE monolayers. *Regenerative Engineering and Translational Medicine*. pp 1-13 (**2019**).
10. Kozielski K, Ruiz-Valls A, Tzeng S, Guerrero-Caszares H, **Rui Y**, Vaughan H, Gionet-Gonzales M, Vantucci C, Kim J, Schiapparelli P, Alkharboosh R, Quinones-Hinojosa A, Green JJ. Cancer-selective nanoparticles for combinatorial siRNA delivery to primary human GBM in vitro and in vivo. *Biomaterials*. 209 pp79-87. (**2019**).
11. **Rui Y**, Wilson DR, Sanders K, Green JJ. Reducible branched ester amine quadpolymers (rBEAQs) co-delivering plasmid DNA and RNA oligonucleotides enable CRISPR/Cas9 genome editing. *ACS Applied Materials & Interfaces*. 11 (11), pp 10472-10480 (**2019**).
12. Wilson DR, **Rui Y**, Siddiq K, Routkevitch D, Green JJ. Differentially branched ester amine quadpolymers with amphiphilic pH-sensitive properties for efficient plasmid DNA delivery. *Molecular Pharmaceutics*. 16 (2), pp 655-668 (**2019**).
13. Lopez-Bertoni H*, Kozielski KL*, **Rui Y***, Lal B, Vaughan H, Wilson DR, Mihelson N, Eberhart CG, Laterra J, Green JJ. Bioreducible polymeric nanoparticles containing multiplexed cancer stem cell-

regulating miRNAs inhibit glioblastoma growth and prolong survival. *Nano Letters*. 18 (7), pp 4086–4094 (**2018**). *These authors contributed equally.

14. Wilson DR, Routkevitch D, **Rui Y**, Quinones-Hinojosa A, Zack DJ, Green JJ. A triple-fluorophore labeled nucleic acid pH nanosensor to investigate non-viral gene delivery. *Molecular Therapy*. 25 (7), pp 1697-1709. (**2017**).
15. **Rui Y,** Guo J, Harwell J, Nakanishi T, Kotera S, Grady BP. Electrical, mechanical and crystallization properties of ethylene-tetrafluoroethylene copolymer/multiwalled carbon nanotube composites. *Journal of Polymer Science, Polymer Physics*, 131 (22). (**2014**).
16. **Rui Y,** Grady BP. Long-time crystallization kinetics in zinc-neutralized ethylene-methacrylic acid ionomers. *Thermochimica Acta*, 565 pp 183-193. (**2013**).

Review Articles

1. **Rui Y** and Green JJ. Overcoming Delivery Barriers in Immunotherapy for Glioblastoma. *Drug Delivery and Translational Research*. In press (**2021**).
2. Luly KM, Choi J, **Rui Y,** Green JJ, Jackson EM. Safety considerations for nanoparticle gene delivery in pediatric brain tumors. *Nanomedicine*. (**2020**).
3. **Rui Y***, Wilson DR*, Green JJ. Non-viral delivery to enable genome editing. *Trends in Biotechnology*, 37 (3), pp 281-293. (**2018**). *These authors contributed equally.
4. **Rui Y**, Quiñones G, Green JJ. Biodegradable and bioreducible poly(beta-amino ester) nanoparticles for intracellular delivery to treat brain cancer. *AIChE Journal*, 63 (5) pp 1470-1482. (**2017**)
5. Kozielski K*, **Rui Y*,** Green JJ. Non-viral nucleic acid containing nanoparticles as cancer therapeutics. *Expert Opinion on Drug Delivery,* 13 (10) pp 1475-1487. (**2016**). *These authors contributed equally.

Abstracts

Talks

1. **Rui Y,** Wilson DR, Sanders K, Green JJ. Carboxylated branched poly(B-amino ester) nanoparticles enable robust intracellular protein delivery and CRISPR/Cas9 gene editing. Society for Biomaterials National Conference. Seattle, WA. 2019
2. **Rui Y,** Wilson DR, Sanders K, Green JJ. Carboxylated branched poly(B-amino ester) nanoparticles enable robust intracellular protein delivery and CRISPR/Cas9 gene editing. Wilmer Eye Institute Research Discussion (W.E.I.R.D.) Seminar Series. Baltimore, MD. 2019.
3. **Rui Y,** Lopez-Bertoni H, Kozielski KL, Lal B, Wilson DR, Laterra J, Green JJ. Environmentally-responsive polymeric nanoparticles for brain cancer gene therapy. Johns Hopkins Institute for Nanobiotechnology Student Research Forum. Baltimore, MD. 2019.
4. **Rui Y,** Wilson DR, Green JJ. Poly(beta-amino ester) nanoparticles for the delivery of CRISPR/Cas9 achieves efficient genome editing. Mid-Atlantic Biomaterials Day. Baltimore, MD. 2018.
5. **Rui Y,** Wilson DR, Sanders K, Green JJ. Hyperbranched bioreducible poly(beta-amino ester)s for efficient delivery of siRNA. Biomedical Engineering Society National conference. Phoenix, AZ. 2017.

Posters

1. **Rui Y,** Wilson DR, Choi J, Varanasi M, Sanders K, Karlsson J, Lim M, Green JJ. Carboxylated branched poly(β-amino ester) nanoparticles enable robust intracellular protein delivery and CRISPR/Cas9 gene editing. US-Japan Symposium on Drug Delivery Systems. Maui, HI. 2019.
2. **Rui Y,** Wilson DR, Sanders K, Green JJ. Carboxylated branched poly(beta-amino ester) nanoparticles enable non-viral CRISPR/Cas9 gene editing via intracellular ribonucleoprotein delivery. American Society of Gene & Cell Therapy Annual Meeting. Washington D.C. 2019

3. **Rui Y,** Wilson DR, Green JJ. Hyperbranched bioreducible poly(beta-amino ester)s for efficient delivery of siRNA. Johns Hopkins Women in STEM Symposium. Baltimore, MD. 2018.
4. **Rui Y,** Kozielski K, Wilson DR, Green JJ. Poly(β-amino ester) nanoparticles for delivery of CRISPR/Cas9 to primary human brain cancer cells. International Nanomedicine & Drug Delivery Symposium. Baltimore, MD. 2016
5. **Rui Y,** Grady BP. Long-time crystallization kinetics in zinc-neutralized ethylene methacrylic acid ionomers. American Chemical Society National Meeting. New Orleans, LA. 2013.
6. **Rui Y,** Grady BP. Effects of neutralization level on the fractional crystallinity of ethylene/methacrylic acid ionomers. Oklahoma American Chemical Society Pentasectional Meeting. Lawton, OK. 2012.

Teaching Experience

- Instructor for *JHU Biomedical Engineering Innovations*: 6-week, three credit summer online course for high school students (32 students) 2020
- Graduate Research Mentor. Directly mentored six JHU undergraduates and two high school students in the Green lab. Six have published research articles with me. 2016-Present
- JHU HEART Course Instructor*: Engineering Genome Editing Systems for Gene Therapy*. Ten-week, one credit course taught to two sessions of 12 undergraduate students. 2019
- JHU Intersession Course Instructor: *Practical Genome Editing and Gene Therapy*. Three-week, two credit JHU intersession course taught to 13 undergraduate students. 2019
- Head Teaching Assistant for *Cell Engineering:* Semester long, three credit undergraduate elective course (63 students) in Biomedical Engineering under Dr. Jordan Green and Dr. Kevin Yarema 2017
- Teaching Assistant for *General Chemistry Lab* at University of Oklahoma (24 students). 2014